STUDIES OF EXCITON INTERACTIONS IN MOLECULAR AGGREGATES

LEON PAUL GIANNESCHI, B.Sc.(Hons.)

Department of Physical and Inorganic Chemistry,

University of Adelaide.

Thesis presented for the degree of

Doctor of Philosophy

January, 1977

To Elizabeth

and Ben

Summary

Exciton effects were studied in three types of molecular aggregate. These studies involved a predominantly theoretical analysis of the exciton migration phenomenon in molecular dimers and experimental investigations of exciton transfer effects in mixed molecular crystals and dye-polymer complexes.

The adiabatic approximation was applied to the problem of vibronic exciton interactions in dimers. It was determined that a weak interaction, arising from the nuclear kinetic energy, exists between the ground and excited states within each molecule in the dimer and that, indirectly, this interaction introduces an additional significant coupling between the excited states of the dimer. The problem which includes such "kinetically induced" effects was formulated and solved for the usual tight-binding exciton model of dimers. The results of this analysis were used to calculate theoretical absorption spectra which were compared with those from a previous crude adiabatic exciton theory. An experimental verification of the theory developed in this work was carried out by the study of the dimeric species spectra of three xanthene dyes; Pyronine Y, Pyronine B and Rhodamine B. In particular, the Pyronine Y system was the subject of the application of an experimental planning technique known as prediction analysis which was aimed at optimizing the experimental conditions in order to reduce the errors in determining the dimeric species spectra. The spectra of the various dimeric species were fitted to, and compared with, theoretical spectra calculated from the adiabatic and crude adiabatic theories. The existence of the weak kinetically induced interaction predicted by the adiabatic theory was confirmed and was interpreted as an

exciton-nuclear momentum interaction.

The study of mixed molecular crystals was aimed at investigating the extent to which the properties of the guest could be interpreted in terms of variations in the orientation of the guest transition moment. The systems 1- and 2- aminoanthracene as guests in anthracene as the host provide excellent examples as each of these appear to produce two crystallographically distinct orientations of the guest. This was confirmed by the measurements of the polarized guest absorption as a function of the angle of incidence at very low temperatures in these mixed molecular crystals. By the application of classical optics, effective transition moment orientations for the guests were calculated, measurements of the system tetracene in anthracene providing a test of the method used. Classical local field corrections were carried out and appeared to be only slightly anisotropic. The results of computer simulations of the crystal packing were used to assign specific guest orientations to the measured transition moment directions. In this way, the directions of the transition moments were fixed with respect to the molecular axes and provided additional, important verifications of the crystallographic inequivalence of the observed guest transitions. It was concluded that the differences in excitation energy observed for the different orientations of the same guest species could be accounted for purely in terms of the guest-host resonance interaction, although the effects of differences in dispersion forces may need to be included as well.

Preliminary investigations were effected in a study aimed at examining the presence of exciton band structure in polymers. In analogy to similar studies with shallow traps in mixed molecular crystals, the absorption spectra of dye-polymer complexes were measured at low temperatures.

Mixed films of the phenothiazine dyes, Methylene Blue and Thionine, in poly (vinyl alcohol) (PVA) and atactic sodium poly (styrenesulphonate) (NaPSS) were studied at liquid nitrogen temperatures and at room temperature. The results of this work indicated that spectral shifts caused by solvent effects would tend to out-weigh expected exciton resonance shifts. As well, the spectral region of interest in the proximity of the host absorption band was not resolved at low temperatures so that a deconvolution technique was employed. Differences in absorption intensity were observed between the free dye transitions and transitions for the dyes bound to NaPSS. This effect was not observed for dyes held within a PVA matrix. However, the intensity differences observed are larger than would be expected for exciton interactions in an atactic polymer such as NaPSS. Although inconclusive, the results of this study have indicated the limits faced in attempting an investigation of this type for polymeric aggregates.

To the best of my knowledge and belief, this thesis contains no material previously published or written by another person, nor any material previously submitted for a degree or diploma at any university, except were due reference is made in the text.

L.P. Gianneschi

Acknowledgements

I wish to express my appreciation to Dr. T. Kurucsev for his encouragement and astute guidance throughout the duration of this work. My thanks also are extended to Dr. N.J. Bridge who helped make my stay at the University of Kent at Canterbury, where the crystal studies were carried out, both fruitful and enjoyable.

I wish to thank the various members of the technical staff who helped in the construction of the apparatus required as well as my fellow students for their continuing support and friendship. I also thank Mrs. J. Schilling for the typing of this thesis and the Advisory Centre for University Education for the photo-reduction of some of the diagrams and tables.

A Commonwealth Postgraduate Research Award is also acknowledged.

L.P. Gianneschi

Department of Physical and
Inorganic Chemistry,
The University of Adelaide,
South Australia.

January, 1977.

Contents

..... the whole is more than the sum of its parts and ..... the constructive interplay of complementary processes is the secret of all creative activity in life.

J.M. Jauch in

"Are Quanta Real?"

CHAPTER I

Introduction

1. THE EXCITON

From a quantum-mechanical viewpoint, the electronic or nuclear excitation of an aggregate of identical, oriented, non-interacting molecules or atoms cannot be associated with any particular component of that aggregate. As a result of this indistinguishability, the absolute location of the excitation cannot be known and a manifold degeneracy is associated with the excitation of any one of the components within the totality of the aggregate. The independence of these components or oscillators ensures the separability of each individual excited state so that the set of degenerate excited states of the aggregate are product states of the separate component wavefunctions. In itself, this picture does not describe any motion of the excitation but rather is a reflection of the probabilistic interpretation of quantum mechanics. The concept of excitation energy migration emerges from the inclusion of an interaction between the components of the aggregate which, in reality, must be expected if the aggregate is to exist at all. The existence of such an interaction makes it possible to describe the states of excitation of the aggregate as superpositions of the product states so that each of these superposed or stationary states describes the delocalization of a single excitation over the entire aggregate. The delocalization is ascribed to the interaction between the components of the aggregate and this interaction takes the form of a potential exchanging the excitation energy from one oscillator to the next. As a result of this type of interaction, the degeneracy of the overall system is removed and the set of stationary states forms a manifold of separate energy levels equal in number to the number of oscillators in the aggregate. Various interpretations of the excitation energy migration evolve from this argument[1] but that due to

Frenkel[2] has enjoyed the widest appeal, particularly in its applicability to molecular systems.

As described in the pioneering work of Frenkel,[2,3] the migration of excitation energy is envisaged as a wave-like propagation. Wave "packets", formally constructed from the stationary states of the aggregate, travel through the aggregate carrying with them the excitation energy and have been termed *excitons*. Consequently, the stationary excited states of the aggregate are termed exciton states and are structured into an exciton band. Since the concept of the exciton had its inception in the field of solid state physics, its development has been influenced a great deal by its resultant interpretation as a quasi-particle. As such, the exciton will have an effective mass and thus a particle momentum so that the exciton band structure reflects the momentum dependence of the exciton energies and of the symmetry-controlled selection rules. In the Frenkel model of the exciton, it is further assumed that there is negligible electron density overlap between neighbouring oscillators in both the ground and excited states — the so-called "tight-binding" model. This implies that no charge-transfer component is included in the process of exciton migration within this model. The application of these fundamental concepts to the various excitation modes possible in atomic, ionic and molecular systems is far-ranging but, within the scope of this thesis, the area of interest has been restricted to singlet state, tight-binding excitons in molecular aggregates.

It is apparent that the exciton, with its basis in the excitation exchange potential, has no real classical analogue. The process involves a radiationless exchange of energy between neighbouring oscillators by a resonant interaction of electron densities. That is, the de-excitation of

one oscillator is accompanied by an almost simultaneous excitation of a neighbouring oscillator and thus involves an interaction between the respective transition moments. Furthermore, the simple model of the exciton so far described will be inadequate when factors such as the nuclear vibrations, deformations of the aggregate structure and the actual process of forming the exciton from a radiation field are probed more fully. Thus, from the initial applications of exciton theory to molecular crystals[4] and polymeric aggregates,[5] this field of study has expanded in various directions encompassing the two major aspects of the energetic and transport properties of the exciton. The present state of these developments in the case of molecular crystals is indicated by the relatively large number of the more recent monographs and review articles[6-21] while reviews related to the more general group of molecular aggregates,[1, 18-21] including polymers and lamellar systems, have not been as plentiful.

2. TOPICS IN THE STUDY OF EXCITON EFFECTS

While the most important advances in the theory of excitons have occurred in the study of crystalline solids due to their high order, the most significant applications would appear to be in the biological sphere[1, 18,20,21] involving a variety of other molecular aggregates. Although the principles are necessarily identical in applying exciton theory to a diversity of molecular aggregates, the particular emphasis and technique will be characteristic of each example. Conversely, the experimental information obtainable from various systems will add constructively to the understanding of the general phenomena involved. It has been in the aim of this work to investigate specific aspects of the exciton phenomenon in a variety of molecular aggregates within particular guidelines. The method of electronic absorption spectroscopy formed the basis of all the experimental studies carried out and each topic utilized a specific property characteristic of the molecular aggregate investigated. In order to systematize the following discussion, the terminolgy used by Birks[20] will be adopted. The exchange of excitation energy from one molecule to a molecule of a different species will be termed exciton *transfer* while such exchange between identical molecules will be termed exciton *migration*. The excitation exchange potential is most commonly known as the exciton resonance interaction.

2.1 Exciton Migration Effects

The phenomenon of exciton migration has many spectroscopic ramifications encompassing both static and dynamic properties of the exciton.[8,12,21] These include a variety of effects from such fundamental static properties as the nature of the exciton wavefunctions and energies to such dynamic

properties as the interaction of the exciton with lattice vibrations. The particular facet of interest in this work has been the interaction of the exciton with the nuclear vibrations — the so-called vibronic interactions. Such interactions play a most important part in the mechanism of exciton decay since the exciton motion is retarded by the nuclear displacements. The effects of nuclear motion on the electronic states of molecules have long been recognized[22] and the application of these concepts to the exciton problem followed from experimental observations on a variety of molecular aggregates.[23-26] Earlier measurements of the spectra of crystals and polymers showed the existence of two limiting cases where the pattern of vibronic levels is determined either by electronic considerations[23, 24, 26] or by the vibrational structure.[25] This effect was qualitatively classified[27] in terms of strong, intermediate and weak coupling, referring to the strength of the exciton resonance interaction as compared to the vibrational energy increment. Theoretical formulations of the vibronic interaction have been presented for crystalline[10,12,14,28] and polymeric aggregates.[19,21,29] However, the experimental and theoretical study of dimeric aggregates has been involved to a very great extent with the problem of vibronic interactions in view of the simplicity of these systems.

2.1.1 *The Interpretation of the Spectra of Dimers*

From the earliest qualitative discussions,[26,33] the formal analyses of vibronic interactions in dimers have been developed in several ways but most of these treatments have been based on specific models which require some amplification at this stage. The mathematical treatment of molecular behaviour may be formulated in terms of the adiabatic approxima-

tion[34-36] in which it is reasoned that nuclear and electronic energies may be calculated separately due to the difference in the magnitude of these terms. The separability of these energies is the basic premise of the well-known Born-Oppenheimer approximation.[37] In recognizing that the potential in which the electrons move depends on the position of the nuclei, the electronic wavefunctions are formulated so as tc retain a nuclear position coordinate dependence. However, as this nuclear dependence in the electronic wavefunctions causes computational difficulties, the nuclear position coordinate in the molecular potential may be fixed at the equilibrium position corresponding to the minimum in this potential. This is the basis of the simpler crude adiabatic approximation in which the electronic wavefunctions retain only a dependence on the electronic coordinates and the effects of the electronic-nuclear interaction are relegated to the molecular potential only. The crude adiabatic approximation has provided instructive and often reasonably accurate treatments of molecular behaviour despite the simplicity of this model.

From the original general discussions[26,33] and theoretical formulations,[26,38] the theory of vibronic interactions in dimers has developed through perturbational[39,40] and variational[41,42] calculations culminating in the symmetry operator treatment of Fulton and Gouterman.[43] These are all crude adiabatic models. In addition, a second quantization method[44] and various stationary state,[45] Born-Oppenheimer state,[46] perturbational[47] and transformation methods[48] based on the adiabatic approximation have been presented. In general, none of these treatments have attained the completeness and computational elegance of the Fulton and Gouterman theory and, although some have been attempts to use more physically realistic

models, they have been simplified to such an extent to be of practical use[44-52] that they have had relatively little to add to the quantitative interpretation of the spectra of dimers. Nevertheless, various discrepancies between the Fulton and Gouterman theory and experiment have been recognized[53,54] and attempts have been made to extend the theory so as to explain these inaccuracies.[51,52] However, the validity of using the crude adiabatic approximation as the basis to these formulations has remained uncertain, although entirely practical. Fulton's[55] treatment of the adiabatic approach to vibronic interactions in *molecules* has provided a concise matrix method of dealing with the adiabatic wavefunctions. This technique has presented the opportunity of applying the adiabatic approximation to the dimer problem in a way analogous to the formulation of the Fulton and Gouterman theory. Such a theoretical treatment and subsequent experimental verification are the subject of a study on the dimeric aggregate presented in this work.

2.2 Exciton Transfer Effects

It has been recognized for some time[56] that, for systems containing very small quantities of an impurity, or guest, in a host crystal, the fluorescence emission induced by light absorbed by the host occurs preferentially from the guest molecules. This observation has two important implications. Firstly, since guest concentrations can be very low, the excitation energy has apparently migrated through the host to the guest. Secondly, the actual process of energy transfer from the host to the guest suggests some form of host-guest resonance interaction. The study of the effects of exciton transfer then provides information about the exciton states of the host as well as about the process by which the exciton looses

its excess energy to become localized at the guest site. Such studies have been the subject of many experimental and theoretical investigations which are extensively reviewed in the literature.[7-12, 14, 57] However, the points of interest in this work are involved with the nature of the guest-host resonance interaction and of its use as a probe of the exciton band structure of the host.

Two limiting cases of the guest-host interaction are distinguished. The shallow trap limit corresponds to the situation where the host exciton bandwidth is comparable with the energy difference between the host and guest transitions so that the localized excitation involves both host and guest molecules and the host band structure must be taken into account. In the deep trap limit, the host and guest energy separation is much larger than the exciton bandwidth and only nearest neighbour interactions need be considered. The more recent theoretical analyses of the spectral properties associated with the exciton transfer process in molecular crystals[58-64] have determined and quantified two basic effects expected from the guest-host interaction. Firstly, as the shallow trap limit is approached, the excitation energy of the guest shifts further to the red as the bottom on the exciton band is approached and as the exciton becomes increasingly delocalized. Secondly, the guest transition exhibits anomalous intensity behaviour near the host exciton band. This behaviour for both shallow and deep traps has indicated that there is a mixing of the excited states of the guest molecules with the excited states of the neighbouring host molecules. Such effects then not only show the presence of an exciton band structure but also indicate the position of the band edge and of the optical, zero wavevector exciton state.

2.2.1 *The Guest-Host Interaction in Molecular Crystals*

Direct spectroscopic evidence for the guest-host interaction[9,10,12] in molecular crystals has encompassed both of the expected effects so far discussed. However, many such studies have probed the nature of the host-guest interaction by observation of the spectral properties of the guest as a function of the energy difference between guest and host excitation energies. The effects of the orientation of the guest have provided an additional area of study, particularly in crystalline systems where the high symmetry and order of these aggregates produces guest sites of determinable alignment. Several instances are known where a particular guest molecule produces several distinct types of trap sites and three such cases may be differentiated. Firstly, if the host molecules are non-rigid,[65-67] the guest molecules may be accommodated in various slightly different orientations. Secondly, a similar result occurs when the guest molecule is a particularly bad fit[68] and causes gross distortions of the host lattice. Variations in the excitation energy of the guest will be relatively small for these two cases. Larger differences would be expected in the third case where the guest molecules replace crystallographically inequivalent host molecules.[69] In such a case, the host molecules are all very close to being equivalent and differences between guest sites arise from a gross change in the orientation of the guest with respect to the host lattice.[70-72]

Anthracene doped with an anthracene derivative having a small substituent at the 1- or 2- position provides a useful example. Firstly, the distortion of the host lattice may be expected to be marginal. There are then eight ways of substituting a host molecule with such a guest. However, crystal symmetry,[73] which includes a site symmetry C_i, reduces

this to only two distinct orientations which are not connected by any *crystal symmetry* operation. If the guest molecule replaces a host molecule with absolute coincidence of molecular axes, these two distinct, crystallographically inequivalent orientations are related by a half-turn about the long-axis of the molecule[69,74,75] which is not a crystal symmetry operation. However, in practice, it would be expected that displacements caused by the steric constraints on the substituents in each case would make this relationship only approximate. In relation to the guest-host resonance interaction, the guest transition energy will depend on the orientation of the guest transition moment with respect to the crystal lattice. The systems 1- and 2- aminoanthracene in anthracene[71] appear to be excellent examples of this effect. In fluorescence, two distinct traps have been identified for each of these systems by a measurement of the positions of spectral lines identified with the guest species. The energy separations, measured at 4.2°K, were 156cm^{-1} and 279cm^{-1} for the 1- and 2- aminoanthracene systems, respectively; energy differences substantially larger than for small misalignments[66] but comparable to those associated with crystallographic inequivalence.[69] The aim of this part of the work has been to confirm this interpretation of such crystalline aggregates by a measurement of the guest transition moment orientations and to interpret the results obtained in terms of the guest-host resonance interaction.

2.2.2 *The Guest-Host Interaction as an Exciton Probe in Polymers*

The theoretical application of the concepts discussed in Section 2.2 for crystalline systems has not been widely implemented in the case of analogous polymeric aggregates. Apart from discussions of energy transfer

in linear crystals,[58,61] the work by Philpott[76-79] appears to be the most extensive contribution in this area. The results of these theoretical analyses have been quite analogous to the effects expected and observed in molecular crystals; these including energy shifts and anomalous transition intensity behaviour near the exciton band edge. The types of guest-host systems possible for polymeric aggregates are of two forms — copolymers and interstitially substituted dye-polymer complexes. Emission spectroscopy of pure polymers and copolymers forms the greater part of the experimental work so far presented, dealing with prompt and delayed fluorescence[80-84] and excitation spectroscopy[85] of both solutions and films at temperatures between room values and 77°K. On the other hand, absorption spectroscopy of pure polymers[86,87] has not yielded a great deal of conclusive information, with the exception of studies with associated dye aggregates,[88] due to the generally small resonance interactions involved. However, the study of dye-polymer complexes[89,90] of biopolymers has provided an overwhelming volume of information involving both fluorescence and absorption spectroscopy, although typically of deep trap systems. The motivation for these latter studies has been based on an interest in the binding and conformation aspects rather than on the investigation of exciton resonance phenomena. The study of polymeric aggregates undertaken in this work was directed at determining the existence of exciton band structures from shallow trap effects.

2.3 Structure of the Thesis

The three aspects of the exciton phenomenon presented in Sections 2.1.1, 2.2.1 and 2.2.2 deal with three types of molecular aggregate — dimers, crystals and polymers. The theoretical formulation of the adiabatic

approach to exciton interactions in dimeric aggregates and a subsequent experimental verification of this theory are presented in Chapter III. The more experimentally-based study of the effects of guest orientation on the guest-host resonance interaction in crystalline aggregates is described in Chapter IV. The third study aimed at investigating the presence of an exciton band structure in polymeric aggregates is given in Chapter V. However, it must be mentioned that this latter experimental investigation is of a preliminary nature as it has not been fully developed. Chapter II describes the experimental details of all the studies carried out from the instrumental and material handling aspects. Standard statistical terminology is used in this thesis without definition and S I units are used unless otherwise specified. Wavenumbers are given *in vacuo*.

REFERENCES

1. M. Kasha, *Rev. Mod. Phys.*, 31, 162 (1959).

2. J. Frenkel, *Phys. Rev.*, 37, 17, 1276 (1931).

3. J. Frenkel, *Z. Sowjetunion*, 9, 158 (1936).

4. A.S. Davydov, *Zhur. Eksptl. Teoret. Fiz.*, 18, 210 (1948).

5. Th. Förster, *Naturwissenshaften*, 33, 166 (1946).

6. (a) R.S. Knox, *Theory of Excitons, Solid State Physics. Supplement 5*, (Ed. F. Seitz and D. Turnbull; Academic Press. 1963).

   (b) D.L. Dexter and R.S. Knox, *Excitons*, (John Wiley and Son, 1965).

7. D.P. Craig and S.H. Walmsley, *Physics and Chemistry of the Organic Solid State*, (Ed. D. Fox, M.M. Labes and A. Weissberger; Wiley-Interscience, 1963). Vol I. p. 585.

8. J.Jortner, S.A. Rice and R. Silbey, *Modern Quantum Chemistry*, (Ed. O. Sinanoğlu; Academic Press. 1965). Part III. p. 139.

9. M.W. Windsor, *Physics and Chemistry of the Organic Solid State*, (Ed. D. Fox, M.M. Labes and A. Weissberger; Wiley-Interscience. 1967). Vol. II. p. 345.

10. S.A. Rice and J. Jortner, *Physics and Chemistry of the Organic Solid State*, (Ed. D. Fox, M.M. Labes and A. Weissberger; Wiley-Interscience. 1967). Vol. III.p. 199.

11. V.M. Agranovich and V.L. Ginsburg, *Spatial Dispersion in Crystal Optics and the Theory of Excitons*. (Wiley-Interscience. 1966).

12. D.P. Craig and S.H. Walmsley, *Excitons in Molecular Crystals*, (W.A. Benjamin. 1968).

13. D.S. McClure, *Optical Properties of Solids*, (Ed. S. Nudelman and S.S. Mitra; Plenum Press. 1969). p.555.

14. G.W. Robinson, *Ann. Rev. Phys. Chem.*, 21, 429 (1970).

15. A.S. Davydov, *Theory of Molecular Excitons*, (Plenum Press. 1971).

16. V.M. Agranovich, *Optical Properties of Solids*, (Ed. F. Abelés; North-Holland.1972).

17. R. Kopelman, *Excited States*, (Ed. E.C. Lim; Academic Press. 1975). Vol 2. p. 33.

18. M. Kasha, *Radiation Res.*, 20, 55 (1963).

19. Th. Förster, *Modern Quantum Chemistry*, (Ed. O. Sinanoğlu. 1965). Part III. p. 93.

20. J.B. Birks, *Photophysics of Aromatic Molecules*, (Wiley-Interscience. 1970). pp. 518-624.

21. M.R. Philpott, *Adv. Chem. Phys.* 23, 227 (1973).

22. H.A. Jahn and E. Teller, *Proc. Roy. Soc. (London)*, A161, 22 (1937).

23. J. Franck and E. Teller, *J. Chem. Phys.*, 6, 861 (1938).

24. D.P. Craig and P.C. Hobbins, *J. Chem. Soc.*, 539 (1955).

25. (a) D.P. Craig, *J. Chem. Soc.*, 2302 (1955).
(b) D.P. Craig and P.C. Hobbins, *J. Chem. Soc.* 2309 (1955).

26. G.S. Levinson, W.T. Simpson and W. Curtis, *J. Amer. Chem. Soc.*, 79, 4314 (1957).

27. W.T. Simpson and D.L. Peterson, *J. Chem. Phys.*, 26, 588 (1957).

28. R.M. Hockstrasser and P.N. Prasad, *Excited States*, (Ed. E.C. Lim; Academic Press. 1974). Vol. 1, p. 79.

29. T. Sanematu and Y. Mizuno, *J.Phys. Soc. Japan*, 40, 1733 (1976).

30. A.V. Lukashin, *Optics and Spectr.*, 30, 470 (1971).

31. M.R. Philpott, *J. Chem. Phys.*, 55, 2039 (1971).

32. E.G. McRae, *Aust. J. Chem.*, 14, 354 (1961).

33. D.S. McClure, *Can. J. Chem.*, 36, 59 (1958).

34. M. Born and K. Huang, *Dynamical Theory of Crystal Lattices*, (Oxford Univ. Press, 1954). pp. 170, 406-407.

35. W.D. Hobey and A.D. McLachlan, *J. Chem. Phys.*, 33, 1695 (1960).

36. H.C. Longuet-Higgins, *Advan. Spectry.*, 2, 429 (1961).

37. M. Born and J.R. Oppenheimer, *Ann. Physik*, 84, 457 (1927).

38. A. Witkowski and W. Moffit, *J. Chem. Phys.*, 33, 872 (1960).

39. A. Witkowski, *Roczniki Chemii*, 35, 1399, 1409 (1961).

40. E.G. McRae, *Aust. J. Chem.*, 14, 344 (1961).

41. R.E. Merrifield, *Radiation Res.*, 20, 154 (1963).

42. W. Siebrand, *J. Chem. Phys.*, 40, 2223 (1964).

43. (a) R.L. Fulton and M. Gouterman, *J.Chem.Phys.*, 35, 1059 (1961).
(b) R.L. Fulton and M. Gouterman, *ibid*, 41, 2280 (1964).

44. J.H. Young, *J.Chem.Phys.*, 49, 2566 (1968).

45. A.D. McLachlan, *Mol.Phys.*, 4, 417 (1961).

46. R. Lefebvre and M. Sucre, *Intern. J. Quantum Chem. Symposium*, 1, 339 (1967).

47. A. Bierman, *J.Chem.Phys.*, 45, 647 (1966).

48. M. Gouterman, *J.Chem.Phys.*, 42, 351 (1965).

49. M. Sucre, F. Gény and R. Lefebvre, *J.Chem.Phys.*, 49, 458 (1968).

50. A. Witkowski and M. Zgierski, *Intern. J. Quantum Chem.*, 4, 427 (1970).

51. M. Zgierski, *Chem. Phys. Lett.*, 21, 525 (1973).

52. M. Zgierski, *J.Chem.Phys.*, 59, 3319 (1973).

53. E.A. Chandross, J. Ferguson and E.G. McRae, *J. Chem. Phys.*, 45, 3546, 3554 (1966).

54. R. Englman, *The Jahn-Teller Effect in Molecules and Crystals*, (Wiley-Interscience. 1972). pp. 90-96.

55. R.L. Fulton, *J. Chem. Phys.*, 56, 1210 (1972).

56. E.J. Bowen, E. Mikiewicz and F.W. Smith, *Proc. Roy. Soc.*, A62, 26 (1949).

57. H.C. Wolf, *Advan. Atom. Mol. Phys.*, 3, 119 (1967).

58. R.E. Merrifield, *J. Chem. Phys.*, 38, 920 (1963).

59. E.I. Rashba, *Soviet Phys. Solid State*, 4, 2417 (1963).

60. D.P. Craig and T. Thirunamachandran, *Proc. Roy. Soc.*, A271, 207 (1963).

61. D.P. Craig, *Advan. Chem. Phys.*, 8, 27 (1965).

62. R.G. Body and I.G. Ross, *Aust. J. Chem.*, 19, 1 (1966).

63. (a) D.P. Craig and M.R. Philpott, *Proc. Roy. Soc.*, A290, 583, 602(1966).
(b) D.P. Craig and M.R. Philpott, *ibid*, A293, 213 (1966).

64. M.R. Philpott, *J. Chem. Phys.*, 53, 136 (1970).

65. R.M. McNab and K. Sauer, *J. Chem. Phys.*, 53, 2805 (1970).

66. R.M. Hockstrasser and G.J. Small, *J. Chem. Phys.*, 48, 3612 (1968).

67. G.J. Small, *J. Chem. Phys.*, 52, 656 (1970).

68. e.g. A. Brillante and D.P. Craig, *Chem. Phys. Lett.*, 29, 17 (1974).

69. R.G. Bray and D.P. Craig, *Cnem. Phys. Lett.*, 13, 577 (1972).

70. N.D. Kurmei, A.V. Soloviev and M.T. Shpak, *Ukr. Fiz. Zhur.*, 19, 94 (1974).

71. N.J. Bridge and D. Vincent, *J. Chem. Soc., Faraday II*, 70, 30 (1974).

72. A. Brillante, D.P. Craig, A.-H. Mau and R. Rajikan, *Chem. Phys. Lett.*, 51, 215 (1975).

73. V.M. Robertson, A.M. Mathieson and V.C. Sinclair, *Acta Cryst.*, 3, 245 (1950).

74. J.S. Vincent and A.H. Maki, *J. Chem. Phys.*, 42, 865 (1965).

75. G. Fischer, *Mol. Cryst. Liquid Cryst.*, 11, 85 (1970).

76. M.R. Philpott, *J. Chem. Phys.*, 53, 968 (1970).

77. M.R. Philpott, *J. Chem. Phys.*, 54, 4223 (1971).

78. M.R. Philpott, *J. Chem. Phys.*, 55, 4005 (1971).

79. M.R. Philpott, *Chem.Phys.Lett.*, 17, 60 (1972).

80. W. Klöpffer, *J. Chem. Phys.*, 50, 2337 (1969).

81. R.B. Fox, *Pure Appl. Chem.*, 34, 235 (1973).

82. R.B. Fox, T.R. Price, R.F. Cozzens and W.H. Echols, *Macromolecules*, 7, 937 (1974) and all previous papers.

83. C.David, M. Piens and G. Geuskens, *Eur.Poly. J.*, 12, 621 (1976) and all previous papers.

84. C.David, V. Naegelen, W. Piret and G. Geuskens, *Eur. Poly. J.*, 11, 569 (1975) and all previous papers.

85. M. Leibowitz and A. Weinreb, *J. Chem. Phys.*, 46, 4652 (1967).

86. M.T. Vala, J. Haebig and S.A. Rice, *J. Chem. Phys.*, 43, 886 (1965).

87. J.W. Longworth, *Biopolymers*, 4, 1131 (1966).

88. S.P. McGlynn, T. Azumi and M. Kinoshita, *The Triplet State*, (Prentice-Hall. 1971).

89. e.g. A. Blake and A.R. Peacocke, *Biopolymers*, 6, 1225 (1968).

90. e.g. G. Lober, *Z. Chem.*, 11, 135 (1971).

CHAPTER II

General Experimental Details

3. CRYOSTATS

Two types of cryostats were used in the experimental studies undertaken. A liquid helium cryostat was available for the spectroscopic studies of crystals down to 4.2°K and a liquid nitrogen cryostat was constructed for the absorption spectroscopy of polymer films at 77.4°K. Very complete descriptions of the many aspects of cryogenics are to be found in the works of White[1] and Meyer[2].

3.1 Liquid Helium Cryostat

The liquid helium cryostat was of conventional design constructed wholly from metal with two viewing ports closed with silica windows. A schematic diagram of the overall structure of this cryostat is presented in figure 3.1. The essential basis of its cooling operation is so-called open cycle refrigeration — the boiling refrigerant cools the sample by conduction. Thermal insulation is a particularly critical factor when dealing with liquid helium as any heat leak could act over a temperature gradient of about 300°K. The liquid helium chamber is generally insulated by radiation shields and a vacuum and the temperature differentials may be reduced to about 70°K by jacketing the low temperature chamber with a liquid nitrogen container at 77°K.

Referring to figure 3.1, it can be seen that the cryostat consists of three separate parts; an internal section (A) supported completely on the upper flange, a middle section (B) which holds the o-ring seals and a lower section (C). The internal section consists of an inner liquid helium chamber (1), of 1.8 dm^3 in volume, jacketed by a liquid nitrogen container (2) and the evacuated space (3). The sample mounting platform

Fig. 3.1 SCHEMATIC VIEW IN CROSS-SECTION OF THE LIQUID HELIUM CRYOSTAT

A. Internal Section

1. Liquid helium chamber
2. Liquid nitrogen chamber
3. Evacuated space
4. Sample mounting platform
5. Sample disc
6. Radiation shields

B. Middle Section

C. Lower Section

7. Removable silica windows

D. Supporting Frame

8. Supporting Bolts
9. Angle of incidence scale

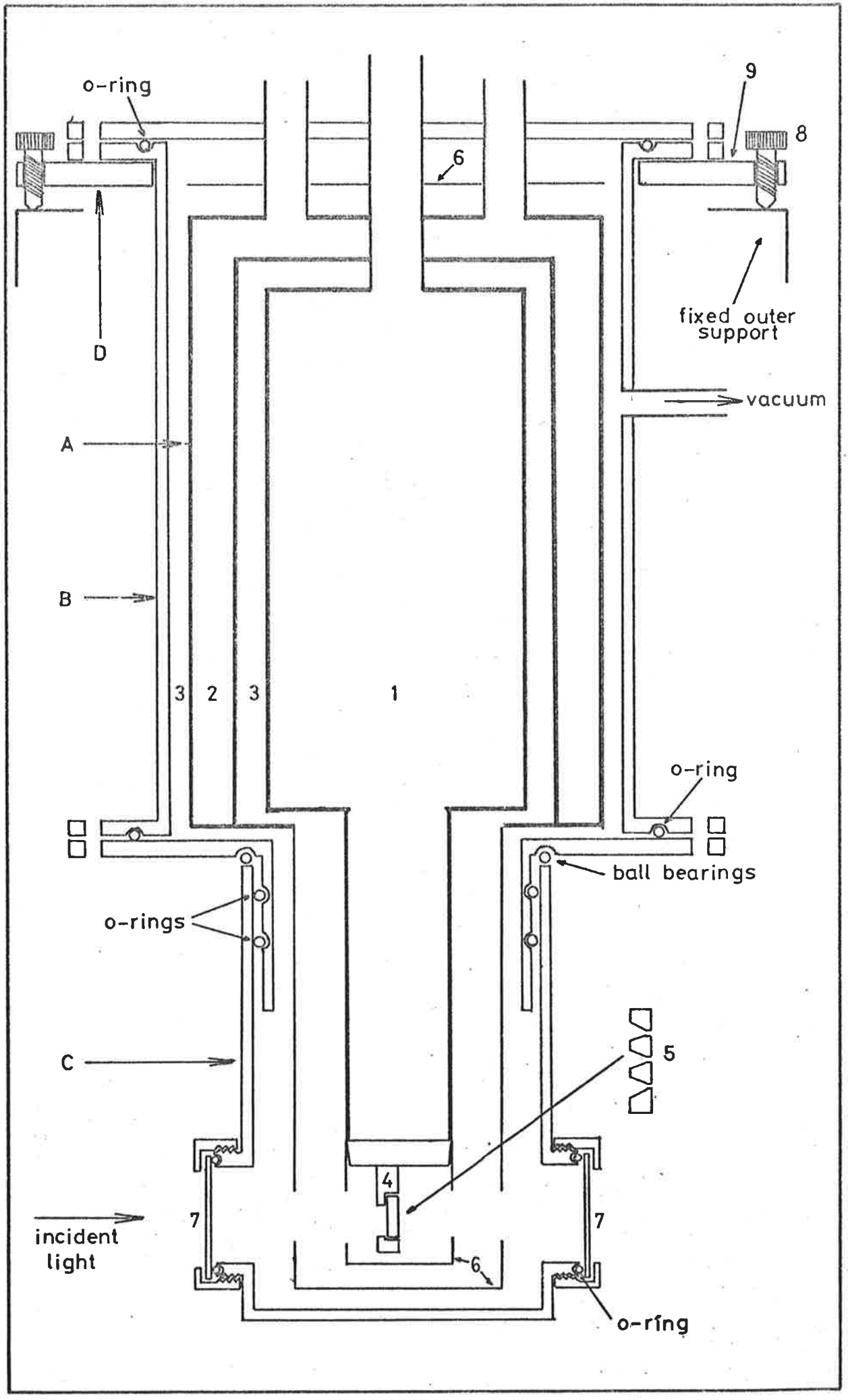
o-ring
9
8
6
D
fixed outer support
vacuum
A
B
3
2
3
1
o-ring
ball bearings
o-rings
C
5
4
7
7
incident light
6
o-ring

(4), made of solid copper, is bolted to the liquid helium container. However, the samples are mounted onto a copper disc (5) which is bolted to the mounting platform when required. This sample disc is a circular copper plate 3cm in diameter and 3mm. thick, with three holes each 1mm. in diameter drilled through it, as shown in figure 3.1. While the sample face of this plate is flat and the holes are flush with it to guarantee a good thermal contact with the samples, these holes have been milled out in approximate conical shapes to the rear of the sample face. This ensures that, when the incident light falls at an angle to the sample face, the disc does not obstruct the light beam. The sample area is surrounded by the lower radiation shields (6) at both 77^{o}K and 4^{o}K. All internal surfaces are silvered to reduce radiation heat transfer except those surfaces in the light path which are blackened to reduce scattering effects. The removable silica windows (7) are mounted into a rotatable section moving on two o-ring seals which maintain the necessary vacuum. The ball-bearings prevent this rotatable section from jamming up against the lower flange under vacuum which would thereby render it immovable. Once the whole cryostat assembly is mounted onto the supporting frame (D), the lower section may be easily removed to replace samples as required. The position of any of the samples with respect to the light beam may be fixed by means of four supporting bolts (8) which tilt and lift or lower the cryostat. A scale (9), graduated in angular degrees, is set onto the supporting frame to indicate the angle of incidence of the incoming light beam on the sample surface. A reference mark on the cryostat, corresponding to the position of normal incidence, was determined from the geometry of the cryostat. The cryostat may then be rotated to a known angle of incidence and the lower rotatable section is turned so that the silica

windows are normal to the light beam. The temperature of the samples is monitored in two ranges with thermometers inserted into the mounting platform. A calibrated copper-constantan thermocouple[3] with the reference junction at 77.4°K was used in the range 300°K to 77°K and a carbon resistance thermometer[4] was used in the range 20°K to 4°K. The connecting wires were attached firmly to the mounting platform to counter the heating of the thermometers by thermal leaks down these leads.

The subsequent procedure was followed in operating this cryostat. Three samples were attached to the sample disc using glycerol as the adhesive. This material neither fluoresces nor dissolves the crystals nor evaporates away under vacuum. Being liquid, it does not appear to strain the crystal at the time of mounting and on cooling sets to a glass which retains useful thermal conductivity at 4°K. The sample disc may then be bolted to the mounting platform, the lower section attached and the evacuation of the vacuum jacket is then commenced by means of a rotary backing pump. Immediately that the pressure has started dropping, the cooling of the samples must be commenced to avoid damaging the crystals by evaporation. To minimize thermal shock to the samples, the inner liquid helium chamber is pre-cooled to 77°K by dripping in liquid nitrogen over a period of about 90 minutes while pumping progresses and the temperature is monitored with the thermocouple. When the inner chamber is thoroughly cooled to 77°K and the vacuum approaches 10^{-5} torr, the liquid nitrogen chamber is filled and any excess liquid nitrogen in the inner container is washed out with gaseous helium. The liquid helium is transferred into the cryostat from a storage dewar by means of a vacuum insulated transfer siphon. This siphon consists of two concentric U-shaped tubes, sealed from one another with an insulating vacuum between them.

One end of the siphon is inserted below the surface of the liquid helium in the storage dewar while the other end engages into the entrance of the inner chamber of the cryostat. By means of a rubber bladder, helium gas is forced down onto the liquid helium in the storage vessel and the refrigerant is impelled into the cryostat through the inner tube of the siphon. There is no direct method of monitoring the quantity of liquid helium transferred except to observe the temperature drop with the carbon resistance thermometer and the rate at which gaseous helium is being vented from the cryostat. With the refrigerant transferred, the cryostat is isolated from the vacuum. The actual volume of liquid helium transferred may be measured with a thermo-acoustical "stick". This consists of a thin-walled, stainless steel tube, about 6mm in diameter, with a small funnel on one end. A thin rubber diaphragm is fastened across the top of this funnel so that the gas vibrations which set in when the tube reaches the liquid surface are observed by the vibration of this diaphragm. There is a marked change in vibration frequency when the end of the "stick" passes from the gas to the liquid so that the volume of liquid helium can be measured against the length of the pre-calibrated tube. The boil-off rate of the liquid helium was generally such that a volume of 1 to 1.5 dm^3 provided between 6 and 8 hours of operating time.

3.2 Liquid Nitrogen Cryostat

The liquid nitrogen cryostat to be described was designed and built as a general purpose instrument for spectroscopic studies. However, certain specific design characteristics were included as the prime aim was the study of the absorption spectra of solid polymer films. The design of this cryostat is quite conventional[1,2] and similar to that of the liquid

helium cryostat previously described. In addition, since the cryostat was to be used with a single beam Ziess PMQII absorption spectrophotometer, a support assembly was required to allow for the measurement of both a sample and a reference. Furthermore, the design of the cryostat was supported by standard heat transfer calculations[1] for such assemblies.

The structure of the cryostat is presented in figure 3.2. Constructed mainly from brass, it consists of three main parts - the internal (A), middle (B) and lower sections (C). The internal section is made up of the 700 cm^3 liquid nitrogen chamber (1), supported from the upper flange by four stainless steel tubes (2), and the sample mounting platform (3). Heat conduction in stainless steel is much less than in brass[1] so that this major heat leak to the liquid nitrogen container is somewhat reduced by the use of stainless steel. The solid copper mounting platform has a separate brass plate (4), held on by two spring clips, which retains the samples firmly over the apertures in the mounting platform. A platinum resistance thermometer (5) is inserted into the mounting platform between the reference and sample apertures. The middle section of the cryostat holds the o-ring seals which maintain the insulating vacuum (6), as well as the vacuum outlet and tap (7) and the glass-to-metal seal (8) which allows entry of the thermometer leads into the cryostat. The surfaces between the middle and internal sections are highly polished to reduce radiation heat transfer. The removable silica windows (9), wide enough to allow a full view of both the apertures in the sample platform, are mounted into the lower section which has been so constructed as to allow the sample mounting platform to be off-set as shown in figure 3.2. In this way, the sample is as close as possible to the

Fig. 3.2 SCHEMATIC VIEW IN CROSS-SECTION OF THE LIQUID NITROGEN CRYOSTAT

A. Internal Section

1. Liquid nitrogen chamber
2. Stainless steel support tubes
3. Sample mounting platform
4. Sample retaining plate
5. Platinum resistance thermometer

B. Middle Section

6. Insulating vacuum
7. Vacuum outlet and tap
8. Glass-to-metal seal

C. Lower Section

9. Removable silica windows

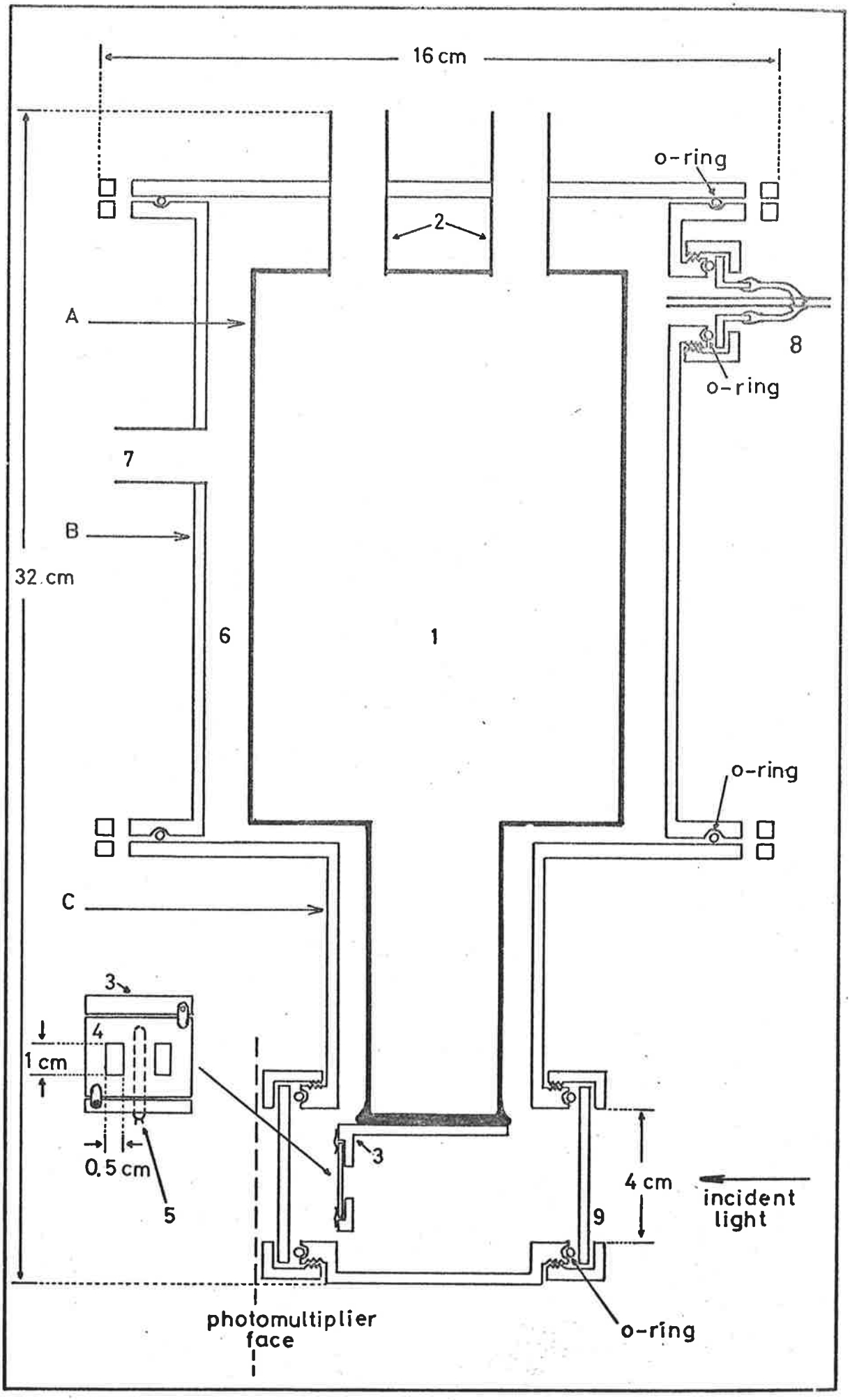
16 cm
o-ring
2
A
8
o-ring
7
B
32 cm
6
1
o-ring
C
3
4
1 cm
0.5 cm
5
3
4 cm
incident light
9
photomultiplier face
o-ring

photomultiplier, thus reducing scattering errors in the measurement of the absorption spectra of polymer films.[5] All exposed surfaces in the sample area have been blackened to reduce stray light reflections.

Figure 3.3 provides a schematic view of the support assembly designed for the use of this cryostat with the Ziess manual spectrophotometer. Only the lower section of the cryostat is supported inside this assembly which must be kept light-tight to protect the photomultiplier. The lower flange of the cryostat is clamped to the upper plate assembly (A) which consists of two main parts. These are the support plate (1), which stands on four large bolts, and the moving plate (2), which rides on two linear ball-races (3) attached to the support plate. The cryostat fits through the openings in the upper section and into the box assembly (B). These openings are rectangular in the stationary parts of the overall assembly and allow the cryostat to move back and forth across the face of the photomultiplier (7). A double-layered "bag" (8), made from black photographer's cloth, is sealed to the edges of the opening in the box assembly and is tied around the "neck" of the cryostat once it is in place. This arrangement ensures that the box is light-tight while allowing free movement of the cryostat. The box assembly is a rectangular box with a door hinged to the front giving access to the whole of the interior. The photomultiplier is supported freely within a tubular external section and by an internal plastic support (9). This plastic support also protects the photomultiplier by separating the cryostat and photomultiplier by about 2mm. The lens assembly (10) consists of a metal tube, which holds the lens of 8cm focal length, sliding within an outer sheath attached to the box assembly. The lens, when set at a distance of two times the focal length from the light source, produces an

Fig. 3.3 SCHEMATIC DESIGN OF CRYOSTAT SUPPORT ASSEMBLY IN CROSS-SECTION

A. Upper Plate Assembly

1. Support plate
2. Moving plate
3. Ball-race
4. Spring-loaded stop
5. Slot plate
6. Microswitch

B. Box Assembly

7. Photomultiplier
8. Light-tight cloth "bag"
9. Internal photomultiplier support
10. Lens assembly

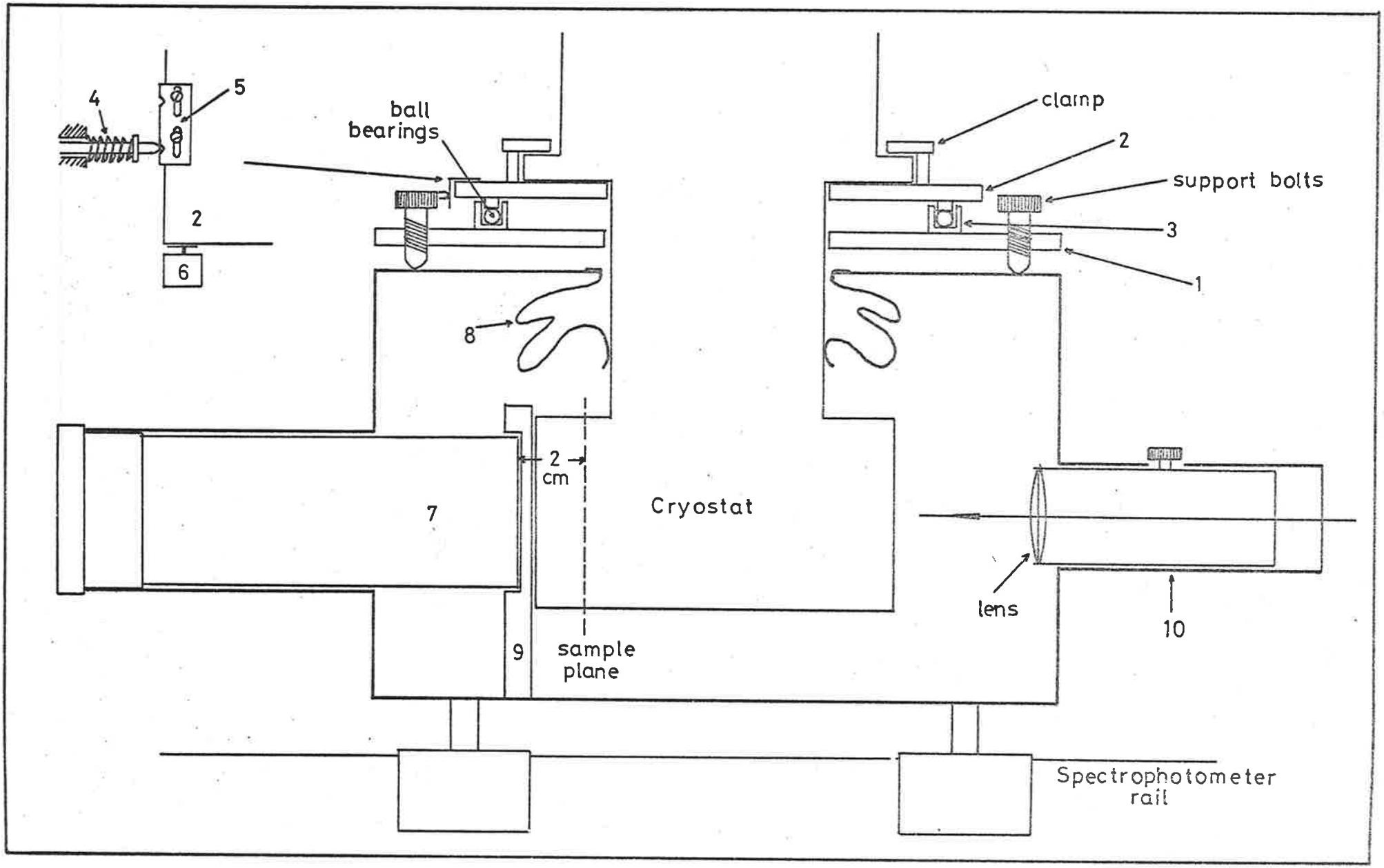
4
5
ball
bearings
2
6
8
clamp
2
support bolts
3
1
2
cm
7
Cryostat
lens
10
9
sample
plane
Spectrophotometer
rail

image the same size as the source at the position of the sample. With the focus set, the lens can be clamped and does not require readjustment since the photomultiplier support (9) ensures that the cryostat is always in the same position. At each wavelength, the 100% transmittance level is set with the light beam through the reference aperture in the sample mounting platform and, then, the sample absorbance may be measured. The reference and sample positions are fixed by means of the spring-loaded stop (4) which locks into either one of the two grooves in the slot plate (5). Each of these grooves corresponds to the situation where the light beam passes through either the reference or sample aperture.

The procedure for the operation of the cryostat and accompanying assembly is as follows. The sample is secured over the sample aperture in the mounting platform with a little apiezon grease to retain thermal contact and is held in place with the retaining plate. The lower section of the cryostat is bolted on and the cryostat is evacuated on a separate vacuum line. The pressure is lowered to less than 10^{-3} torr with a mercury diffusion pump backed by a rotary pump and liquid nitrogen is poured into the cryostat. This is done reasonably slowly at first so as not to strain the cryostat unduly but, when the temperature drops to $77^{o}K$ at the sample platform, the liquid nitrogen may be added more quickly. Once isolated from the vacuum, the cryostat is lowered into the support assembly and clamped into position on the support plate as shown in figure 3.3. This is carried out without the photomultiplier in place so that the direction of the light beam may be viewed directly as it passes through the sample. The cryostat is raised or lowered by means of the four bolts supporting the upper section of the box assembly and the lateral movement

of the cryostat is fixed by means of the stop previously described. The sample and reference positions are adjusted by the mechanism shown as an inset to figure 3,3. The spring-loaded stop (4) is tightened securely into one of the grooves in the slot plate (5). The screws retaining the slot plate to the support plate are loosened so that the cryostat can be moved in relation to both the light beam and the position of the stop. Once the cryostat is positioned with the light beam through the appropriate aperture, the slot plate is secured and the stop is released to a suitable pressure to allow the cryostat to move freely but firmly from one groove to the next. The cryostat is moved by means of a handle (not shown) attached to the moving plate (2) and a microswitch (6) connects the automatic slit control when the cryostat is in the reference position so that the 100% transmittance level is set. When the cryostat is moved to the sample position, the microswitch is turned off and the slit remains fixed at the required width. A full complement of liquid nitrogen allows over one hour of operating time.

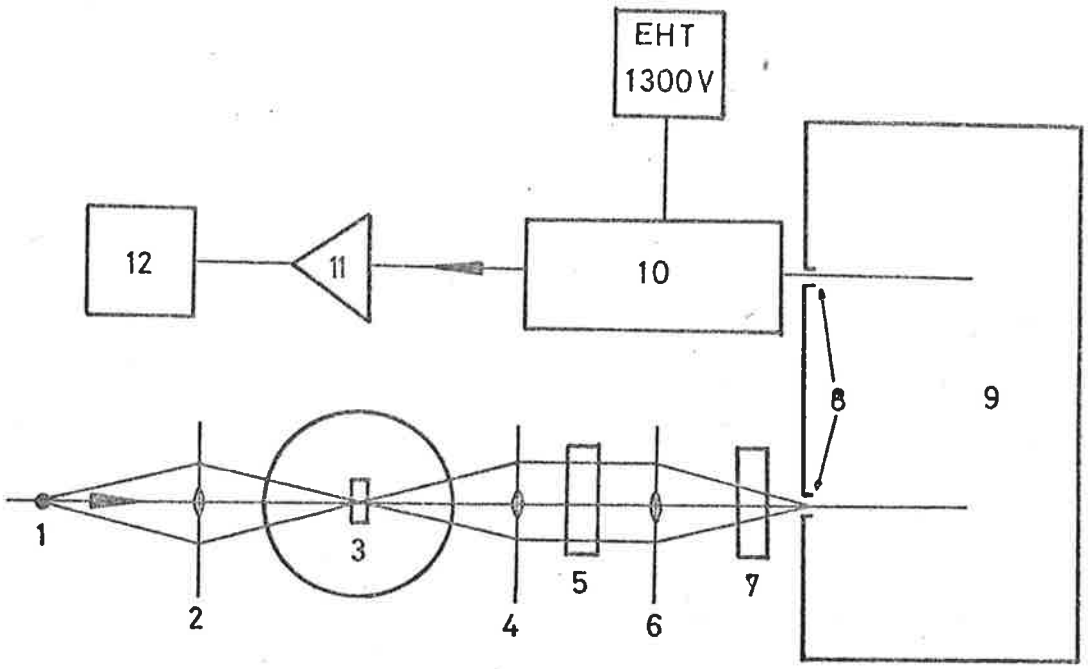

1. Tungsten Light Source
2. Focussing Lens
3. Sample
4. Collimating Lens
5. Polarizer
6. Focussing Lens
7. "Scrambler" Prism
8. Manual Slits
9. Monochromator
10. Photomultiplier (EMI 9558Q)
11. DC Amplifier
12. Chart Recorder

FIG. 4.1 SCHEMATIC DIAGRAM OF HILGER D460 ASSEMBLY.

4. SPECTROPHOTOMETRY

Two main spectrophotometers were used; a Hilger D460 monochromator in conjunction with the liquid helium cryostat and a Ziess PMQII manual spectrophotometer in conjunction with the liquid nitrogen cryostat and for the dye solution experiments.

4.1 Hilger D460

The Hilger D460 monochromator was used for absorption measurements in the visible and ultraviolet regions between 350nm and 460nm. Maximum resolution was found to be better than $2cm^{-1}$ but with a normal slit width of 50nm, the resolution was of the order of $4cm^{-1}$. Figure 4.1 illustrates the experimental design of the spectrophotometer assembly for the measurement of crystal spectra at $4.2^{o}K$. A tungsten lamp is the source of light which is focussed by a lens onto the sample inside the cryostat. The light passes into a collimating lens, through a rotatable calcite polarizer and then is focussed onto the manual inlet slit. A Rochon prism is placed in front of the slit to act as a "scrambler" which rotates the polarized light into an orientation which counters the polarizing effects of the components of the monochromator.[6] Thus, crystals can be mounted at any angle and polarized absorption spectra can be measured without correcting for bias in the monochromator. The signal from the photomultiplier is fed into a highly stabilized DC amplifier which allows gains of 0.1, 1 and 10 times the input signal. The output is recorded as a continuous spectrum on a chart recorder.

A wavelength calibration was carried out using 20 spectral lines from a mercury arc in the range 350nm to 460nm. The error in wavelength

was found to be random in this range giving rise to a required mean correction of +0.4nm to the measured value. No direct check was made of the absorbance error since scattering effects will be an important contribution to this for solid samples. The procedure, to be described, for the calculation of absorbances from measured crystal spectra does much to account for these effects. Absorbance errors were estimated, however, from the observed variations in the measured values and this is summarized in Section 4.3.

4.2 Ziess PMQII

The Ziess PMQII manual spectrophotometer was used for absorption measurements in the visible and ultraviolet regions in the range 200nm to 700nm. The structure of this spectrophotometer is illustrated in figure 4.2 for the measurement of solution spectra with the silica cell assembly and for the measurement of polymer film spectra with the liquid nitrogen cryostat. This is a conventional scheme with the sample between the monochromator and detector and the slit is adjusted at each wavelength by an automatic slit control unit triggered by a microswitch on the sample changing assembly. Resolution was generally maintained between $100cm^{-1}$ and $200cm^{-1}$ throughout the spectral range by judicious use of signal amplification. However, maximum resolution of $50cm^{-1}$ could be achieved in certain regions of the spectrum. The signal output is shown as a galvanometer deflection in terms of absorbance or transmittance.

A wavelength calibration, reported elsewhere,[7] indicated that no correction was required in the ultraviolet region but, in the visible region, the mean correction was $-20cm^{-1}$ to the measured values. In view of

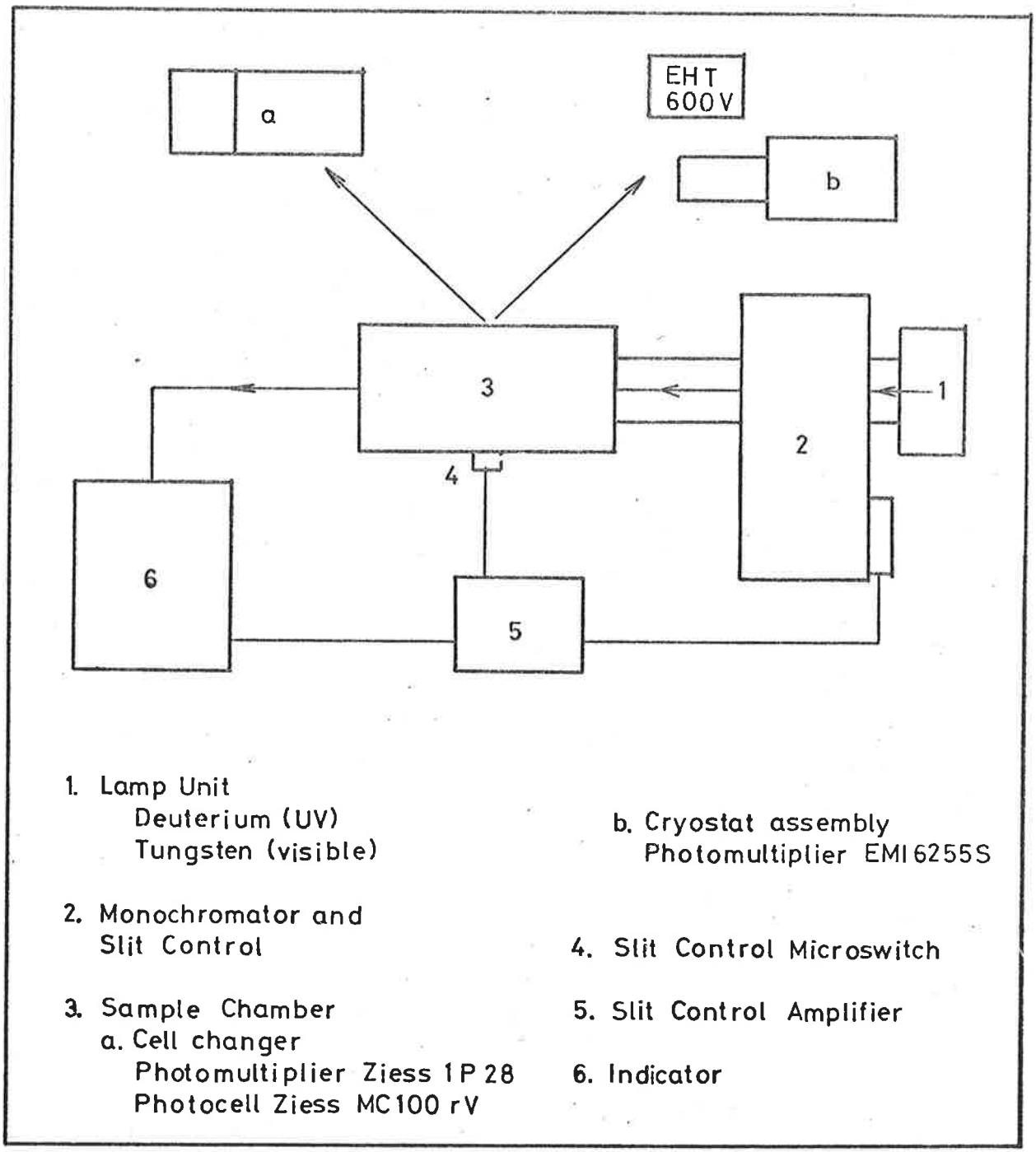

1. Lamp Unit
   Deuterium (UV)
   Tungsten (visible)

2. Monochromator and
   Slit Control

3. Sample Chamber
   a. Cell changer
   Photomultiplier Ziess 1P 28
   Photocell Ziess MC100 rV

b. Cryostat assembly
   Photomultiplier EMI 6255S

4. Slit Control Microswitch

5. Slit Control Amplifier

6. Indicator

FIG. 4.2 SCHEMATIC DIAGRAM OF ZIESS PMQII SPECTROPHOTOMETER.

the resolution limit, this correction was not considered necessary. The photometric accuracy of this instrument was checked with standard cobalt ammonium sulphate solutions.[8] Five solutions of differing concentrations were prepared and measured at 410nm, 510nm and 550nm covering a transmittance range of between 19% and 86%. The standard deviation in transmittance based on 45 determinations over three days was found to be 0.13%. However, a larger standard deviation in the transmittance, 0.2%, was taken since this is the value which corresponds to the manufacturers recommendation. The standard deviation in absorbance was calculated from this constant error in transmittance. Both conventional and short path length silica cells (UV-01, Beckman-RCCI) were used for the spectrophotometric measurements. Pathlengths of the cells were determined by the use of standard potassium chromate solutions.[9] The relative standard deviation in the pathlengths was found to be very nearly constant, of value 0.35%.

4.3 Summary of Experimental Errors

The experimental errors summarized in this section constitute the necessary values required for the data analyses undertaken in the various parts of this work. Apart from those calibrations already described, the following errors were calculated. Estimates of the transmittance error in the measurement of the polarized crystal spectra with the Hilger D460 assembly were calculated from observed variations in the experimental data. The measurement of each crystal spectrum involved two separate observations for each of the two polarizations taken. The differences between the calculated transmittances so measured provided an estimate of the mean transmittance error which was used to compute the absorbance

errors. Crystal and polymer film thickness errors were estimated by measuring the respective thicknesses at five points over the area of each sample and, consequently, obtaining a mean thickness error for all samples. Estimated errors in dye solution concentrations were calculated by the usual procedures and were found to be reasonably constant for all solutions prepared. Table 4.1 summarizes these experimental errors, taken to be standard deviations.

Table 4.1 Standard Deviations in Experimental Variables

Variable	Standard Deviation	Relative Standard Deviation
Crystal Studies:		
Polarized Transmittance	0.3%	-
Crystal Thickness	-	10%
Dimer Studies:		
Transmittance	0.2%	-
Pathlength	-	0.35%
Concentration	-	0.29%
Polymer Studies:		
Transmittance	0.2%	-
Film Thickness	-	15%

5. MATERIALS

5.1 Purification of Materials

The purification of materials for use in spectroscopic experiments is an important requirement if the integrity of the result is to be guaranteed. Unfortunately, there is no absolute criterion of purity as there is no unique method of purification. The method used in each case will depend on the properties of the sample and, most importantly, on the cost in terms of sample loss. This must be balanced against the degrees of purity required to ensure a meaningful result from the experiment undertaken. In the final analysis, it is the results of the experiment which will indicate the influence of any impurities present.

5.1.1 *Materials for Crystal Studies*

The absorption spectroscopy of mixed crystal systems need not be as demanding, from the point of view of sample purity, as the study of the fluorescence of these systems.[10,11] Fluorescence occurs predominantly from the guest so that the effects of impurities must be systematically studied. On the other hand, in the absorption studies of these systems, guest concentrations need only exceed impurity levels to the extent that the spectra can be safely associated with the guest or host. The purification procedures described in this section were used in conjunction with fluorescence experiments[10,12] so that this requirement is fulfilled.

Anthracene

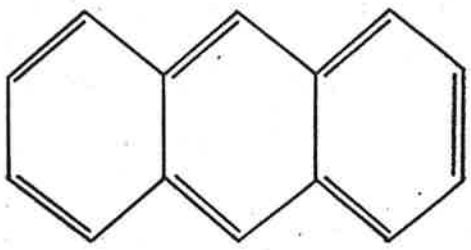

Blue fluorescence grade anthracene, purchased from BDH, was used. 15g of anthracene were chromatographed over about 100g of alumina of activity I on the Brockman scale. A continuous elution method[13] was utilized whereby the elutant passes through the column and into a lower vessel in which the solvent is boiled leaving behind the purified solid and passing up a lagged tube to a condenser above the column. In this way the solvent was recycled through the column of alumina, which was about 4cm in diameter and 25cm long, over a period of about 4 hours until all the anthracene was eluted. Chromatography was carried out under nitrogen with about 250cm^3 of redistilled AR toluene as the solvent and the column was maintained at 40°C, with a water jacket, to sustain a reasonable elution rate. The only impurity band observed on the column, under both visible and ultraviolet light, was a green area near the top of the column. The anthracene recrystallized in the lower vessel and the crystals so obtained were dried *in vacuo* for about 24 hours. Further purification was carried out by zone refining.[14-16] A vertical 5-stage zone refiner was used, passing 5mm zones through a 120mm, ingot at the rate of 25mm / hour. The zone refining tube, of 5mm internal diameter, was filled with chromatographed anthracene under helium at a pressure of 100 torr. At this pressure, sublimation of the anthracene is at a practical minimum so that the ingot remains intact throughout the procedure. A visible band of impurities generally appears at the bottom of the tube. However, impurities are also expected to migrate to the top of the tube[14] so that, generally, only the middle portion was used. After 100 passes, the middle halves of two ingots were combined in a single tube and refined by a further 100 passes. Fluorescence spectra of sublimation grown crystals from these samples were comparable to those of the purest samples

so far reported[10,11] and the absorption spectra were clear of any observable impurity bands in the regions of interest.

Aminoanthracenes

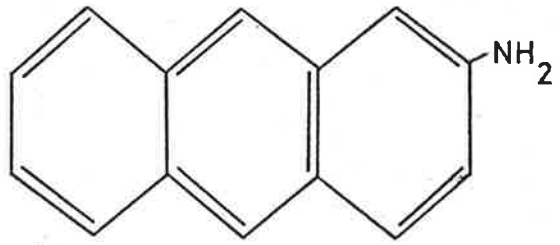

2-aminoanthracene

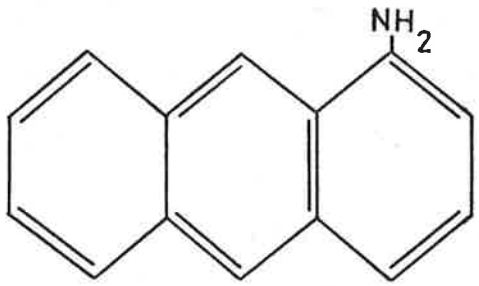

1-aminoanthracene

The purification of the aminoanthracenes was carried out by slight modifications to the method of Bridge and Vincent.[12] 2-aminoanthracene was obtained from Koch-Light and 1-aminoanthracene, with a stated purity of 90%, was purchased from R.N. Emanuel. It has been found that aminoanthracenes are susceptible to atmospheric oxidation, particularly in solution, to heating and to chromatography over strong absorbents.[12] However, rapid chromatography over deactivated alumina proved satisfactory. 0.1g of the aminoanthracene were dissolved in about $3cm^3$ of toluene and applied to a light-tight column containing 10g of alumina of activity III on the Brockman scale. The column was 1.5cm in diameter and 8cm in height. Eluting with toluene, about 25 to $50cm^3$ of clear yellow solution were collected. Dark bands of impurities were absorbed to the top of the column and a brownish material was eluted ahead of the yellow aminoanthracenes. The aminoanthracenes were identified by means of their visible and ultraviolet spectra.[17,18] From 1 to 2.5g of purified anthracene were added to

the chromatographed solutions of the aminoanthracenes so that mixed crystals were formed from solution. In this way, the aminoanthracenes were stabilized in a solid matrix and these mixed crystals formed a ready-made mixture for producing the sublimation-grown flakes required. This sublimation procedure proved to act as an additional purification step since, often, darkened material was left behind on sublimation. Neat samples of the aminoanthracenes were also prepared by the technique described, without the addition of anthracene. Chromatography was generally carried out twice and the solids were retrieved by freeze-drying under vacuum. These materials were obtained as yellow crystals which were found to darken quickly in air, underlining the need for storage in an inert atmosphere.

Tetracene

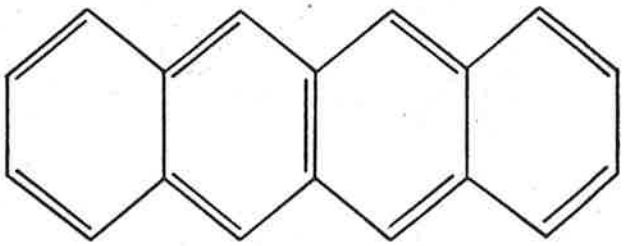

Only a small quantity of this expensive material was available so that sublimation under helium was the only purification procedure employed. A small amount of the tetracene was sealed in a glass tube of 1.2cm internal diameter and 10cm length under 200 torr of helium and heated to about 240°C. Crystals formed at the room temperature end of the tube leaving behind a black residue which was not observed on subsequent passes.

5.1.2 *Materials for Dimer Studies*

The basic aim of these studies was the determination of the species spectra from the association behaviour of particular dyes in solution.

This was done by the theoretical analysis of the *shape* of the spectra as a function of dye concentration so that any impurities which affect this property must be removed. As the spectral properties associated with dye aggregation are well-known, the effects of impurities may be determined.

Pyronine Y (G)

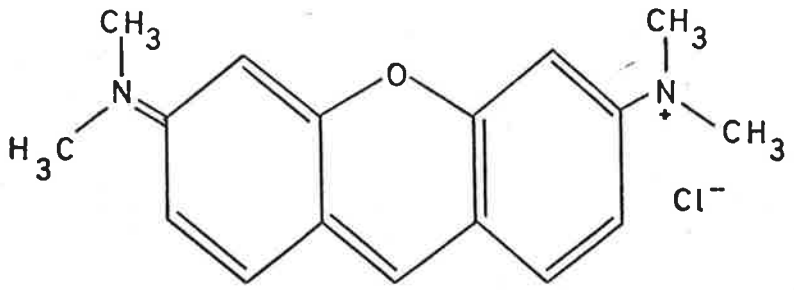

Pyronine Y, purchased from Eastman Kodak Co., had a stated dye content of about 49%. Previous work with this xanthene dye[19] has revealed that samples from various sources contain large amounts of "dextrin and salt". This appeared to apply to this particular sample as it would not dissolve completely in a variety of solvents. The soluble dye was removed from the remaining matrix of insoluble impurities by the Soxhlet extraction procedure[20] under reduced pressure. Chloroform was used as the solvent and the extraction temperature was maintained below 40°C to reduce heat damage to the dye. Solid dye was recovered in a powdery form by freeze-drying and, although the nuclear magnetic resonance, visible and ultraviolet absorption spectra were in agreement with previous information,[19,21] elemental analysis (CSIRO, Melbourne) indicated a high level of impurities. Consequently, column chromatography over activity I alumina was attempted[19] with the result that the dye was found to decompose under this procedure. This occurred for very efficient columns having sample to absorbent mass ratios of 1:100 and length to width ratios of 50:1. The

decomposition may have been reduced by the use of lower activity alumina but an alternate procedure was found to be most satisfactory.

Elemental and X-ray fluorescence analysis (Geology Department, University of Adelaide) indicated high levels of zinc and of some iron in the solvent extracted dye. Such impurities are expected to be present from the manufacture of these dyes[22] and, in addition, it has been reported for the analogous dye Pyronine B[23] that dye-metal complexes form with iron. A metal-free sample of Pyronine Y was prepared by the following procedure. 1g of the commercial product was dissolved in 50cm^3 of hot water, together with 5g of sodium ethylene-diamino-acetate to complex any metal ions present. The solution was cooled to 0^{o}C and filtered to remove much of the pulpy, insoluble material. The resultant filtrate was freeze-dried and the residue extracted with ethanol to leave behind the bulk of the sodium-ethylene-diamine-acetate complexes. This ethanolic solution was reduced to between 5 and 10cm^3, filtered and the dye precipitated by an excess of dry diethyl ether. The dye was separated by centrifugation and the above precipitation procedure was repeated three times. In this way, the dye precipitate lost its original tackiness, which was due to the presence of water, and assumed a more flocculent nature. This material was dissolved in a minimum amount of chloroform, filtered and recovered by freeze-drying. The crystals were hygroscopic and thus were stored under vacuum. The final yield was about 30% and elemental analysis indicated that sulphated ash residues at 300^{o}C had been reduced from about 16% to less than 1%. In addition, table 5.1 shows that the molar absorptivity compares favourably with the highest value reported.[24]

Table 5.1 Molar Absorptivity of Pyronine Y at the Visible Maximum

Sample	Concentration (mol dm^{-3})	Molar Absorptivity (dm^3 mol^{-1} cm^{-1})
Fujiki *et alia*[25,a]	1×10^{-5}	12 200
Porro *et alia*[21]	3×10^{-5}	46 200
Fujiki *et alia*[25,b]	1×10^{-5}	~69 900
Jakobi *et alia*[24]	1×10^{-6}	~85 100
This work[c]	5×10^{-6}	55 600
This work[d]	5×10^{-6}	81 100

a. Crude reagent.
b. Recrystallized reagent.
c. Solvent extracted reagent.
d. EDTA extracted reagent.

5.1.3 *Materials for Polymer Studies*

These experiments involved the study of the spectra of certain dyes in polymer matrices. As the results of this work were of a preliminary nature, the major concern was with the presence of any complexing metal ions. In this way, for the concentrations at which the dye-polymer films were prepared, it could be safely assumed that the dye was predominantly in its monomeric form. The polymers were used without further purification.

Phenothiazine Dyes

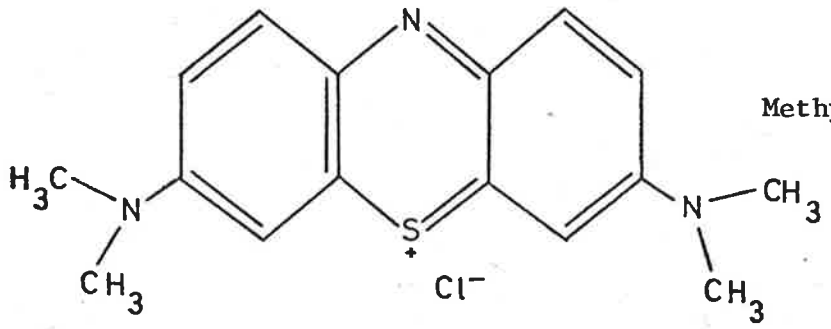

Methylene Blue

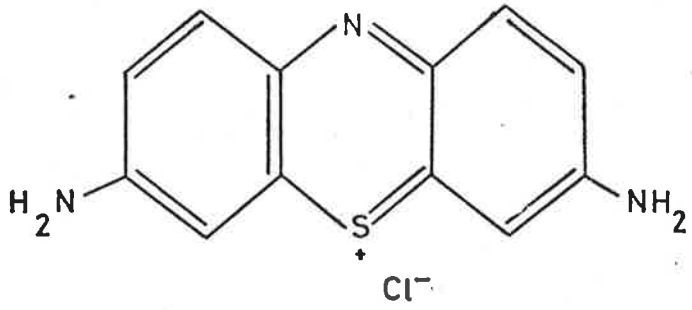

Thionine

Methylene Blue was obtained from May and Baker Ltd. and had a stated purity of 85%. Thionine, of unknown purity, was obtained from Gurr and Co. Both of these dyes were purified by a modification of the method of Pal and Schubert.[26] A concentrated solution was prepared from 3g of dye in boiling 0.1M hydrochloric acid. 5g of sodium ethylene-diamino-acetate were dissolved into this solution which then was filtered hot. The resultant filtrate was chilled and the crystals so obtained were dried *in vacuo* and redissolved in a minimum amount of hot ethanol. On cooling the solution to $0^{o}C$, the dye was then reprecipitated by the slow addition of an excess of cold diethyl ether. The resultant precipitate was washed with cold ethanol and diethyl ether, dried under vacuum and the procedure was repeated one further time. The visible and ultraviolet absorption spectra of these dyes were in agreement with those previously reported[27-33] and, as can be seen from table 5.2, the measured molar absorptivity for Methylene Blue indicates a reasonable purity. The measured molar absorptivity for Thionine was not as favourable. However, micro-

analytical measurements (Perkin-Elmer 240 Elemental Analyser) of the residue after combustion for these samples indicated that the residue for Methylene Blue was reduced from just above 1% to about 0.5% while that for Thionine was reduced from 16% to about 2%. The purification procedure has removed almost all metal ions so that the dyes are known to be in uncomplexed form. As was seen from the results of the dye-polymer experiments, the impurities present had no significant effect.

Table 5.2 Molar Absorptivities of Phenothiazine Dyes at the Visible Maximum.

Sample	Concentration (mol dm^{-3})	Molar Absorptivity (dm^3 mol^{-1} cm^{-1})
Methylene Blue:		
Rabinowitch *et alia*[27]	2×10^{-6}	39 000
Vickestaff *et alia*[28]	2.5×10^{-6}	61 000
Braswell[29]	6×10^{-7}	78 000
Michaelis *et alia*[30]	6.4×10^{-6}	80 000
Lewis *et alia*[31]	6.3×10^{-7}	84 000
Bergmann *et alia*[32]	$\sim 1 \times 10^{-6}$	85 000
This work	5×10^{-6}	73 300
Thionine:		
Haugens *et alia*[33]	1.9×10^{-6}	~48 600
Rabinowitch *et alia*[27]	2.5×10^{-7}	58 000
This work	5×10^{-6}	26 600

5.2 Preparation of Samples

5.2.1 *Mixed Crystals*

All crystals were grown by gradient sublimation as this method is known to produce fewer dislocations[34] while melt-grown crystals are reported to give spectra with intense continuous fluorescence, attributed to excitons trapped at lattice defects.[35] Crystals were grown in a sealed glass tube of 1.2cm internal diameter and of 10cm in length. Between 0.1g and 0.2g of material were placed into an open tube which was then evacuated to a pressure of less than 10^{-3} torr. The tube was flushed several times with helium and then filled to a pressure of about 200 torr with this gas and the tube was sealed hermetically. The sublimation heater consists of a glass tube 4cm in diameter and 25cm long with a heater wire wound around it in an uneven way so that the temperature gradient from one end of the tube to the other is about 3.6°C/cm at normal operating voltages. One end of the sample tube was placed at the hottest end of the heater, which is usually at 240°C, and crystals form at the cooler end, usually at 150°C, over the period of between 30 min and one hour. The first attempt usually gave poor results, with a powdery covering to the walls of the tube. As a consequence, the sublimation procedure was repeated once more with the tube reversed, producing well-formed flat platelets growing out from the sides of the tube. The starting material contained a mixture of guest and host prepared either in the purification procedure, as in the case of the aminoanthracenes, or by mixing known amounts of the guest and host, as in the case of tetracene. The starting mixtures for the aminoanthracenes were estimated as having guest concentrations of about 10^{-3} mol/mol while the tetracene mixtures were prepared at concentrations of between 0.1 and 0.001 mol/mol. Mixed crystals grow under sublimation with a wide range of guest concentrations, usually with the higher guest content being formed

at the hottest part of the tube. This provides a convenient way of obtaining mixed crystals of various concentrations from the one starting mixture.

5.2.2 *Dye Solutions*

Aqueous dye solutions for both the dimer and polymer studies were prepared by the same procedure. A stock solution was prepared volumetrically in a one dm^3 vessel at the highest concentration required. The lower concentrations then were prepared by weight assuming that the density of the stock solution was 1g cm^{-3} so that the concentrations could be converted into molarities (mol dm^{-3}). It was determined, by density measurements within an experimental error of 0.2%, that the density assumption was valid for the Pyronine Y stock solution of concentration 1×10^{-3} mol dm^{-3} and was assumed to apply to the similar phenothiazine dyes. The method of preparing solutions by weight results in far lower errors than would be produced by preparing solutions by volumetric dilution. Such errors are kept to a minimum by diluting stock solutions only, using stock weights of 0.5g or more, instead of employing a stepwise dilution procedure. While the relative standard deviation in the stock concentrations were of the order of 0.07%, the same errors in the lower concentrations were found to be a constant 0.29%, including the 0.2% error in the density assumption.

5.2.3 *Dye-Polymer and Polymer Films*

All films were cast, from solutions of the polymers or dye-polymer mixtures, in perspex trays constructed from two pieces of perspex. Four

evenly spaced cylindrical holes, 1.9cm in diameter, were drilled through the top plate which is 1.3cm thick. Both plates, cleaned prior to use by wiping with ethanol and rinsing with distilled water, were held firmly together by four corner screws which passed through the top plate and into the base plate. An appropriately shaped thin rubber gasket, made from medium gauge "dental dam", was placed between the plates to ensure a water-tight seal. Solutions of the polymers or dye-polymer mixtures were then placed into the holes in the perspex trays which were floated on a pool of mercury and protected from the light. In this way, homogeneous polymer films formed in two to three days and were removed by dismantling the perspex trays. These films then were trimmed to a diameter of about 1.5cm to remove the thick and uneven edges. The starting solutions were prepared from 5% w/w solutions of the pure polymers in cold water, for sodium poly (styrenesulphonate), or in a hot 5:1 mixture of water and ethanol for poly (vinyl alcohol). To produce mixed films, a weighed amount of the polymer was dissolved in the relevant solvent, allowed to cool and then a weighed amount of dye solution could be added to make the polymer concentration up to 5% w/w. In this way, the dye concentrations could be calculated in terms of the number of moles of dye to the number of moles of monomeric unit of the polymer. One cm^{-3} of these solutions was placed in each of the holes in the perspex trays to form the required films which were generally about 0.005cm in thickness.

REFERENCES

1. G.K. White, *Experimental Techniques in Low-Temperature Physics*, (Oxford Univ.Press. 1959).

2. B. Meyer, *Low Temperature Spectroscopy*, (American Elsevier. 1971).

3. R.L. Powell, M.D. Bunch and R.J. Corruccini, *Cryogenics*, 1, 139 (1961).

4. C. Terry, *Rev. Sci. Instrum.*, 39, 925 (1968).

5. e.g. G.R. Kelly and T. Kurucsev, *Eur.Poly. J.*, 11, 581 (1975).

6. e.g. D. Clarke and J.F. Grainger, *Polarized Light and Optical Measurement*, (Pergamon, 1971). pp. 170-172.

7. G.R. Kelly, *Ph.D. Thesis*, (University of Adelaide. 1974).

8. Nat. Bur. Stand. Circular No. 484 (1949).

9. G.W. Haupt, *J. Opt. Soc. Amer.*, 42, 441 (1952).

10. e.g. N.J. Bridge and D. Vincent, *J. Chem. Soc., Faraday II*, 68, 1522 (1972).

11. e.g. L.E. Lyons and L.J. Warren, *Aust. J. Chem.*, 25, 1411, 1427 (1972).

12. N.J. Bridge and D. Vincent, *J. Chem. Soc., Faraday II*, 70, 30 (1974).

13. J.N. Sherwood, *Fractional Crystallization*, (Ed. M. Zief; Marcel Dekker. 1969). Vol. 2, p.157.

14. W.G. Pfann, *Zone Melting*, (Wiley and Sons. 1966).

15. W.R. Willcox, R.Friedenberg and N. Back, *Chem. Rev.*, 64, 187 (1964).

16. G.J. Sloan, *Physics and Chemistry of the Organic Solid State*, (Ed. D. Fox, M.M. Labes and A. Weissberger; Interscience. 1963). Vol I, p. 180.

17. M. Tichy and R. Zahradnik, *J. Phys. Chem.*, 73, 534 (1969).

18. S. Suzuki and H. Babi, *Bull. Chem. Soc. Japan*, 37, 519 (1964).

19. R.W. Horobin and L.B. Murgatroyd, *Stain Tech.*, 44, 297 (1969).

20. e.g. A. Vogel, *Quantitative Inorganic Analysis*, (Longmans, Green and Co. 1961), p. 904.

21. T. Porro and H.Morse, *Stain Tech.*, 40, 173 (1965).

22. J. Hewitt, *Dyestuffs Derived from Pyridine, Quinoline, Acridine and Xanthene*, (Longmans, Green and Co. 1922). p. 250.

23. E.M. Chamberlain, B.F. Powell, D.E. Williams and J. Conn, *J. Org. Chem.*, 27, 2263 (1962).

24. H. Jakobi and H. Kuhn, *Z. Elecktrochem.*, 66, 47 (1962).

25. K. Fujiki, C. Iwanaga and M. Koizumi, *Bull. Chem. Soc. Japan*, 35, 185 (1962).

26. M.K. Pal and M. Schubert, *J. Amer. Chem. Soc.*, 84, 4384 (1962).

27. E. Rabinowitch and L.F. Epstein, *J. Amer. Chem. Soc.*, 63, 69 (1941).

28. T. Vickerstaff and D.R. Lemin, *Nature*, 157, 373 (1946).

29. E. Braswell, *J. Phys. Chem.*, 72, 2477 (1968).

30. L. Michaelis and S. Granick, *J. Amer. Chem. Soc.*, 67, 1212 (1945).

31. G.N. Lewis, O. Goldschmid, T.T. Magel and J. Bigeleisen, *J. Amer. Chem. Soc.*, 65, 1150 (1943).

32. K. Bergmann and C.T. O'Konski, *J. Phys. Chem.*, 67, 2169 (1963).

33. G.R. Haugens and E.R. Hardwick, *J. Phys. Chem.*, 67, 725 (1963).

34. J.O. Williams and J.M. Thomas, *Trans. Faraday Soc.*, 63, 1720 (1967).

35. W. Helfrich and F.R. Lipsett, *J. Chem. Phys.*, 43, 4368 (1965).

CHAPTER III

The Dimeric Aggregate

6 AN ADIABATIC TREATMENT OF EXCITON INTERACTIONS IN DIMERS

In dealing with exciton interactions in associated dimers, one is presented with a two-fold problem. Such dimers have both a molecular and a dimeric nature, each of these being distinguishable yet intimately connected to one another. In the ground and excited states the moieties of the dimer are attracted to one another by the relatively weak dispersion forces and, in both the ground and excited states, molecular orbital overlap is generally accepted as being insignificant for such dimers. Consequently, the Frenkel[1] "tight-binding" model for exciton interactions is applicable in such cases and to a predominant degree the dimeric problem may be described in molecular terms. It has been this capacity to deal with the molecular part of the problem separately which has allowed a successful treatment of the effects of nuclear vibrations on the exciton interaction in dimers. The usual crude adiabatic formulations of these exciton interactions have revealed the essential nature of such effects but, in neglecting the nuclear position dependence of the electronic wavefunctions, this form of approximation has led to an oversimplification of the molecular part of the problem. The use of the adiabatic approximation, as undertaken in the following work, will show that further electronic-nuclear interactions are present arising from purely molecular terms which have not been previously considered but which play a significant rôle in a quantitative theory of exciton interactions in dimers.

In the subsequent treatment, the following notations and conventions will be used:

(i) N and M will denote the ground and excited electronic states, respectively, residing within a particular molecular moeity of the dimer;

(ii) P and Q are the nuclear momentum and position coordinates while m_e and r are the corresponding electronic coordinates, again referring to each molecular moiety of the dimer;

(iii) $\underline{\sigma}_1$, $\underline{\sigma}_2$ and $\underline{\sigma}_3$ are the Pauli spin matrices[2],

$$\underline{\sigma}_1 = \begin{pmatrix} 0 & -1 \\ 1 & 0 \end{pmatrix}, \quad \underline{\sigma}_2 = \begin{pmatrix} 0 & -i \\ i & 0 \end{pmatrix}, \quad \underline{\sigma}_3 = \begin{pmatrix} 1 & 0 \\ 0 & -1 \end{pmatrix}$$

while $\underline{1}$ is the identity matrix;

(iv) the Dirac notation[2] for the wavefunctions will be used when dealing with integrals. That is

$$\langle \psi(x) | A(x) | \psi(x) \rangle = \int dx \, \psi^*(x) A(x) \psi(x)$$

where A(x) is an operator acting on the wavefunction $\psi(x)$. Unless otherwise stated all integrals will be over the electronic position coordinate r;

(v) the usual anti-commutator and commutator expressions will be used for general operators A and B, namely

$$[A,B]_{\pm} = AB \pm BA.$$

This formulation of exciton interactions in dimers will be constructed as follows. The molecular aspect of the problem will be dealt with initially, deriving and solving the eigenvalue equation for each moiety of the dimer. The overall dimeric eigenvalue equation is then constructed and solved followed by the derivation of the transition intensities. The solutions are in terms of absorption spectra only, these being the ones of practical interest in this work. However, solutions in terms of fluorescence spectra may be derived from the general formulation presented.

6.1 Treatment for Each Moiety

In keeping with the usual approximations,[3-6] the model of the molecular moiety of the dimer is assumed to be a single molecule with the ground state and one excited state being the only electronic energy levels to be considered. Each moiety is further assumed to behave as a harmonic oscillator of effective mass M_n with only one mode of vibration. Translational and rotational motions and spin effects are neglected.

Fulton[6] has presented a novel application of the adiabatic approximation to the problem of a single molecule with n nearly-degenerate electronic states using a stationary state argument. The major result of this treatment has been that the various nuclear wavefunctions associated with the set of n nearly-degenerate states, and hence the electronic states themselves, are coupled by terms arising from the nuclear kinetic energy. Such an effect has been described previously[7,8] but has been generally neglected for non-degenerate states[8-10] since the magnitude of the coupling terms is proportional to the energy separation between the electronic states. However, conceptually, such coupling is still possible between more widely separated states so that the limit at which this coupling becomes negligible is arbitrary and needs to be decided upon in view of the magnitude of other perturbations present. Thus this kinetically induced coupling, henceforth referred to as KI coupling, may be a small perturbation when compared to the transition energy between the ground and excited state *within* each moiety of the dimer but is more significant when compared to the magnitude of the exciton interaction *between* the moieties of the dimer.

The use of one stationary state to describe the coupling of a set of degenerate or nearly-degenerate states simply replaces many energies by

one mean energy and many states by one state. This formulation leads to the construction of a set of coupled eigenvalue equations which, when decoupled, yield the original set of energy levels with the coupling interaction included as a perturbation.[4] The stationary state description remains applicable as long as the coupling between the states in question is taken to be significant. Fulton's stationary state formulation of the KI coupling terms in matrix form is then applicable to the case of a weaker KI coupling between the ground and excited states within a molecular moiety of the dimer. However, the resultant coupled molecular Hamiltonian must be decoupled into separate ground and excited state forms if the dimeric Hamiltonian is to be constructed in the usual way.[3,4] This argument introduces the use of a modified stationary state approach in the case of more widely separated or non-degenerate states, the form of which is now described.

6.1.1 *The Molecular Hamiltonian in Coupled Form*

The total Hamiltonian H is generally written as the sum of the nuclear kinetic energy T_n and the electronic Hamiltonian H_e[3,4,6]

$$H = T_n(P) + H_e(m_e, r, Q), \tag{6.1}$$

In putting the electronic ground and excited states ψ_N and ψ_M, respectively, into vector form

$$\underline{\psi} = \begin{pmatrix} \psi_N(r,Q) \\ \psi_M(r,Q) \end{pmatrix}, \tag{6.2}$$

one may express the electronic eigenvalue equation in the matrix form

$$H_e\underline{\psi}^T = \underline{\psi}^T \underline{V} \tag{6.3}$$

where

$$\underline{V} = \begin{pmatrix} E_N(Q) & 0 \\ 0 & E_M(Q) \end{pmatrix}. \tag{6.4}$$

$\underline{\psi}^T$ is the transpose of $\underline{\psi}$ and E_N and E_M are the respective electronic energies corresponding to the states in the vector $\underline{\psi}$. Postulating that a weak KI coupling exists between these two widely separated states, the wavefunctions associated with the total Hamiltonian H may be formulated as the stationary states

$$\Psi_\nu = \underline{\psi}^T \underline{\phi}_\nu \tag{6.5}$$

where

$$\underline{\phi}_\nu = \begin{pmatrix} \phi_{N\nu}(Q) \\ \phi_{M\nu}(Q) \end{pmatrix}. \tag{6.6}$$

$\phi_{N\nu}$ and $\phi_{M\nu}$ are the nuclear wavefunctions associated with the electronic states ψ_N and ψ_M, respectively, and both refer to the vibrational state ν in the one mode of vibration being considered.

Fulton[6] describes the derivation of the coupled form of the total eigenvalue equation resulting from the operation of the total Hamiltonian in eqn (6.1) on the wavefunctions Ψ_ν in eqn (6.5). Thus, in this case, writing the coupled Hamiltonian $\underline{\mathcal{H}}$ as

$$\underline{\mathcal{H}} = \langle \underline{\psi} | H | \Psi_\nu \rangle$$

then

$$\underline{\mathcal{H}}\, \underline{\phi}_\nu = \underline{\mathcal{T}}_n \underline{\phi}_\nu + \underline{V}\underline{\phi}_\nu = \epsilon_\nu \underline{\phi}_\nu \tag{6.7}$$

where

$$\underline{\mathcal{T}}_n(-i\hbar\, \partial/\partial Q) = \langle \underline{\psi} | T_n | \underline{\psi}^T \rangle \tag{6.8}$$

for one mode of vibration only. This treatment results in the premise[6] that $\underline{\mathcal{T}}_n$ may be found from T_n by the replacement

$$\underline{\mathcal{T}}_n(-i\hbar\, \partial/\partial Q\underline{1}) = T_n(-i\hbar\, \partial/\partial Q\underline{1} + \underline{\Lambda}). \tag{6.9}$$

The form of $\underline{\Lambda}$, in this case, is a two-dimensional matrix whose elements are

$$\underline{\Lambda} = f(Q)\underline{\sigma}_2$$

where

$$f(Q) = \hbar(E_M - E_N)^{-1}\langle\psi_N|\partial H_e/\partial Q|\psi_M\rangle. \tag{6.10}$$

Note that, due to the fact that E_M and E_N are used in this example, the elements of $\underline{\Lambda}$ have opposite signs to the corresponding elements in the case described by Fulton.

It is seen from the form of $\underline{V}$ in eqn (6.4) that

$$\underline{V} = \tfrac{1}{2}(E_M + E_N)\underline{1} + \tfrac{1}{2}(E_M - E_N)\underline{\sigma}_3. \tag{6.11}$$

In addition, using the replacement described by expression (6.9), $\underline{\mathcal{T}}_n$ may be written as

$$\underline{\mathcal{T}}_n = (2M_n)^{-1}[P + f(Q)\underline{\sigma}_2]^2\underline{1} \tag{6.12}$$

so that the coupled eigenvalue equation in expression (6.7) takes the form

$$\begin{aligned}(T + V_o - V_a)\phi_{N\nu} \; - iV_p\phi_{M\nu} &= \varepsilon_\nu\phi_{N\nu}\\ (T + V_o + V_a)\phi_{M\nu} + iV_p\phi_{N\nu} &= \varepsilon_\nu\phi_{M\nu}\end{aligned} \tag{6.13}$$

where use is made of the following substitutions

$$\begin{aligned}T &= (2M_n)^{-1}[P^2 + f^2(Q)]\\ V_o &= \tfrac{1}{2}(E_M + E_N)\\ V_a &= \tfrac{1}{2}(E_M - E_N)\\ V_p &= f(Q)P/M_n\end{aligned} \tag{6.14}$$

That is, the coupled molecular Hamiltonian $\underline{\mathcal{H}}$ has the form

$$\underline{\mathcal{H}} = (T + V_o)\underline{1} + V_p\underline{\sigma}_2 - V_a\underline{\sigma}_3. \tag{6.15}$$

This stationary state approach as applied to the case of non-degenerate levels has resulted in the Hamiltonian in eqn (6.15) being coupled by the KI terms Vp. These terms, however, impart only a weak coupling as Vp is of the order of f(Q) in eqn (6.10) and this allows the subsequent decoupling

technique to be utilized.

6.1.2 *The Molecular Hamiltonian in Decoupled Form*

In general, the decoupling technique of Fulton and Gouterman[4] will be followed. It is convenient to transform $\underline{\mathcal{H}}$ by the unitary transformation

$$\underline{\mathcal{H}}_T = U_S^\dagger \underline{\mathcal{H}} U_S$$

where

$$U_S = 2^{-\frac{1}{2}}(\underline{\sigma}_1 + \underline{\sigma}_3). \tag{6.16}$$

In this way, the eigenvalue equation (6.7) becomes

$$\underline{\mathcal{H}}_T \underline{\phi}_\nu' = \varepsilon_\nu \underline{\phi}_\nu' \tag{6.17}$$

where the transformed nuclear wavefunctions $\underline{\phi}_\nu'$ are given by

$$\underline{\phi}_\nu' = U_S^\dagger \underline{\phi}_\nu = 2^{-\frac{1}{2}} \begin{pmatrix} \phi_{N\nu} + \phi_{M\nu} \\ \phi_{N\nu} - \phi_{M\nu} \end{pmatrix}. \tag{6.18}$$

The transformed Hamiltonian $\underline{\mathcal{H}}_T$ is then

$$\underline{\mathcal{H}}_T = (T + V_o)\underline{1} - V_p\underline{\sigma}_2 - V_a\underline{\sigma}_1. \tag{6.19}$$

As has been shown,[4] the assumption that ψ_N and ψ_M are of different symmetry guarantees, for most groups, that a molecular symmetry operator G exists. The properties of this operator, adding that it reflects the momentum coordinate[6] P, are summarized as follows:

$$[G, T]_- = [G, V_o]_- = [G, V_a]_- = [G, V_p]_+ = 0$$

$$G^2 = 1. \tag{6.20}$$

As a consequence, the commutation relation

$$[G\underline{\sigma}_1, \underline{\mathcal{H}}_T]_- = 0 \tag{6.21}$$

is obtained indicating that two possible solutions of the coupled eigenvalue equation (6.17) may be constructed. That is, the eigenstates of

$G\underline{\sigma_1}^4$ as expressed in vector form

$$\underline{\phi_\nu}^{\pm} = \begin{pmatrix} \phi_\nu^{\pm} \\ \pm G\phi_\nu^{\pm} \end{pmatrix} \tag{6.22}$$

are also eigenstates of $\underline{\mathcal{H}}_T$. Using either of these forms as possible solutions, the Hamiltonian $\underline{\mathcal{H}}_T$ in expression (6.19) is reduced to two one-dimensional Hamiltonaians $\mathcal{H}_+$ and $\mathcal{H}_-$ where

$$\underline{\mathcal{H}}_{\pm}\, \phi_\nu^{\pm} = [T + V_o \pm (-V_a + iV_p)G]\phi_\nu^{\pm} = \varepsilon_\nu^{\pm}\phi_\nu^{\pm}. \tag{6.23}$$

Choosing ϕ_ν^{+} and ϕ_ν^{-} to be normalized to unity, it follows from the eigenfunctions in eqn (6.18) that

$$\begin{pmatrix} \phi_{N\nu} \\ \phi_{M\nu} \end{pmatrix} = \tfrac{1}{2} \begin{pmatrix} \phi_\nu^{+} + G\phi_\nu^{+} \\ \phi_\nu^{+} - G\phi_\nu^{+} \end{pmatrix}$$

or

$$\begin{pmatrix} \phi_{N\nu} \\ \phi_{M\nu} \end{pmatrix} = \tfrac{1}{2} \begin{pmatrix} \phi_\nu^{-} - G\phi_\nu^{-} \\ \phi_\nu^{-} + G\phi_\nu^{-} \end{pmatrix}. \tag{6.24}$$

The Hamiltonians $\mathcal{H}_+$ in equation (6.23) are decoupled forms of the coupled Hamiltonian $\underline{\mathcal{H}}_T$. However, if the dimeric part of the problem is to be simply formulated, it will be necessary to express the decoupled eigenvalue equations in terms of the original set of eigenfunctions $\underline{\phi_\nu}$ in eqn (6.6). That is, separate ground and excited state forms of the decoupled Hamiltonians are required whereas the presence of the symmetry operator G in expression (6.23) makes such forms unclear. This stationary state approach has thus resulted in something of an impasse which, in the final analysis, lies in the form of the total wavefunctions Ψ_ν. However, an escape presents itself if it is recognized that the KI coupling between the electronic states of the molecular moiety is small when compared to the transition energy between these states. Thus, two limits may be imposed on

the stationary states Ψ_ν in eqn (6.5) to yield the separate zeroth order forms while still retaining the KI terms as perturbations in the decoupled Hamiltonians. As the states $\phi_{N\nu}$ and $\phi_{M\nu}$ are coefficients in the expansion of the Ψ_ν in eqn (6.5), these are the quantities to be dealt with.

LIMIT 1:

If

$$\phi_{M\nu} << \phi_{N\nu},$$

then

$$\Psi_\nu \rightarrow \psi_N \phi_{N\nu}.$$

That is, the molecule is in the unperturbed electronic ground state in vibrational state ν in this limit so that, using the wavefunctions in expression (6.24),

$$G\phi_\nu^+ \rightarrow \phi_\nu^+$$

or

$$G\phi_\nu^- \rightarrow -\phi_\nu^-.$$

This results in reducing the two one-dimensional Hamiltonians in eqn (6.23) to only one independent component

$$\mathcal{H}_N \phi_{N\nu} = (T + V_o - V_a + iV_p)\phi_{N\nu} = \varepsilon_{N\nu}\phi_{N\nu} \qquad (6.25)$$

because, from (6.24),

$$\phi_\nu^\pm \equiv \phi_{N\nu}$$

and

$$\varepsilon^\pm \equiv \varepsilon_{N\nu}$$

where $\varepsilon_{N\nu}$ is the overall energy for the electronic ground state in vibrational state ν.

LIMIT 2:

In this case, $\phi_{N\nu}$ is taken to be much smaller than $\phi_{M\nu}$ so that

the form of the total wavefunction approaches that for the unperturbed excited state in vibrational state ν. The one independent component which results from this is

$$\mathcal{H}_M \phi_{M\nu} = (T + V_o + V_a - iV_p)\phi_{M\nu} = \varepsilon_{M\nu}\phi_{M\nu} \tag{6.26}$$

where $\varepsilon_{M\nu}$ is the overall excited state energy.

Equations (6.25) and (6.26) yield the separate ground and excited state energies perturbed by the weak KI coupling which exists between them, while the zeroth order wavefunctions are taken to be valid in this approximation. Making the substitutions given in eqn (6.14) into equations (6.25) and (6.26), one obtains the following forms of the Hamiltonians $\mathcal{H}_M$ and $\mathcal{H}_N$.

$$\mathcal{H}_N = (2M_n)^{-1} [P^2 + 2if(Q)P + 2f^2(Q)] + E_N$$

$$\mathcal{H}_M = (2M_n)^{-1} [P^2 - 2if(Q)P + 2f^2(Q)] + E_M. \tag{6.27}$$

As the energy gap $E_M - E_N$ increases, $f(Q)$, given in expression (6.10), decreases so that these forms of $\mathcal{H}_N$ and $\mathcal{H}_M$ will approach the form of the unperturbed Hamiltonian derived in the crude adiabatic approximation.[10] It is important to note, then, that the KI coupling terms have been formulated solely by the proper inclusion of the nuclear position dependence in the electronic wavefunctions - a property intrinsic only to the adiabatic approximation. While the terms in $f(Q)$ would normally be considered negligible, it will be subsequently shown that such terms are indeed significant in the overall picture of exciton interactions in dimers.

Having decoupled the original Hamiltonian given in eqn (6.15), the resultant pair of Hamiltonians in eqns (6.25) and (6.26) retain the KI coupling terms only as perturbations. In the "tight-binding" formulation of the dimeric problem[3,4] the dimeric states are derived as product states

of the monomeric wavefunctions. Consequently, the KI coupling between monomeric states must lead to an *indirect* KI coupling between the relevant dimeric states. In having achieved the simplicity of eqns (6.25) and (6.26), this form of coupling will be lost in the treatment of the dimeric part of the problem. However, a systematic method is available for routinely coupling and decoupling the eigenvalue equation given in expression (6.13) as follows. A comparison of the coupled eigenvalue equation (6.13) with the decoupled forms in eqns (6.25) and (6.26) reveals a great similarity between them brought about by the use of the zeroth order wavefunctions in the case of the latter two. Thus, taking the coupled form eqn (6.13) and considering only the KI coupling terms in V_p, one replaces $\phi_{M\nu}$ by $-\phi_{N\nu}$ in the first of equations (6.13) and replaces $\phi_{N\nu}$ by $-\phi_{M\nu}$ in the second of these equations. The result is that this set of equations is effectively decoupled to yield the pair of equations (6.25) and (6.26). This straightforward replacement method provides a *schematic technique* for the coupling and decoupling of the KI terms as required. The validity of this technique lies, firstly, in the formal connexion between the coupled and decoupled forms described and, secondly, in the ultimate success of this method.

6.2 Treatment for the Dimer

The model dimer is assumed to be made up of two identical molecules the properties of which have been described in Section 6.1. It is further assumed that these moieties are in a fixed spatial arrangement so that the intermolecular potential is constant. It is well-known that the degenerate excited states of the dimer are coupled to one another via the intermolecular potential - the so-called exciton coupling or exciton inter-

action. As mentioned previously, the tight-binding model for such exciton interactions will be used.

As was discussed in the previous section, it is expected that the KI coupling between the monomeric states will lead to an indirect coupling between certain of the dimeric states. Such a KI coupling cannot exist as a *direct* consequence of a nuclear momentum interaction between degenerate dimeric states from both a physical and a formal stand-point. Physically, the tight-binding model ensures that the electronic states of one moiety of the dimer are unaffected by the nuclear momenta of the other. Thus, in physical terms, there is no vehicle for the direct KI coupling between dimeric states in the same way that the intermolecular potential acts as a vehicle for the exciton coupling. Formally, the relevant dimeric states are constructed from orthonormal monomeric states so that necessarily the off-diagonal KI terms vanish in the dimeric formulation - again a result of the tight-binding model. The following procedure will then be adopted. Firstly, the exciton coupling terms will be introduced by using the decoupled molecular Hamiltonians in eqns (6.25) and (6.26) to derive the usual coupled eigenvalue equations for the dimer. The KI terms arising from the moiety states will then be introduced as coupling terms between the relevant dimeric states by means of the schematic method discussed in Section 6.1.2. The overall dimeric eigenvalue problem may then be solved.

6.2.1 *Exciton Coupling Between Dimeric States*

The subsequent derivation follows well-established procedure[3,4] for the formulation of exciton interactions in dimers. Where necessary, symbols will be primed to indicate a dimer term corresponding to a similar molecular term. Each particular moiety of the dimer will be differentiated

by A or B as a subscript or superscript.

The dimeric Hamiltonian H' is written as the sum

$$H' = T_n'(P') + H_e^A(m_e^A, r^A, Q^A) + H_e^B(M_e^B, r^B, Q^B) + V^{AB}(r', Q') \quad (6.28)$$

where H_e^A and H_e^B are the molecular electronic Hamiltonians corresponding to the form given in eqn (6.3), V^{AB} is the intermolecular potential and T_n' is the dimeric nuclear kinetic energy. This kinetic energy may be expressed as the sum of various intra- and intermolecular terms[4] but, as the moieties are assumed fixed, T_n' reduces to the sum of the nuclear kinetic energies for each moiety, T_n^A and T_n^B. Thus, H' simplifies to

$$H' = H^A + H^B + V^{AB} \quad (6.29)$$

where

$$H^A = T_n^A(P^A) + H_e^A(M_e^A, r^A, Q^A). \quad (6.30)$$

H^A and H^B are directly identifiable with the molecular Hamiltonian in expression (6.1). The electronic and nuclear wavefunctions for the moieites A and B will be given by the forms presented in eqns (6.2) and (6.6), with the relevant moiety superscripts. The dimeric wavefunctions may be constructed as product states of these molecular wavefunctions[4] due to the separability of the dimeric Hamiltonian[11] as shown in eqn (6.29). This mathematical separability is a consequence of the tight-binding model for the physical situation. In this way, the following dimeric states may be defined:

$$\theta_o = \psi_N^A \psi_N^B; \quad \theta_1 = \psi_M^A \psi_N^B; \quad \theta_2 = \psi_N^A \psi_M^B, \quad (6.31)$$

for the dimeric electronic states and

$$\chi_{o\nu} = \phi_{N\nu}^A \phi_{N\nu}^B; \quad \chi_{1\nu} = \phi_{M\nu}^A \phi_{N\nu}^B; \quad \chi_{2\nu} = \phi_{N\nu}^A \phi_{M\nu}^B, \quad (6.32)$$

for the dimeric nuclear states. The degenerate excited states of the dimer are conveniently written in the vector forms

$$\underline{\theta} = \begin{pmatrix} \theta_1 \\ \theta_2 \end{pmatrix}; \quad \underline{\chi}_\nu = \begin{pmatrix} \chi_{1\nu} \\ \chi_{2\nu} \end{pmatrix} . \tag{6.33}$$

Similar eigenvalue equations to the molecular form in eqn (6.3) may be established for each moiety in terms of these dimeric wavefunctions; that is,

$$H_e{}^A \, \underline{\theta}^T = \underline{\theta}^T \, \underline{V}^A, \tag{6.34}$$

where, for moiety A,

$$\underline{V}^A = \begin{pmatrix} E_M{}^A & 0 \\ 0 & E_N{}^A \end{pmatrix} . \tag{6.35}$$

However, for moiety B,

$$\underline{V}^B = \begin{pmatrix} E_N{}^B & 0 \\ 0 & E_M{}^B \end{pmatrix} . \tag{6.36}$$

The solutions of the eigenvalue equation for H' in eqn (6.28) may be formulated as stationary states in terms of the degenerate electronic and corresponding nuclear states of the dimer,

$$\Psi_\nu' = \underline{\theta}^T \underline{\chi}_\nu \tag{6.37}$$

which is analogous to eqn (6.5). Following the procedure for deriving the corresponding molecular eigvenvalue equation, the eigenvalue equation for H' and Ψ_ν' is expanded into the coupled form

$$\underline{\mathcal{H}}' \underline{\chi}_\nu = \underline{\mathcal{H}}^A \underline{\chi}_\nu + \underline{\mathcal{H}}^B \underline{\chi}_\nu + \underline{\mathcal{V}}^{AB} \underline{\chi}_\nu = \varepsilon_\nu' \underline{\chi}_\nu \tag{6.38}$$

where

$$\underline{\mathcal{H}}^A = \langle \underline{\theta} | H^A | \underline{\theta}^T \rangle \; ; \; \underline{\mathcal{V}}^{AB} = \langle \underline{\theta} | V^{AB} | \underline{\theta}^T \rangle . \tag{6.39}$$

The elements of the two-dimensional matrix $\underline{\mathcal{V}}^{AB}$ are such that the following replacements are possible[4]:

$$\mathcal{V}_{11}^{AB} = \mathcal{V}_{22}^{AB} = W_{AB}$$

$$\mathcal{V}_{12}^{AB} + \mathcal{V}_{21}^{AB} = W_s . \tag{6.40}$$

Because of the orthonormality of the monomer wavefunctions, $\underline{\mathcal{H}}^A$ is a

diagonal matrix whose non-zero elements are

$$\mathcal{H}^{A}_{11} = \langle \psi_M^A | H^A | \psi_M^A \rangle$$

$$\mathcal{H}^{A}_{22} = \langle \psi_N^A | H^A | \psi_N^A \rangle .$$

Thus, $\mathcal{H}^{A}_{11}$ is analogous to $\mathcal{H}_M$ in eqn (6.26) and $\mathcal{H}^{A}_{22}$ is identified with $\mathcal{H}_N$ in eqn (6.25) while, in the case of $\underline{\mathcal{H}}^B$, $\mathcal{H}^{B}_{11}$ and $\mathcal{H}^{B}_{22}$ are analogous to $\mathcal{H}_N$ and $\mathcal{H}_M$, respectively. By substituting into expression (6.38) for $\underline{\mathcal{H}}^A$, $\underline{\mathcal{H}}^B$ and $\underline{V}^{AB}$ as described above, one obtains the coupled dimeric eigenvalue equation

$$\begin{aligned} (T' + E_{11} - i\, W_p)\chi_{1\nu} + W_s\, \chi_{2\nu} &= \varepsilon_\nu' \chi_{1\nu} \\ (T' + E_{22} + i\, W_p)\chi_{2\nu} + W_s\, \chi_{1\nu} &= \varepsilon_\nu' \chi_{2\nu} \end{aligned} \qquad (6.41)$$

where

$$\begin{aligned} T' &= T_n^A + T_n^B + (2M_n)^{-1}\, [f^2(Q^A) + f^2(Q^B)] \\ E_{11} &= E_M^A + E_N^B + W_{AB} \\ E_{22} &= E_N^A + E_M^B + W_{AB} \\ W_p &= V_p^A - V_p^B . \end{aligned} \qquad (6.42)$$

This form of the coupled dimeric eigenvalue equation clearly shows that the exciton coupling parameter[4] W_s produces the only apparent coupling between the states $\chi_{1\nu}$ and $\chi_{2\nu}$ while the KI terms are present in decoupled form.

6.2.2 *Kinetically Induced Coupling Between Dimeric States*

The KI terms V_p^A and V_p^B for the separate moiety states are present in the coupled equation (6.41) but in a decoupled form. The schematic method is applicable here because the nuclear wavefunctions for the dimer are product states whose components are the separate moiety wavefunctions as given in expression (6.32). In this way, the coupling between the moiety

states $\phi_{N\nu}$ and $\phi_{M\nu}$ produces an indirect coupling between the dimeric states $\chi_{1\nu}$ and $\chi_{2\nu}$.

Taking the appropriate KI coupling terms in eqn (6.41), namely,

(i) $(-i\,V_p^A + i\,V_p^A)\chi_{1\nu} = (-i\,V_p^A + i\,V_p^B)\ \phi_{M\nu}^A\,\phi_{N\nu}^B$

from the first equation, and

(ii) $(i\,V_p^A - i\,V_p^B)\chi_{2\nu} = (i\,V_p^A - i\,V_p^B)\ \phi_{N\nu}^A\,\phi_{M\nu}^B$

from the second, $\phi_{M\nu}^A$ is replaced by $-\phi_{N\nu}^A$ and $\phi_{N\nu}^B$ is replaced by $-\phi_{M\nu}^B$ in (i). Similarly, $\phi_{N\nu}^A$ is replaced by $-\phi_{M\nu}^A$ and $\phi_{M\nu}^B$ is replaced by $-\phi_{N\nu}^B$ in (ii). This results in $\chi_{1\nu}$ being effectively replaced by $\chi_{2\nu}$ in (i) while the opposite occurs in (ii). In this way, eqn (6.41) becomes

$$(T' + W_o + W_a)\chi_{1\nu} + (-i\,W_p + W_s)\chi_{2\nu} = \varepsilon_\nu'\chi_{1\nu}$$
$$(T' + W_o - W_a)\chi_{2\nu} + (i\,W_p + W_s)\chi_{1\nu} = \varepsilon_\nu'\chi_{2\nu} \qquad (6.43)$$

where

$$W_o = \tfrac{1}{2}(E_{11} + E_{22})$$
$$W_a = \tfrac{1}{2}(E_{11} - E_{22}). \qquad (6.44)$$

The coupled dimeric eigenvalue equation (6.43) now contains both the exciton and KI coupling terms in the required forms. The corresponding coupled Hamiltonian is given as

$$\underline{\mathcal{H}}' = (T' + W_o)\,\underline{1} + W_a\underline{\sigma}_3 + W_p\underline{\sigma}_2 + W_s\underline{\sigma}_1 \qquad (6.45)$$

6.2.3 *Solution of the Coupled Eigenvalue Equation for the Dimer*

The solution of the coupled eigenvalue equation for the dimer given by expression (6.43) is based on the technique of Fulton and Gouterman[4,5] previously used to decouple the molecular Hamiltonian in Section 6.1.2.

From eqn (6.10)

$$f(Q^A) = \hbar\,(E_M^A - E_N^A)\,\langle\psi_N^A|\partial H_e^A/\partial Q^A|\psi_M^A\rangle$$

for moiety A. In the so-called harmonic approximation, the molecular potentials E_M^A and E_N^A are expanded as Taylor series such that the term $\partial H_e^A/\partial Q^A$ is the first-order coefficient. To a first approximation,[6] the integral in the expression for $f(Q^A)$ is set equal to this first-order coefficient which is the displacement term in the classical displaced oscillator potential. This will be denoted 1. In addition, since the moieties are identical,

$$(E_M^A - E_N^A) = (E_M^B - E_N^B) = \Delta E,$$

neglecting the Q dependence of these quantities. Thus,

$$f(Q^A) \equiv f(Q^B) = \hbar 1/\Delta E. \tag{6.46}$$

The Hamiltonian $\underline{\mathcal{H}}'$ in eqn (6.45) is converted into a more convenient form by means of the unitary transformation

$$\underline{\mathcal{H}}_T' = U_D^\dagger \underline{\mathcal{H}}' U_D,$$

where

$$U_D = 2^{-\frac{1}{2}}(\underline{1} - i\underline{\sigma}_1). \tag{6.47}$$

The resultant transformed Hamiltonian is given as

$$\underline{\mathcal{H}}_T' = (T' + W_o)\underline{1} - W_p\underline{\sigma}_3 + W_a\underline{\sigma}_2 + W_s\underline{\sigma}_1 \tag{6.48}$$

and the transformed wavefunctions of this Hamiltonian are

$$\underline{\chi}_\nu' = U_D^\dagger \underline{\chi}_\nu. \tag{6.49}$$

In the case of dimers, it can be shown[4] that, if a symmetry operation exchanging moieties A and B exists, then a dimeric symmetry operator G' will also exist with the properties

$$[G', T']_- = [G', W_o]_- = [G', W_s]_- = [G', W_a]_+ = [G', W_p]_+ = 0,$$
$$(G')^2 = 1 \tag{6.50}$$

the last commutation relation arising from the fact that G' interchanges the molecular momenta P^A and P^B.[4] G' is analogous to but not the same in general as the molecular symmetry operator G in Section 6.1.2. It

follows from such properties above that

$$[G\underline{\sigma}_1, \underline{\mathcal{H}}_T']_- = 0,$$

with the result that the Hamiltonian in expression (6.48) may be reduced to two one-dimensional Hamiltonians $\mathcal{H}_+'$ and $\mathcal{H}_-'$ given as

$$\mathcal{H}_\pm' = T' + W_o - W_p \pm (W_s - iW_a)G', \tag{6.51}$$

with corresponding wavefunctions

$$\underline{\chi}_\nu^\pm = \begin{pmatrix} \chi_\nu^\pm \\ \pm G\chi_\nu^\pm \end{pmatrix}. \tag{6.52}$$

The harmonic approximation is applied to the potentials W_o and W_a; that is, quadratic forms are assumed for the molecular potentials E_N and E_M with the same force constant k being used in both the ground and excited states. In addition, the replacements in expressions (6.14), (6.42), (6.44) and (6.46) are used to express the Hamiltonians $\mathcal{H}_\pm'$ in terms of the separate moiety coordinates. In using the transformed normal coordinates[4,5]

$$P^\pm = 2^{-\frac{1}{2}}(P^A \pm P^B)$$

$$Q^\pm = 2^{-\frac{1}{2}}(Q^A \pm Q^B),$$

these latter Hamiltonians assume the forms

$$\mathcal{H}_\pm' = (2M_n)^{-1}\,[(P^+)^2 + (P^-)^2 + 2\hbar^2 l^2/(\Delta E)^2] +$$
$$\text{CONSTANT (1)} + 2^{-\frac{1}{2}} l\, Q^+ + 2^{-1} k\,(Q^+)^2 + 2^{-1} k\,(Q^-)^2 +$$
$$2^{\frac{1}{2}} \hbar l\, P^-/\,(\Delta E.M_n) \pm\{W_s - i[\text{CONSTANT(2)} + 2^{-\frac{1}{2}} l\, Q^-]\}G'. \tag{6.53}$$

CONSTANT(1) is a constant potential and is neglected[4] as it simply causes spectral shifts and not band shape changes. CONSTANT(2) is of the order of W_{AB} which is the intermolecular potential when both molecules are excited. Assuming that only one of the moieties of the dimer will be excited at one time, W_{AB} may be neglected. The Hamiltonians resulting from such exclusions are converted to reduced form by dividing through by $\hbar\,\omega$

where ω is the classical harmonic oscillator frequency of vibration. The following dimensionless quantities[4,5] are then substituted into these reduced Hamiltonians:

$$p^{\pm} = (\hbar\omega M_n)^{-\frac{1}{2}} P^{\pm}$$
$$q^{\pm} = (M_n\omega/\hbar)^{\frac{1}{2}} Q^{\pm}$$
$$\lambda = (2M_n\hbar\omega^3)^{-\frac{1}{2}} l$$
$$\varepsilon = (\hbar\omega)^{-1} W_s$$
$$d = (2\hbar\omega)^{-1}\Delta E$$
$$\kappa = \lambda/d, \qquad (6.54)$$

the last two quantities being specific to this derivation. The results of these substitutions is that the reduced Hamiltonians may be separated into two commuting forms denoted h' and $h^{\pm}$ where

$$h' = \tfrac{1}{2}(p^+)^2 + \tfrac{1}{2}(q^+)^2 + \kappa^2/2 + \lambda q^+$$
$$h^{\pm} = \tfrac{1}{2}(p^-)^2 + \tfrac{1}{2}(q^-)^2 - \kappa p^- \pm(\varepsilon - i\lambda q^-)G'. \qquad (6.55)$$

These equations illustrate explicitly two forms of electronic-nuclear interaction. The exciton interaction ε, having its basis in the electronic states of the dimer, is modified by the positions of the nuclei, represented by the terms in λ. This is the well-known vibronic interaction which has been formulated in a very similar way in the crude adiabatic analogues[5] of eqns (6.55). The second type of interaction, being exclusive to this adiabatic approach, is that between the momenta of the nuclei, represented by the term κp^-, and the exciton interaction. Therefore, a more concise nomeclature may refer to *exciton-nuclear position interaction* and *exciton-nuclear momentum interaction* in order to distinguish between these two effects while retaining the term vibronic interaction to describe all electronic-nuclear interactions in general. The terms ε, λ and κ may then be referred to as the exciton exchange, nuclear position and

nuclear momentum parameters, respectively. From its definition in eqns (6.54), it follows that κ will always be significantly less than λ for real dimers so that, in general, the exciton-nuclear position interaction will predominate. In keeping with the accepted classification,[12] the exciton-nuclear position and exciton-nuclear momentum interactions may be categorized as strong ($\lambda>>\varepsilon$; $\kappa>>\varepsilon$), intermediate ($\lambda\sim\varepsilon$, $\kappa\sim\varepsilon$) and weak ($\lambda<<\varepsilon$; $\kappa<<\varepsilon$).

If $\chi_\nu^{\pm}$ are the wavefunctions of the reduced Hamiltonians giving rise to the commuting forms in eqn (6.55), then this separability of the Hamiltonians quarantees that these wavefunctions may be constructed as product states of the wavefunctions for h' and $h^{\pm}$. The sets of co-ordinate p^+, q^+ and p^-, q^- are associated with symmetric and asymmetric (or in-phase and out-of-phase) modes of vibration,[5,13] respectively. That is, one may refer to separate vibrational states for each of these plus and minus polarizations but, within each polarization, both moieties of the dimer must be in the same vibrational state as required by the form of the nuclear states in eqns (6.32). Thus, the states $\chi_\nu^{\pm}$ are replaced by the states $\chi_{nm}^{\pm}$ for vibrational state n in the plus polarization and m in the minus polarization. That is,

$$\chi_{nm}^{\pm}(q^+,q^-) = \chi_n'(q^+)\chi_m^{\pm}(q^-) \tag{6.56}$$

where

$$h'\chi_n' = \varepsilon_n'\chi_n'$$
$$h^{\pm}\chi_m^{\pm} = \varepsilon_m^{\pm}\chi_m^{\pm}. \tag{6.57}$$

The wavefunctions χ_n' and $\chi_m^{\pm}$ may be expanded in terms of the ground state monomer wavefunctions,[5] denoted ϕ_ρ and ϕ_σ, where ρ and σ are the vibrational levels considered. That is,

$$\chi_n' = \sum_\rho b_{n,\rho}\phi_\rho$$

$$\chi_m^\pm = \sum_\sigma c_{m,\sigma}^\pm \phi_\sigma \qquad (6.58)$$

where $b_{n,\rho}$ and $c_{m,\sigma}^\pm$ are the coefficients of expansion. While the coefficients $b_{n,\rho}$ are the overlap integrals given in Appendix IV of reference (4), a possibly better alternative source of these quantities are the solutions to the matrix equation

$$[\rho + \tfrac{1}{2} + \tfrac{1}{2}\kappa^2]b_{n,\rho} + (\rho/2)^{\frac{1}{2}}\lambda b_{n,\rho-1} + [(\rho+1)/2]^{\frac{1}{2}} b_{n,\rho+1} = \varepsilon_n' b_{n,\rho}. \qquad (6.59)$$

This matrix equation is obtained by using Merrifield's[14] variational method with the first of equations (6.55). A similar variational calculation for complex coefficients[15] based on Merrifield's method yields the matrix equation

$$[\sigma + \tfrac{1}{2} \pm (-1)^\sigma\varepsilon]c_{m,\sigma}^\pm + i(\sigma/2)^{\frac{1}{2}}[\kappa\pm(-1)^\sigma(-\lambda)]\, c_{m,\sigma-1}^\pm$$
$$-i[(\sigma+1)/2]^{\frac{1}{2}}[\kappa\pm(-1)^\sigma\lambda]\, c_{m,\sigma+1}^\pm = \varepsilon_m^\pm c_{m,\sigma}^\pm , \qquad (6.60)$$

from the second of equations (6.55). Both matrix equations (6.59) and (6.60) involve infinite, tridiagonal, hermitian matrices whose eigenfunctions are the coefficients $b_{n,\rho}$ and $c_{m,\sigma}^\pm$, respectively, and whose eigenvalues are the energies ε_n' and $\varepsilon_m^\pm$, respectively. These matrix equations may be solved numerically by standard techniques if truncated to a suitable size. Finally, the required energies of the absorption bands for transitions between the pure ground state Ψ_{00} and the excited states $\Psi_{nm}^\pm$ are given in units of ε by

$$\varepsilon_n' + \varepsilon_m^\pm - 1. \qquad (6.61)$$

6.3 The Transition Moments for Absorption

The dimeric transition moment is usually written as the sum of the molecular transitions moments of each monomeric moiety in terms of the dimeric states.[4] In this case, however, the dimeric states are coupled

directly by the exciton interaction and indirectly by the KI effect. This latter effect is localized in the molecular states and results in coupled molecular transition moments which may be decoupled using the states in eqn (6.22). The former interaction gives rise to the usual forms of dimeric transition moments which may be decoupled using the states in expression (6.52). By analogy to the derivation of the dimer Hamiltonians from the suitably decoupled molecular forms, the dimeric transition moments will be constructed from the decoupled molecular moments.

6.3.1 *The Molecular Transition Moments*

The derivation of the transition moment expression in this case presents the difficulty that the transition occurs between two electronic states which are coupled to one another. The usual type of problem[4-6] deals with the transition between an unperturbed ground state and a manifold of coupled excited states. Such an analysis, however, is possible even in this situation by virtue of the fact that the limits used to derive the form of the schematic coupling technique described in Section 6.1.2 reduce the coupled wavefunctions to their zeroth order forms. As can be seen from the form of the coupled molecular Hamiltonian in eqn (6.7), the complete set of nuclear wavefunctions associated with the electronic ground state are coupled with the set of nuclear wavefunctions for the excited state. The transition of interest is that between the overall vibrationally-unexcited ground state Ψ_0 and a vibronic level in the excited state Ψ_ν, this latter wavefunction being the stationary state in expression (6.5). The zeroth order form of Ψ_0, however, is given by

$$\Psi_0 = \psi_N \phi_{N0} \tag{6.62}$$

the components of which are also components of the coupled states Ψ_ν.

Thus, the transition in absorption incorporating the KI effect between the ground and excited electronic states, occurs within a manifold of coupled vibrational states.

The molecular transition moment $\underline{R}^{mol}$ for a transition $\Psi_\nu \leftarrow \Psi_0$ is given by

$$\underline{R}^{mol} = \langle \Psi_\nu | \underline{M} | \Psi_0 \rangle \tag{6.63}$$

where $\underline{M}$ is the electric dipole moment, Ψ_0 and Ψ_ν are defined by equations (6.62) and (6.5), respectively, and integration is over the coordinates r and Q. $\underline{R}^{mol}$ is further reduced by use of the quantity[6]

$$\underline{\mathcal{D}}_s(Q) = \langle \underline{\psi} | \underline{M} | \psi_N \rangle. \tag{6.64}$$

That is, integrating over the coordinate Q,

$$\underline{R}^{mol} = \langle \underline{\phi}_\nu | \underline{\mathcal{D}}_s(Q) | \phi_{N0} \rangle \tag{6.65}$$

where the $\underline{\phi}_\nu$ are defined in eqn (6.6). Within the framework of the adiabatic approximation, Fulton[6] has shown that

$$\partial \underline{\mathcal{D}}_s / \partial Q \simeq -i\hbar\Lambda \underline{\mathcal{D}}_s, \tag{6.66}$$

so that, transforming to the reduced coordinate q (analogous to $q^{\pm}$ in eqns (6.54) for the dimer) and substituting expressions (6.10), (6.46) and (6.54), it follows that

$$\partial \underline{\mathcal{D}}_s(q) / \partial q \simeq i2^{-\frac{1}{2}} \kappa \underline{\sigma}_2 \underline{\mathcal{D}}_s(q). \tag{6.67}$$

The form of eqn (6.67) implies that

$$\underline{\mathcal{D}}_s(q) \simeq \exp(-i\kappa' q \underline{\sigma}_2) \underline{\mathcal{D}}^0_{mol} \tag{6.68}$$

where

$$\kappa' = \kappa / 2^{\frac{1}{2}} \tag{6.69}$$

and $\underline{\mathcal{D}}^0_{mol}$ is the constant vector

$$\underline{\mathcal{D}}^0_{mol} = \begin{pmatrix} \underline{\mathcal{D}}^0_N \\ \underline{\mathcal{D}}^0_M \end{pmatrix}. \tag{6.70}$$

Expression (6.68) for $\underline{\mathcal{D}}_s(q)$ could now be substituted into eqn (6.63) to obtain the required molecular transition moment. However, the set of wavefunctions $\underline{\phi}_\nu$ have been replaced by the set $\underline{\phi}_\nu'$ by the unitary transformation described in eqns (6.16) and (6.18). Under this transformation, $\underline{\mathcal{D}}_s(q)$ in eqn (6.68) is found to take the form

$$\underline{\mathcal{D}}_s(q) \simeq \exp\ (i\kappa' q\underline{\sigma}_2)\,\underline{\mathcal{D}}^0_{mol} \qquad (6.71)$$

so that, making use of eqn (6.18) for the $\underline{\phi}_\nu'$, the following coupled transition moments are derived:

$$\underline{R}^{mol} = \tfrac{1}{2}\langle\underline{\phi}_\nu'|\exp\ (i\kappa' q\underline{\sigma}_2)U_s^\dagger|\phi_{N0}\rangle, \qquad (6.72)$$

integration now being over the reduced coordinate q.

These transition moments may be decoupled by a well-established procedure,[4-6] via the wavefunctions in eqn (6.22), to yield separate transition moments, denoted $\underline{R}_+^{mol}$ and $\underline{R}_-^{mol}$, for transitions from the pure monomeric ground state Ψ_0 to the decoupled plus and minus polarizations of the molecule (eqns (6.22) to (6.24)). $\underline{R}_\pm^{mol}$ are given by

$$\underline{R}_\pm^{mol} = \tfrac{1}{2}\langle(\phi_\nu^\pm \quad \pm G\phi_\nu^\pm)|\exp\ (i\kappa' q\underline{\sigma}_2)\,|\,(\underline{\sigma}_1+\underline{\sigma}_3)\phi_{N0}\rangle\underline{\mathcal{D}}^0_{mol} \qquad (6.73)$$

integrating over q. If the limiting conditions that were used in arriving from eqn (6.23) to the pair of equations (6.25) and (6.26) are applied to the transition moments in eqn (6.73), then these adopt the following forms:

$$\underline{R}_\pm^{mol} = \tfrac{1}{2}\langle(\phi_\nu^\pm \qquad \phi_\nu^\pm)|\ \exp\ (i\kappa' q\underline{\sigma}_2)\,|\,(\underline{\sigma}_1+\underline{\sigma}_3)\ \phi_{N0}\rangle\underline{\mathcal{D}}^0_{mol}$$

from limit 1 in Section 6.1.2 and

$$\underline{R}_\pm^{mol} = \tfrac{1}{2}\langle(\phi_\nu^\pm \qquad -\phi_\nu^\pm)|\exp\ (i\kappa' q\underline{\sigma}_2)\,|\,(\underline{\sigma}_1+\underline{\sigma}_3)\phi_{N0}\rangle\underline{\mathcal{D}}^0_{mol}$$

from limit 2. Applying these constraints to the wavefunctions in eqn (6.24) and substituting for $\underline{\sigma}_1$, $\underline{\sigma}_3$ and $\underline{\mathcal{D}}^0_{mol}$, it follows that the four transition moments above reduce to two independent solutions

$$\underline{R}_{NN}^{mol} = \langle \phi_{N\nu} | \exp(i\kappa' q\underline{\sigma}_2) | \phi_{N0} \rangle \underline{\mathcal{D}}_N^0 \qquad (6.74)$$

and

$$\underline{R}_{MN}^{mol} = \langle \phi_{M\nu} | \exp(i\kappa' q\underline{\sigma}_2) | \phi_{N0} \rangle \underline{\mathcal{D}}_M^0, \qquad (6.75)$$

these integrals being over q. These final forms of the decoupled transition moments are an interesting illustration of the significance of the limits discussed in Section 6.1.2. While the initial transition moments $\underline{R}^{mol}$ in eqn (6.63) describe transitions between the pure ground state and a series of excited vibronic states coupled to it, the forms in eqns (6.74) and (6.75) describe essentially the same transitions except that the two excited states involved have been effectively decoupled from one another. However, the terms arising from the KI effect have been retained also in a decoupled form. Thus, eqn (6.74) describes a transition between the vibrationally-unexcited ground state to a higher vibrational level in the same electronic state and is subsequently denoted $\underline{R}_{NN}^{mol}$. On the other hand, eqn (6.75) describes the transition from the same ground state to a vibronic level in the excited electronic state and is thus denoted $\underline{R}_{NM}^{mol}$. The influence of the KI effect is retained in the exponential factor in both those cases which brings to notice an important point.

The term κ' is related to the function f(Q) via eqns (6.54), (6.46) and (6.10) and as such is strictly a function of nuclear displacement. Thus, κ' should vary for each different vibrational state ν in each of the two electronic state N and M in eqns (6.74) and (6.75). If this were taken into account, eqn (6.74) would describe the effect of KI coupling between different vibrational levels in the same electronic state[8] where the κ' terms could be quite large. In the case of $\underline{R}_{MN}^{mol}$, however, the κ' terms are much smaller, as the coupling is between more widely separated states, so that the use of the approximation in eqn (6.46) is expected to be more accurate in this case. However, discrepancies in predicted

intensities may occur for the higher vibronic levels in the excited state where nuclear displacements and energy differences have increased, while the theory has accounted for only first order terms of this kind.

As the dimeric transition moments are to be constructed from the molecular transition moments in eqn (6.75), these latter forms will need to be expressed in terms of the dimeric states in eqn (6.32). This is achieved in a straightforward manner because these dimeric states are product states of the separate molecular moieties of the dimer. Thus, if the molecule A is to be excited, eqn (6.75) is multiplied by the left and right forms of the eigenstates $\phi^{A}_{M\nu}$. Similarly, multiplication by the eigenstates $\phi^{B}_{M\nu}$ describe the excitation of molecule B. The result of these operations are two transition moments

$$\underline{R}^{A}_{MN} = \langle \chi_{1\nu} | \exp(i\kappa' q^{A} \underline{\sigma}_2) | \chi_{00} \rangle (\underline{\mathcal{D}}^{A}_{M})^{0}$$

$$\underline{R}^{B}_{MN} = \langle \chi_{2\nu} | \exp(i\kappa' q^{B} \underline{\sigma}_2) | \chi_{00} \rangle (\underline{\mathcal{D}}^{B}_{M})^{0} \qquad (6.76)$$

where χ_{00}, $\chi_{1\nu}$ and $\chi_{2\nu}$ are the dimeric nuclear states in eqn (6.32) and $(\underline{\mathcal{D}}^{A}_{M})^{0}$ and $(\underline{\mathcal{D}}^{B}_{M})^{0}$ are specific molecular forms of the constant vector $\underline{\mathcal{D}}^{0}_{M}$ in eqn (6.70).

6.3.2 *The Dimeric Transition Moments*

For a vibrational state ν in *both* moieties, the dimeric transition $\underline{R}$ may be written as the sum of the molecular moments $\underline{R}^{A}_{MN}$ and $\underline{R}^{B}_{MN}$ from expression (6.76). If it is postulated that a coordinate q' exists which acts as q^{A} for moiety A and as q^{B} for moiety B then this sum may condense into the matrix form

$$\underline{R} = \langle \underline{\chi}_{\nu} | \exp(i\kappa' q' \underline{\sigma}_2) | \chi_{00} \rangle \underline{\mathcal{D}}^{0} \qquad (6.77)$$

where integration is over this reduced coordinate q' and where $\underline{\mathcal{D}}^{0}$ is the

$$\underline{\mathcal{D}}^{0} = \begin{bmatrix} (\underline{\mathcal{D}}_{M}^{A})^{0} \\ (\underline{\mathcal{D}}_{M}^{B})^{0} \end{bmatrix} . \qquad (6.78)$$

It is evident that the form of $\underline{\mathcal{D}}_{s}(q')$ in eqn (6.77) is identical to $\underline{\mathcal{D}}_{s}(q)$ in reference (6) and that the unitary transformations used in both cases are identical. Thus, Fulton's resultant forms of the decoupled transition moments for the separate plus and minus polarizations will apply in this case. These dimeric transition moments are then

$$\underline{R}^{\pm} = \tfrac{1}{2}\underline{\mathcal{D}}_{+}^{0} \langle \chi_{\nu}^{\pm} | e^{-i\kappa' q'} | \chi_{00} \rangle \pm \tfrac{1}{2}\underline{\mathcal{D}}_{-}^{0} \langle \chi_{\nu}^{\pm} | G' e^{i\kappa' q'} | \chi_{00} \rangle \qquad (6.79)$$

where

$$\underline{\mathcal{D}}_{\pm}^{0} = (\underline{\mathcal{D}}_{M}^{A})^{0} \pm i(\underline{\mathcal{D}}_{M}^{B})^{0} \qquad (6.80)$$

and integration is over q'.

The form of the decoupled wavefunctions for different vibrational states in each of the two polarizations is obtained on the basis of the wavefunctions in eqn (6.56). Thus, the wavefunctions $\chi_{\nu}^{\pm}$ in eqn (6.79) are replaced by the forms $\chi_{nm}^{\pm}$ and, ultimately, by the state χ_{n}' and $\chi_{m}^{\pm}$ from eqn (6.56) and this results in the following dimeric transition moments:

$$\underline{R}_{nm}^{\pm} = \tfrac{1}{2}\underline{\mathcal{D}}_{+}^{0} \langle \chi_{m}^{\pm} | e^{-i\kappa' q'} | 0,0 \rangle \langle \chi_{n}' | e^{-i\kappa' q'} | 0,0 \rangle$$
$$\pm \tfrac{1}{2}\underline{\mathcal{D}}_{-}^{0} \langle \chi_{m}^{\pm} | G' e^{i\kappa' q'} | 0,0 \rangle \langle \chi_{n}' | G' e^{i\kappa' q'} | 0,0 \rangle . \qquad (6.81)$$

Here $|0,0\rangle$ corresponds to the pure, undisplaced nuclear ground state while the $|\sigma,\kappa'\rangle$ are the momentum displaced harmonic oscillator states in vibrational levels σ. Since[6]

$$e^{-i\kappa' q'} |n,o\rangle = |n,\kappa'\rangle ,$$

further expansion of the transition moment expression (6.81) may be achieved by the technique described in Appendix IV of reference (4). That is,

$$\langle\chi_m^{\pm}|e^{-i\kappa' q'}|0,0\rangle = \langle\chi_m^{\pm}|Ge^{i\kappa' q'}|0,0\rangle = \sum_\sigma (c_m^{\pm})^*\langle\sigma,-\kappa'|0,0\rangle$$
$$\langle\chi_n'|e^{-i\kappa' q'}|0,0\rangle = \langle\chi_n'|Ge^{i\kappa' q'}|0,0\rangle = \sum_\sigma b_{n,\rho}\langle\rho, -\kappa'|0,0\rangle \qquad (6.82)$$

using the expansions of χ_n' and $\chi_m^{\pm}$ given in eqns (6.58). Substituting expressions (6.82) into eqn (6.81), the dimeric transition moments reduce into the forms

$$\underline{R}_{mn}^{\pm} = \tfrac{1}{2}\sum_\sigma (c_{m,\sigma}^{\pm})^*\langle\sigma, -\kappa'|0,0\rangle\sum_\rho b_{\mu,\rho}\langle\rho, -\kappa'|0,0\rangle(\underline{\mathcal{D}}_+^0 \pm \underline{\mathcal{D}}_-^0) \qquad (6.83)$$

where the vectors $\underline{\mathcal{D}}_+^0$ and $\underline{\mathcal{D}}_-^0$ enclose an angle α in the complex plane. That is,

$$|\underline{\mathcal{D}}_+^0 \pm \underline{\mathcal{D}}^0| = \text{CONSTANT}\ (1 \pm \cos\alpha) \qquad (6.84)$$

where α determines the plus or minus character of the spectrum and is consequently viewed as the angle between the monomeric moieties of the dimer. The intensity $I_{nm}^{\pm}$ of the transitions between the vibrationally unexcited ground state Ψ_0 and the excited states $\Psi_{nm}^{\pm}$ are given by

$$I_{nm}^{\pm} = |R_{nm}^{\pm}|^2$$
$$= \text{CONSTANT}\ |\sum_\rho b_{n,\rho}\langle\rho, -\kappa'|0,0\rangle|^2 |\sum_\sigma (c_{m,\sigma}^{\pm})^*\langle\sigma, -\kappa'|0,0\rangle|^2$$
$$\text{X}\ (1 \pm \cos\alpha) \qquad (6.85)$$

using eqns (6.83) and (6.84). The general integrals in this expression are given by[4,6,16]

$$\langle\beta, -\kappa'|0,0\rangle = (-1)^\beta \exp(-\kappa'^2/4)\ (i\kappa'/2^{\frac{1}{2}})\ (\beta!)^{-\frac{1}{2}}. \qquad (6.86)$$

6.4 Summary

The computation of the dimeric absorption spectra for the transition from state Ψ_0 to the states $\Psi_{nm}^{\pm}$ is summarized as follows. Suitably truncated versions of the matrix equations (6.59) and (6.60) may be solved numerically to yield the coefficients $b_{n,\rho}$ and $c_{m,\sigma}^{\pm}$ and the

eigenvalues ϵ_n' and $\epsilon_m^{\pm}$. Consequently, the transition energies and intensities are calculated via eqns (6.61) and (6.85), respectively. Of the required parameters ε, λ, κ and α, λ and κ may be obtained from the properties of the monomeric moieties of the dimer, while ε and α may be obtained by a fitting procedure to be described. Ideally, however, even the parameters ε and λ could be determined from direct experimental or alternative theoretical analyses of the dimer.

7. EXPERIMENTAL STUDY OF THE DIMERIC SPECTRUM

Only two experimental systems appear to be available for the study of exciton interactions in non-chemically bonded dimers — dimers formed in glassy matrices at low temperatures[17,18] and dimers formed by aggregation in solution.[19] While interpretations of the spectra of associated dimers in solution in terms of exciton interactions were proposed only relatively recently,[20,21] work in this area has been both rapid and plentiful. The predominant interest has been in the phenomenon of vibronic coupling or, in terms of the terminology suggested in Section 6.2.3, the exciton-nuclear position interaction. The study of dimers in glassy matrices at low temperatures has been well-suited to this particular problem because of the experimental determination of reasonably well-resolved vibrational structure in these cases. On the other hand, the interpretation of the associated dimer spectra of dyes in solution involve two main difficulties. Firstly, because both monomeric and dimeric species coexist in solution, the separate spectra must be resolved from the total spectrum observed as a function of total dye concentration. Secondly, these derived spectra do not display well-resolved vibrational structure in absorption. However, the successful treatment of these two problems lays the foundations for proper theoretical and experimental analyses of more complex systems of biological interest which are entirely analogous to these simpler dimeric systems.

These difficulties with the spectra of dimers in solution have been resolved to a major degree by the use of statistically-based deconvolution techniques[24] to obtain separate monomer and dimer spectra and by the fitting of single vibrational progressions to monomeric spectra to obtain the

necessary vibrational parameters.[25] This latter aspect of the analysis, while having a reasonable theoretical basis,[26] is particularly applicable to present theories of exciton interactions in dimers because these are based on single progressions in the monomeric moieties. The fitting of a single vibrational progression has been successfully extended[27] to determine the parameter λ in the theory of Fulton and Gouterman[5] by use of the assumptions that each vibronic band is described satisfactorily by a Gaussian curve[28] and that the squares of the overlap integrals for the vibronic states in the ground and excited levels are described by a Poisson distribution.[29] A similar analysis of the monomeric spectrum is applicable to the theory presented in this work, giving access to the nuclear position parameter λ and the nuclear momentum parameter κ.

While various statistical methods of analysis for multicomponent systems have been developed, the weighted non-linear least squares method described in reference (27) has proven to be very successful for the deconvolution of the spectroscopic data into its various components. An additional statistical aid in this respect is that of factor analysis[30] by means of which the minimum number of independent components in a system may be determined from the relationship between these and the rank of the matrix of measured data. However, no efforts appear to have been made to increase the experimental accuracy of the *primary* data, this being the variation of the overall absorption spectrum of the dye with concentration in this particular case. Whatever the method of analysis, the ultimate accuracy of the derived component spectra must depend on the accuracy of the primary data. To this end an experimental planning technique, referred to as prediction analysis,[31] was undertaken in this work in an effort to quantify and optimize the relevant experimental conditions.

Systems characteristic of strong exciton-nuclear position interactions have been studied[32-34] with particular reference to the theory of Fulton and Gouterman[5] in the interpretation of the observed dimer spectra. However, spectral changes on dimerization for such systems are relatively small and deviations from this theory due to the weaker exciton-nuclear momentum interactions described in this work are less likely to be observed. More obvious discrepancies between experimental and theoretical spectra have been found in certain dimeric dye systems[27] where exciton-nuclear position interactions are much weaker and spectral changes on dimerization are consequently more pronounced. Thus, the spectra of more strongly interacting dye systems are more suitable for a proper quantitative study of the effects predicted by the adiabatic theory presented here. However, apart from the optimization of the experimental conditions to obtain accurate spectra, one must be guarded in accepting all spectral changes as being due to aggregation. Other effects, such as dissociative equilibria[35] of the monomer, also may need to be accounted for, while it must be established that any impurities present do not result in erroneous computed dimer spectra. Finally, it should be mentioned that while alternative interpretations have been presented[36] and have failed, the aggregation view of the spectra of dyes has been strongly supported not only by a large group of spectroscopic studies but also by vapour pressure osmometry,[37] partition equilbria,[38] micro-calorimetric measurements of heats of dilution[39] and nuclear magnetic resonance.[40]

The xanthene dye Pyronine Y(G) was chosen for the following experimental study in view of four necessary requirements. Firstly, a dimer species spectrum was required and previous solution studies of this dye[41,42] indicate a monomer-dimer equilibrium. Secondly, as also indicated

by these solution experiments for Pyronine Y, it would be preferred that the monomer-dimer equilibrium is sufficiently extensive to ensure accurate dimer spectra. Thirdly, the dimer exciton theories discussed in this work assume a single electronic transition. This dye has an intense band in the visible part of the spectrum which has been attributed to a single electronic transition by fluorescence polarization and linear dichroism measurements.[43] Finally, studies on similar dyes[27,44] have shown that exciton interactions are generally large in such systems so that spectral changes on dimerization are usually quite marked. Specific details of dye purification, sample preparation and apparatus used for the study of Pyronine Y have been presented in Chapter II. The monomeric and dimeric spectra of two further xanthene dyes, Rhodamine B and Pyronine B, were available from other sources[27,45] as additional tests for the theories discussed in this work.

7.1 The Application of Prediction Analysis

The essential postulates and formalism of prediction analysis are summarized in Appendix A together with a discussion of the application of this technique to a model monomer-dimer system in equilibrium. The purpose of prediction analysis is to make some estimate of the precision of the unknown parameters to be measured by a particular experiment with a view to optimizing the experimental conditions. As a consequence, some estimate of the values of these parameters is required from the outset and thus excludes the application of prediction analysis to an entirely "pioneering" experiment. In applying this experimental planning technique to the solution measurements of Pyronine Y, it initially can be assumed that a monomer-dimer equilibrium is involved,[41,42] Under these circum-

stances, the absorbance of the solution at wavelength λ is given by[44]

$$A_i^{\lambda} = (\varepsilon_1^{\lambda} C_1 + 2K\bar{\varepsilon}_2^{\lambda} C_1^2) b_i$$

where

$$C_1 = [(1 + 8KC_i)^{\frac{1}{2}} - 1]/4K. \qquad (7.1)$$

b_i is the cell path length, C_i is the stoichiometric dye concentration, K is the association constant, ε_1^{λ} is the molar absorptivity of the monomer at wavelength λ and $\bar{\varepsilon}_2^{\lambda}$ is the corresponding quantity for the dimer expressed in terms of each monomer unit. The quantities A_i^{λ}, b_i and C_i are experimentally accessible while K, ε_1^{λ} and $\bar{\varepsilon}_2^{\lambda}$ are the three sets of unknown parameters to be determined. Such a determination may be achieved by a non-linear least squares fit of equation (7.1) to a series of absorbances as a function of concentration for each wavelength in the spectrum of interest. It is found, from the covariance matrix for such analyses, that at each wavelength the quantities K, ε_1^{λ} and $\bar{\varepsilon}_2^{\lambda}$ are statistically correlated. This is illustrated by the application of prediction analysis to a model monomer-dimer system as given in Appendix A. It is seen that the error of determination in each of these quantities is very dependent on the values of the other parameters. As is expected intuitively, the association constant is most accurately determined at those points in the spectrum where ε_1^{λ} and $\bar{\varepsilon}_2^{\lambda}$ are well separated. Prediction analysis then quantifies the usual procedure of determining the association constant at the maximum molar absorptivity of the monomer where, at least for strongly exciton coupled dye dimers, ε_1^{λ} and $\bar{\varepsilon}_2^{\lambda}$ are usually well separated. This value may then be used to calculate the overall monomer and dimer spectra from equation (7.1) by fitting only the two parameters ε_1^{λ} and $\bar{\varepsilon}_2^{\lambda}$.

7.1.1 *Optimization of Experimental Conditions*

It is apparent that, within the context of this experiment, prediction analysis will be used with the aim of reducing the error of determination of the association constant. As the unknown parameters are correlated, this more accurate value of K will result in more accurate monomer and dimer spectra. Prediction analysis will indicate the set of experimental conditions required to achieve this optimum degree of precision with the least expenditure of time, material and labour. In this case, the experimental conditions include the number of data points taken, the distribution of these data points, the accuracy of the spectrophotometer and cells and the precision with which the solutions are prepared. Of these conditions, only the former two may be considered to be sufficiently alterable to achieve a satisfactory reduction in the errors of determination of the unknown parameters. The number and distribution of data points were altered by dividing the concentration range under consideration into five equal regions so that the number of solutions within each region could be changed independently of the others. In this study three quantities, the standard deviations in K, ε_1^λ and $\bar{\varepsilon}_2^\lambda$, are to be minimized simultaneously. This may be achieved by minimizing either the determinant[46] or the sum of the diagonal elements[47] of the covariance matrix; the latter suggestion was employed in this work as it is the total of the standard deviations for all the unknown parameters.

A prediction analysis computer programme (PREDAN) was written using the basic scheme prescribed by Wolberg[48] and is reproduced in Appendix C. This basic scheme, however, simply computes estimates of the standard deviations in the unknown parameters from a static set of experimental variables. To adapt this procedure to the purposes of minimizing the

total standard deviation, a linear optimization procedure referred to as the "simplex" method[49] was introduced. The simplex method simply maximizes or minimizes the value of a particular function by a programmed alterations of the relevant variables. It is a sequential search method particularly suitable for large numbers of variable quantities. In this case, the total standard deviation or the total relative standard deviation is the quantity to be minimized while the number of data points within each of the five concentration regions are the variables. The simplex part of the programme then uses the prediction analysis procedure as a "black-box" function which generates values of the total relative standard deviation for different data point distributions.

As the prediction analytical procedure requires some estimates of the unknown parameters, a preliminary experiment was carried out to obtain such estimates. It was known[41,42] that the dimer species for Pyronine Y occurs, without observable perturbations from higher aggregates, for concentrations below about 1×10^{-3} mol dm^{-3}. A stock solution at this concentration was prepared volumetrically while the lowest concentration to be studied ($\sim 5 \times 10^{-6}$ mol dm^{-3}) and one of intermediate value ($\sim 5 \times 10^{-5}$ mol dm^{-3}) were prepared by weight. Assuming that the maximum absorptivity of the most dilute solution corresponded closely to the value for the monomer spectrum, estimates of K and $\bar{\varepsilon}_2^{\lambda}$ were used to reproduce the observed absorbance values at a series of wavelengths for the spectra measured. The resulting estimated values of the unknown parameters were taken to be

$$\varepsilon_1^0 = 81{,}000 \text{ dm}^3 \text{ mol}^{-1} \text{cm}^{-1}$$

$$\varepsilon_2^0 = 70 \text{ dm}^3 \text{ mol}^{-1} \text{cm}^{-1}$$

$$K = 1030 \text{ dm}^{-3} \text{mol}^{-1},$$

where the superscript zeros denote values taken at the monomer maximum.

Using this set of estimates, as well as the estimates for the standard deviations in the experimental variables given in Appendix A, the predicted total relative standard deviation in these parameters was computed by PREDAN for a series of *even* distributions of between 15 and 30 data points. The result of these computations is illustrated by the continuous line in figure 7.1 which shows that the total relative standard deviation has little tendency to level out with increasing number of data points. The absolute value of the total relative standard deviation has no real significance since predicted errors are based on estimated parameters as well as estimated standard deviations in the absorbances, path lengths and concentrations. However, it serves to illustrate the behaviour of the various errors as the experimental conditions are varied.

The effect of the *distribution* of points on the precision of the results was considered next by the following procedure. The simplex search method was started with a set of 11 points in the distribution (3,3, 3,3,3). The distributions are described by giving the number of solutions in successive regions, noting that data points corresponding to each of the four boundary concentrations demarking these regions are counted twice. The simplex procedure not only redistributed but also increased the number of data points, as would be expected. However, two basic trends emerged. Firstly, the number of points in the second and last concentration regions were increased while those in the other regions remained reasonably constant in number. Secondly, the reduction in the total relative error was generally more significant in a non-even distribution of an odd number of points compared to a similar distribution of an even number of points. As examples, in figure 7.1 the total relative errors corresponding to a 20 point distribution (4,7,3,4,6) and the 21 point distribution (4,8,3,4,6)

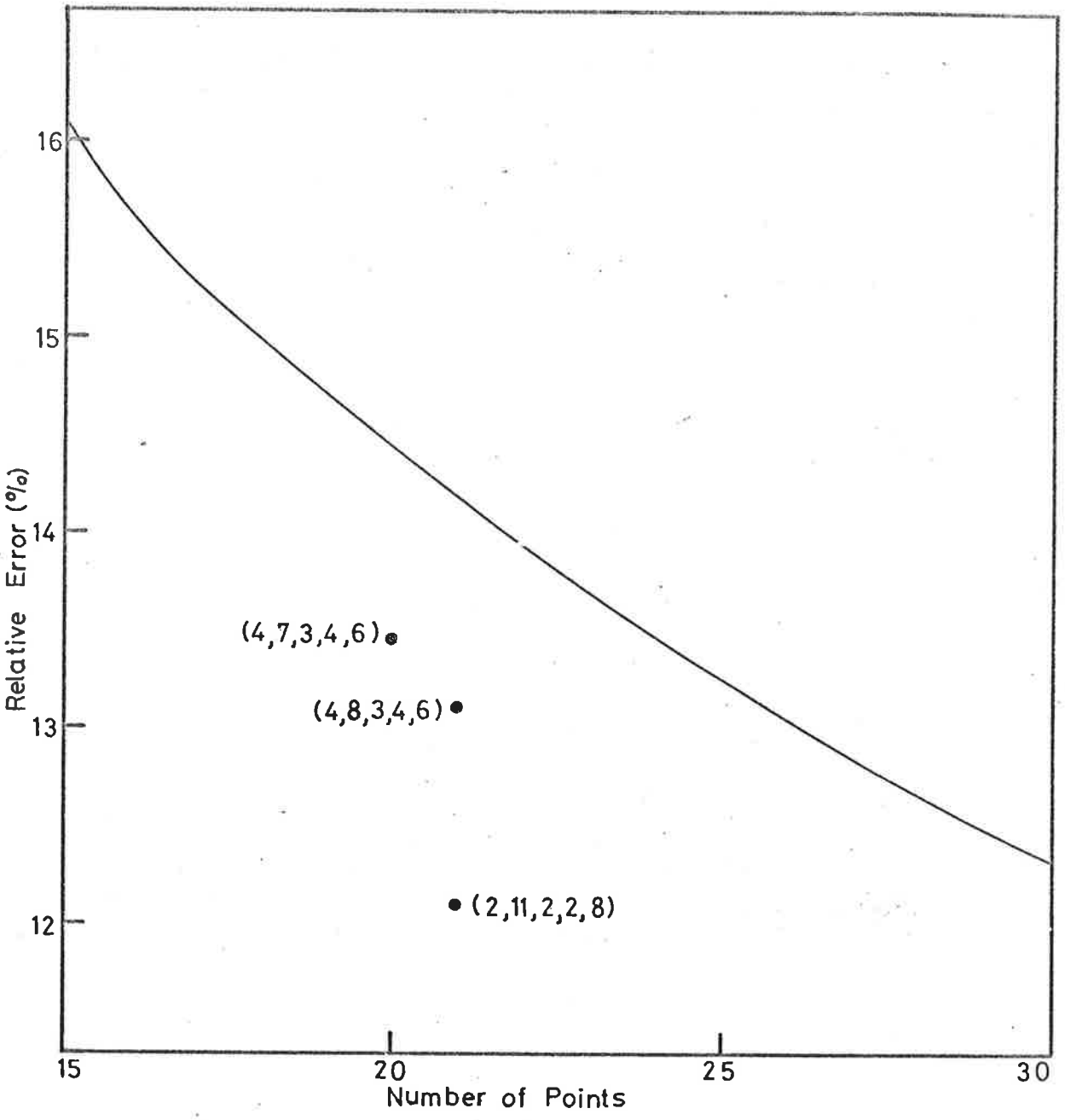

FIG. 7.1 PREDICTED TOTAL RELATIVE STANDARD DEVIATION AS FUNCTION OF NUMBER AND DISTRIBUTION OF DATA POINTS.
Curve refers to points distributed evenly along concentration axis. See text for description of non-even distributions.

are compared. As 30 data points were reasoned to be a maximum number to work with, redistributed sets of points with comparable total relative standard deviations were sought. Starting with distributions which followed the basic trend observed, it was possible to achieve this aim and it was finally determined that the distribution (2,11,2,2,8) for 21 points had a predicted total relative error of less than that for 30 evenly distributed points (see figure 7.1) and yet represented about a 30% reduction in work load. The prediction analytical procedure was subsequently used to calculate the concentrations and most probable path lengths to be used such that the peak absorbances would fall in the range 0.2 to 0.5 where absorbance errors are at a minimum. This was done for the 21 point *optimum* distribution and the 21 point *even* distribution such that a total of 30 *quasi-evenly* distributed points were measured in all. In this way, the predictions of this experimental planning technique could be corroborated experimentally.

7.1.2 *Determination of Species Spectra*

Thirty dye solutions of concentrations between 4.805×10^{-6} mol dm^{-3} and 1.0003×10^{-3} mol dm^{-3} were prepared in water as prescribed by the prediction analytical procedure in accordance with the distribution of points required. The absorbances of these solutions were measured at intervals of either 100 cm^{-1} or 200 cm^{-1} between 16,000 cm^{-1} and 22,000 cm^{-1} using the Ziess PMQII manual spectrophotometer and both conventional and short pathlength silica cells which had been suitably calibrated. Measured molar absorptivities, concentrations and path lengths are given in Appendix B. Blank cell readings were determined before and after each solution measurement and, typically, variations of no larger than about

0.002 absorbance units were found. Absorption of the dye onto the silica surfaces was consequently insignificant. The pH value measured at the lowest and highest concentrations were 4 and 3, respectively, so that amounts of protolytic reaction products of the Pyronine cation were negligible.[50] Figure 7.2 shows the behaviour of the spectrum of Pyronine Y in aqueous solution as a function of dye concentration. The two isosbestic points present remain well-defined indicating two important points. Firstly, this result supports the premise of a monomer-dimer equilibrium. Secondly, any impurities which may be present have not observably distorted the shape of the measured spectra which would lead to errors in the determined species spectra.

The dimerization equilibrium model was applied separately to the spectra belonging to the three distributions defined above using a weighted, non-linear least squares procedure[27] which utilizes a gradient search method[51] for rapid convergence. The standard deviations in the relevant experimental variables are summarized in Section 4.3. The values and relative standard deviations of the resulting paramters ε_1^0, $\bar{\varepsilon}_2^0$ and K, determined at the wavelength of maximum molar absorptivity, are presented in table 7.1, together with the respective total relative standard deviations. It is seen from the table that results derived from the experimental spectra are in complete agreement with predicted trends illustrated in figure 7.1.

A least squares calculation of the complete species spectra may be achieved in three ways; by a total matrix solution of the entire spectral data set, by a three parameter analysis at each wavelength, or by a two parameter analysis at each wavelength where the parameter K is introduced as a constant in eqn (7.1). The first of these possibilities

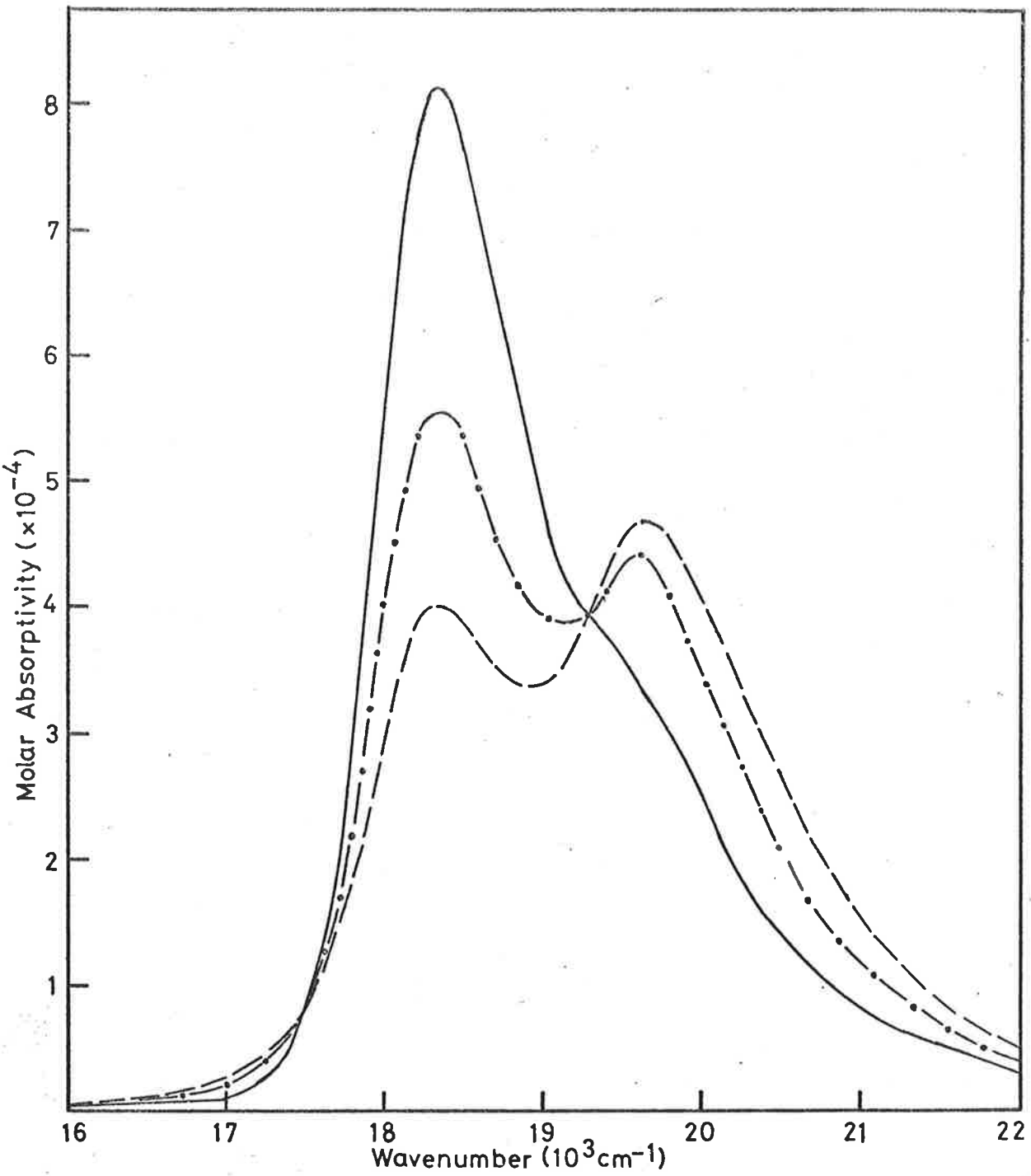

FIG. 7.2 SPECTRUM OF PYRONINE Y AS A FUNCTION OF STOICHIOMETRIC CONCENTRATION.
Approximate dye concentrations are as follows: 5×10^{-6} (——); 3×10^{-4} (—·—·—); 1×10^{-3} mol dm^{-3} (— — —).

Table 7.1 Parameters Derived from Experimental Spectra.
(Relative standard deviations in brackets for each case).

Distribution	ε_1^0($dm^3 mol^{-1} cm^{-1}$)	$\bar{\varepsilon}_1^0$($dm^3 mol^{-1} cm^{-1}$)	K($dm^3 mol^{-1}$)	Total Relative Standard Deviation
30 points, quasi-even	81136 (0.0011)	2970 (0.57)	1151 (0.089)	0.660
20 points, even	81213 (0.0012)	3810 (0.57)	1192 (0.108)	0.679
21 points, optimum	82249 (0.0010)	3990 (0.33)	1243 (0.075)	0.406

is computationally cumbersome while the second is subject to large errors in the estimation of K at certain values of ε_1^{λ} and $\bar{\varepsilon}_2^{\lambda}$, as indicated by the prediction analytical results in Appendix A, leading to a possible over-estimation of the computed errors. In the last possibility, the error in the association constant is neglected and the number of degrees of freedom increases as only two unknown parameters are involved. This will result in a possible under-estimation of the computed standard deviations. However, of these three methods, the last was chosen as being the simplest from a computational viewpoint. In addition, by using an accurate K value, as obtained by the prediction analytical procedure, the effect of the under-estimation of the standard deviations will be reduced. Table 7.2 shows the relative standard deviations in the computed molar absorptivities of the monomer and dimer species at particular points over the energy range measured. These were calculated with the K values given in table 7.1 in the case of each of the three data point distributions studied. The trends in the relative standard deviations presented in table 7.2 show that the 21 point optimum distribution produces generally more precise results particularly when the greater precision of the K value for this case is taken into consideration.

The spectra of the monomer and dimer species of Pyronine Y in aqueous solution, as obtained from the 21 point optimum distribution, are presented in figure 7.3. In view of the difficulty in assessing how the error in K is distributed between ε_1^{λ} and $\bar{\varepsilon}_2^{\lambda}$, the computed standard deviations have been accepted as a lower limit and of being representative of the trends in the behaviour of the errors over the species spectra. It is apparent, nonetheless, that the prediction analytical procedure has successfully optimized the relevant experimental conditions so as to achieve,

Table 7.2 Computed Molar Absorptivities at Particular Wavenumbers.
(Relative standard deviations as percentages given in brackets)

Wavenumber (cm^{-1})	Distribution							
	30 Quasi-Even		21 Even		21 Optimum			
	ε_1^λ	ε_2^λ	ε_1^λ	ε_2^λ	ε_1^λ	ε_2^λ
16000	331 (11.8)	401 (19.2)	302 (10.9)	430 (17.9)	334 (13.2)	384 (23.4)
17000	955 (6.1)	4648 (2.5)	951 (4.8)	4659 (2.3)	965 (6.0)	4497 (2.6)
18000	58192 (0.9)	6174 (13.6)	58266 (0.7)	5584 (13.2)	58826 (0.7)	6424 (11.2)
18300	81440 (0.8)	2500 (27.0)	81462 (0.5)	2446 (26.7)	82313 (0.5)	3893 (16.5)
19000	47766 (0.6)	21112 (2.1)	47889 (0.5)	21058 (2.0)	48336 (0.5)	21395 (2.0)
20000	24023 (0.9)	56397 (0.7)	24073 (0.5)	56280 (0.5)	24127 (0.7)	55204 (0.6)
21000	7606 (2.9)	21169 (2.0)	7627 (1.9)	21111 (1.6)	7642 (2.9)	20535 (2.1)
22000	2605 (4.0)	6762 (3.0)	2634 (2.5)	6786 (2.2)	2676 (4.0)	6530 (3.3)

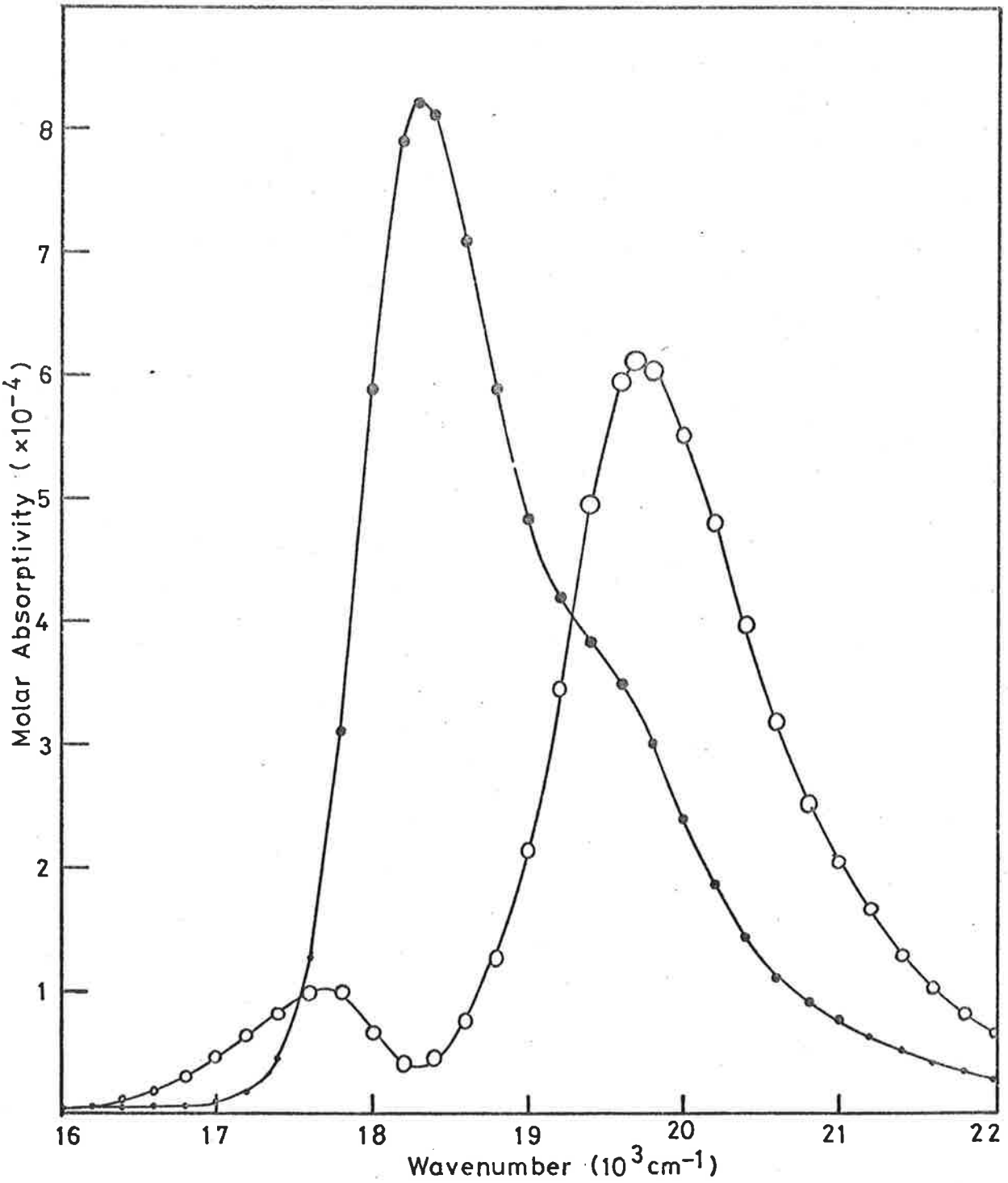

FIG. 7.3 SPECTRA OF MONOMERIC AND DIMERIC SPECIES OF PYRONINE Y. Monomer (●) and dimer (O) spectra computed from optimum distribution of data points. Size of circle indicates standard deviation in each case.

by the measurement of 21 specially selected points, an overall precision not bettered by the measurement of 30 evenly-distributed points.

7.2 Computation of Species Spectra

The following discussions deal with the analysis of the monomeric and dimeric species spectra for the three xanthane dyes, Rhodamine B, Pyronine B and Pyronine Y, noting that these spectra were determined for the former two dyes from 18 randomly-distributed and 30 evenly-distributed points, respectively. Furthermore, it has been shown,[43] for Rhodamine B and Pyronine Y, that the visible band corresponds to a single electronic transition. This may be safely assumed to apply to Pyronine B as well since this dye is a very close analogue of Pyronine Y.

7.2.1 *The Monomer Spectrum*

The monomer spectra were fitted by a weighted, non-linear least squares procedure to a 5-parameter Gaussian equation which has been described previously:[27]

$$I(\bar{\nu}) = (I_{00})_{max} \sum_m \frac{X^m}{m!}\left(1 + \frac{m\Delta\bar{\nu}}{\bar{\nu}_{00}}\right) \exp\left[-(\bar{\nu} - \bar{\nu}_{00} - m\Delta\bar{\nu})^2/b^2\right], \quad (7.2)$$

where $I(\bar{\nu})$ is the intensity as a function of wavenumber for each vibrational state m, $(I_{00})_{max}$ is the maximum intensity in the spectrum at wavenumber $\bar{\nu}_{00}$, $\Delta\bar{\nu}$ is the separation between successive vibrational levels in the monomer spectrum, b is the bandwidth parameter related to the bandwidth at half-maximal intensity b_g by

$$b_g = 2b(\ln 2)^{\frac{1}{2}} \quad (7.3)$$

and X is a parameter related to the equilibrium nuclear conformation in the two electronic states considered in each moiety of the dimer. In the case of the crude adiabatic approximation, it can be shown that[27]

$$\lambda = X^{\frac{1}{2}} \tag{7.4}$$

where X is the ratio of the (1,0) intensity to the (0,0) intensity within the monomer band since there is no coupling interaction considered between the ground and excited states. λ is the nuclear position parameter introduced in the dimer theory discussion. However, in the adiabatic theory, in which an interaction between the ground and excited states within each monomer moiety is postulated, equation (7.4) cannot hold strictly. The adiabatic λ value may be obtained from the monomeric spectrum, on the other hand, by the following experimental procedure.

Consider, initially, the case when $\varepsilon = 0$ in the dimer Hamiltonian of equation (6.55) and in its crude adiabatic analogue derived by Fulton and Gouterman.[5] In the latter case, when $\varepsilon = 0$ the Hamiltonian fortuitously reduces to the equation for a position displaced harmonic oscillator and yields the energies and intensities for a single, isolated molecule within the context of the crude adiabatic approximation. However, when $\varepsilon = 0$ in the adiabatic equation (6.55), the dimeric states still remain coupled by the κ term implying that the plus and minus series will not converge to the same form. This situation is best viewed as corresponding to the spectrum of an idealized dimer in which the intermolecular potential is non-existent so that the indirect KI coupling between dimeric states alone produces the differences between the predicted plus and minus series spectra. In general, the plus series corresponds to parallel molecular transition moments in the dimer so that the monomeric moieties, in such a case, are environmentally identical with the overall dimeric configuration. In the case of $\varepsilon = 0$, then, the plus series spectrum has the *shape* expected for an isolated monomer treated by the adiabatic approximation. The adiabatic λ value may then be obtained by fitting the

experimental monomer spectrum to the adiabatic plus series spectrum with the exciton exchange parameter, ε, set equal to zero. Finally, the nuclear momentum parameter κ required for calculations involving the adiabatic dimer theory and defined in eqn (6.54) is given by

$$\kappa = 2\Delta\bar{\nu}\lambda / \bar{\nu}_{00} \qquad (7.5)$$

in terms of the monomeric fitting parameters.

7.2.2 *The Dimeric Spectrum*

Theoretical absorption spectra for the adiabatic model were calculated as summarized in Section 6.4 by means of the computer programme ADFULGO given in Appendix C. The infinite matrix equations (6.59) and (6.60) were truncated and solved by library programmes available with a CDC 6400 computer. The size of the matrices was limited to a dimension of 20 as this was found to yield at least 10 eigenvalues and eigenfunctions well clear of any significant truncation errors. The sums in eqn (6.85) converged rapidly for the usual values of κ'. The dimeric absorption spectra were constructed by superimposing Gaussian bandshapes, of the form in expression (7.2), onto the computed line spectra[5] normalizing the overall spectrum to the maximum of the experimental spectrum. An identical procedure was adopted in calculating theoretical spectra based on the crude adiabatic model of Fulton and Gouterman using an available computer programme.[27] Of the necessary parameters for these calculations, the exciton exchange parameter, ε, and the angle between the moieties of the dimer, α, were fitting parameters. The bandwidth parameter, b, was assumed to be identical for both the monomer and dimer species[27] while "crude adiabatic" values of λ and κ were obtained from eqns (7.4) and (7.5).

8 COMPARISONS OF THEORY AND EXPERIMENT

8.1 Theoretical Comparisons

Figures 8.1(a) and 8.1(b) compare theoretical spectra computed by the adiabatic model with those obtained by the crude adiabatic approach due to Fulton and Gouterman. The following set of parameters were used in both cases

$$(I_{00})_{max} = 5$$
$$\bar{\nu}_{00} = 12.5$$
$$\Delta\bar{\nu} = 1.4$$
$$b_g = 0.5,$$

all those quantities being in arbitrary units. All spectra have been normalized to $(I_{00})_{max}$ and the plus series for both models have been superimposed at this maximum intensity, where possible, to aid comparison. The spectra have been plotted on an arbitrary energy scale with the monomer (0,0) band at 11.8. The variable parameters ε, λ and κ are shown in each case applying to both the plus and minus series of each model, that is for parallel and anti-parallel molecular transition moments in the dimer, respectively.

In relation to the phenomenon of the exciton-nuclear position interaction, it is apparent that both models provide, in a similar way, the gross spectral trends expected for various degrees of competition between the exciton interaction (ε) and the nuclear displacements (λ).[52] However, in agreement with the situation discussed by Fulton,[6] the adiabatic and crude adiabatic models diverge as the KI effect increases and the influence of nuclear momentum (κ) becomes comparable with the exciton interaction. Both theories predict very similar negative series spectra which appear as normal

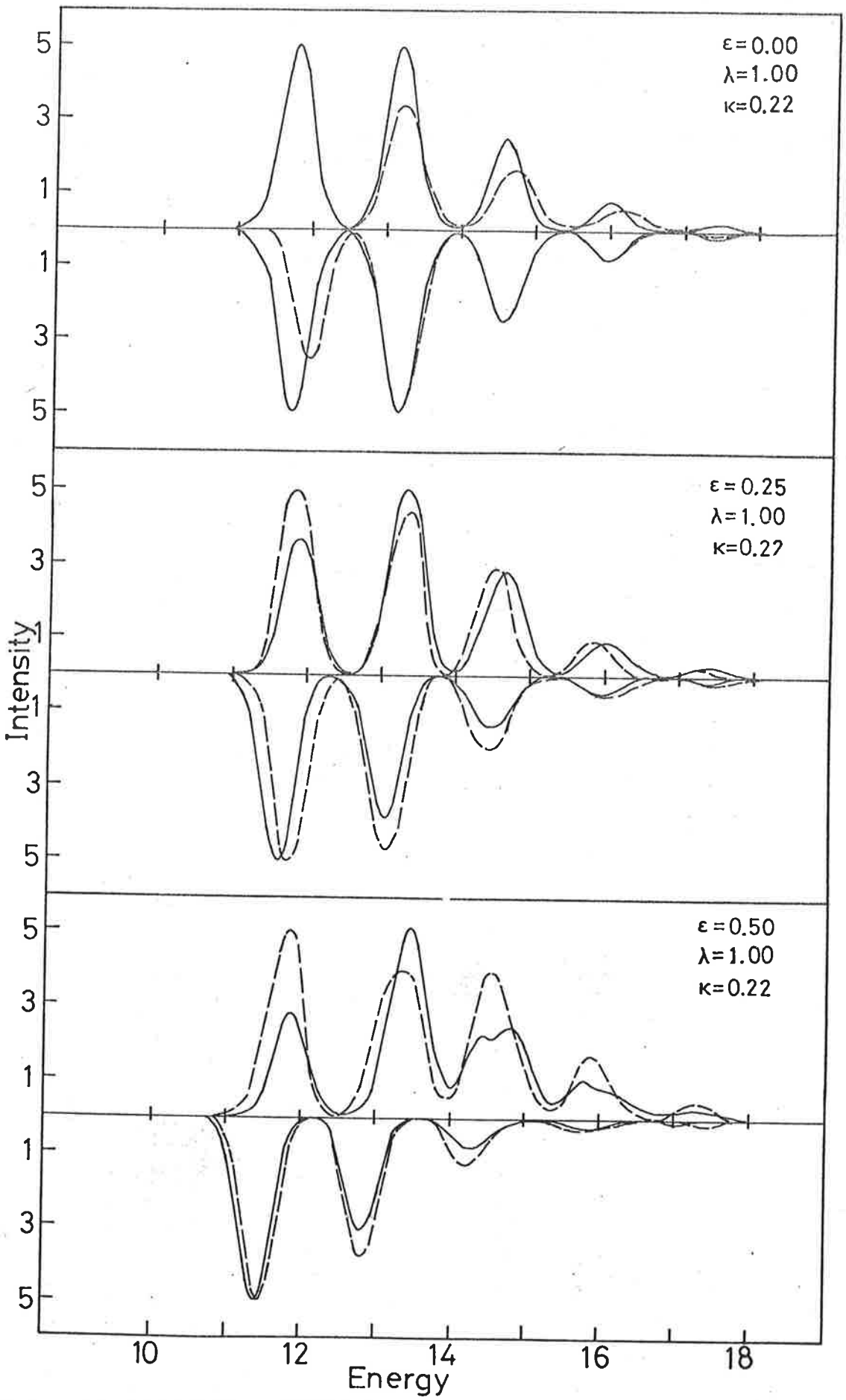

FIG. 8.1(a) THEORETICAL ABSORPTION SPECTRA. Continued in Fig. 8.1(b)

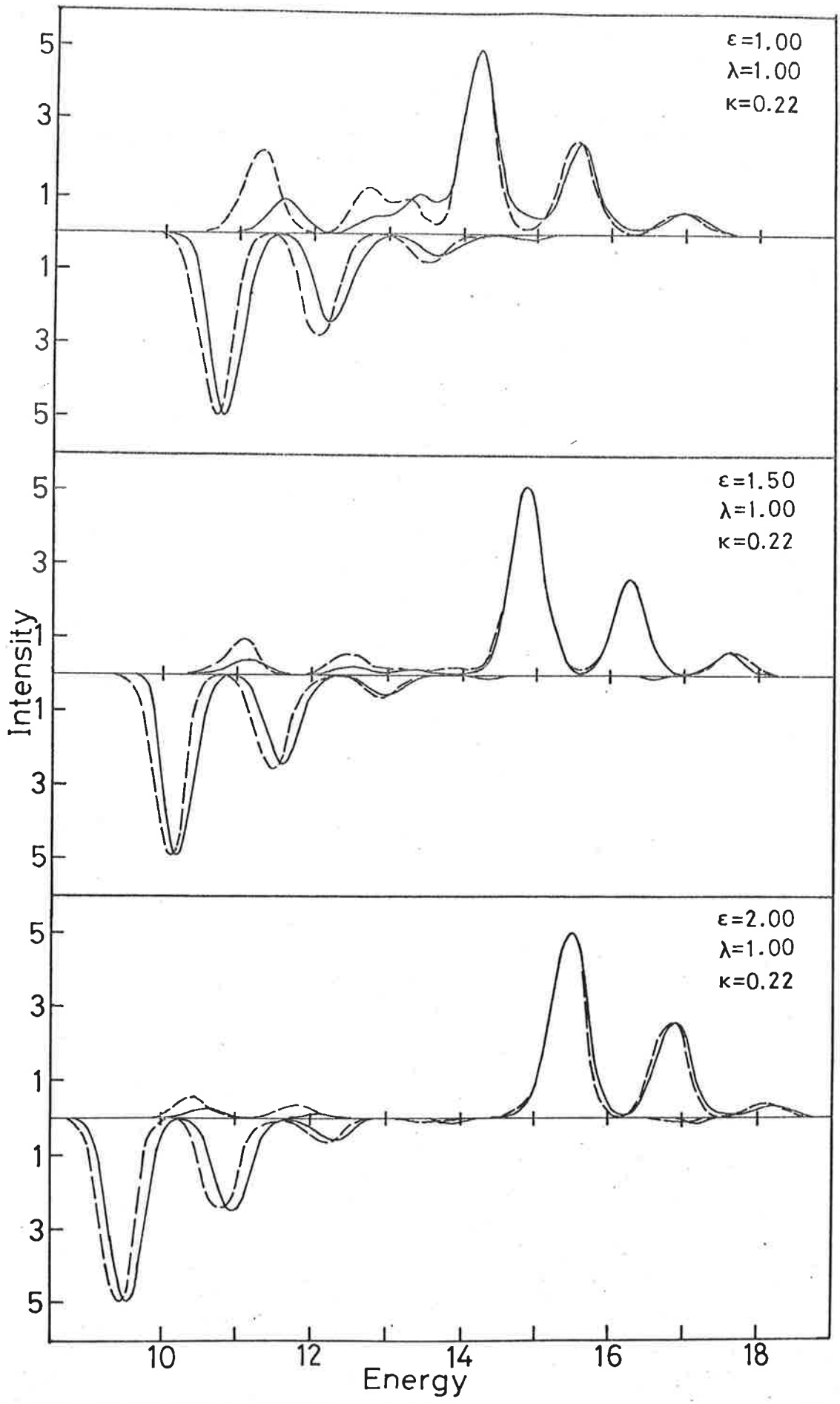

FIG. 8.1(b) THEORETICAL ABSORPTION SPECTRA. Plus and minus series for each spectrum are shown above and below x-axis, respectively.
——, crude adiabatic model (parameters ε and λ);
– –, adiabatic model of this work (parameters ε, λ and κ)

vibrational progressions throughout the whole range of coupling strengths. The positive series, on the other hand, shows a more varied behaviour for both models. In the limit where the exciton-nuclear momentum interaction is substantial (figure 8.1(a)), the adiabatic theory predicts positive series spectra which appear to be much broader than the corresponding crude adiabatic spectra. The only real correlation between the models in this coupling region is in the position of the vibronic bands but not in their intensities. However, in the region of much weaker exciton-nuclear momentum interaction (figure 8.1(b)), predicted intensities and band positions are almost identical at higher energies. This limit also corresponds to the situation of weak exciton-nuclear position interaction of which it is qualitatively[52] predicted that the two series are very well separated, as is observed in figure 8.1(b). However, both theories predict additional weak bands at low energy for the plus series and at high energy for the minus series. These have been ascribed[5] to "vibrational borrowing" between the two coupled electronic states of the dimer due to the asymmetric vibrational mode q^-. In the plus series, the adiabatic model predicts much larger intensities in this region of the spectrum which supports the vibrational borrowing interpretation. This is seen to be so because the KI effect operates via the asymmetric momentum coordinate p^- as may be seen from eqn (6.55).

As was discussed in Section 7.2.1, there is a difference between the plus and minus adiabatic spectra when $\varepsilon = 0$ which has been attributed to the KI coupling between dimeric states. It is of interest to assess the deviation between the predicted crude adiabatic monomer spectra and the corresponding adiabatic spectra for various values of λ and κ, for practical purposes. Adiabatic monomer spectra, corresponding to the

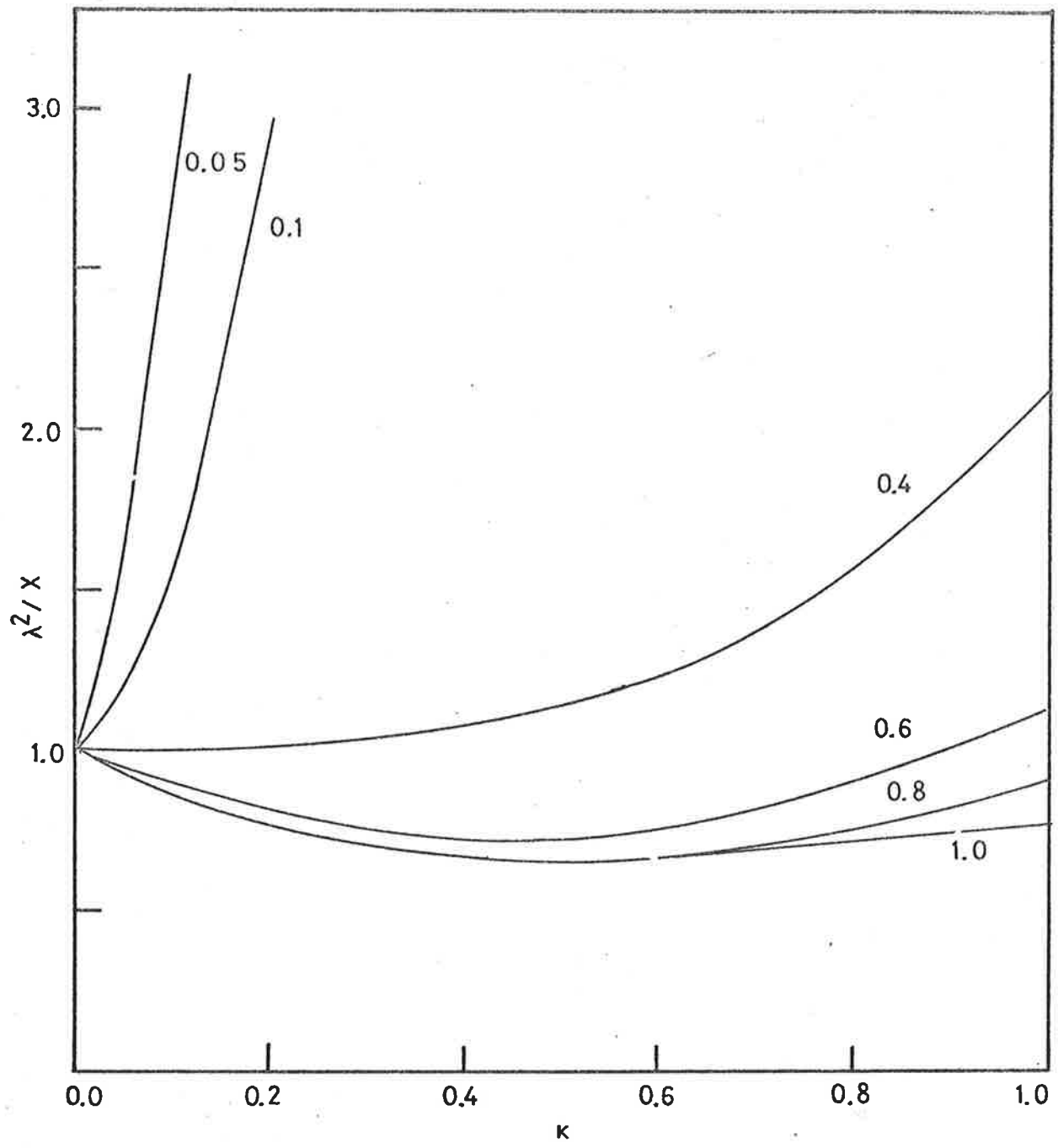

FIG. 8.2 NUCLEAR POSITION PARAMETER IN THE ADIABATIC THEORY. The value of λ corresponding to each curve is indicated.

plus series for $\varepsilon = 0$ as discussed earlier, were computed for a range of pairs of λ and κ values and then X values for these spectra were calculated from the ratio of the (1,0) to the (0,0) band intensities. The ratio λ^2/X is unity for the crude adiabatic monomer, as can be seen from eqn (7.4). However, plots of this quantity versus κ are a direct measure of the deviation of the adiabatic model of the monomer from eqn (7.4) and are presented in figure 8.2.

8.2 Experimental Comparisons

The computed monomer spectra of the xanthene dyes considered, as analysed by means of the Gaussian equation described in Section 7.2.1, are presented in figure 8.3. The resultant five fitting parameters are given in table 8.1 for each of these dyes. The last two entries in this table have been calculated from equations (7.4) and (7.5) so that these quantities are strictly valid only in the crude adiabatic approximation. However, comparing these values to the curves in figure 8.2, it is seen that, for these three dye systems, the ratios λ^2/X are close to unity within experimental error. Accordingly, no significant error is introduced by the use of the λ and κ values given in table 8.1 for both models as required.

The relevant dimer spectra were calculated as described in Section 7.2.2 for both theoretical models using the parameters in table 8.1 and varying only the exciton exchange parameter ε and the angle between the moieties in the dimer, α. These theoretical spectra and the dimer absorption spectra as derived experimentally are presented in figure 8.4. It is seen that the dimer spectra of Rhodamine B, Pyronine B and Pyronine Y correspond to a series of decreasing exciton-nuclear position and exciton-nuclear momentum interaction, as reflected by the increase of ε with respect

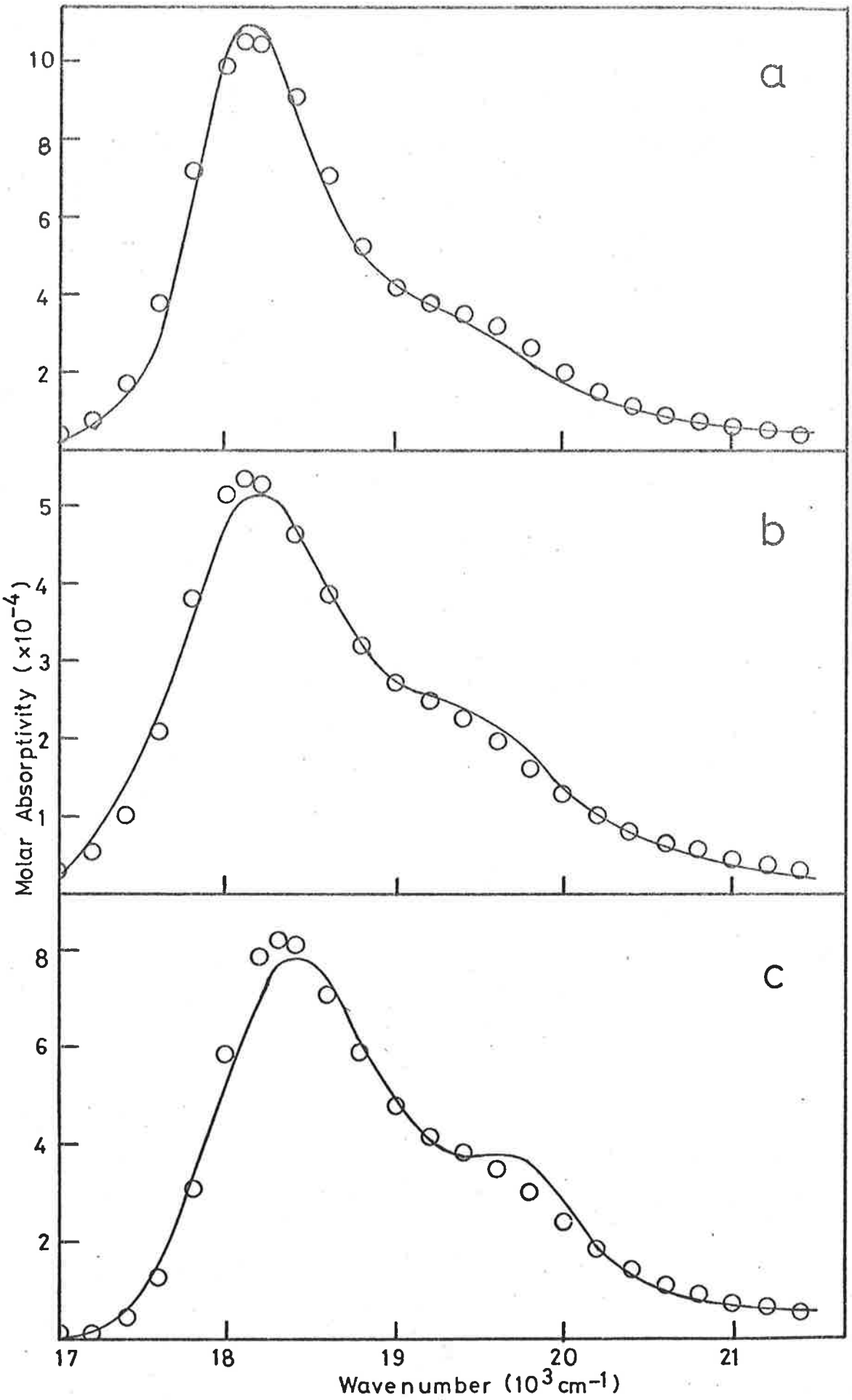

FIG. 8.3 COMPARISON OF EXPERIMENTAL AND THEORETICAL MONOMER SPECTRA. (a) Rhodamine B, (b) Pyronine B, (c) Pyronine Y. Experimental data: (O); theoretical curve: (——).

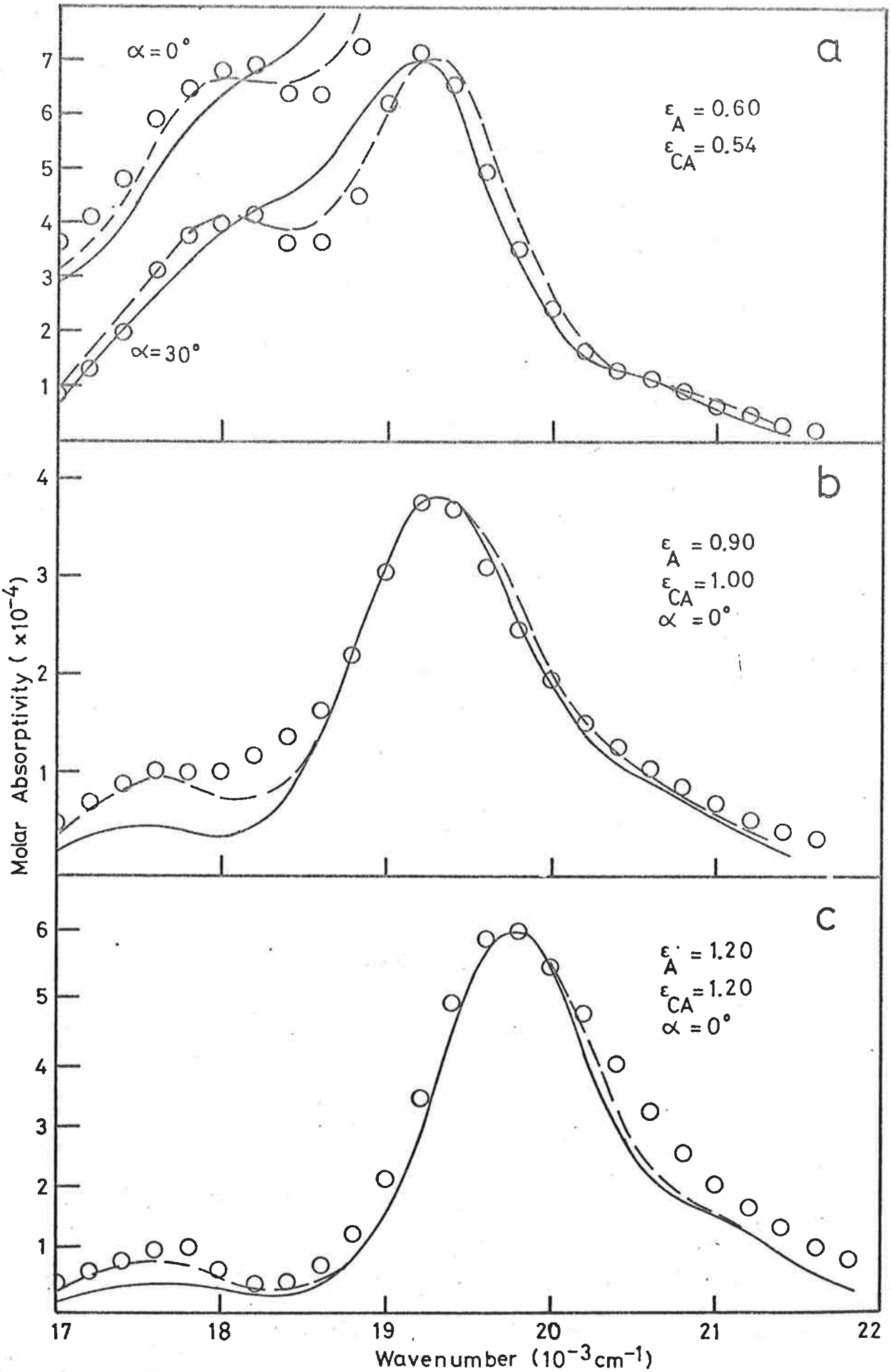

FIG.8.4 COMPARISON OF EXPERIMENTAL AND THEORETICAL DIMER SPECTRA. (a) Rhodamine B, (b) Pyronine B, (c) Pyronine Y. Experimental data: (O). Adiabatic spectra, parameter ε_A: (———). Crude adiabatic spectra, parameter ε_{CA}: (——). Angle parameter α applies to both models. See text concerning inset to (a).

Table 8.1 Monomer Parameters for the Three Dye Spectra
(Errors shown are standard deviations)

Parameter	Rhodamine B	Pyronine B	Pyronine Y
$(I_{00})_{max}$	101 800 ± 2300	51 390 ± 950	78 850 ± 1700
$\bar{\nu}_{00}$ (cm^{-1})	18 188 ± 20	18 170 ± 20	18 392 ± 10
$\Delta\bar{\nu}$ (cm^{-1})	1 348 ± 30	1 260 ± 30	1 194 ± 20
X	0.34 ± 0.02	0.43 ±0.02	0.46 ± 0.02
b_g	1 115 ± 30	1 140 ± 20	1 052 ± 20
λ	0.58	0.66	0.68
κ	0.086	0.091	0.088

to λ and κ. Although the exciton-nuclear momentum interaction is weak in these cases, there are significant differences between the two models, predominantly in the low energy region of the spectra. This observation parallels the difference in behaviour for the two models on a theoretical basis as seen in figures 8.1(a) and 8.1(b).

Both models predict an angle of about 30^{o} between the monomer moieties of the Rhodamine B dimer and 0^{o} for the Pyronine dyes. Theoretically, the minus series affects predominantly the low energy region of the spectrum as can be seen from the results in figures 8.1(a) and 8.1(b). However, no amount of contribution from the minus series can explain, as does the adiabatic model, the discrepancy between the crude adiabatic and experimental spectra for these dye systems. However, in the case of Rhodamine B, the minus series is included to produce the longer low energy "tail" which is not observed in the spectra of the Pyronines. The effect

of the minus series on the Rhodamine spectrum, as shown as an inset to figure 8.4, indicates the only change incurred on the whole of the theoretical spectrum as the angle α is altered in each model.

The interpretation of the spectrum of Rhodamine B is complicated by two factors. Firstly, a component of the minus series is present, as brought about by the non-zero angle between the monomer moieties of the dimer. Secondly, this dimer is an example of the intermediate exciton-nuclear position interaction limit where the redistribution of intensities is complicated. However, the adiabatic model provides an obvious improvement over the crude adiabatic result in this case. The spectra for the Pyronine dyes, on the other hand, have no minus series component and are representative of weak to very weak exciton-nuclear position interaction. Only the adiabatic model predicts quantitative intensities for these examples in the low energy region of the spectra which, as discussed in Section 8.1, corresponds to vibrationally borrowed intensity from the forbidden negative series. Apart from the generally more accurate predictions of the adiabatic theory, this latter result adds great weight in favour of the premise of a kinetically induced coupling between non-degenerate states of the monomer moieties leading to an exciton-nuclear momentum interaction.

As the exciton-nuclear position interaction decreases, neither model predicts accurate intensities in the high energy region of the experimental spectra, although the adiabatic model provides some improvements even here. As was discussed in Section 6.3.1, such a discrepancy would be expected from the form of the κ term used. This form of the nuclear momentum parameter is based on the harmonic approximation to the

potential energy and thus depends only on the displacement in and the energy of the zero vibrational level in the excited state. It is suggested that the discrepancies observed in the high energy region of the predicted spectra may be due to not accounting for the larger displacements, energies and anharmonicities of the higher vibronic states.

9 CONCLUSIONS

9.1 Prediction Analysis

The important prediction, that by the judicious choice of the distribution of points a significant improvement may be achieved in the precision of the physical parameters to be determined, has been experimentally vindicated. As a consequence, the use of prediction analysis in the optimization of experiments concerned with the concentration dependence of the spectra of solutions, can achieve significant savings in labour, time and material. In addition, prediction analysis provides a powerful tool for assessing the feasibility of any data collecting experiment where the physical law of the phenomenon in question and the accuracy of the experimental variables are known.

9.2 Exciton Interactions in Dimers

In general, the adiabatic theory appears to provide a more accurate description of exciton interactions in dimers than does the simpler crude adiabatic theory. In particular, the adiabatic model predicts a weak coupling between the ground and excited states within each moiety of the dimer arising from the nuclear kinetic energy. While this kinetically

induced coupling is small, experimental evidence presented indicates that it is nonetheless significant when introduced as a competition to the exciton interaction in dimers. This competition has subsequently been interpreted as an exciton-nuclear momentum interaction.

While studies such as this for dimer systems have no direct *mathematical* application to the many-body problem of the polymer or crystal, the *processes* involved would be expected to be quite applicable to these more complex aggregates. The exciton migrating through a crystal or along a polymer chain will experience perturbations due to the various inter- and intramolecular vibrations inherent in each of these cases. In general, this type of perturbation has been dealt with only in a static sense. That is, only the effect of the instantaneous positions of the nuclei on the exciton have been considered, giving rise to, what is termed in this work, the exciton-nuclear position interaction. However, it must be presumed that the exciton will be affected by the *change* in the potential energy as the nuclei move. This, in fact, is the physical basis of the exciton-nuclear momentum interaction.

REFERENCES

1. J. Frenkel, *Phys. Rev.*, 37, 17, 1276 (1931).

2. e.g. L.I. Schiff, *Quantum Mechanics*, (McGraw-Hill, 1966). pp.164-166 and p.206.

3. A. Witkowski and W. Moffit, *J. Chem. Phys.*, 33, 872 (1960).

4. R.L. Fulton and M. Gouterman, *J. Chem. Phys.*, 35, 1059 (1961).

5. R.L. Fulton and M. Gouterman, *J. Chem. Phys.*, 41, 2280 (1964).

6. R.L. Fulton, *J. Chem. Phys.*, 56, 1210 (1972).

7. M. Born, *Gött. Nachr. Math. Phys.*, K1, 1 (1951).

8. e.g. R.M. Hochstrasser and P.N. Prasad, *Excited States*, (Ed. E.C.Lim; Academic Press, 1974). Vol. 1, p.79.

9. e.g. R. Englman, *The Jahn-Teller Effect in Molecules and Crystals*, (Wiley-Interscience, 1972), pp. 9-18.

10. H.C. Longuet-Higgins, *Advan. Spectry.*, 2, 429 (1961).

11. e.g. A. Messiah, *Quantum Mechanics*, (North-Holland. 1969). Vol. 1, pp.252-254, 307-309.

12. W.T. Simpson and D.L. Peterson, *J. Chem. Phys.*, 26, 588 (1957).

13. (a) A. Witkowski, *Roczniki Chemii*, 35, 1399, 1409 (1961).

    (b) A. Witkowski, *Modern Quantum Chemistry*, (Ed. O. Sinanoğlu; Academic Press, 1965). Part III, p. 161.

14. R.E. Merrifield, *Radiation Res.*, 20, 154 (1963).

15. e.g. B.L. Moiseiwitsch, *Variational Principles*, (Interscience. 1966). p. 166.

16. S. Koide, *Z. Naturforsch.*, 15a, 123 (1960).

17. E.A. Chandross, *J. Chem. Phys.*, 43, 4175 (1965).

18. J. Ferguson, *J. Chem. Phys.*, 43, 306 (1965).

19. (a) S.E. Sheppard, *Proc. Roy. Soc.*, A82, 256 (1909)

    (b) S.E. Sheppard and A.L. Geddes, *J. Amer. Chem. Soc.* 66, 2003 (1944).

20. Th. Förster, *Naturwissenschaften*, 33, 166 (1946).

21. G.S. Levinson, W.T. Simpson and W. Curtis, *J. Am. Chem. Soc.*, 79, 4314 (1957).

22 (a) E.A. Chandross, J. Ferguson and E.G. McRae, *J. Chem. Phys.* 45, 3546 (1966).

(b) E.A. Chandross and J. Ferguson, *J. Chem. Phys.*, 45, 3554 (1966).

23. B. Badger and B. Brocklehurst, *Trans. Farad. Soc.*, 65, 2576, 2582, 2588, (1969).

24. M.E. Lamm and D.M. Neville, *J. Phys. Chem.*, 69, 3872 (1965).

25. E.G. McRae, *Aust. J. Chem.*, 14, 344 (1961).

26. e.g. E.F. McCoy and I.G. Ross, *Aust. J. Chem.*, 15, 573 (1962).

27. M.E. Gál, G.R. Kelly and T. Kuruscev, *J. Chem. Soc., Farad. Trans. II*, 69, 395 (1973).

28. e.g. J.T. Bell and R.E. Biggers, *J. Mol. Spect.*, 18, 247 (1965).

29. C. Manneback, *Physica*, 17, 1001 (1951).

30. e.g. B. Higman, *Applied Group-Theoretic and Matrix Methods*, (Clarendon Press. 1955). p.149.

31. J.R. Wolberg, *Prediction Analysis*, (van Nostrand. 1967).

32. J.N. Kikkert, G.R. Kelly and T. Kurucsev, *Biopolymers*, 12, 1459 (1973).

33. G.R. Kelly and T. Kuruscev, *Biopolymers*, 13, 769 (1974).

34. D.E. Joyce and T. Kurúscev, *Biophys. Chem.*, 2, 273 (1974).

35. e.g. R.W. Ramette and E.B. Sandell, *J. Amer. Chem. Soc.*, 78, 4872 (1956).

36. e.g. See discussion in J.F. Padday, *J. Phys. Chem.*, 72, 1259, (1968).

37. e.g. P. Ts'o and S. Chan, *J. Amer. Chem. Soc.*, 86, 4176 (1964).

38. e.g. D. Guttman and T. Higuchi, *J. Am. Pharm. Assoc., (Scientific Ed.)* 46, 4 (1957).

39. e.g. P. Stoesser and S. Gill, *J. Phys. Chem.*, 71, 564 (1967).

40. e.g. S. Chan, M. Schweizer, P. Ts'o and G. Helmkamp, *J. Amer. Chem. Soc.*, 86, 4182 (1964).

41. K. Fujiki, C. Iwanaga and M. Koizumi, *Bull. Chem. Soc. Japan*, 35, 185 (1962).

42. V. Vitagliano and L. Costantino, *J. Phys. Chem.*, 74, 197 (1970).

43. H. Jakobi and H. Kuhn, *Z. Elektrochem.*, 66, 47 (1962).

44. T. Kuruscev and U.P. Strauss, *J. Phys. Chem.*, 74, 3081 (1970).

45. T. Cant, *Honours Report*, 1973, (University of Adelaide).

46. G. Box and H. Lucus, *Biometrika*, 46, 77 (1959).

47. H. Chernoff, *Ann. Math. Stat.*, 24, 586 (1953).

48. J.R. Wolberg, *Prediction Analysis*, (Van Nostrand. 1967). pp.102-111.

49. e.g. G. Beveridge and R. Schechter, *Optimization: Theory and Practice*, McGraw-Hill, 1970). p. 367.

50. S. Woisławski, *J. Amer. Chem. Soc.*, 75, 5201 (1953).

51. J. Pitha and R.N. Jones, *Canad. J. Chem.*, 44, 3031 (1966).

52. e.g. M. Kasha, *Radiation Res.*, 20, 55 (1963).

CHAPTER IV

The Crystalline Aggregate

10 THE CLASSICAL THEORY OF TRANSMISSION AND ABSORPTION OF LIGHT IN CRYSTALS.

The essential aim of this work is to determine the orientation of the transition moment of a particular guest held within a host matrix. Apart from such methods as the electron spin resonance studies of the triplet states of the guest molecule,[1] the observation of the behaviour of light absorption by the guest as a function of crystal orientation provides a particularly straightforward avenue for achieving this aim. The attraction of the method lies as much in the direct nature of the experimentation required as in the fact that the results may be interpreted by means of the well-established classical optics of crystals.

The theoretical discussion presented here is a specific application of the classical optics of crystals, based predominantly on the work by Born and Wolf,[2] to the problem of the transmission and absorption of light in monoclinic crystals, such as anthracene. The requirement for such an analysis at this point arises from the need to delineate tne necessary experimental conditions for the most facile interpretation of light absorption by a guest molecule within a host lattice. Two major interpretive difficulties may be defined with particular reference to the class of biaxial crystals of which anthracene is one example. Firstly, the incident light will undergo double refraction within a biaxial crystal so that the electric field orientations within the crystal will not be identical to the orientation of the external field. Moreover, the specific orientations of the internal field are related to the mutual alignment of crystal and external field. Secondly, the external field applied to the medium is considered to be further altered by the electric

field of the medium itself. The influence of this local field[3], as distinct from the applied field, at the site of a specific molecule requires consideration when dealing with the problem of a guest molecule in a host lattice. Gaussian units will be used in the subsequent discussion which includes an introductory summary of the necessary classical optics followed by an application of this classical theory to the specific problem on hand.

10.1 The Optics of Anisotropic Media

Born and Wolf[2] have presented a very complete work on the theory of classical optics and this has been used as the source for the summary of the fundamental concepts which follows. The absorption of light by a dopant in a host molecular crystal concerns the interaction of the electric field of the incident electromagnetic radiation and the transition moment of the guest molecule. The direction of the electric field in such a crystal is then of central importance to the derivation of the transition moment orientation. In the treatment of most insulating crystals it may be assumed that the medium is homogenous, non-conducting, magnetically isotropic and electrically anisotropic so that the macroscopic electric field *within* the medium, as distinct from the applied external field, is related to the electrical displacement $\underline{D}$ by

$$\underline{D} = \underline{\underline{\varepsilon}}\,\underline{E}. \qquad (10.1)$$

$\underline{\underline{\varepsilon}}$ is the dielectric tensor which, being symmetric, may be diagonalized by taking as the coordinate system the so-called principal dielectric axes having the principal dielectric constants ε_{xx}, ε_{yy} and ε_{zz} in the x, y, and z directions, respectively. These axes are labelled such that

$$\varepsilon_{xx} < \varepsilon_{yy} < \varepsilon_{zz} \tag{10.2}$$

thus establishing a unique coordinate system.

An electromagnetic wave is assumed to propagate in the direction represented by the unit vector $\underline{w}$, the so-called wavenormal, at a velocity v_w, known as the wavenormal or phase velocity, such that $\underline{D}$ is perpendicular to $\underline{w}$. On the other hand, the magnitude and direction of the energy flux of the electromagnetic field is given by the Poynting vector $\underline{S}$,

$$\underline{S} = \frac{c}{4\pi} (\underline{E} \times \underline{H}) \tag{10.3}$$

where c is the velocity of light *in vacuo* and $\underline{H}$ is the magnetic vector. For convenience, the direction of this energy flux is represented by the unit vector $\underline{r}$, the so-called ray, and the velocity of energy propagation is the ray velocity v_r. The vector $\underline{E}$ is perpendicular to $\underline{r}$ and is not collinear with $\underline{D}$, in general. The wavenormal velocities and directions are interrelated by Fresnel's equation of wavenormals

$$\frac{w_x^2}{v_w^2 - v_x^2} + \frac{w_y^2}{v_w^2 - v_y^2} + \frac{w_z^2}{v_w^2 - v_z^2} = 0 \tag{10.4}$$

where w_x, w_y and w_z are the x, y and z components of the wavenormal vector and v_x, v_y and v_z are the principal velocities of propagation. An analogous equation to (10.4) relates the ray directions and velocities.

Attention is now centred on the refraction of light in the specific case of biaxial crystals. It is found that each incident wave gives rise to two refracted waves, each of these transmitted waves having a unique velocity of propagation. Each transmitted wave may have only one direction of polarization of the vector $\underline{D}$ and both waves are in the plane of incidence. This is known as the phenomenon of *double refraction* or

birefringence. The refracted waves obey the general law of refraction

$$\frac{\sin \theta_i}{\sin \theta_w} = \frac{c}{v_w} = \eta_w \qquad (10.5)$$

where θ_i and θ_w are the angles of incidence and refraction, respectively, for the wavenormal and η_w is the refractive index of wavenormals which is direction dependent. In general, the orientation of the vector $\underline{D}$, and thus of $\underline{E}$, is not easily determined. On the other hand, it is known that propagation in any coordinate plane of the principal dielectric axis system gives rise to an *ordinary* and an *extraordinary* wave such that the directions of vibration of the vector $\underline{D}$ are perpendicular and parallel to the coordinate plane, respectively. Equation (10.5) applies to the extraordinary wave while the form

$$\frac{\sin \theta_i}{\sin \theta_w} = n_w, \qquad (10.6)$$

where n_w is the refractive index of wavenormals independent of the direction of propagation, applies to the ordinary wave.

There exists in the x z -plane, known as the principal plane, certain unique directions along which there is only one allowed velocity of propagation but an infinity of allowed directions of polarization for the vectors $\underline{E}$ or $\underline{D}$. A maximum of two such directions are possible, corresponding to the case of biaxial crystals, situated symmetrically about the z-axis for each of the wavenormal and ray directions and are termed the optic axes of wavenormals and the optic ray axes, respectively. The important consequence of propagation of a wavenormal in the direction of an optic axis is that the light is depolarized and consequently indicates the position of the axis in question. This is known as *internal conical refraction* in the case of a wavenormal propagating in the direction of an optic axis of wavenormals and *external conical refraction* in the case of a ray propagating along a ray

optic axis.

10.2 Doped Crystal Absorption

The principles described above will now be applied to the problem of energy absorption by a dopant molecule in a host lattice. Specifically, the host crystal is anthracene. The following facts and assumptions will be defined at first.

(i) The crystal structure of anthracene is described by space group $P2_1/a$. The unit cell is bimolecular and monoclinic[4] and thus optically biaxial.[2,5] As a result, it is known that one of the dielectric axes is parallel to the two-fold crystallographic axis while the other two are dependent on wavelength.[5] Optical data for anthracene[6-9] and the condition in eqn (10,2) then establish that the optical y-axis is coincident with the crystallographic b-axis and the optical x z -plane is in the crystallographic ac-plane.

(ii) Anthracene crystallizes into plates, the extended surface being the crystallographic ab-plane.[4]

(iii) The dopant concentration is assumed to be sufficiently low as not to incur any significant effect on the crystal structure of the host. As well, low dopant concentrations will ensure that there are no guest-guest interactions and that absorption by the dopant at each site occurs in a region smaller than the wavelength of the exciting radiation. There are then no significant boundary effects.

(iv) The host is assumed not to possess any significant absorption in the region of guest absorption so that the host matrix acts as a classical,

non-absorbing, electrically anisotropic medium.

For non-absorbing media, the expression[2]

$$n = (\varepsilon\mu)^{\frac{1}{2}} \tag{10.7}$$

relates the refractive index n to the dielectric constant ε and the magnetic permeability μ. For most non-magnetic materials, μ is very close to unity and will be neglected in all consequent expressions in this analysis. Thus

$$\varepsilon = n^2$$

so that, for electrically anisotropic media,

$$\varepsilon_{xx} = \alpha^2;\ \varepsilon_{yy} = \beta^2;\ \varepsilon_{zz} = \gamma^2 \qquad \alpha < \beta < \gamma \tag{10.8}$$

where α, β and γ are the principal refractive indices and are obtainable experimentally. Due to the nature of the anthracene crystal, absorption is best carried out with light incident on the crystallographic ab-plane, that is the optical xy-plane of the principal dielectric system of axes. It is further known that the evaluation of directions of polarization for the field vectors is much simplified when the wavenormals and rays lie in the coordinate planes. Thus, the incident plane is most suitably selected as to be in the crystallographic ac-plane, that is, the principal optical plane. Figure 10.1 presents a plan view of the ac-plane with a light beam incident on the ab-plane at an angle θ_i. Due to double refraction, two wavenormal (and two ray) directions result within the crystal. One wavenormal undergoes ordinary refraction at an angle θ_w' and the other undergoes extraordinary refraction at angle θ_w''. It is also known that there are two optic axes of wavenormals within this plane equally displaced about the z-axis at an angle Ω_w to the z-axis. The axis perpendicular to the crystallographic a-axis in the ac-plane will be denoted c′ and the angle

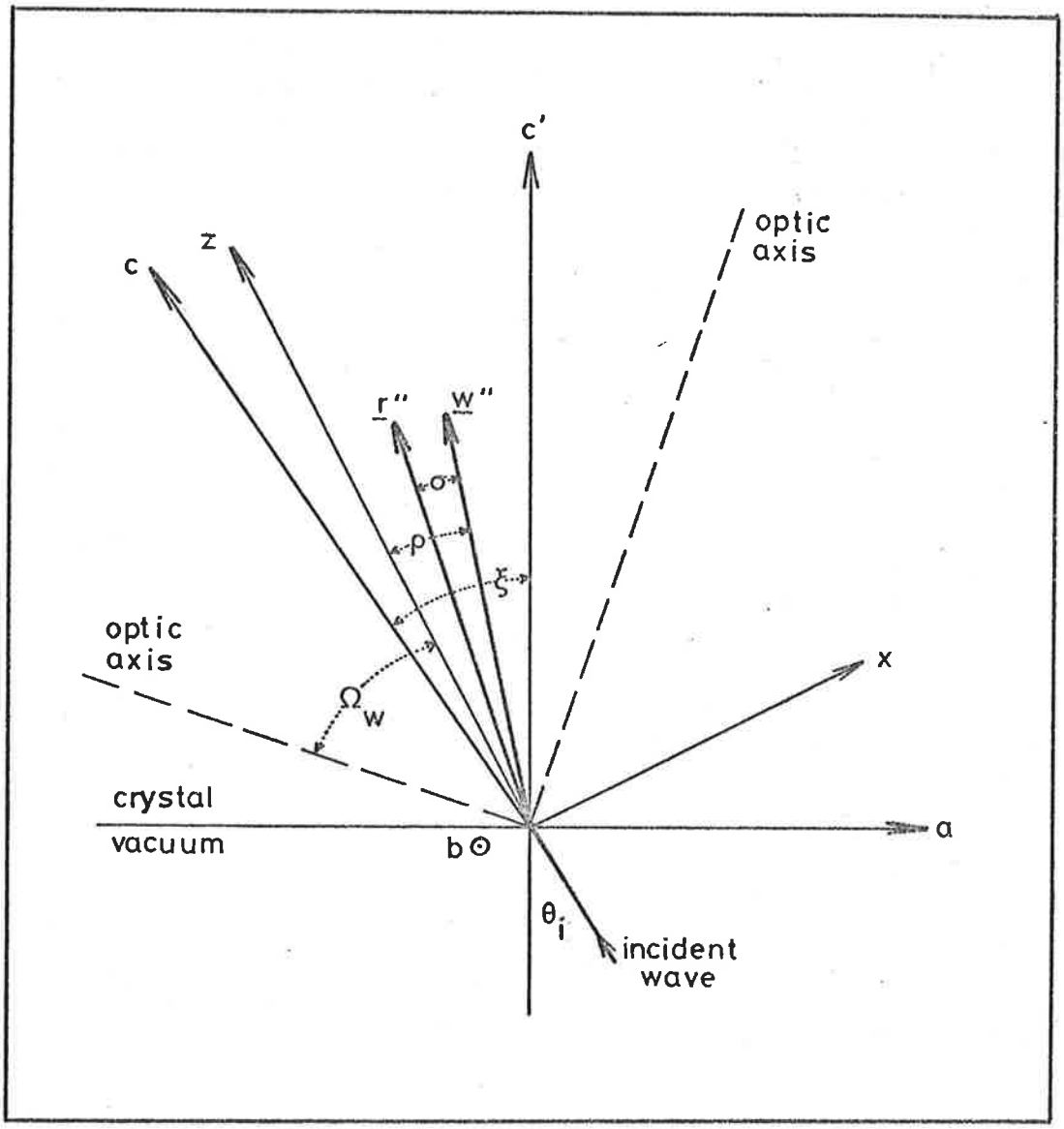

FIG.10.1 OPTICAL AND CRYSTALLOGRAPHIC AXIS. Extraordinary wavenormal and ray are denoted $\underline{w}''$ and $\underline{r}''$, respectively. Ordinary components not shown.

between c' and the z-axis will be denoted ξ. For convenience ρ will denote the angle between the extraordinary wavenormal direction $\underline{w}''$ and the z-axis and σ will denote the angle between $\underline{w}''$ and the extraordinary ray direction $\underline{r}$.

From eqn (10.4), Fresnel's equation of wavenormals in the x z -plane will be

$$(v_w^2 - v_y^2)\,[\,w_x^2(v_w^2 - v_y^2) + w_z^2(v_w^2 - v_x^2)\,] = 0.$$

But

$$w_z = \cos\rho \quad \text{and} \quad w_x = \sin\rho$$

so that

$$(v_w^2 - v_y^2)[(v_w^2 - v_z^2)\sin^2\rho + (v_w^2 - v_x^2)\cos^2\rho] = 0. \qquad (10.9)$$

The roots of this equation are

$$v_w'^2 = v_y^2$$

$$v_w''^2 = v_z^2 \sin^2\rho + v_x^2\cos^2\rho, \qquad (10.10)$$

the first of which gives the wavenormal velocity for the ordinary wavenormal $\underline{w}'$ and the second giving the extraordinary wavenormal velocity. The simple law of refraction, eqn (10.6), will apply to $\underline{w}'$ and corresponds to a vibration direction of the vector $\underline{D}$ along the optical y-axis. That is,

$$\frac{\sin\theta_i}{\sin\theta_w} = \beta \qquad (10.11)$$

where β is the refractive index along the y-axis as described by eqn (10.8). The extraordinary wavenormal obeys the law given in eqn (10.5), specifically

$$\frac{\sin\theta_i}{\sin\theta_w'} = \frac{c}{v_w'} = \eta_w, \qquad (10.12)$$

and represents a vibration direction of $\underline{D}$ in the x z -plane. From eqns (10.8) and (10.10), it may be seen that

$$v_w'' = c(\sin^2\rho/\gamma^2 + \cos^2\rho/\alpha^2)^{\frac{1}{2}}$$

where

$$v_k = c\varepsilon_{kk}^{-\frac{1}{2}} \qquad k = x, y, z,$$

so that eqn (10.12) becomes

$$\sin\theta_i - \sin\theta_w'' \left[\frac{\sin^2(\xi-\theta_w'')}{\gamma^2} + \frac{\cos^2(\xi-\theta_w'')}{\alpha^2}\right]^{-\frac{1}{2}} = 0 \qquad (10.13)$$

since $\rho = \xi - \theta_w''$. This equation may be used to calculate values of θ_w'' from values of θ_i using Newton's method of evaluating the roots of a function.

The $\underline{D}$ vector associated with the extraordinary wavenormal is in the x z -plane and will be denoted $\underline{D}''$. In the same way $\underline{E}''$ is associated with the extraordinary ray and is also in this plane. The vibration directions for the vectors associated with the ordinary wavenormal and ray are denoted $\underline{D}'$ and $\underline{E}'$ and are collinear with the y-axis. It follows from this argument and from eqn (10.1) that

$$D_x'' = -\cos(\xi-\theta_w'')\,|\underline{D}''| = \varepsilon_{xx} E_x'' = -\cos(\xi-\theta_r'')\,\varepsilon_{xx}\,|\underline{E}''| \qquad (10.14)$$

$$D_z'' = \sin(\xi-\theta_w'')\,|\underline{D}''| = \varepsilon_{zz} E_z'' = \sin(\xi-\theta_r'')\varepsilon_{zz}\,|\underline{E}''|$$

where the plus and minus signs arise because of the directions of the components D_x'' and D_z''. Thus, dividing by D_x and D_z results in the expression

$$\tan(\xi-\theta_w'') = \frac{\varepsilon_{zz}}{\varepsilon_{xx}} \tan(\xi-\theta_r'')$$

so that

$$\theta_r'' = \xi - \tan^{-1}\left[\frac{\alpha^2}{\gamma^2} \tan(\xi-\theta_w'')\right] \qquad (10.15)$$

In this way, values of the angles θ_r'' can be computed from the values of θ_w'' obtained from eqn (10.13).

As was discussed in Section 10.1, the energy of an electromagnetic field in an anisotropic medium is propagated in the direction of the ray. By using the Poynting vector $\underline{S}$ in eqn (10.3), the energy flux or intensity in the ray direction may be evaluated. That is, if ρ_r is taken to be the radiation energy density then, from eqn (10.3),

$$\rho_r v_r = \frac{c}{4\pi} (\underline{r} \cdot \underline{E} \times \underline{H})$$

which leads to the expression

$$\rho_r v_r = \frac{n_w c}{4\pi} \overline{E^2} (\theta_r - \theta_w) \qquad (10.16)$$

for the intensity of the electromagnetic field in the direction θ_r, where the bar denotes a time average. The general refractive index of wavenormals may be written as[2]

$$n_w = (|\underline{D}|^2 / \underline{E} \cdot \underline{D})^{\frac{1}{2}}$$

so that the direction-dependent wavenormal refractive index in the x z -plane is given by

$$\eta_w = \left(\frac{|\underline{D}|^2}{\frac{D_x'^2}{\varepsilon_{xx}} + \frac{D_z'^2}{\varepsilon_{zz}}} \right). \qquad (10.17)$$

Substituting the relevant expressions from eqn (10.14) into eqn (10.17) yields the expression

$$\eta_w = \left[\frac{\cos^2(\xi - \theta_w'')}{\alpha^2} + \frac{\sin^2(\xi - \theta_w'')}{\gamma^2} \right]^{-\frac{1}{2}} \qquad (10.18)$$

allowing the computation of the refractive indices η_w at each extraordinary wavenormal angle θ_w''. Returning to eqns (10.11) and (10.12),

$$\sin \theta_i = \sin \theta_w'' \eta_w$$

and

$$\sin \theta_i = \sin \theta_w' \beta$$

so that

$$\sin \theta_w' = \sin \theta_w'' \eta_w/\beta.$$

Thus

$$\cos \theta_w' = (1 - \sin^2\theta_w')^{\frac{1}{2}} = (1 - \sin^2\theta_w'' \eta_w^2/\beta^2)^{-\frac{1}{2}},$$

relating the extraordinary and ordinary wavenormal angles of refraction via the equation

$$\beta\cos\theta_w' = (\beta^2 - \sin^2\theta_w'' \eta_w^2)^{-\frac{1}{2}}. \qquad (10.18)$$

The absorption by a deep trap is assumed to be described by the classical model of a local field $\underline{F}$ acting on a guest molecule. The relationship between $\underline{F}$ and the total macroscopic electric field $\underline{E}$ is[10]

$$\underline{F} = \underline{\underline{d}} \cdot \underline{E} \qquad (10.20)$$

where $\underline{\underline{d}}$ is the local field tensor, the nature of which will be discussed in Section 10.2.1, and $\underline{E}$ is the macroscopic field defined in eqn (10.1). The transition moment $\underline{R}$ for the guest molecule is given by

$$\underline{R} = \text{constant}.\underline{\mu}$$

where $\underline{\mu}$ is the electric dipole moment of the transition. The absorption is determined by a projection of $\underline{R}$ onto the effective field[11] - a scalar product of the form

$$\underline{R} \cdot \underline{F} = \text{constant}.\underline{\mu} \cdot \underline{\underline{d}} \cdot \underline{E}.$$

Defining an *effective* electric dipole moment $\underline{\mu}'$ such that

$$\underline{\mu}' = \underline{\mu} \cdot \underline{\underline{d}} \qquad (10.21)$$

leads to a simplification of this absorption relation. The intensity absorbed per unit volume is proportional to

$$\overline{(\underline{\mu}' \cdot \underline{E})^2}$$

where the bar denotes a time average. If the incident light is polarized in the x z-plane and in the y-direction, respectively, the intensity of absorption will be proportional to

$$(\mu_x' \bar{E}_x + \mu_z' \bar{E}_z)^2$$

and $(\mu_y' \bar{E}_y)^2$, (10.22)

respectively. If t is the crystal thickness, the path lengths, l_y and l_{xz}, for each of the above polarizations will be

$$l_y = t \sec \theta_w'$$

$$l_{xz} = t \sec \theta_w'' \ . \tag{10.23}$$

A monochromatic beam of light of incident intensity I_0 falling on a specimen of thickness l containing m molecules of the absorbing species per cm^3, will have a transmitted intensity I given by

$$I = I_0 e^{-\alpha^c l}$$

where α^c is the absorption coefficient[12] and implicitly contains the m dependence. That is,

$$\frac{dI}{dl} = -I\alpha^c$$

so that integration over a path of unit length results in the expression

$$\alpha^c = - K(\lambda) \, I'/I$$

where I' is the *absorbed* intensity and K(λ) is the constant of integration which is wavelength dependent (λ). The intensities in the x z - and y-polarizations are given by eqns (10.22) while the intensity of the transmitted light is given by eqn (10.16). Consequently, the components of the absorption coefficient are found to be

$$\alpha^c_y = K(\lambda) \ (\mu_y' \bar{E}_y')^2 / \frac{c}{4\pi} \beta \cos 0 \ \overline{E'^2} \tag{10.24}$$

where

$$\theta_r' - \theta_w' = 0$$

for ordinary refraction and

$$\alpha^c_{xy} = K(\lambda)\ (\mu_x' \overline{E_x''} + \mu_z' \overline{E_z''})^2 / \frac{c}{4\pi}\eta_w \cos(\theta_r' - \theta_w'')\overline{E''^2}$$

for extraordinary refraction where the refractive index η_w is given by eqn (10.18). The components E_x'' and E_y'' may be expanded using eqn (10.14) so that

$$\alpha^c_{xy} = K(\lambda)[-\mu_x' \cos(\xi - \theta_r'') + \mu_z' \sin(\xi - \theta_r'')]^2 / \eta_w \cos(\theta_r'' - \theta_w''). \quad (10.25)$$

The absorbance A is defined as

$$A = \alpha^c l$$

so that, by substituting eqns (10.23), (10.24) and (10.25), the y- and xz- polarized absorbances are given by

$$A_y = K(\lambda)\ \mu_y'^2\ t \sec \theta_w'/\beta$$

$$A_{xz} = K(\lambda)[-\mu_x' \cos(\xi - \theta_r'') + \mu_z' \sin(\xi - \theta_r'')]^2 t \sec \theta_w''/\eta_w \cos(\theta_r'' - \theta_w''). \quad (10.26)$$

For convenience, a coordinate transformation is affected by a rotation of $-\xi$ about the y-axis so that the dielectric axis system is brought into coincidence with the crystallographic abc system. It is then appropriate to label quantities in terms of the crystallographic system rather than in terms of the optical coordinates. Thus A_y is labelled A_b and is unaltered while A_{xz} becomes

$$A_{ac} = K(\lambda)[-\mu_a' \cos\theta_r'' - \mu_c' \sin \theta_r'']^2 t \sec\theta_w''/\eta_w \cos(\theta_r'' - \theta_w''). \quad (10.27)$$

Figure 10.2 illustrates the orientation of the effective electric dipole moment within the crystallographic axis system where ζ is the angle between

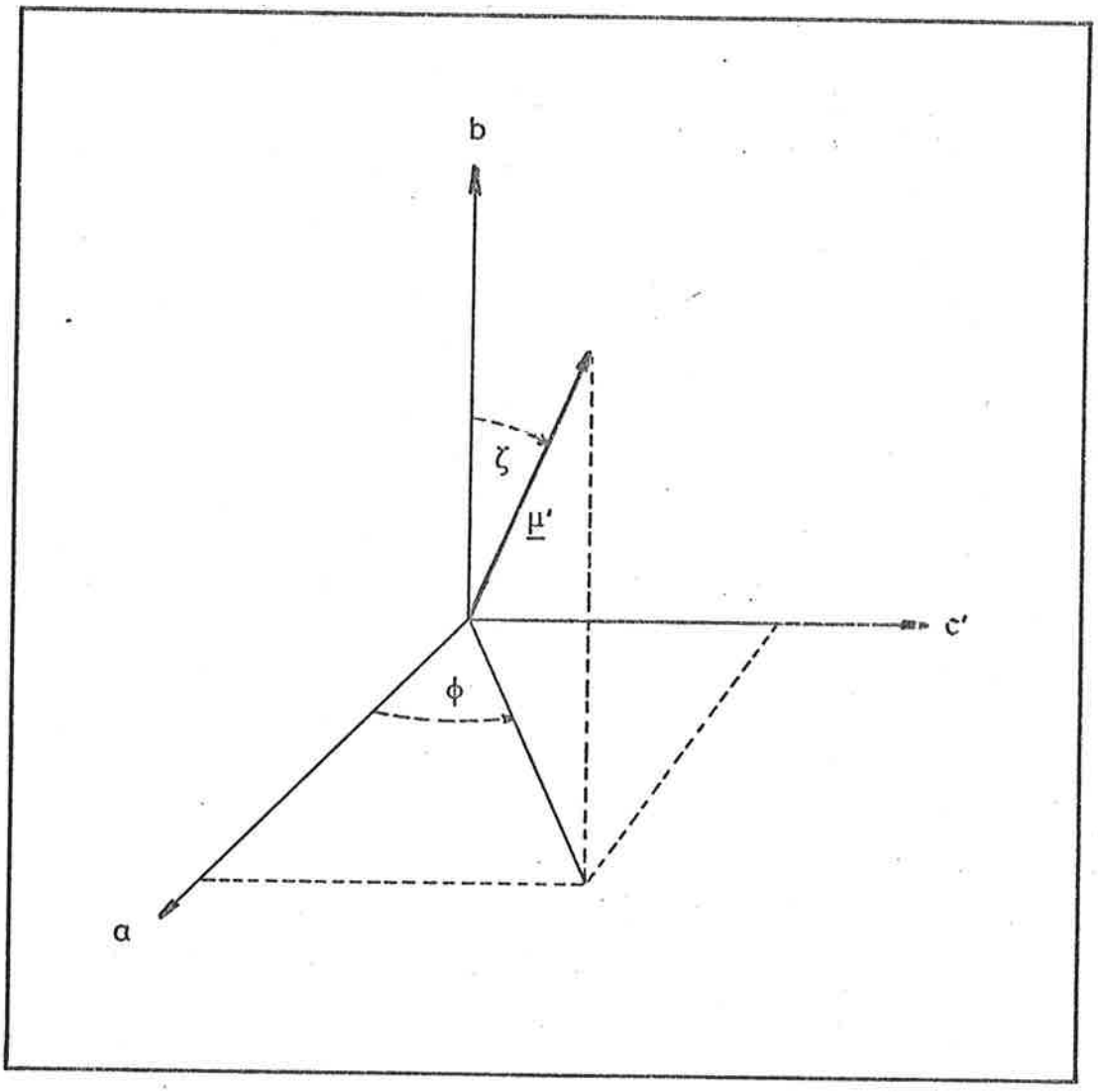

FIG.10.2 ORIENTATION CONVENTION FOR THE EFFECTIVE ELECTRIC DIPOLE MOMENT. (Left-handed coordinate system).

$\underline{\mu}'$ and the positive b-axis and ϕ is the angle between the ac' projection of $\underline{\mu}'$ and the positive a-axis. The axial components of $\underline{\mu}'$ may then be written

$$\mu_a' = |\underline{\mu}'| \sin\zeta \cos\phi$$
$$\mu_b' = |\underline{\mu}'| \cos\zeta \qquad (10.28)$$
$$\mu_c' = |\underline{\mu}'| \sin\zeta \sin\phi.$$

As a result,

$$A_b = K(\lambda)|\underline{\mu}'|^2 \cos\zeta\, t/\beta \cos\theta_w'$$

from eqn (10.26) and, by substituting eqn (10.19), A_b may be written in terms of the extraordinary wavenormal angle of refraction as follows:

$$A_b = K(\lambda)\ |\underline{\mu}'|^2 \cos^2\zeta\, t\ (\beta^2 - \sin^2\theta_w''\ \eta_w^2)^{-\frac{1}{2}}.$$

In the same way

$$A_{ac} = K(\lambda)|\underline{\mu}'|^2 \sin^2\zeta t[\cos\phi\cos\theta_r'' + \sin\phi\sin\theta_r'']^2/\eta_w\cos(\theta_r''-\theta_w'')\cos\theta_w''.$$

Letting

$$K = K(\lambda)|\underline{\mu}'|^2 t\ \cos^2\zeta,$$

the equations for A_b and A_{ac} simplify to

$$A_b = K(\beta^2 - \sin^2\theta_w''\ \eta_w^2)^{-\frac{1}{2}} \qquad (10.29)$$

and

$$A_{ac} = K \tan^2\zeta(\cos\phi\cos\theta_r'' + \sin\phi\sin\theta_r'')^2/\eta_w\cos(\theta_r'' - \theta_w'')\cos\theta_w'' \qquad (10.30)$$

where K, as a function of wavelength, describes the shape of the absorption band and A_b and A_{ac} are now expressed completely in terms of the effective electric dipole orientation and the extraordinary refraction angles θ_w'' and θ_r''.

It is of further interest to define an isotropic absorbance A_{iso} which is of use in estimating the dopant concentration, as a practical point. This is defined as

$$A_{iso} = \frac{1}{3}\,(A_a^0 + A_b^0 + A_{c'}^0) \tag{10.31}$$

where A_a^0, A_b^0 and $A_{c'}^0$ are the purely a-, b- and c′- polarized components of absorbance. The A_b^0 component arises when the $\underline{E}$ vector is collinear with the b- axis and consequently occurs when the ray is collinear with the c- axis. Thus θ_r'' is zero and simplifies eqn (10.15) to the form

$$(\theta_w'')_b^0 = \xi - \tan^{-1}\left\{\frac{\gamma^2}{\alpha^2}\tan\xi\right\}. \tag{10.32}$$

The angle $(\theta_w'')_b^0$ corresponding to the b- polarized component of $\underline{E}$ may then be calculated from eqn (10.32) and is used to evaluate A_b^0 from eqn (10.29). From eqns (10.28)

$$\begin{aligned} A_a^0 &= A_b^0 \tan^2\zeta\cos^2\phi \\ A_{c'}^0 &= A_a^0 \tan^2\phi \end{aligned} \tag{10.33}$$

so that A_a^0 and $A_{c'}^0$ may be computed from the A_b^0 component.

Summary

By way of a summary, the following is the procedure for the computation of the orientation of the transition moment in terms of the angles ϕ and ζ from the experimental data.

Required experimental data:

(i) measured b- and ac- polarized absorbances as functions of the angles of incidence θ_i;

(ii) the refractive indices α, β, γ;

(iii) the angle ξ between the optical z- axis and the crystallographic c´- axis in the ac-plane (see figure 10.1);

(iv) the optic axial angle Ω_w.

Procedure for computation:

(i) compute the set of wavenormal angles θ_w'' for extraordinary refraction from the measured angles of incidence using Newton's method of evaluating the roots of equation (10.13);

(ii) using eqn (10.15), the set of corresponding ray angles θ_r'' may be computed from the θ_w'' ;

(iii) the refractive indices of wavenormals in the ac-plane, η_w, may be computed from eqn (10.18);

(iv) the absorbances A_{ac} computed from eqn (10.30) may be fitted to the measured ac-polarized absorbances using the method of non-linear least squares. The variables are the absorbances A_{ac} and the angles θ_r'' and θ_w'' while the fitting parameters are the total entity $K \tan^2\zeta$ and the angle ϕ;

(v) using a linear least squares procedure, the computed absorbances A_b from eqn (10.29) may be fitted to the measured values. The variables are the absorbances A_b and the angles θ_w'' while the only parameter is the constant K. In this way, the angle ζ can be evaluated from the non-linear least squares parameter $K \tan^2 \zeta$.

(vi) finally, the isotropic absorbance is calculated from eqns (10.29), (10.31), (10.32) and (10.33).

10.2.1 *Optical Data for Anthracene*

The optical data required for these calculations include the principal refractive indices α, β and γ and the angle ξ between the z-axis and the crystallographic c′- axis in the ac-plane at 4.2°K, the temperature at which the absorption spectra were measured. While there is no published data for the dispersion curves of α and γ at low temperatures for anthracene, there is data for β and the refractive indices of wavenormals η_w in the ac-plane measured at normal incidence at 300°K,[6,8] 140°K,[7] 95°K,[8] and 20.4°K.[9] This data will allow a computation of the other refractive indices α and γ as follows.

The angle of indicence I_w for which the wavenormal is refracted along the direction of the optic axis of wavenormals is given by the equation for ordinary refraction (10.11). Furthermore it can be seen from figure 10.1 that the wavenormal optic axis angle Ω_w would then be given by

$$\Omega_w = \xi + \sin^{-1} (\beta^{-1} \sin I_w). \qquad (10.34)$$

Equation (10.8) gives the extraordinary refractive index of wavenormals for a general direction of propagation. When refraction of the wavenormal is along the crystallographic c′- axis, that is at normal incidence, this equation reduces to

$$\frac{1}{\eta^2} = \frac{\cos^2\xi}{\alpha^2} + \frac{\sin^2\xi}{\gamma^2}, \qquad (10.35)$$

where η is the extraordinary refractive index of wavenormals for *normal incidence*. When refraction of the extraordinary wave lies in the direction of an optic axis of wavenormals, the b- and ac- polarized waves are parallel and $\eta_w = \beta$. In such a case, eqn (10.18) reduces to

$$\frac{1}{\beta^2} = \frac{\cos^2\Omega_w}{\alpha^2} + \frac{\sin^2\xi_w}{\gamma^2} \qquad (10.36)$$

β being independent of the direction of propagation. Solving eqns (10.35) and (10.36) simultaneously in terms of β and η yields the results

$$\frac{1}{\alpha^2} = \left(\frac{1}{\beta^2\sin^2\Omega_w} - \frac{1}{\eta^2\sin^2\xi}\right) \Big/ \left(\frac{1}{\tan^2\Omega_w} - \frac{1}{\tan^2\xi}\right) \qquad (10.37)$$

and

$$\frac{1}{\gamma^2} = \left(\frac{1}{\beta^2\cos^2\Omega_w} - \frac{1}{\eta^2\cos^2\xi}\right) \Big/ (\tan^2\Omega_w - \tan^2\xi). \qquad (10.38)$$

In this way, using published data for β and η at normal incidence and measured values of I_w, the quantities α and γ may be obtained from eqns (10.34), (10.37) and (10.38). The determination of the angles I_w and ξ and the extrapolations necessary to estimate the required refractive indices α, β and γ at 4.2°K from the data at higher temperatures will be discussed in Section 11.

10.2.2 *The Local Electric Field.*

In the classical theory of dielectric media, the polarizability of each atom (or oscillator) is assumed to be the same in the crystal as in the gas. However, the presence of an applied macroscopic field produces an induced dipole field within the neighbouring region and is taken to reinforce the macroscopic field at the site of the oscillator. This is the basis to the concept of the local electric field. Such a concept, however, is unnecessary in a proper quantum-mechanical approach because the very presence of a neighbour modifies the wavefunction, and thus the polarizability, of each oscillator even in the absence of the macroscopic field. In this way, the calculated wavefunctions include all interactions

between oscillators and the correct value of the field would be the macroscopic field and not a local field. This point has been illustrated by perturbational and self-consistent field calculations of the non-resonant interaction between a crystal and an incident macroscopic field[13] where, for at least cubic crystals, the quantum-mechanical result reduces to the classical local field model. It is to be appreciated, however, that the extension of such a theory to real, anisotropic molecular crystals would be no mean task and, as a consequence, the quantum-mechanical theory is beyond the scope of this work.

A simple classical approach[3] has been to consider a sphere, large relative to atomic dimensions and centred on the oscillator in question, as being the boundary of a continuous dielectric within a specimen. If the applied macroscopic field is defined as the field produced *outside* the specimen and incident on it, then the local field at a general lattice site within the crystal is the sum of the depolarization field produced by a surface charge on the outer surface of the sample, the Lorentz field from the induced charges on the inside surface of the boundary sphere and the field of the oscillators within this cavity. It is then clear that the macroscopic field $\underline{E}$, which is dealt with in the optics of anisotropic media (eqn 10.1), is the sum of the applied field and the depolarization field. Assuming that the applied field is uniform and induces a uniform polarization $\underline{P}$ in a *cubic* sample, which may be considered as being a continuous isotropic dielectric, the local field $\underline{F}$ may be written[3] as

$$\underline{F} = \underline{E} + \frac{4\pi}{3}\underline{P} \qquad (10.39)$$

where

$$\underline{P} = \underline{\underline{\chi}}\,\underline{E}. \qquad (10.40)$$

$\underline{\underline{\chi}}$ is the dielectric susceptibility tensor being a diagonal matrix with all non-zero elements equal to χ for isotropic media. The dielectric constant ε for an isotropic medium is related to the isotropic dielectric susceptibility χ by[2]

$$\varepsilon = 1 + 4\pi\chi. \tag{10.41}$$

This then allows an application of these equations to anisotropic media since eqn (10.41) may be used to describe each of the principal dielectric constants ε_{xx}, ε_{yy} and ε_{zz}. Applying eqns (10.39), (10.40) and (10.41) to the local field equation (10.20) and replacing the isotropic dielectric susceptibility tensor by an anisotropic form $\underline{\underline{\chi}}'_{anis}$, results in the following form of the local field tensor $\underline{\underline{d}}$:

$$\underline{\underline{d}} = \underline{\underline{1}} + \frac{1}{3}\underline{\underline{\chi}}'_{anis} \tag{10.42}$$

where

$$\underline{\underline{\chi}}'_{anis} = \begin{pmatrix} \varepsilon_{xx}-1 & 0 & 0 \\ 0 & \varepsilon_{yy}-1 & 0 \\ 0 & 0 & \varepsilon_{zz}-1 \end{pmatrix}, \tag{10.43}$$

for the principal dielectric coordinate system. Since the computation of the orientation of the transition moment given in Section 10.2 was carried out with respect to the crystallographic axis system, a coordinate transformation on eqn (10.42) is required. The matrix $\underline{\underline{\chi}}'_{anis}$ is described with respect to the crystallographic coordinate system by a similarity transformation using the rotation matrix $\underline{R}_0$. That is,

$$\underline{\underline{\chi}}'_{anis} = \underline{R}_0^{-1}\, \underline{\underline{\chi}}'_{anis}\, \underline{R}_0 .$$

where

$$\underline{R}_0 = \begin{pmatrix} \cos\xi & 0 & -\sin\xi \\ 0 & 1 & 0 \\ \sin\xi & 0 & \cos\xi \end{pmatrix}$$

and $\underline{\underline{\chi}}_{anis}$ is the transformed tensor. Thus, making the further replacements from eqns (10.8),

$$\underline{\underline{\chi}}_{anis} = \begin{bmatrix} (\alpha^2-1)\cos^2\xi + (\gamma^2-1)\sin^2\xi & 0 & -(\alpha^2-1)\cos\xi\sin\xi + (\gamma^2-1)\cos\xi\sin\xi \\ 0 & \beta^2-1 & 0 \\ -(\alpha^2-1)\cos\xi\sin\xi + (\gamma^2-1)\cos\xi\sin\xi & & (\alpha^2-1)\sin^2\xi + (\gamma^2-1)\cos^2\xi \end{bmatrix} \tag{10.44}$$

and eqn (10.42) becomes

$$\underline{\underline{d}}_{anis} = 1 + \frac{1}{3}\underline{\underline{\chi}}_{anis} \tag{10.45}$$

where $\underline{\underline{d}}_{anis}$ will denote the anisotropic Lorentz local field tensor[14] in the crystallographic axis system.

Vuks[15] has defined the classical Lorentz field in terms of an average refractive index

$$n^2_{ave} = (\alpha^2 + \beta^2 + \gamma^2)/3$$

so that[14]

$$\underline{\underline{d}}_{iso} = \left(\frac{n^2_{ave}+2}{3}\right)\underline{1}, \tag{10.46}$$

which is an entirely isotropic local field tensor used to describe anisotropic media. Local field tensors for molecular crystals have also been derived using a self-consistent, classical point-dipole approximation.[10] Chen *et alia*,[16] Cummins *et alia*[17] and Bridge[18] have independently illustrated that this theory for two molecules per unit cell has two degrees of freedom and thus a continuum of solutions. By selecting most probable[14] or constrained[18,19] solutions of the point-dipole approximation, local field tensors have been derived which are at some variance with the forms

given in eqns (10.45) and (10.46). In particular, work by Bridge[18] has shown that corrected electric dipole moments for guest molecules obtained by the application of point-dipole local field tensors to eqn (10.21) are highly localized about a preferred axis and are not within the plane of a host molecule. This adds further weight to the belief that the point-dipole approximation is not valid for a crystal such as anthracene where the distance between nearest neighbours is much less than the length of the molecule itself. In such a situation, the atomic nature of the molecule would be expected to be of some significance. On the other hand, a very recent point-dipole analysis of this problem,[20] based on a fourier analysis method, has been suggested as being more accurate than former theories. However, an application of the theory is, as yet, unavailable. Thus, only the local field tensors of eqns (10.45) and (10.46) will be investigated in this work and applied to eqn (10.21) to calculate the actual electric dipole moment $\underline{\mu}$ from the effective moment $\underline{\mu}'$ measured from experiment. That is,

$$\underline{\mu} = \underline{\mu}' \cdot \underline{d}^{-1}. \qquad (10.47)$$

11 EXPERIMENTAL STUDY

The two traps observed for each of the systems 1-aminoanthracene in anthracene and 2-aminoanthracene in anthracene[21] are resolved only at very low temperatures and appear as two separate but overlapping systems of bands in fluorescence. In absorption, however, only the two traps of the 2-aminoanthracene case are observed while, in the case of 1-aminoanthracene, the higher energy trap appears to be masked by the phonon structure of the low energy trap. Thus, only the orientations of the three observed traps can be determined by the absorption method discussed in the previous section. However, the complete results for 2-aminoanthracene make it possible to also discuss the analogous 1-aminoanthracene case.

The necessary absorption spectra are to be determined with light polarized in and perpendicular to the crystallographic ac-plane as a function of the angle of incidence. It is then necessary to identify the position of the b-axis for each crystal and to orient it in the direction of the axis of rotation. The subsequent determination of the absorption spectra is complicated by various factors such as the shape of the background to the spectral lines of interest, the depolarizing effects of misalignment of the crystal and scattering effects. The methods by which these problems have been approached in this work will be described but, as a test of the overall procedure, the system tetracene in anthracene was also studied since the orientation of the tetracene molecules has been determined by other methods.[1, 22]

11.1 Materials

The purification and sample preparation procedures for the materials

used in this study are described in detail in Chapter II. Crystal thickness and dopant concentration are not required as part of the computation of the transition moment orientation. However, these quantities are of interest from a practical viewpoint and, with respect to dopant concentrations, it is necessary to know whether guest-guest interactions may be significant.

Crystal thickness was measured by means of a polarizing microscope in the conoscopic mode.[23] The Bertrand method was employed whereby the interference figure could be viewed against a micrometer scale in the ocular. In this way, the number of fringes per scale division yielded the crystal thickness directly. Estimates of dopant concentration may be obtained using solution values of the molar absorptivities, room temperature crystal thicknesses as measured above and isotropic absorbances as defined in eqn (10,38). The molar concentrations of dopant thus calculated may be converted to mole/mole concentrations if the density of the host is known. Of the several approximations involved in this method, the estimation of the correct molar absorptivity presents the greatest problem since, for example, the transitions being observed for 1- and 2- aminoanthracene at $4.2^{o}K$[21] is hidden beneath a wide, structureless band at room temperature in solution.[24] Thus an independent method of concentration determination was also attempted. Beer's law for two independent species in solution with overlapping absorption bands is given as

$$A_T^{\lambda} = (\varepsilon_1^{\lambda} C_1 + \varepsilon_2^{\lambda} C_2)b \qquad (11.1)$$

where A_T^{λ} is the total absorbance at wavelength λ, ε_1^{λ} and ε_2^{λ} are the molar absorptivities at wavelength λ for each of the species denoted 1 and 2, b is the cell path length and C_1 and C_2 are the respective molar concentra-

tions. A non-linear least squares fit of eqn (11.1) to measured total absorbance data will yield the concentrations C_1 and C_2 with ε_1^{λ} and ε_2^{λ} being set as constants. The procedure involves dissolving an individual crystal in a suitable solvent and carrying out the above analysis to determine the concentrations of host and guest and thus to obtain the mole/mole concentrations. In practice, however, the very low dopant concentration is a severe restriction which can be countered, to some extent, by the use of a low volume "trough" cell. Such a cell was used, having a calibrated path length of 1.016cm and a volume of only $0.5cm^3$ compared to the usual $3cm^3$ for a normal 1cm cell. This means that concentrations would be some seven times higher than could be usually expected.

The orientation of the crystals could be established by observation under a polarizing microscope in the conoscopic mode. Since the extended face of the anthracene platelets is the crystallographic ab-plane, the optic axis plane (ac-plane) will be normal to the direction of the b-axis. Thus the optic axes emerge from the extended face of the crystal. The interference figure seen in the conoscopic mode appears as a black spot surrounded by interference fringes.[23] This spot is the point of emergence of one of the optic axes while the other occurs outside the field of view, being at a more acute angle to the ab-plane, as shown in figure 11.1. The position of this "*observed*" optic axis, as well as the points of maximum and zero extinction as the crystal is rotated between crossed polars, consequently fixes the direction of the crystallographic b-axis.

The overall procedure for sample handling was as follows. Single sublimation-grown crystals of doped anthracene were mounted, three at a time, over the small holes in the sample disc of the liquid helium cryostat

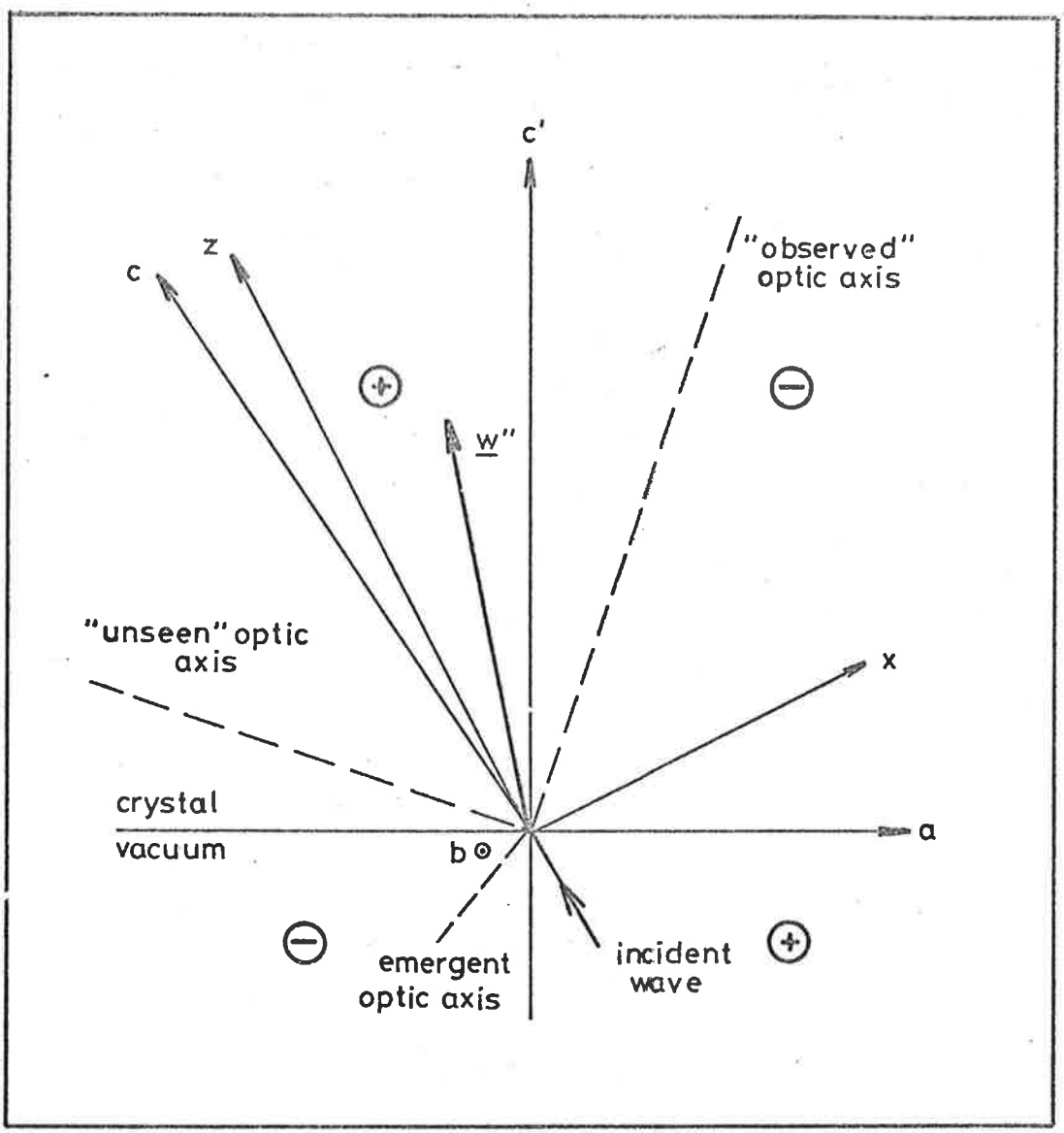

FIG. 11.1 SIGN CONVENTION FOR ANGLES IN ac-PLANE. Sign given in each quadrant of the abc-coordinate system in the ac-plane.

described in Chapter II. The adhesive used was glycerol which enables the crystals to be oriented on the disc as required and yet freezes to a clear, glassy matrix at low temperatures providing a useful thermal contact between cryostat and sample. However, no glycerol was allowed to cover the crystal over the aperture in the sample disc. Each crystal could then be viewed under the microscope to determine the orientation of the b-axis which was fixed along a fudicial mark on the sample disc. As well, the position of the optic axis was noted since, referring to figure 11.1, the crystals had to be oriented in such a way that light was refracted either in the dielectric z-axis side of the crystallographic c-axis or in the opposite quadrant containing the observed optic axis. This restriction was necessary because the cryostat could be turned only 15^{o} one way and 43.5^{o} the other. As a means of identifying in which quadrant the refracted beam lay, a sign convention was adopted as shown in figure 11.1. In this way, negative angles of incidence identify refracted waves in the x-axis quadrant while positive angles occur in the z-axis quadrant. Once the crystals were oriented on the sample disc, the crystal thickness was determined, as described, at five points over the aperture in the disc. The average thickness could then be measured with some indication of the variation in uniformity. The sample disc was then bolted to the mounting platform of the liquid helium cryostat, aligning the fudicial mark on the disc with the marked rotation axis of the cryostat. If, after the relevant low temperature spectra were measured, crystals were required for dopant concentration measurements by the solution method described earlier, the crystals could be floated off the sample disc onto water.

11.2 Spectrophotometry

Specific details of the Hilger D-460 spectrophotometer used in conjunction with the liquid helium cryostat are given in Chapter II. Before spectral measurements were taken, a check was made of the effects of crystal misalignment and depolarization caused by gross variations in the uniformity of a crystal which may appear as the angle of incidence is varied. With the crystal set at normal incidence, the polarizer on the spectrophotometer and another polarizer placed between light source and crystal were adjusted to eliminate any transmitted light. This implies that one of the polarizers is parallel to the b-axis of the crystal while the other is perpendicular to it. The cryostat was then rotated through 43.5^{o} and any misalignment or crystal distortion was revealed by the consequent depolarization, this generally being of the order of 1% or less.

Transmission spectra was recorded for angles of incidence between -15^{o} and $+43.5^{o}$, using the sign convention introduced in Section 11.1, at intervals of 5^{o}. On the fewer occasions where the position of the optic axis was to be determined, the angle of incidence was varied between 0^{o} and -43.5^{o}. In all cases, the angle was first increased then decreased in the range selected and at each setting the transmission spectrum was recorded four times with the spectrophotometer polarizer set successively at 0^{o}, 90^{o}, 180^{o} and 270^{o} to the vertical. In this way, errors due to non-uniformities in the crystal and to possible small misalignments of the cryostat are expected to be randomized. Figure 11.2 illustrates full transmission spectra for tetracene, 1-aminoanthracene and 2-aminoanthracene in anthracene at angles of incidence of 0^{o} and 30^{o}. The spectral lines

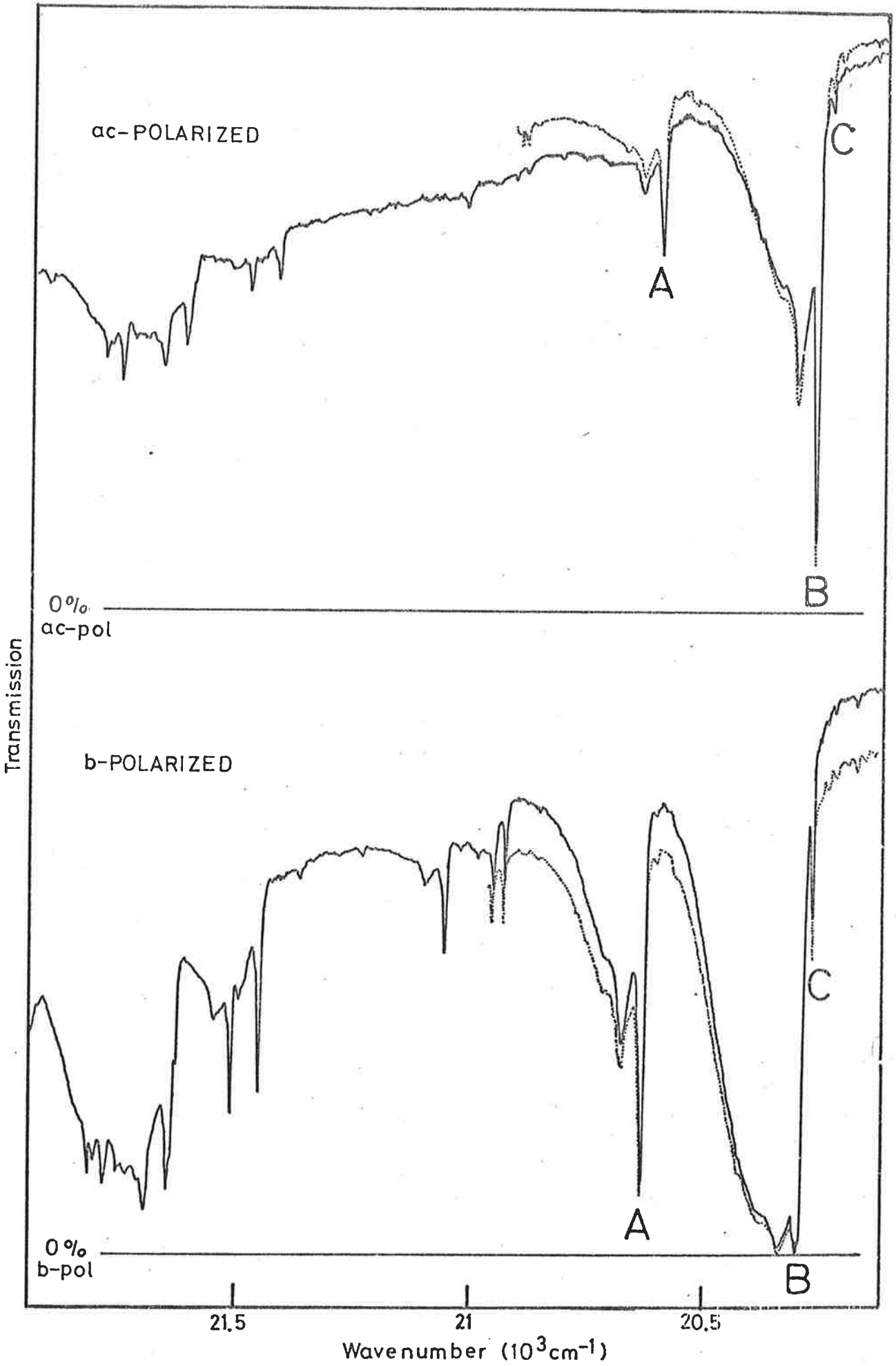

FIG. 11.2(a) ABSORPTION OF TETRACENE IN ANTHRACENE. Guest concentration 0.002 mol/mol. Angle of incidence 0° (——); 30° (- - - - - - - -). Traps TETA, TETB and TETC indicated.

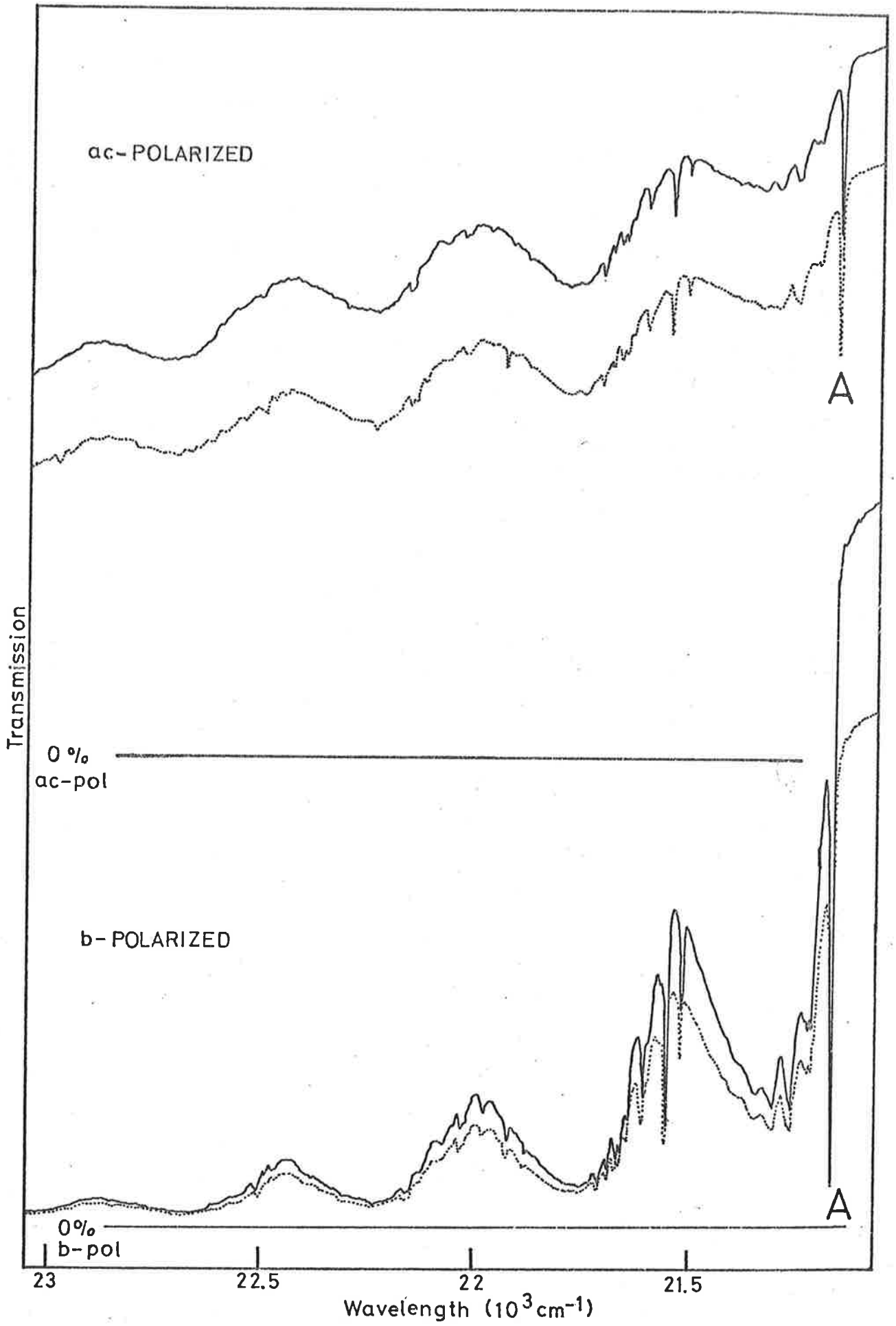

FIG. 11.2 (b) ABSORPTION OF 1-AMINOANTHRACENE IN ANTHRACENE. Guest concentration 0.003 mol/mol. Angle of incidence 0° (——); 30° (·····). Trap 1A indicated.

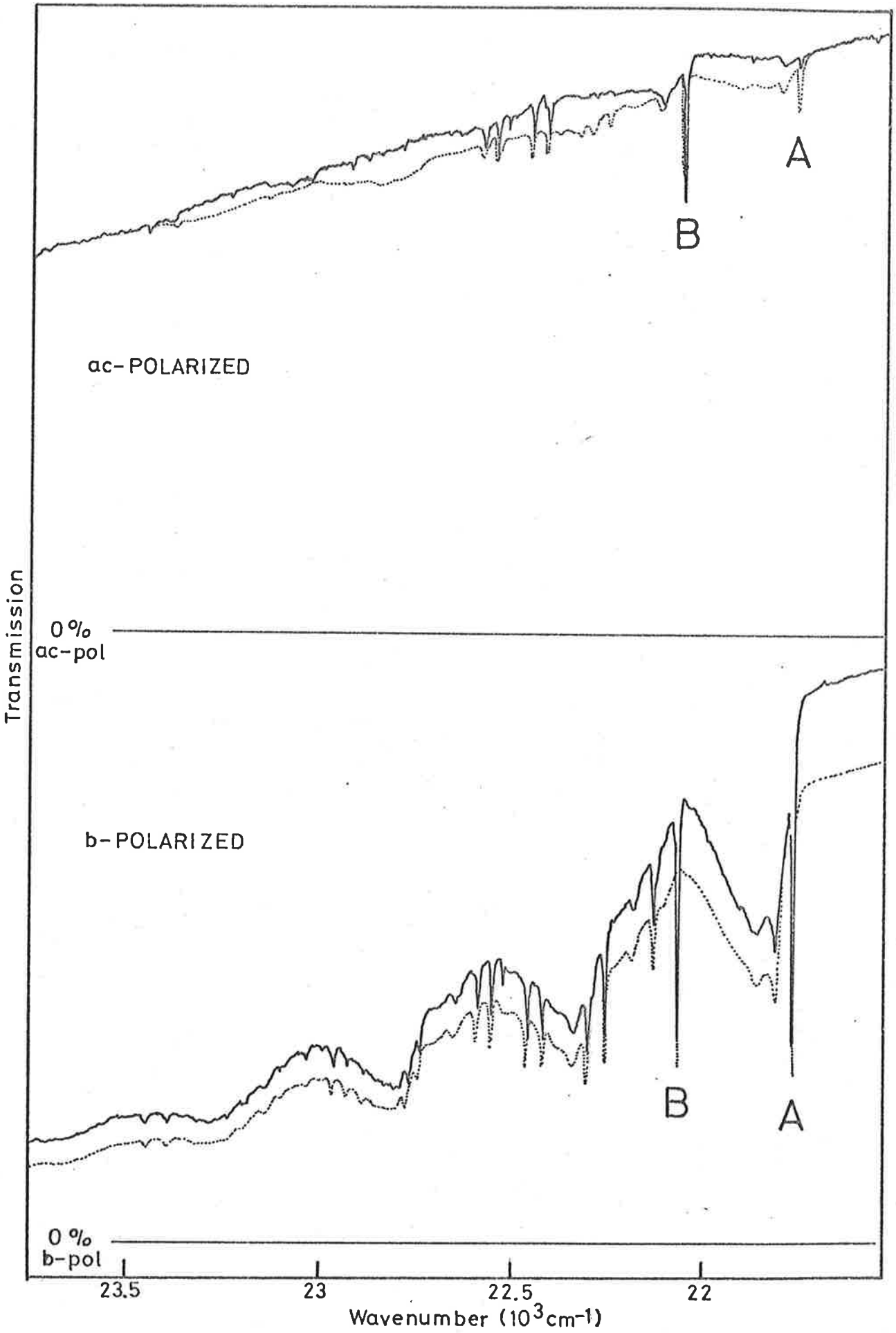

FIG. 11.2(c) ABSORPTION OF 2-AMINOANTHRACENE IN ANTHRACENE. Guest concentration 0.004 mol/mol. Angle of incidence 0° (——); 30° (– – –). Traps 2A and 2B indicated.

of interest have been labelled TETA, TETB and TETC for tetracene, 1A for 1-aminoanthracene and 2A and 2B for 2-aminoanthracene. The latter three labels correspond to the notation used by Bridge and Vincent[21] to distinguish the double traps produced by these materials. In order to calculate the absorbances of each of these spectral lines, one must determine the 0% and 100% transmittance levels. The zero transmittance level is set on the spectrum, as shown in figure 11.2, by closing the entrance slit on the spectrophotometer. The 100% level is taken to be the background baseline on which the spectral lines stand. The form of this baseline in each case is not intrinsically assessable. However its position may be estimated and it is considered that, if a consistent method is used to reproduce it for each spectrum measured, then absorbances calculated at the various angles of incidence would be little affected. In addition, the use of such a baseline corrects somewhat for variations caused by scattering losses because it would be expected that both line intensities and the background baseline would be altered by such effects. Figure 11.3 shows the way in which these baselines were established for each of the traps studied, the same method being used at each angle of incidence.

Referring to figure 11.3, I is the intensity of the spectral line of interest while I_0 is the incident light intensity obtained from the position of the baseline. In this way, the transmittance of each line was obtained from the ratio I/I_0. The procedure yielded two b-polarized and two ac-polarized transmittances at each angle of incidence so that an average measurement could be obtained with some indication of the possible error in transmittance. As a result, b-polarized and ac-polarized absorbances were calculated from these transmittances as a function of the

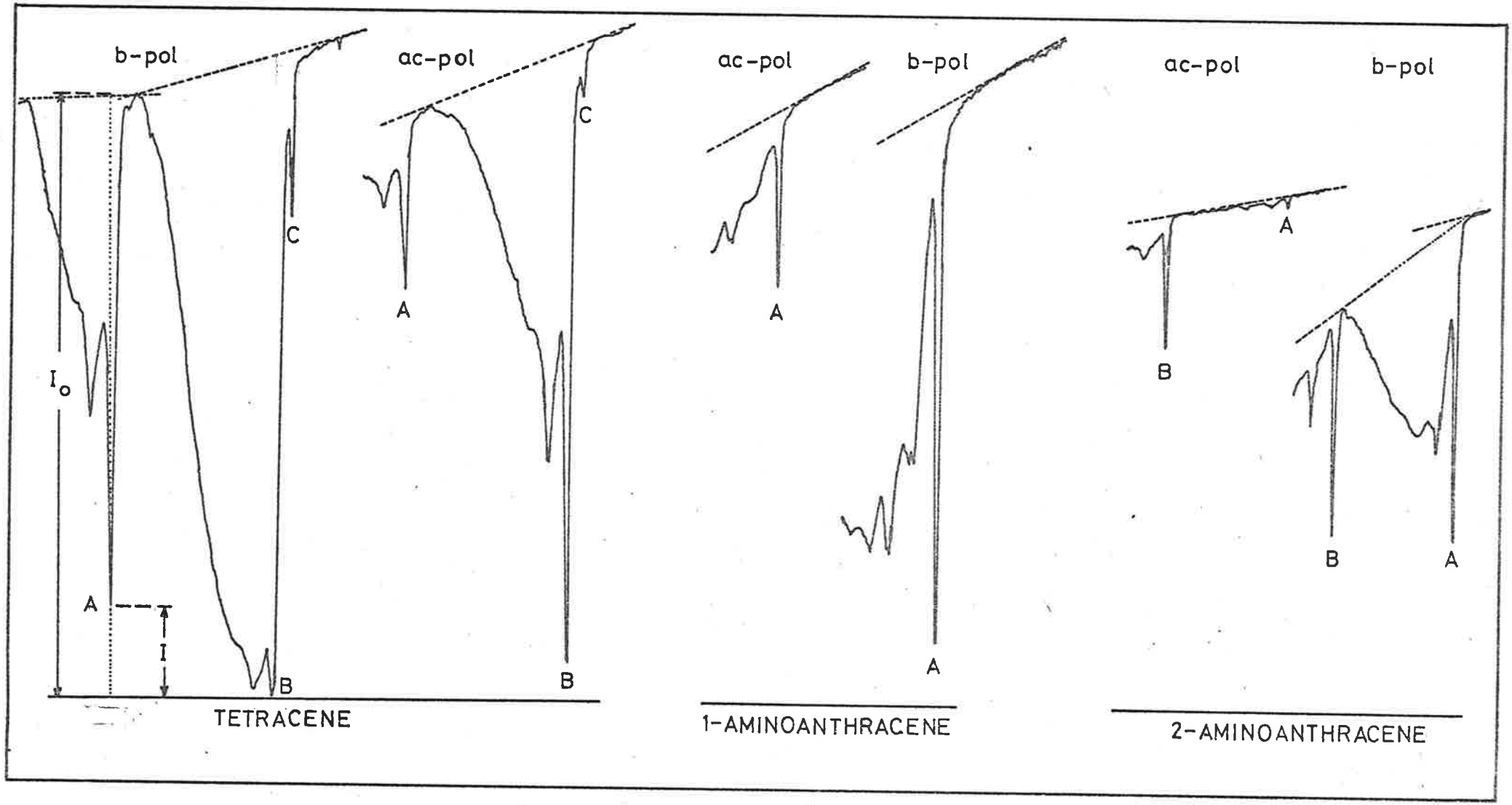

FIG. 11.3 BASELINE PLACEMENTS FOR GUEST-HOST SYSTEMS STUDIED.
Baselines shown as broken lines:---------.

angle of incidence together with estimates of the errors in absorbance. This constitutes the basic data needed to compute the transition moment orientations.

11.3 Calculation of Ancillary Data

11.3.1 *Optical Data*

To calculate transition moment orientations from the above absorbance data, optical data at 4.2°K was required. However, as noted in Section 10.2.1, only values of the refractive indices β and η_w at normal incidence are available for temperatures between 20.4°K and 298°K.[6-9] The computation of the refractive indices α, β and γ at 4.2°K then requires a knowledge of the angles ξ and Ω_w and a method by which optical data at the higher temperatures can be extrapolated to 4.2°K.

The room temperature results of Obreimov *et alia*[6] show that the dispersion of the angle ξ is negligible for wavelengths between 578nm and 405nm. That is, $\xi = 29.6^\circ$ with a standard deviation of 0.7° in this wavelength range. From room temperature crystallographic data[25] for anthracene, the ac projection of the long (L) axis of the anthracene molecule lies at 29.9° to the c′- axis, which coincides with the value of ξ above to within the standard deviation noted. This fact endorses the idea that the dielectric z-axis, being the direction of maximum *crystal* polarizability, lies very closely in the direction of maximum *molecular* polarizability. It is assumed that this coincidence also applies at lower temperatures and hence, from crystal data at 95°K,[25] $\xi = 31.1^\circ$. As this represents a change of only about 5% from the room temperature value, it is further assumed that the value of 31.1° applies at all temper-

atures below 140°K.

By measuring the behaviour of the dopant absorption for angles of incidence between 0° and -43.5°, the apparently anomalous effects caused by internal conical refraction indicate the position of the optic axis of wavenormals which lies on the x-axis side of the c′-axis. The form of this anomalous absorption is illustrated in figure 11.4 which shows plots of measured b- and ac- polarized absorbances for light refracted in the x-axis quadrant containing the "observed" optic axis as given in figure 11.1. The quite apparent localized depolarization of this absorbance data gives either direct or estimated values of the angles of incidence I_w at which light is refracted along each of the optic axes of wavenormals corresponding to the wavelengths of absorption for the traps TETA, 1A, 2A and 2B. That is, figure 11.4 clearly demonstrates the dispersion of the optic axis of wavenormals. The optic axial angle Ω_w at each of the relevant wavelengths may be computed from eqn (10.34). This was done using the values of I_w measured at 4.2°K with β values interpolated from the published data[6-9] at various wavelengths and at temperatures between 140°K and 20.4°K. The results of these calculations are given in table 11.1 which also includes the interpolated Ω_w values obtained from eqns (10.36)-(10.38) using the complete set of room temperature refractive indices of Obreimov *et alia*.[6] Although values of I_w measured at 4.2°K were used to calculate the Ω_w values below 140°K, a continuous correspondence appears to exist even with the independent room temperature data.

Having obtained the necessary values for the angles ξ and Ω_w, the refractive indices α were calculated from eqns (10.37) and (10.38) using

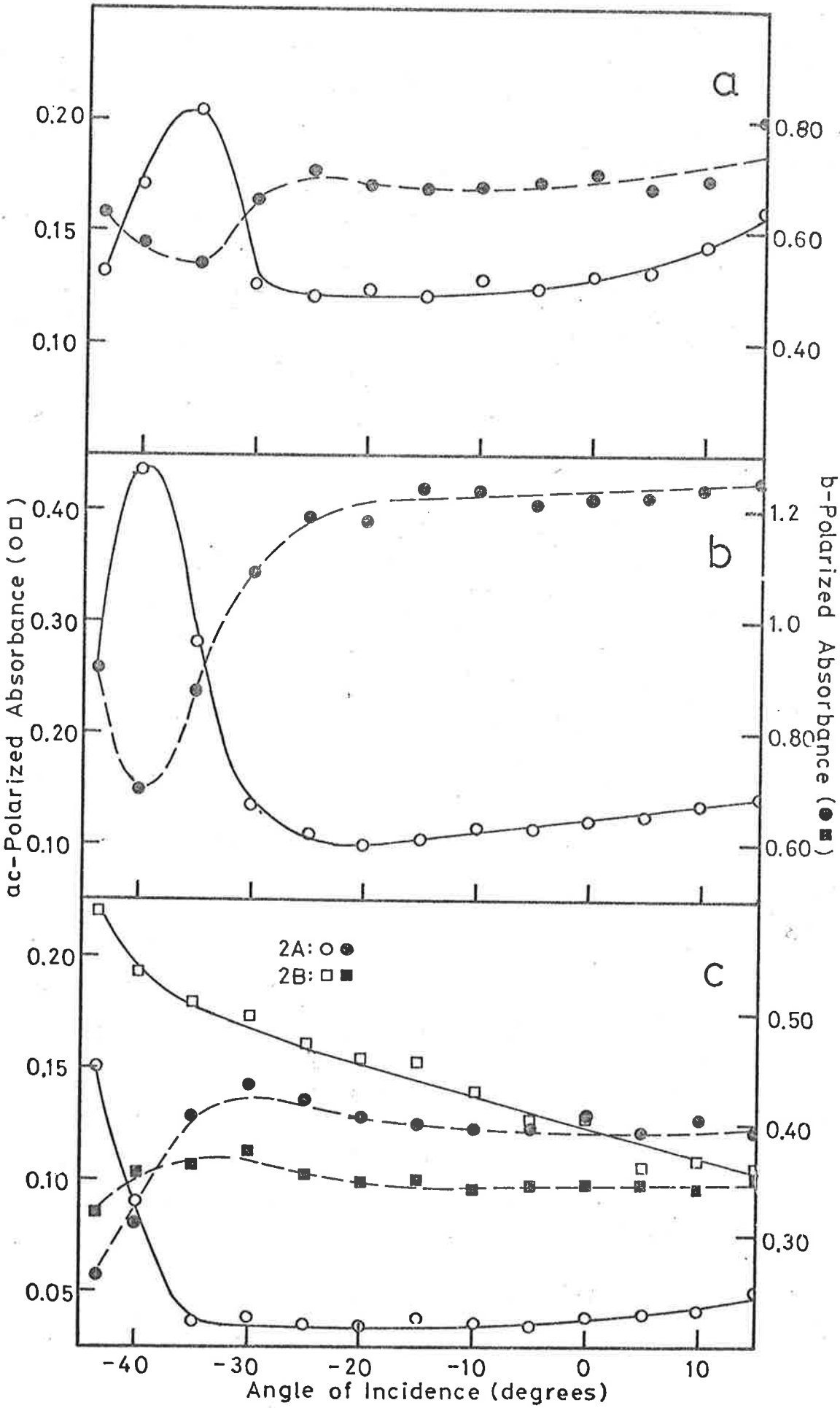

FIG. 11.4 EXPERIMENTAL EFFECTS OF INTERNAL CONICAL REFRACTION. (a) Tetracene, trap TETA; (b) 1-aminoanthracene, trap 1A; (c) 2-aminoanthracene, traps 2A and 2B.

TABLE 11.1

Optical Constants for Anthracene

(Quantities are shown at each temperature of interest)

Trap	Wavelength of Trap Absorption (nm)	I_w (degrees)	298° K *				140° K				95° K				20.4° K				4.2° K		
			Ω_w	α	β	γ	Ω_w	α	β	γ	Ω_w	α	β	γ	Ω_w	α	β	γ	α	β	γ
TETA	486.2	37	47.0	1.590	1.863	2.264	49.6	1.611	1.895	2.229	50.1	1.534	1.847	2.230	50.3	1.643	1.830	2.003	1.627	1.816	1.992
1A	472.2	39	47.6	1.595	1.880	2.286	50.3	1.605	1.915	2.275	50.5	1.548	1.892	2.322	51.0	1.635	1.850	2.048	1.624	1.842	2.047
2A	458.6	45	48.7	1.600	1.904	2.310	52.2	1.614	1.944	2.277	52.5	1.583	1.938	2.306	53.1	1.624	1.889	2.111	1.618	1.885	2.109
2B	452.8	46	49.3	1.603	1.917	2.320	52.6	1.615	1.960	2.305	52.7	1.598	1.954	2.314	53.2	1.615	1.910	2.167	1.611	1.906	2.162

* from ref (6)

the available β and η_w data.[6-9] The refractive indices at the wavelengths of interest were interpolated from the resultant dispersion curves. The behaviour of these refractive indices with temperature in the range 298°K to 20.4°K is not linear. However, in the range 20.4°K to 140°K the behaviour is very close to being linear so that a linear extrapolation was used in this range to obtain the refractive indices at 4.2°K. The results of all the above calculations are also presented in table 11.1. Calculations of the transition moment orientations could then be carried out with each set of data so that the effects of the various extrapolations, interpolations and other approximations could be quantified.

11.3.2 *Doped Crystal Parameters*

Some results of dopant concentration determinations by the solution method described in Section 11.1 are presented in table 11.2 for the systems tetracene in anthracene and 2-aminoanthracene in anthracene. Accurate absorption spectra of these separate materials in toluene were measured using the purified samples prepared for the transition moment orientation experiments, yielding the required ε^{λ} values for the host and guests. Absorption spectra of particular crystals were subsequently determined, using the trough cell, for about 12 wavelengths between 380 and 420nm on a Unicam SP 500 manual spectrophotometer. Equation (11.1) was fitted to this data by a weighted, non-linear least squares procedure described by Wolberg.[26] Using the crystallographic data of Mason,[25] the density of anthracene at 290°K was found to be 1.245g cm^{-3} while, at 95°K, this became 1.291g cm^{-3} — a change of only 3.6%. It would then appear reasonable to assume that this latter value applies at 4.2°K.

Table 11.2 Solution Determinations of Dopant Concentrations (Relative standard deviations given in brackets).

Crystal Label	Dopant Concentration mole/mole	Dopant Concentration $mole\ dm^{-3}$	Crystal Thickness (cm)
Tetracene(5)	0.002 (15%)	0.014 (15%)	0.0024 (10%)
Tetracene(7)	0.001 (50%)	0.007 (50%)	0.0048 (10%)
Tetracene(8)	0.0005(60%)	0.004 (60%)	0.0022 (10%)
2-aminoanthracene(3)	0.002 (12%)	0.015 (12%)	0.0015 (10%)
2-aminoanthracene(6)	0.003 (7%)	0.024 (7%)	0.0038 (10%)
2-aminoanthracene(8)	0.002 (5%)	0.013 (5%)	0.0039 (10%)

As can be seen from table 11.2, the errors in the concentrations vary widely between 5 and 60% with the larger errors being characteristically more common. While this method was not pursued since the results did not generally warrant the effort, the more accurate of these results did serve a useful purpose. Using the tetracene(5) and the 2-aminoanthracene (6) and (8) results in table 11.2, together with the room temperature crystal thicknesses and calculated isotropic absorbances, the following estimates for the isotropic molar absorptivities of the traps TETA, 1A and 2A were obtained:

$$\varepsilon_{TETA} = 5000 dm^3\ mol^{-1}\ cm^{-1}$$

$$\varepsilon_{1A} = \varepsilon_{2A} = 3000 dm^3\ mol^{-1}\ cm^{-1}$$

The 1A value was taken to be about the same as the 2A result due to the similarity between the spectra of 1- and 2- aminoanthracene. These molar absorptivities were then used for the reverse procedure of obtaining mole/mole concentrations from the calculated isotropic absorbances of all

crystals measured, as originally suggested in Section 11.1. While such concentrations can only be taken as approximate estimates, it is apparent that dopant concentrations are generally very low with about 1 dopant molecule to every 300 host molecules.

Room temperature crystal thicknesses, estimated dopant concentrations, calculated isotropic dopant absorbances and measured absorbance versus angle of incidence data for all the crystals studied are presented in Appendix B.

12 RESULTS AND DISCUSSION OF TRANSITION MOMENT ORIENTATIONS

The computational procedure for determining the orientation of a guest transition moment with respect to the crystallographic axes of the host has been summarized at the end of Section 10.2. However, it must be established that a measured transition moment orientation is indeed associated with a particular possible orientation of a guest molecule. This connects the optical and crystallographic aspects of the problem and is the only way in which the crystallographic inequivalence properties of the double traps can be proved. To this end, a complete analysis entails deriving the transition moment direction with respect to the guest molecular axes as a means of allowing an independent verification of the results. The following assumptions and restrictions were employed in achieving these aims.

(i) All calculations were made for an undistorted host lattice using the structure determined by Mason[25] at 290°K and 95°K. It was then assumed that the 95°K data was applicable at temperatures between 140°K and 4.2°K with reasonable accuracy. Figure 12.1 presents the ac and ab projections of the anthracene crystal structure, as derived from the 95°K crystallographic data, in a left-handed coordinate system. The translationally inequivalent molecules in this structure have been arbitrarily labelled A and B. The numbering of the carbon atoms indicates those atoms which are equivalent under crystal symmetry. As shown in figure 12.1, the molecular axes are denoted L, M and N being the long and short in-plane and out-of-plane axes, respectively.

(ii) It was assumed that the guest molecule replaces a host molecule in

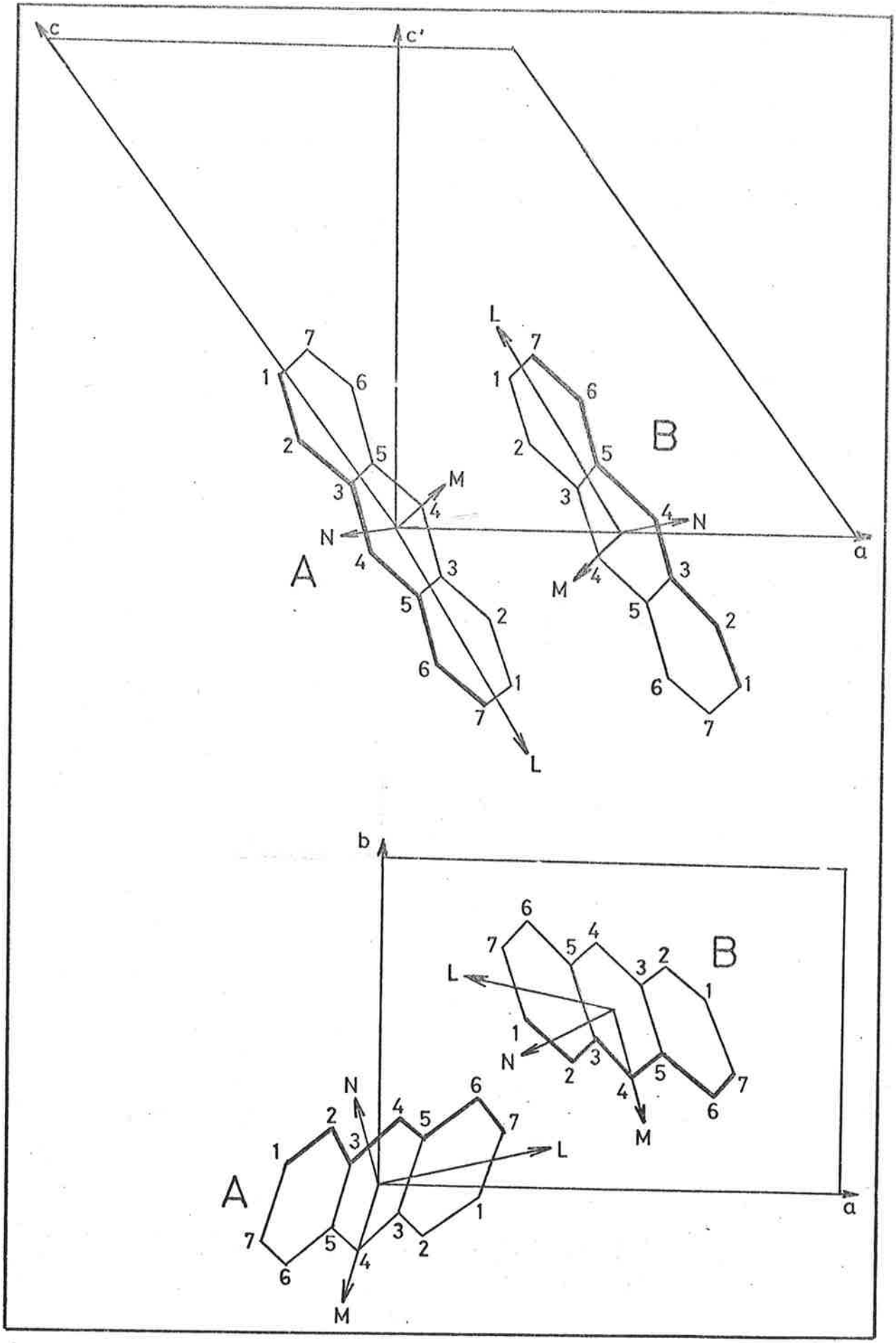

FIG. 12.1 ac AND ab PROJECTIONS OF ANTHRACENE CRYSTAL STRUCTURE. Left-handed coordinate system. A and B label translationally inequivalent molecules. Numbering of carbon atoms shown.

such a way that the long and short axes are coincident. This assumption need not be overly restrictive as any reasonably small realignment of the guest molecule may be accounted for as a final correction to the method.

(iii) The angle ζ, being the angle between the transition moment and the positive b-axis is constrained to the domain

$$0^{o} \leqslant \zeta \leqslant 90^{o},$$

while the angle ϕ, between the ac projection of the transition moment and the positive a-axis, is fixed such that

$$0^{o} \leqslant \phi \leqslant 180^{o}.$$

These restrictions have the effect of simplifying the analysis by taking account of only the necessary projections of the transition moments in the ac-plane without loss of generality. For example, consider a transition moment lying in the direction through the centre and the atoms labelled 1 of either anthracene molecule in figure 12.1. The two such possible directions corresponding to transitions in molecules A or B are labelled A´OA and B´OB, respectively, in figure 12.2. These two directions are related to one another by a half-turn about the b-axis and, consequently, share a common ac projection, labelled G´OG in figure 12.2. Applying the first restriction such that the angle between the directions A´OA and B´OB and the positive b-axis must be between 0^{o} and 90^{o}, results in the elimination of the directions OA´ and OB so that OA and OB´ alone define the directions A´OA and B´OB. Now applying the second restriction so that the angle between G´OG and the positive a-axis is restricted to the range 0^{o} to 180^{o}, eliminates the direction OB´. In this way, the projection OG may

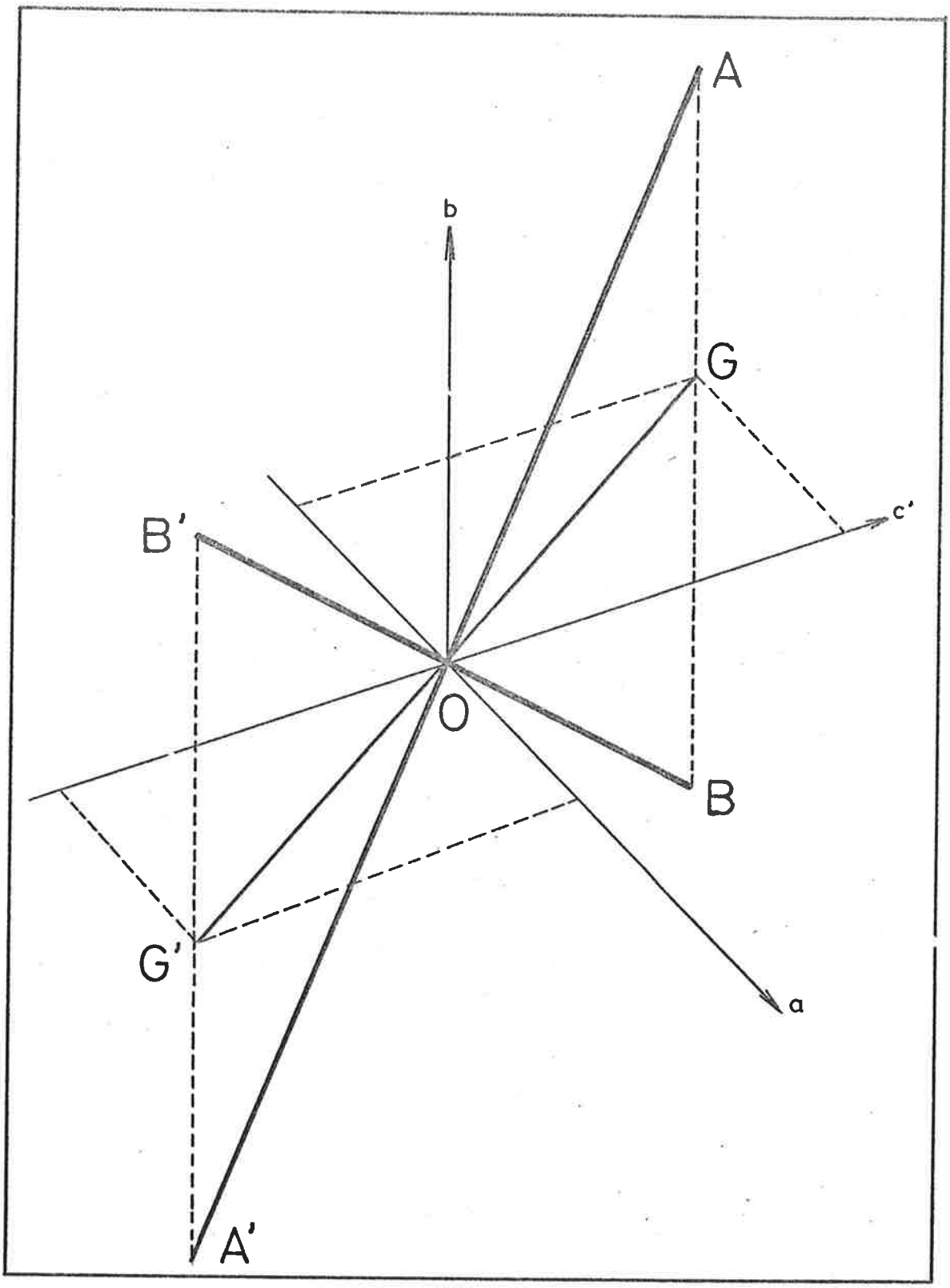

FIG. 12. 2 CONSTRAINED REGION OF CRYSTAL SPACE.
See text.

be related to the direction OA which, in turn, defines all the other possible orientations of the original transition moment considered.

(iv) It was assumed that the guest transitions observed were in, or very close to, the molecular plane.

(v) The results of computer simulations, carried out by N.J. Bridge,[18] concerning the molecular packing of guest molecules in a host lattice were used, In these calculations, the potential energy of the guest was computed by summing atom-atom interactions, following the method of Williams[27] and using his parameter set IV, including both attractive and repulsive terms. Calculations were carried out with the crystallographic data[25] at 290°K and 95°K to give some indication of how the potential energy of the guest might be affected by a displacement of the adjacent host molecules. The guest-host interaction potential was calculated for small displacements of the guest in order to locate the optimum orientation and a check of the method carried out for an unsubstituted host molecule revealed that the largest deviation predicted was a 2° rotation about the L-axis. This procedure was used to calculate guest-host interaction potentials for substituted anthracene molecules with an amino group at one of the positions 1, 2, 6 or 7 given in figure 12.1. It was found, irrespective of temperature or conformation of the amino group, that

$$U_7 > U_1$$

and $$U_2 > U_6$$

where U_1, U_2, U_6 and U_7 are the guest-host interaction potentials

for the substitutions noted above, where positions 1 and 7 correspond to the 2-aminoanthracene case and positions 2 and 6 correspond to 1-aminoanthracene. Assuming an equilibrium distribution of guest molecules between available sites, the actual energy difference in practice can be determined from the equation

$$U_j - U_i = kT \ln (x_i/x_j) \qquad (12.1)$$

derived from the Boltzman distribution, where k is the Boltzman constant, T is the temperature of interest, x_i and x_j are the mole ratios of guests at sites i and j and U_i and U_j are the corresponding guest-host interaction potentials. In the case of 2-aminoanthracene, the guest site concentrations were estimated from absorbances integrated over the origin lines and associated phonon bands since the spectra of the 2A and 2B traps differ in both polarization and phonon structure.[21] In the case of 1-aminoanthracene, the absence of the 1B site in absorption was considered to be due predominantly to concentration effects. Thus, it was determined that

$$x_{2A} > x_{2B}$$

$$x_{1A} > x_{1B}$$

so that

$$U_{2B} > U_{2A}$$

$$U_{1B} > U_{1A},$$

at 150°C, the temperature at which the sublimation grown crystals formed. Thus, an amino group substitution at the atomic positions 1, 7, 6 and 2 corresponds to the trap sites 2A, 2B, 1A and 1B, respectively.

12.1 Theoretical Calculations

Figure 12.3 presents theoretical absorbance curves, computed from eqns (10.29) and (10.30) with K=1, for selected values of the orientation angles ζ and ϕ, with angles of incidence between -15^{o} and 45^{o}, refractive indices α, β and γ of 1.6, 1.8 and 2.0, respectively and $\xi = 30^{o}$. It is quite apparent that the expected behaviour of absorbance with angle of incidence is smooth and continuous, unlike the obvious depolarization effects caused by internal conical refraction as illustrated in figure 11.4. No such unusual changes in absorbance were noted for any of the guests studied in the angle of incidence range -15^{o} to 43.5^{o}, as can be seen from the data in Appendix B.

In the following discussion, the molecular L, M and N axes will be taken as being fixed in the left-handed coordinate system as given in figure 12.1. That is, as shown in figure 12.4, the positive directions of these molecular axes are defined by the vectorial directions $L_A'L_A$, $M_A'M_A$, $L_B'L_B$, $M_B'M_B$, O_AN_A and O_BN_B for the translationally inequivalent molecules A and B. In this way, angles in the molecular plane can be uniquely specified. Thus, ψ is defined as the angle between any theoretical transition moment and the positive L-axis taken in the direction of the positive M-axis on either molecule A or B. Such a transition moment on one of these molecules is related to the corresponding moment on the other molecule by a half-turn about the b-axis. Using the equation[28] for the angle σ between two unit vectors defined by the direction angles a_1, b_1, c_1 and a_2, b_2, c_2, respectively, in the crystallographic coordinate system,

$$\cos\sigma = \cos a_1 \cos a_2 + \cos b_1 \cos b_2 + \cos c_1 \cos c_2, \quad (12.2)$$

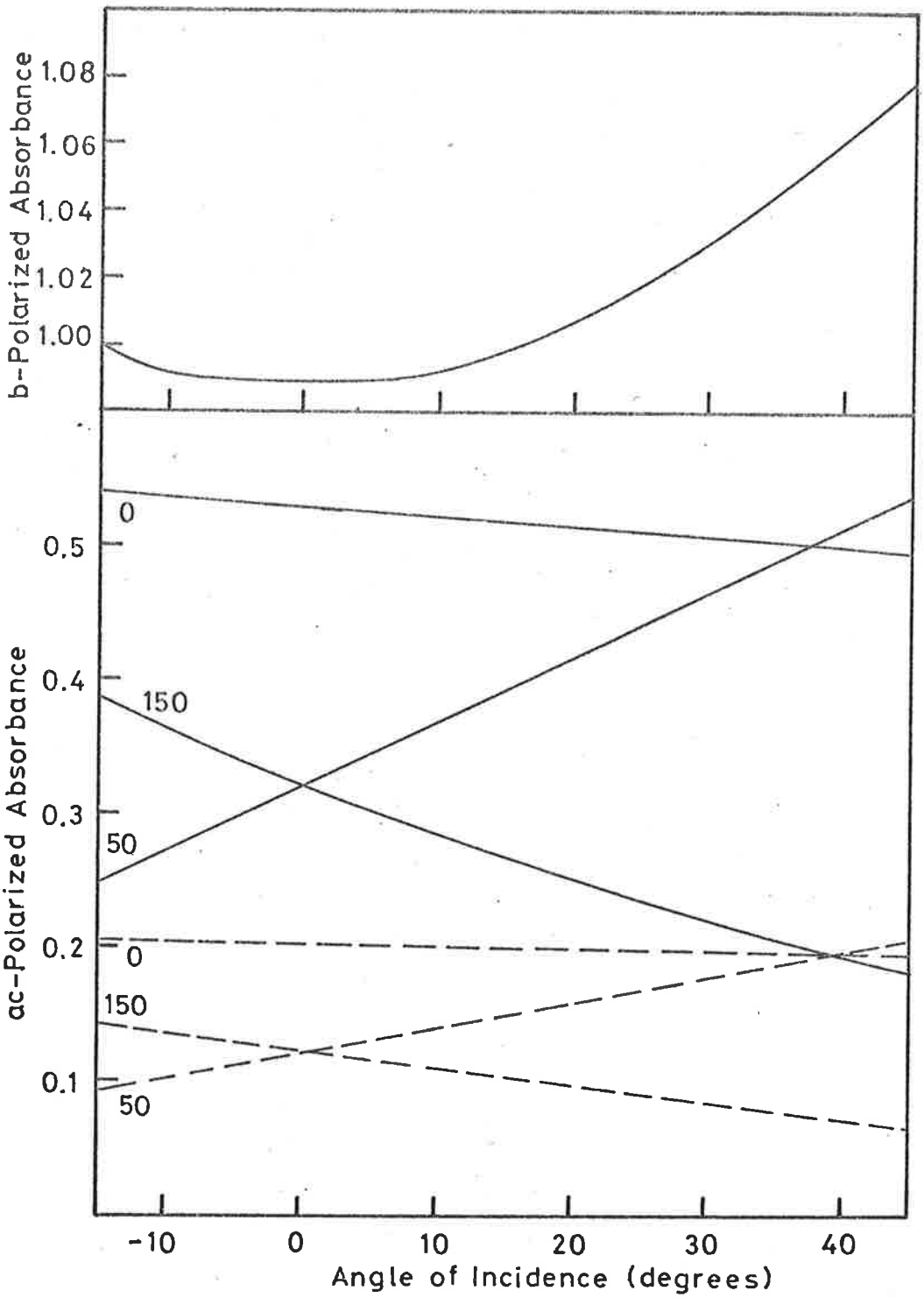

FIG. 12.3 THEORETICAL ABSORBANCE CURVES. Parameter K set equal to unity. For ac-polarized absorbances, angle ϕ corresponding to each curve shown; $\zeta=40°$: ----, $\zeta=70°$: ——. b-pol. curve common to all angles ζ and ϕ, being scaled by constant K only.

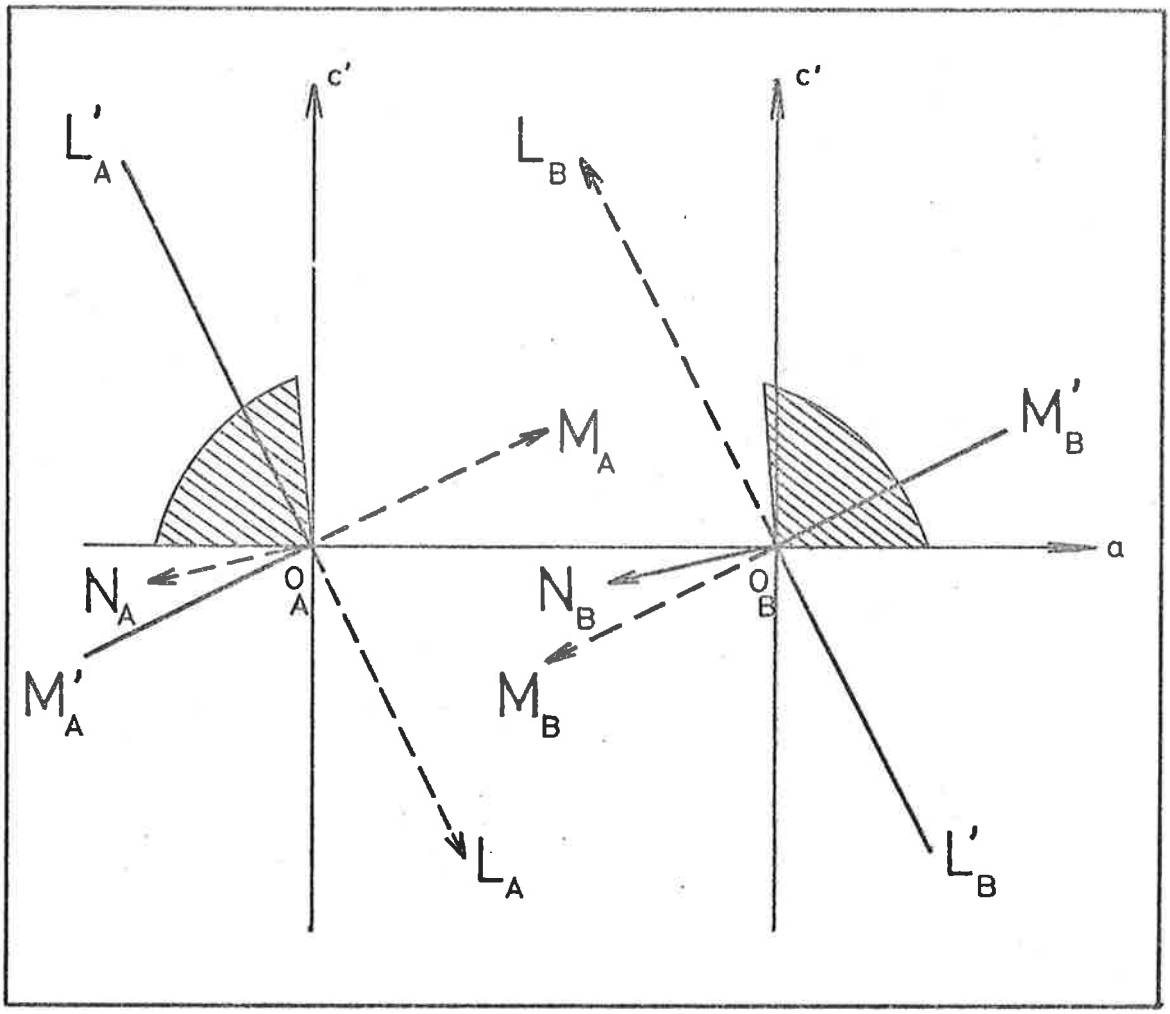

FIG. 12.4 SCHEMATIC VIEW OF MOLECULAR AXES IN ANTHRACENE STRUCTURE. Viewed down b-axis. Directions up from ac-plane: (——); down from ac-plane: (— — —). Hatched areas indicate allowed values of angle ϕ associated with either molecule A or B.

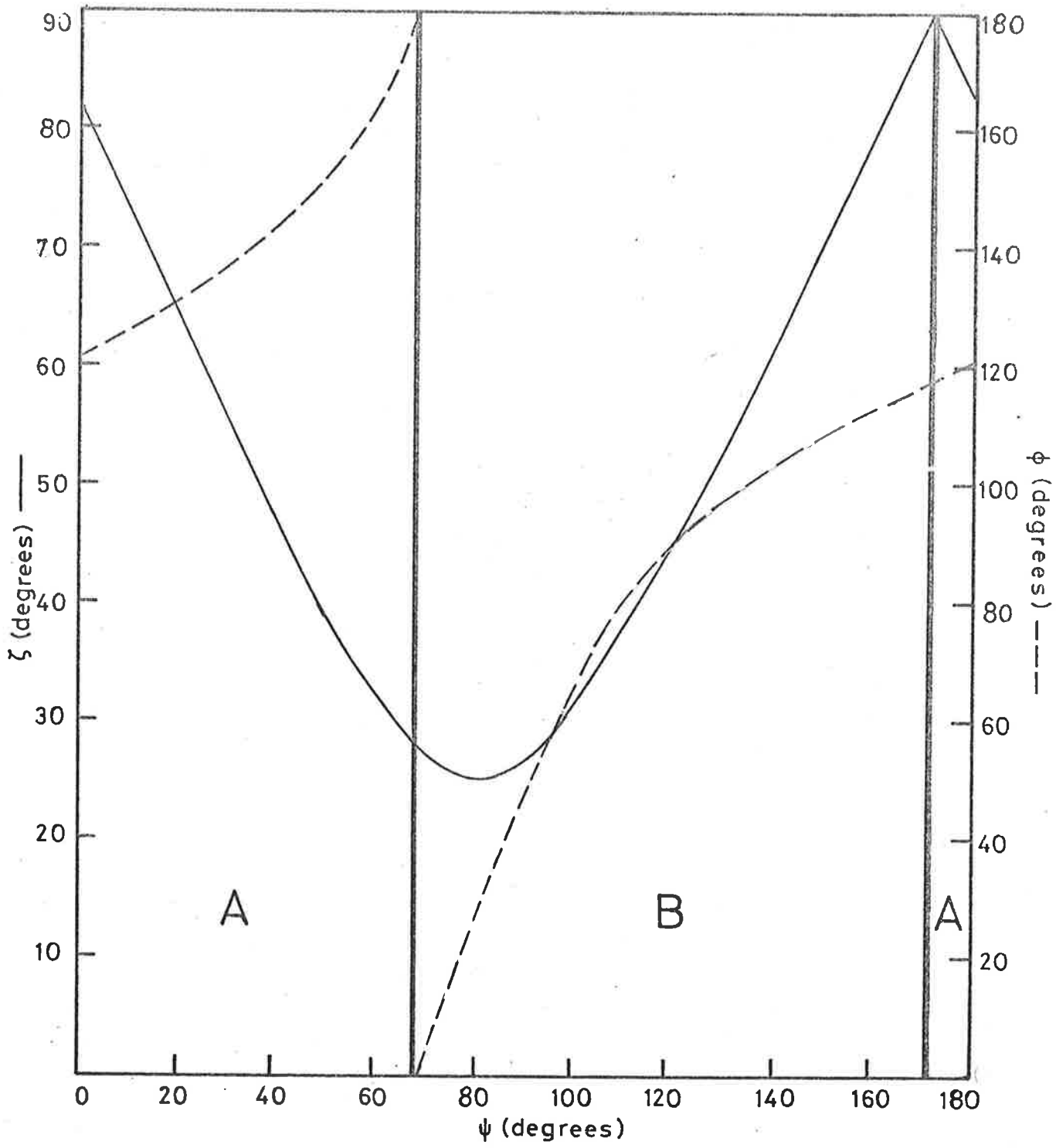

FIG. 12.5 BEHAVIOUR OF ANGLES ζ AND ϕ WITH TRANSITION MOMENT ANGLE ψ. Only angles within allowed limits are shown. Regions A and B define angles associated with molecules A and B in the unit cell.

a set of three equations may be established relating the angle ψ to the directions of the positive L, M and N directions. These may be solved simultaneously to evaluate the orientation of any particular molecular transition moment with respect to the crystallographic axes. Angles ζ and ϕ so calculated with the 95°K crystallographic data, within the constraints established by assumption (iii) above, are presented in figure 12.5. The allowed domain for the angles ζ and ϕ is illustrated schematically in figure 12.4 where only those angles ϕ in the upper region of the ac-plane and those angles ζ associated with directions above this plane are allowed. Relating the results shown in figure 12.5 with the constraints illustrated in figure 12.4 and the symmetry properties of the transition moments, it was determined that the regions of ζ and ϕ values indicated in figure 12.5 correspond to specific transition moment orientations on either molecule A or B. That is, for angles ψ between 0° and 69°, the transition moment observed in the *constrained* region is associated with molecule A. Similarly, ψ values between 69° and 172° are associated with molecule B and the 172° to 180° region is associated with molecule A. The allowed ϕ values corresponding to each molecule A or B are indicated by the hatched areas in figure 12.4.

12.2 Experimental Calculations and Results

A computer programme (TROP), given in Appendix C, was formulated for the calculation of the orientation angles ζ and ϕ from the absorbance data given in Appendix B. Reiterating the procedure described in Section 10.2, the ac polarized absorbances are analysed by a weighted, non-linear least squares procedure[26] to obtain the parameters $K \tan^2\zeta$ and ϕ. A linear least squares analysis of the b polarized absorbances yields

the quantity K so that the angle ζ can be isolated. Isotropic absorbances were also calculated for use in estimating dopant concentrations. Figure 12.6 presents typical fits of the theoretical absorbance curves, calculated with the optical data from Section 11.3.1 at $4.2^{o}K$, to the experimental data. The correspondence between theory and experiment is seen to be very good, yielding values of the orientation angles with standard deviations of no more than $\pm 5^{o}$. Using these standard deviations as weights, weighted means of the angles ζ and ϕ were calculated from all available samples, as given in table 12.1. The errors given are linear estimates of the standard deviations in the set of calculated angles for each guest. Also presented in table 12.1 are some results for the trap sites TETB and TETC, other vibronic lines in the tetracene spectrum given in figure 11.2(a), which appear to be in reasonable agreement with the average TETA values. To establish the effects of variations in the optical constants, the angles ζ and ϕ were also calculated with optical data at the higher temperatures. Specific samples were selected as being representative of their particular group since the individual ζ and ϕ values in these cases were the closest to the weighted means in table 12.1. The largest variation in the calculated angles from one end of the temperature range to the other for these samples was about 15% while variations of the order of 5% to 10% were more common. Such variations will be taken into account when discussing the final results.

The angles ζ and ϕ define the directions of the *effective* transition moments, as discussed in Section 10.2. However, in an effort to account for the possibility of a local field effect, actual transition moment orientations may be calculated from eqn (10.47). Two classical local

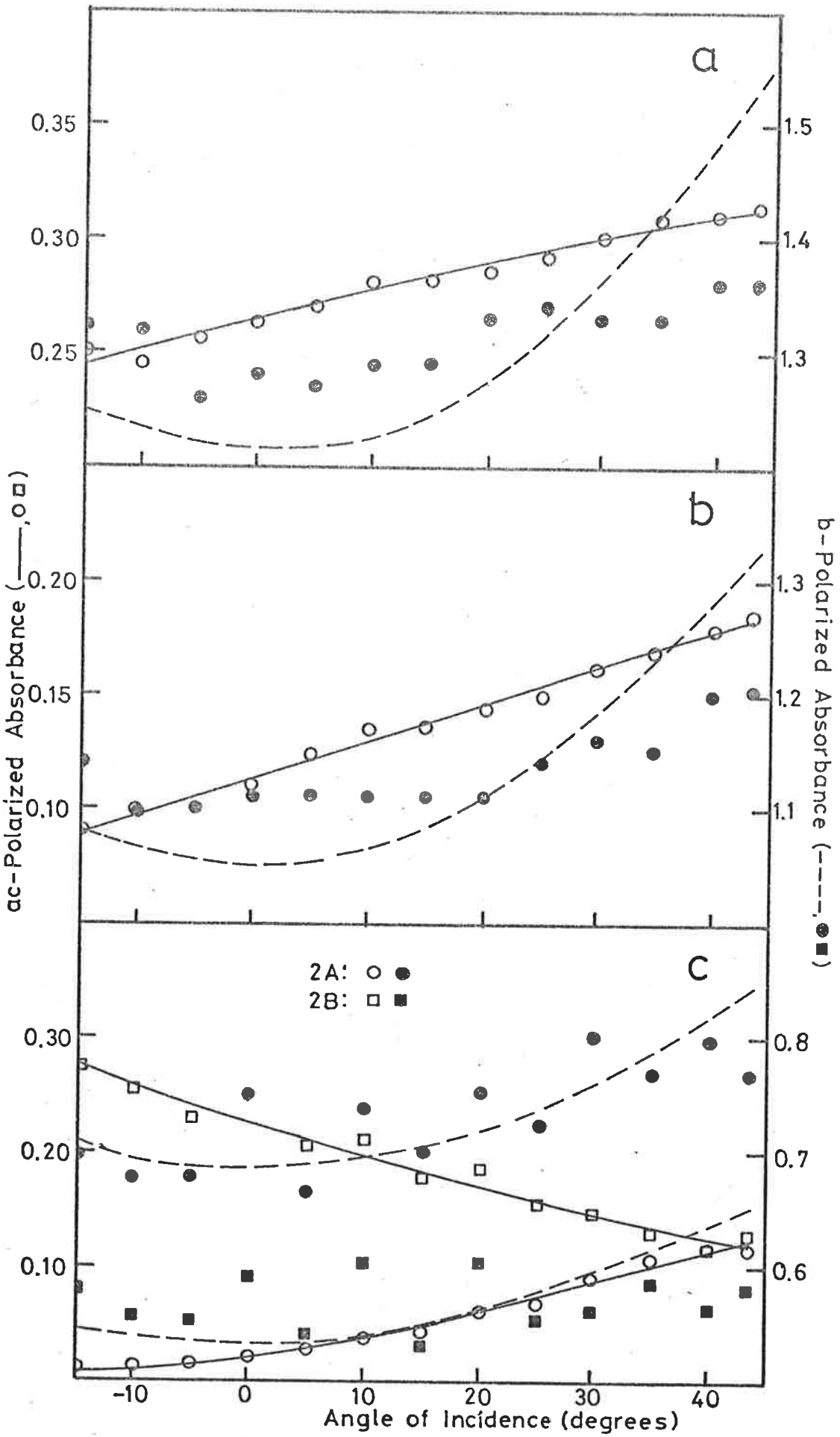

FIG.12.6 CORRESPONDENCE BETWEEN THEORETICAL AND EXPERIMENTAL ABSORBANCE CURVES. (a) Tetracene, trap TETA; (b) 1-aminoanthracene, trap 1A; (c) 2-amino-anthracene, traps 2A and 2B. Theoretical: (——); experimental: (○ ● □ ■).

Table 12.1 Calculated Orientation Angles at 4.2°K

Trap Label	Weighted Mean Angles	
	ζ(degrees)	ϕ(degrees)
TETA	24.1 ± 1.2	23.2 ± 0.7
TETB(1)	-	19.9 ± 1.7
TETC(1)	22.0 ± 2.7	25.0 ± 2.4
1A	21.8 ± 2.4	47.4 ± 6.0
2A	37.5 ± 4.7	89.3 ±11.2
2B	41.3 ± 7.0	147.0 ±19

field tensors have been discussed in Section 10.2.2, $\underline{\underline{d}}_{anis}$ from eqn (10.45) and $\underline{\underline{d}}_{iso}$ from eqn (10.46). The latter local field tensor is entirely isotropic implying that the effective moments are, in fact, the actual ones. The guest molecule is consequently regarded as being immersed in a medium of matched dielectric properties so that the field at the guest site is essentially equal to the macroscopic field. $\underline{\underline{d}}_{anis}$, on the other hand, predicts an anisotropic local field based on the anisotropy of the host polarizability within a spherical cavity. Using the appropriate optical data at 4.2°K, these models were applied to obtain actual transition moment orientations. As an example, the isotropic and anisotropic local field tensors in the case of the 2A trap were found to be

$$\underline{\underline{d}}_{iso} = \begin{pmatrix} 1.846 & 0 & 0 \\ 0 & 1.846 & 0 \\ 0 & 0 & 1.846 \end{pmatrix}$$

$$\underline{\underline{d}}_{anis} = \begin{pmatrix} 1.702 & 0 & 0.270 \\ 0 & 1.851 & 0 \\ 0.270 & 0 & 1.987 \end{pmatrix}.$$

Table 12.2 presents the results of applying these local field corrections to the effective transition moment directions, noting the obvious point that the isotropically corrected and effective moments are identical.

Table 12.2 Corrected Transition Moment Orientations at 4.2°K

	Isotropic Correction		Anisotropic Correction	
	ζ(degrees)	ϕ(degrees)	ζ(degrees)	ϕ(degrees)
TETA	24.1	23.2	16.1	23.8
1A	21.8	47.4	19.4	43.7
2A	37.5	89.3	36.4	81.4
2B	41.3	147.0	47.2	147.6

The isotropically and anisotropically corrected transition moment orientations will be referred to as the uncorrected and corrected moments, respectively, in the following discussion. The angles calculated above define the transition moment orientations with respect to the crystallographic axes and, as such, clearly show that the four trap sites studied correspond to different transition moment directions. However, these transition moments now will be related to the molecular axes using the convention adopted in figures 12.1 and 12.4.

The plane of the guest molecule, being taken as coincident with that of the host it replaces, may be defined by the direction of the normal to this plane. This is the molecular N-axis and its direction cosines are available from the crystallographic data. Using the standard equation[28] for the angle ρ between a plane, defined by the direction

numbers A, B and C of the unit normal to the plane, and a line, defined by the coordinates x, y and z:

$$\sin \rho = Ax + By + Cz, \qquad (12.3)$$

the angle between each transition moment and the plane of either translationally inequivalent molecule in the host lattice is calculated. ρ_A and ρ_B are these angles to the molecular planes of molecules A and B in figure 12.1, and are given in table 12.3 for both the corrected and uncorrected sets of transition moments. These results agree with the assignments predicted by figure 12.5 for the set of angles given in table 12.2, and show that the transition moments are in the plane of a unique, replaced host molecule to well within 5^{o}. The corrected and uncorrected moments give only marginally different results and it is apparent that the assumption that these guests replace a host with coincidence of molecular axes is reasonable. Variations in the angles ρ_A and ρ_B brought about by the possible errors in the optical data were found to be only marginally different from those values in table 12.3. Thus, the transition moments were found to remain close to 5^{o} to the molecular planes indicating that variations in the optical data have little effect on this result.

Table 12.3 Angles between Transition Moments and Molecular Planes at $4.2^{o}K$

Trap Label	Uncorrected Moments		Corrected Moments	
	ρ_A(degrees)	ρ_B(degrees)	ρ_A(degrees)	ρ_B(degrees)
TETA	49.0	0.93	48.2	0.91
1A	45.1	4.32	43.5	3.38
2A	36.6	4.23	31.1	4.96
2B	1.32	37.7	1.54	38.3

Figure 12.5 may be used to obtain the angle ψ, between transition moment and positive molecular L-axis, for each set of ζ and ϕ values given in table 12.2. However, these curves were derived for transition moments which were exactly within the molecular plane of a host molecule. Using eqn (12.2), the angle between the actual spatial orientation of the corrected and uncorrected moments and the positive host L-axis can be computed. This is sufficient in the case of tetracene (point group D_{2h}) which is symmetric about the L-axis. However, in the case of the aminoanthracenes (C_s), the position of substitution of the amino group allows a unique definition of the transition moment direction with respect to the molecular axes. Figures 12.7(a) and (b) schematically show the molecular axis orientations for molecules at sites A and B in the anthracene structure when these molecules are viewed in the positive a-axis direction. The transition moment angle ψ may then be related to the position of substitution of the amino group, as shown in figure 12.7(c), by using the results of the computer simulation of molecular packing discussed earlier. These calculations have shown that the atomic positions 1, 7, 6 and 2 correspond to the trap sites 2A, 2B, 1A and 1B, respectively. The above procedure was applied to the available data and the corrected and uncorrected transition moment angles for tetracene, 1-aminoanthracene and 2-aminoanthracene were calculated. Variations in the transition moments brought about by the errors in the optical data did not exceed about 4%. Consequently, it is apparent that the initial 5% to 10% variations in the angles ζ and ϕ, due to the optica data, are of no particular significance in these calculations.

Since two values of the angle ψ were calculated for 2-aminoanthracene from the 2A and 2B trap data, it was only in this case that a true

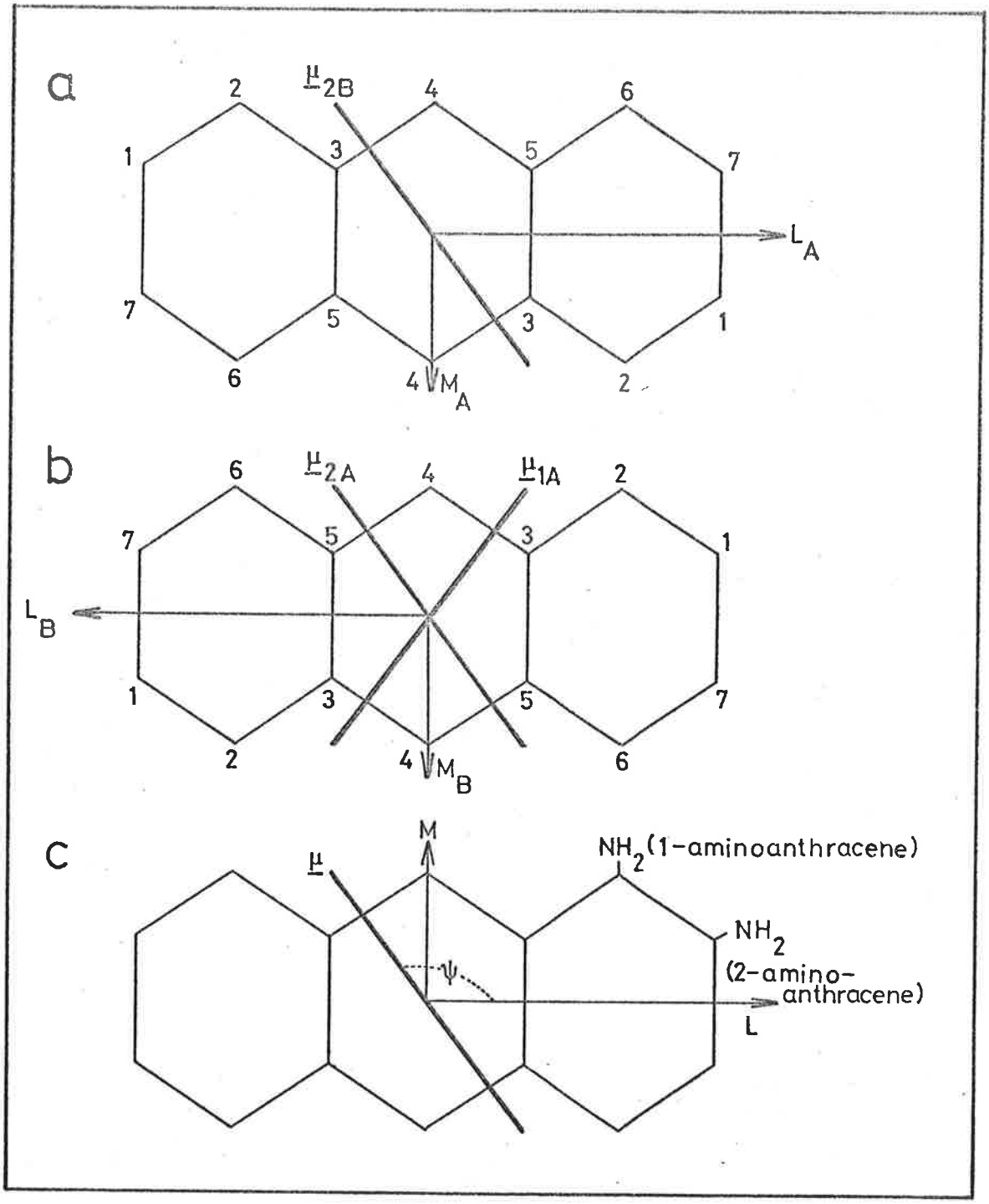

FIG. 12.7 TRANSITION MOMENT ORIENTATIONS FOR AMINOANTHRACENES. (a) and (b) correspond to molecules A and B as viewed in direction of positive a-axis. Orientations of measured electric dipole moments for traps 1A, 2A and 2B shown schematically. (c) defines transition moment angle ψ and molecular axes with respect to amino substituent.

indication of the magnitude of the errors was available. The average of the angles for the 2A and 2B results were $123.8^{o} \pm 9.6^{o}$ and $120.0^{o} \pm 5.9^{o}$ for the uncorrected and corrected results, respectively; deviations of 5% to 10% which may be accounted for by the possible errors in the optical data, Table 12.4 compares the results of this work with other experimental and theoretical results. The errors quoted for tetracene and 1-aminoanthracene have been based on a 10% error suggested by the 2-aminoanthracene results.

Table 12.4 Calculated and Theoretical Transition Moment Angles

	ψ(degrees)		
	Tetracene	1-aminoanthracene	2-aminoanthracene
Experimental:			
Uncorrected moment[a]	100 ± 10	91 ± 10	124 ± 10
Corrected moment[a]	103 ± 10	93 ± 10	120 ± 6
Others	90[b]	89 ± 9[c]	124 ± 2[c]
Theoretical:			
Klevens *et alia*,[32] Pariser[33]	90	-	-
Sadlej *et alia*[34]	-	39	102
Tichy[35]	-	84	116
Tichy *et alia*[36]	-	91	116
Woznicki *et alia*[37]	-	73	135
Jorgensen[30]	-	86	99

a. This work

b. Implied from mixed crystal studies in ref. (29).

c. Unpublished result quoted in ref.(30). Stretched film method of ref.(31).

The tetracene 20246cm^{-1} origin corresponds to a transition polarized along the short in-plane axis.[28] The results of this work, for both corrected and uncorrected moments, thus indicate that there is a systematic discrepancy which would be corrected by a 10° rotation about the N-axis. However, this is contradicted by independent measurements of the tetracene-anthracene system[1,22] which show no such rotation. This error magnitude corresponds to the variation between the 2A and 2B results for 2-aminoanthracene, an error little improved by the application of the anisotropic local field correction. It can only be surmised, then, that there are either experimental or theoretical considerations which have acted to produce the overall errors which are noted. On the other hand, the experimental results for the aminoanthracenes are in very good accord while the calculations in best agreement with these experimental results are those of Tichy and Zahradnik,[36] who employed the LCI-SCF method of Pariser, Parr and Pople, starting from a HMO basis. In this respect, the application of the anisotropic local field correction produces results which are marginally closer to these theoretical expectations than the uncorrected moments.

It is consequently apparent that, within acceptable error limits, the 2A and 2B traps are indeed associated with very different orientations of the same molecular species. Each of the transition moments for the 2A and 2B traps correspond to crystallographically unequivalent substitutions of the amino group. This is best illustrated by figure 12.7 where molecules A and B are presented in the configuration in which they appear in the crystal. It is seen that there is no crystal symmetry operation of the anthracene structure (space group P_{2_1}/a; site symmetry C_i), which connects the transition moment associated with a substituent at any atom 1

with the moment associated with substituent at any other atom 7. The uncorrected transition moment angles for the 2A and 2B traps were 114.2° and 133.4°, respectively which, when related to molecules A and B in figure 12.7, show that the 2A and 2B transition moments are related by an approximate half-turn about the L-axis of the replaced host molecule. The relationship is approximate because each of these orientations of the guest molecule will correspond to differing steric interactions and distortions of the neighbouring host molecules. It is expected, then, that crystallographic inequivalence will apply to the analogous 1-aminoanthracene case where the 1B trap, unobserved in absorption, will be related to the direction of the 1A transition moment by an approximate half-turn about the long axis of the replaced host molecule. From the results presented in table 12.4, it is apparent that 1-aminoanthracene is short-axis polarized so that the 1A and 1B traps are very nearly parallel. However, a possible 10% error exists in this measured orientation of the transition moment. At the very extreme, the transition moment angle ψ could well be about 80°, using the convention of figure 12.7(c). This would be closer to the theoretical predictions of Tichy[32] and Woznicki and Wasilewski[34] and would result in more substantial spatial misalignments between the 1A and 1B traps. This is well illustrated by figure 12.5. Since crystallographically inequivalent pairs are theoretically related by a half-turn about the L-axis, a transition moment angle ψ of 120° has a corresponding inequivalent partner at ψ = 60°. This corresponds approximately to the 2-aminoanthracene case where it is seen that there is a difference of about 12° in the angle ζ and 74° in the angle ϕ, between ψ = 60° and 120°. If the 1-aminoanthracene angles were ψ = 80° and 100°; the difference in ζ would be about 6° with a difference of 42° in ϕ. Thus, a 10° error in the angle ψ for 1-aminoanthracene results in two crystallographically

inequivalent orientations of the transition moment which are spatially misaligned by about 50% of the 2-aminoanthracene result.

13 CONCLUSIONS

The most important conclusion of this work has been that the double traps formed by 1- and 2- aminoanthracene are indeed due to crystallographic inequivalence. From fluorescence and absorption measurements, the difference in excitation energy between the 2A and 2B traps was found to be 279cm^{-1} while the difference between 1A and 1B was 156cm^{-1}. It was demonstrated that, if expected errors are accounted for, the spatial misalignment between the 1A and 1B sites is about half of that between the 2A and 2B orientations. As analogous molecular species are being dealt with, it is reasonable to expect that such variations in transition moment orientations with respect to the crystallographic axes could well account for the energy differences observed. This has been supported by a simple perturbational calculation[18] in the case of 2-aminoanthracene where it was shown that the difference between the 2A and 2B sites arises in large part from the variation of the coupling between the first singlet transition of the guest and the 250nm exciton band of the host. This would imply that the properties of the guest are substantially affected by variations of the orientation of the transition moment. On the other hand, if the error estimates introduced in the 1-aminoanthracene case are too large, spatial misalignment between the 1A and 1B traps could be far less than could account for the difference in excitation energy observed. The model for guest behaviour would then need to go beyond a simple analysis of variations in the guest transition moment orientation but also include the effects of dispersion forces. It is to be expected that different

positions of the guest in the host lattice would induce different dispersion interactions but the importance of these forces has not been unambiguously defined in this work. Nevertheless, there is significant evidence that there is a marked effect on the properties of the guest due to variations in its orientation and that the host-guest resonance interaction is involved by implication.

It is significant that the absorption by deep traps can be described satisfactorily by purely classical optics and that the application of classical local field models is marginally favourable as well. However, more realistic local field calculations may well account for the errors in the measured transition moment angles although point-dipole models do not appear very hopeful at present.

REFERENCES

1. C.A. Hutchison and L. Mangum, *J. Chem. Phys.*, 32, 908 (1961).

2. M.Born and H. Wolf, *Principles of Optics*, (Pergamon Press. 1975).

3. e.g. C. Kittel, *Introduction to Solid State Physics*, (Wiley and Sons. 1971). p.454.

4. A. McL. Mathieson, J.M. Robertson and V.C. Sinclair, *Acta Cryst.*, 3, 245 (1950).

5. R.W. Ditchburn, *Light*, (Blackie and Son. 1953). p. 523.

6. I.V. Obreimov, A.F. Prikhot'ko and I.V. Rodnikova, *Zhur. Eksp. Teor. Fiz.*, 18, 409 (1948).

7. A.Y. Eichis, *Zhur. Eksp. Teor. Fiz.*, 20, 471 (1950).

8. H.C. Wolf, *Z. Naturforsch.*, 13a, 414 (1958).

9. M.S. Brodin and A.F. Prikhot'ko, *Opt. i Spektr.*, 2, 448 (1957).

10. P.G. Cummins, D.A. Dunmur and R.W. Munn, *Chem. Phys. Lett.*, 22, 519 (1973).

11. L. Dissado, *J. Physics C*, 4, 1874 (1971).

12. e.g. J.B. Birks, *Photophysics of Aromatic Molecules*, (Wiley-Interscience 1970). p. 46.

13. S.A. Rice and J. Jortner, *Physics and Chemistry of the Organic Solid State*, (Ed. D. Fox, M.M. Labes and A. Weissberger; Interscience. 1967). Vol.III. p. 199.

14. F.P. Chen, D.M. Hanson and D. Fox, *J. Chem. Phys.*, 63, 3878 (1975).

15. M.F. Vuks, *Opt. & Spectr.*, 20, 361 (1966).

16. F.P. Chen, D.M. Hanson and D. Fox, *Chem. Phys. Lett.*, 30, 337 (1975).

17. P.G. Cummins, D.A. Dunmur and R.W. Munn, *Chem. Phys. Lett.*, 36, 199 (1975).

18. N.J. Bridge, private communication.

19. A.H. Price, J.O. Williams and R.W. Munn, *Chemical Physics*, 14, 413 (1976).

20. D. Fox, *Chemical Physics*, 17, 273 (1976).

21. N.J. Bridge and D. Vincent, *J. Chem. Soc., Farad. Trans. II*, 70, 30 (1974).

22. (a) M. Chabr, J. Fünfschilling and I. Zschokke-Gränacher, *Chem. Phys. Lett.*, 25, 387 (1974).

(b) M. Chabr and I. Zschokke-Gränacher, *Mol. Cryst. Liq. Cryst.* 32, 97 (1976).

23. e.g. N.H. Hartshorne and A. Stuart, *Practical Optical Crystallography*, (Edward Arnold. 1964). pp. 199-240.

24. S. Suzuki and H. Baba, *Bull. Chem. Soc. Japan*, 37, 519 (1964).

25. R. Mason, *Acta Cryst.*, 17, 547 (1964).

26. J.R. Wolberg, *Prediction Analysis*, (Van Nostrand. 1967). pp. 27-74.

27. D.E. Williams, *J. Chem. Phys.*, 45, 3770 (1966).

28. e.g. *Standard Mathematical Tables* (Ed. S.M. Selby; Chemical Rubber Co. 1971). pp. 352-269.

29. J.W. Sidman, *J. Chem. Phys.*, 25, 122 (1956).

30. P. Jorgensen, *J. Chem. Phys.*, 56, 1839 (1972).

31. E.W. Thulstrup, J. Michl and J.H. Eggers, *J. Phys. Chem.*, 74, 3868, 3878 (1970).

32. H.B. Klevens and J.R. Platt, *J. Chem. Phys.*, 17, 470 (1949).

33. P.Pariser, *J. Chem. Phys.*, 24, 250 (1956).

34. A.J. Sadlej and K. Rotkiewicz, *Wiadom. Chem.*, 25, 417 (1967).

35. M. Tichy, Ph.D. Thesis,(Inst, Phys. Chem. Czechoslovak Acad. Sci., Prague).

36. M. Tichy and R. Zahradnik, *J. Phys. Chem.*, 73, 534 (1969).

37. W. Woznicki and J. Wasilewski, unpublished work quoted by K. Rotkiewicz and Z.R. Grabowski, *Trans. Faraday Soc.*, 65, 3263 (1969).

CHAPTER V

The Polymeric Aggregate: A Preliminary Study

14 THEORETICAL BACKGROUND

The results presented here constitute a preliminary study to probe the existence of exciton band structures in some polymeric systems. A summary of the expected theoretical effects will be given in order to justify the basis of the approach used. The theories of dye-polymer complexes presented by Philpott[1-3] and Philpott and Lee[4] have provided very useful guides as to the expectations and difficulties associated with the study of real systems. The most practically oriented of these theoretical formulations has been concerned with the exciton theory of the electronic states of dye-polymer complexes for linear polymers.[1]

14.1 Dye-Polymer Complexes of Linear Polymers

Philpott[1] has discussed the simplest model of a dye-polymer complex involving a dye, with a single excited state, bound to an infinite, single-stranded, linear polymer with one excited state per repeating unit (or monomer). Only primary traps, those involving strong interactions between dye and polymer, were considered and no guest-guest interactions were included. The point-dipole approximation was used and the model was simplified by assuming a strict proportionality between the dye-polymer and polymer resonance interactions, with the parameter α being the constant of proportionality. Within this model, β represents the neighbour resonance interaction between monomers and the exciton bandwidth is $4|\beta|$. The primary trap energy e is defined as the excitation energy of a guest molecule within the dye-polymer aggregate, and thus includes exciton interaction effects, while the trap depth δ is the difference between the excitation energy of the isolated dye and the centre of gravity of the exciton band of the polymer. The trapping probability a^2 is defined as

the probability of finding the excitation on the guest molecule and thus indicates the degree of delocalization of the exciton at or in the neighbourhood of the guest. Finally, I(e) is the trap transition intensity. The following equations, derived by Philpott[1] for trap levels lying *below* the exciton band, yield the required trap parameters:

$$(1 + 2\alpha^2)e^4 - 2\delta\ (1 + \alpha^2)e^3 + [\delta^2 - 4\beta^2(1 + \alpha^2)^2]e^2 + 4\beta^2\delta(1 + \alpha^2)e - 4\beta^2\delta^2 = 0; \qquad (14.1)$$

$$I(e) = [e/(e - 2\beta)]^2 a^2; \qquad (14.2)$$

$$|a|^{-2} = (1 + \alpha^2) - 2\alpha^2(e\ G_o) + \alpha^2(eG_o) \qquad (14.3)$$

where

$$G_o = -(e^2 - 4\beta^2)^{-\frac{1}{2}}.$$

Due to the possible spectral changes incurred by other solvent effects, it is advantageous to discuss the variations in trap parameters with respect to the isolated dye parameter δ, rather than to the primary trap energy.

Figure 14.1 presents the results of solving the above equations for specific values of δ and α where the unit of energy for both e and δ is $2|\beta|$ which is equal to the polymer resonance interaction. The optical exciton state, being of zero wave-vector,[5] is chosen to be either at the bottom of or inside the exciton band. The latter case includes an optical state at the top of the band. It has been suggested that the proportionality between the guest-host and host-host resonance interactions implies that the guest and host transition moments are parallel.[6] The host-guest coupling constant α will indicate the relative importance of guest-host and host-host resonance interactions so that it would appear

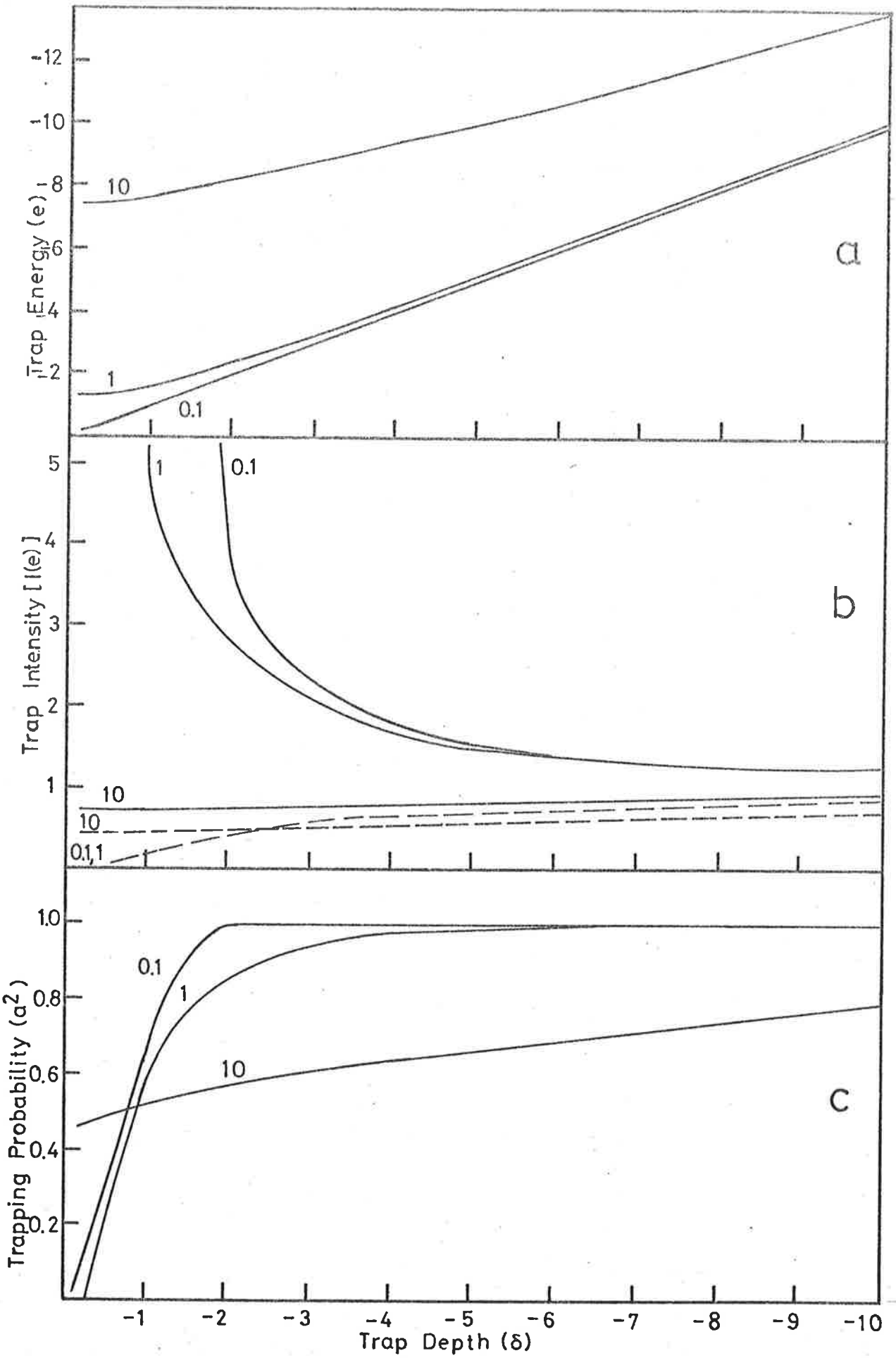

FIG. 14.1 THEORETICAL TRAP PROPERTIES. Energy unit is $|2\beta|$. The value of α corresponding to each curve is shown. Optical level at bottom of band, $e=-1$ (——); inside or at top of band, $e=+1$ (— — —). These are coincident in (a) and (b).

reasonable that the attenuating effects of differences in guest and host transition moment directions are also included in the properties of this parameter. The variations in the quantities e, I(e) and a^2 due to differences in the parameter α are illustrated in figure 14.1 and show that, at any particular trap depth, the exciton becomes more localized at the guest while changes in trap transition intensity become larger as the host-host resonance interaction becomes much larger than the guest-host resonance interaction; that is, as α becomes smaller. This implies that, although the coupling of guest to host may be weak for primary traps, changes in trap transition intensities will still be large. Unfortunately, this result is only truly significant at a trap depth of about $2|\beta|$ and is of little practical advantage for very weak polymer resonance interactions.

Philpott[1] has also discussed the spectral effects expected for a series of vibronic levels in the guest. A strong vibronic coupling situation is predicted when an intense free dye transition lies very close to the bottom of a polymer band corresponding to an intense monomer transition. Under these circumstances, it is expected that a trap state will split away from the rest of the vibronic levels and most of the dye transition intensity will be concentrated in this state. Other perturbations expected to arise from secondary traps and guest-guest interactions[1-4] may be considered negligible at low guest concentrations.

14.2 Real Dye-Polymer Complexes

Real polymers having branch-like chromophores are characterized by medium to short-range order, most often of helical symmetry, and weak exciton exchange interactions. Dye binding to such polymers may be expected to be of two forms - one weak, corresponding to external binding,

and one strong, corresponding to intercalation.[7-9] These two forms would correspond to secondary and primary traps, respectively. The magnitude of the polymer resonance interaction is generally weak. Studies of purine and pyrimidine[10-12] systems suggest that degenerate exciton interactions in nucleic acids could be of the order of several hundred wavenumbers. On the other hand, calculations for isotactic polystyrene[13] indicate values of less than $100cm^{-1}$ for the resonance interaction in this case. For a polymer resonance interaction of $50cm^{-1}$, figure 14.1 shows that a 25% change in trap transition intensity from the free dye value will occur at a trap depth of $300cm^{-1}$ when the guest-host resonance interaction is only $5cm^{-1}$ ($\alpha = 0.1$). Since this represents a trap transition about $200cm^{-1}$ below the bottom of the exciton band, the resolution aspect is critical. However, as a series of dye vibronic levels will be involved, Philpott's calculations indicate that the overall guest spectrum could well be affected.

Ideally, dye-polymer complexes of the more well-ordered biopolymers could be studied with known intercalating dyes. Such dyes with intense transitions very close to the main polymer transitions would be measured at temperatures approaching $4^{o}K$. This would invariably mean that only solid films could be studied and such problems as retaining the interstitial guests within the polymer matrix[14] may occur. However, several practical limitations have required that a compromise be arrived at. Firstly, liquid helium facilities were not available for these studies making the absolute resolution of individual spectral lines impractical. Secondly, polymer absorptions are generally in the ultraviolet region where there appear to be no *intense* transitions[15,16] of suitable dyes. Thirdly, the measurements of spectral shifts is complicated

by solvent effects.[17] The compromise situation entails the study of less intense dye transitions in the ultraviolet which overlap with the polymer absorptions. Techniques will be required to resolve as much of the dye band as possible from the intense polymer absorption so that changes in bandshape for a variety of suitable dyes may be correlated to a possible guest-host interaction in terms of expected exciton effects. While polymer resonance interactions may be small, intensity changes incurred in the dye spectrum close to the exciton band and intensity redistributions among vibronic levels would be expected to cause changes in overall bandshapes.

15 EXPERIMENTAL STUDY

The study of dye-polymer complexes has been very extensive, particularly in the biological sphere. However, comments on the ultraviolet absorption of dyes in such aggregates have not been as plentiful. The absorption spectra of acridine dyes bound to DNA in solution have shown a decrease in the absorption in both the ultraviolet and visible regions which was attributed to a coupling between dye and DNA bases.[18] Certain spectral anomalies were also observed in the ultraviolet band of proflavine bound to DNA but spectral inaccuracies rendered these results inconclusive. Further work with various proflavine-biopolymer complexes[19] have also shown spectral changes between free and bound dye, particularly in the ultraviolet region for DNA deoxyribonucleohistone and apurinic acid. These effects were also attributable to dye-DNA interactions. Some very recent work with quinacrine-nucleic acid complexes in solution has been even more spectacular.[20,21] Difference spectra have revealed a band splitting in that part of the ultraviolet region of the quinacrine spectrum which overlaps into the polynucleotide spectrum and this splitting has been attributed to a host-guest interaction of about $550cm^{-1}$.

The work described above has dealt exclusively with solutions of dye-biopolymer complexes. The study of polymer films, on the other hand, is attractive from the point of view of the wider applicability to measurements at low temperatures and for ease of handling. With the aims of developing techniques for separating overlapping dye and polymer absorption bands in the ultraviolet, the polymers poly(vinyl alcohol) (PVA) and atactic sodium poly(styrenesulphonate)(NaPSS) were studied in conjunction

with the dyes Methylene Blue and Thionine (Erlich). The purification of these dyes and sample preparations are presented in Chapter II. PVA, purchased from J.T. Baker Chemical Co. (99-100% hydrolysed, Baker Grade), was used without further purification. NaPSS was prepared by J.R. Zdysiewicz by the sulphonation[22] of atactic polystyrene (Mean molecular weight ≃ 200,000) obtained from the Dow Chemical Co. Solution spectra of the various film samples and dye solutions were carried out on the Ziess-PMQII manual spectrophotometer using the liquid nitrogen cryostat described in Chapter II. Measurements were carried out at room temperature and 77°K. Film thicknesses were measured with a micrometer screw gauge.

15.1 Experimental Results

15.1.1 *Polymer Spectra*

A major difficulty with the measurement of guest spectra in polymer films is to compensate for the absorption due to the polymer. Scattering is a particularly important contribution which becomes increasingly significant in the ultraviolet. Various methods have been applied in an effort to compensate for polymer absorption[23-25] including the use of a reference film.[26] In the case of NaPSS, the absorption in the ultraviolet is substantial and any mismatch between the sample and reference films introduces significant errors. To investigate the degree to which films can be prepared identically, two separate batches of films were prepared by the same technique and from similar polymer solutions. This was done for both PVA and NaPSS and the resultant room temperature and 77°K absorption spectra and room temperature film thicknesses are presented in Appendix B. These absorbances were measured against air as the reference

and were not extended beyond 45000cm^{-1} for PVA and 36000cm^{-1} for NaPSS due to increased oxygen scattering and large polymer absorption, respectively.

Variations in absorbances between films in the same batch were typically between 5% and 10%, while variations of 10% to 20% often occurred between films from different batches. These variations have little correlation with measured film thicknesses in general since scattering and reflection are important components of the measured absorption although all film measurements were carried out at a constant distance from the photomultiplier of the spectrophotometer. Such variations then make the use of a reference film questionable due to the unpredictability of the overall film absorption and would generally require that a reference film be prepared with each sample film. An alternative method which has been suggested[27] entails the use of the measured absorption spectrum of a single reference film as the basis of all further corrections. The polymer absorption spectrum is divided into a series of linear sections and the absorbance gradient in each of these sections is calculated. This series of absorbance gradients are related to one another by multiplication factors so that the background polymer spectrum can be reproduced for a dye-polymer film using, as a guide, a region where the dye does not absorb. This method is successful for PVA and NaPSS. However, computed standard deviations for the fit of straight line sections to these spectra are typically about 20% and over for PVA and about 10% for NaPSS at both temperatures of measurement. In *statistical* terms, then, this method does not improve the degree of confidence in compensating for polymer absorption.

A particularly simple correlation in the PVA and NaPSS absorption spectra does exist, however, which allows the reproduction of these polymer spectra with very good accuracy. Consider a series of measured absorbances, A_1, A_2, A_3, A_4. . . . A_n, defining the polymer spectrum. Then the ratios A_2/A_1, A_3/A_2, A_4/A_3. . . . A_n/A_{n-1} are calculated so that the spectrum is reproduced by introducing the value of A_1 and recalculating the absorbances A_2 to A_n from these ratios. Applying this principle to the PVA and NaPSS film data in Appendix B, it was found that these ratios calculated for each of the films from *both* batches agreed to well within a standard deviation of 2% at each wavelength within each temperature range. By experience, it was found that this correlation would hold provided the steps in wavenumber were not taken so large as to result in absorbance ratios of larger than about 1.5. A series of such ratios were averaged from the data for PVA and NaPSS at both room temperature and 77°K and these ratios appear in the relevant DATA statements of the subroutines PVA293, PVA77, PSS293 and PSS77 in the computer programme RESPECT presented in Appendix C. Although polymer spectra were measured from 16000cm^{-1}, the ratios were extended down to 13000cm^{-1} assuming that the spectrum was horizontal between 13000cm^{-1} and 16000cm^{-1}. Figure 15.1 illustrates the agreement between the measured and calculated polymer spectra using the averaged absorbance ratios. This degree of agreement was found to hold provided the films measured were reasonably close to the film thicknesses in the basic data given in Appendix B. When films approached thicknesses of twice these values, larger discrepancies occurred making the procedure invalid.

A most important point to be noted from the spectra in figure 15.1 is that there is no apparent improvement in resolution in lowering the

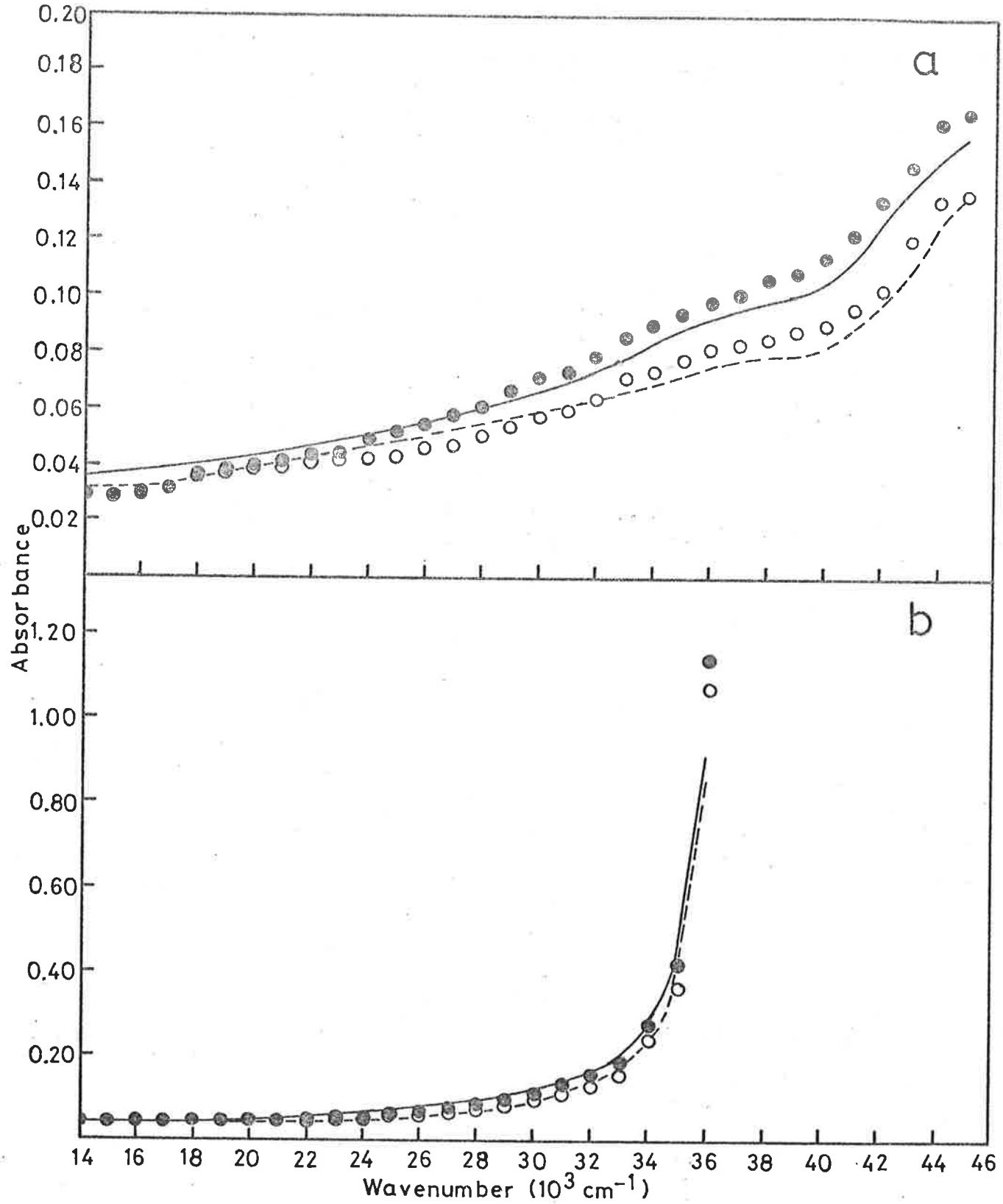

FIG.15.1 COMPARISON OF CALCULATED AND MEASURED POLYMER SPECTRA. (a) PVA; (b) NaPSS. Room temperature values, experimental, o; calculated---. 77°K values, experimental ●; calculated ——.

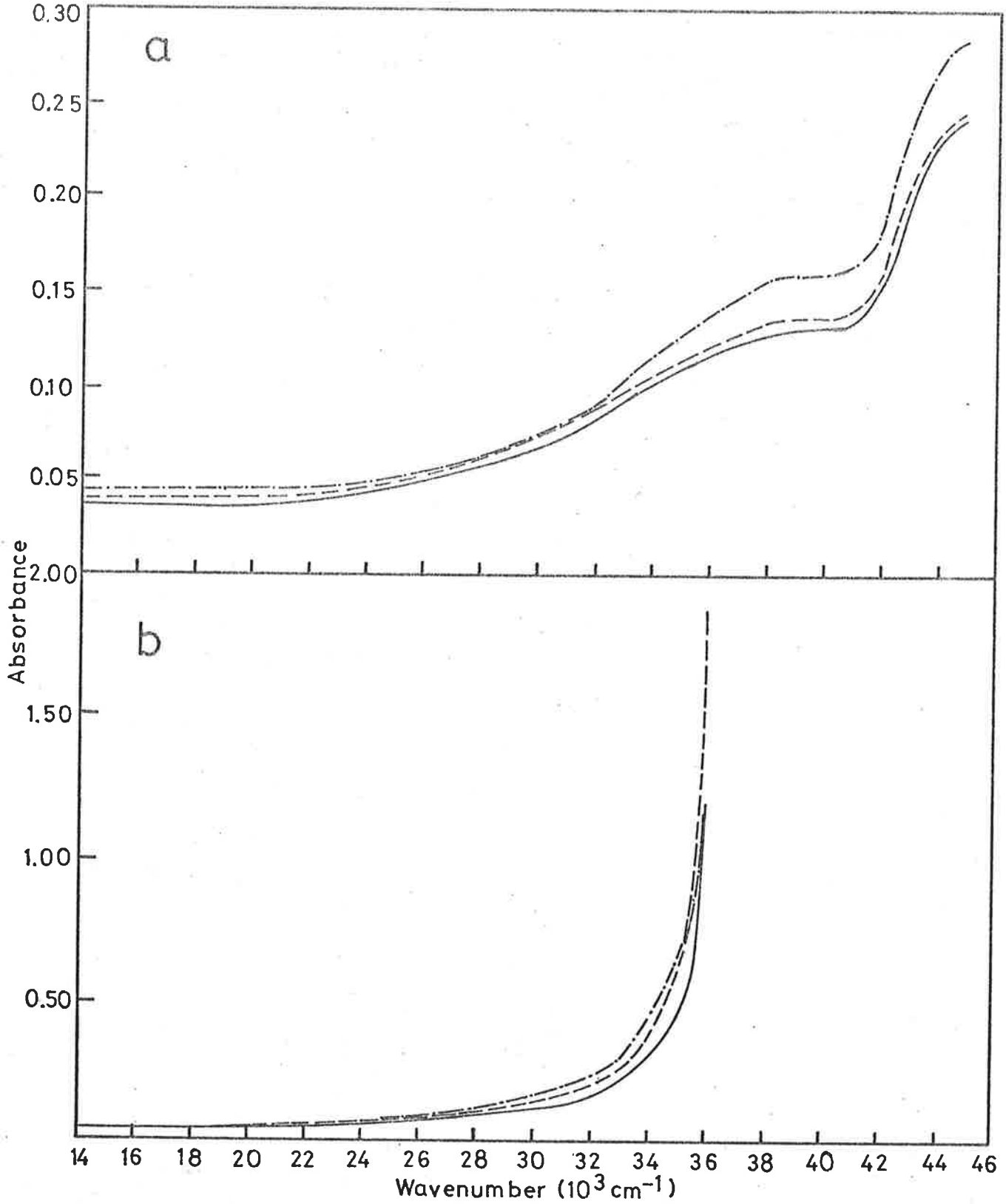

FIG. 15.2 EFFECTS OF VACUUM AND LOW TEMPERATURE ON POLYMER SPECTRA. (a) PVA; (b) NaPSS. Room temp. spectrum: ——; room temp. under vacuum: – – –; 77°K, under vacuum: —·—·—.

temperature to 77°K and thus the procedure described above provides the only accurate method of separating overlapping dye and polymer spectra. In fact, the lowering of temperature does improve resolution but it is countered by the effect of dehydration of the film. Since the films are supported in a high, insulating vacuum at 77°K, the films dehydrate and contract and, presumably, cause increased scattering of the incident light. This is illustrated in figure 15.2 which shows the effect of dehydrating films of PVA and NaPSS at room temperature under vacuum and then cooling them to 77°K.

15.1.2 *Dye Spectra*

Figure 15.3 shows the aqueous solution spectra for the dyes Methylene Blue and Thionine for concentrations at which the dyes are present either in mainly monomeric form or with substantial amounts of dimer. The stability of the isosbestic points indicates that these concentration limits indeed correspond to only monomeric and dimeric species as supported by published data for Methylene Blue[28] and Thionine.[29]

Dye spectra were measured in PVA films to establish two main points. Firstly, the magnitude of spectral shifts incurred by solvent effects in a solid matrix would be indicated by measurements in PVA which acts as a polar solvent. Secondly, since band shape changes are not expected to be marked in the case of dyes dissolved in solid films of PVA,[30] spectra of dye-PVA films provide a test of a technique for separating dye and polymer absorption bands. Dye-polymer films were prepared by the same method used to prepare pure polymer films except that weighed amounts of concentrated dye solution were added. In this way, film thicknesses were in the same range as for the pure polymer films in Appendix B and dye

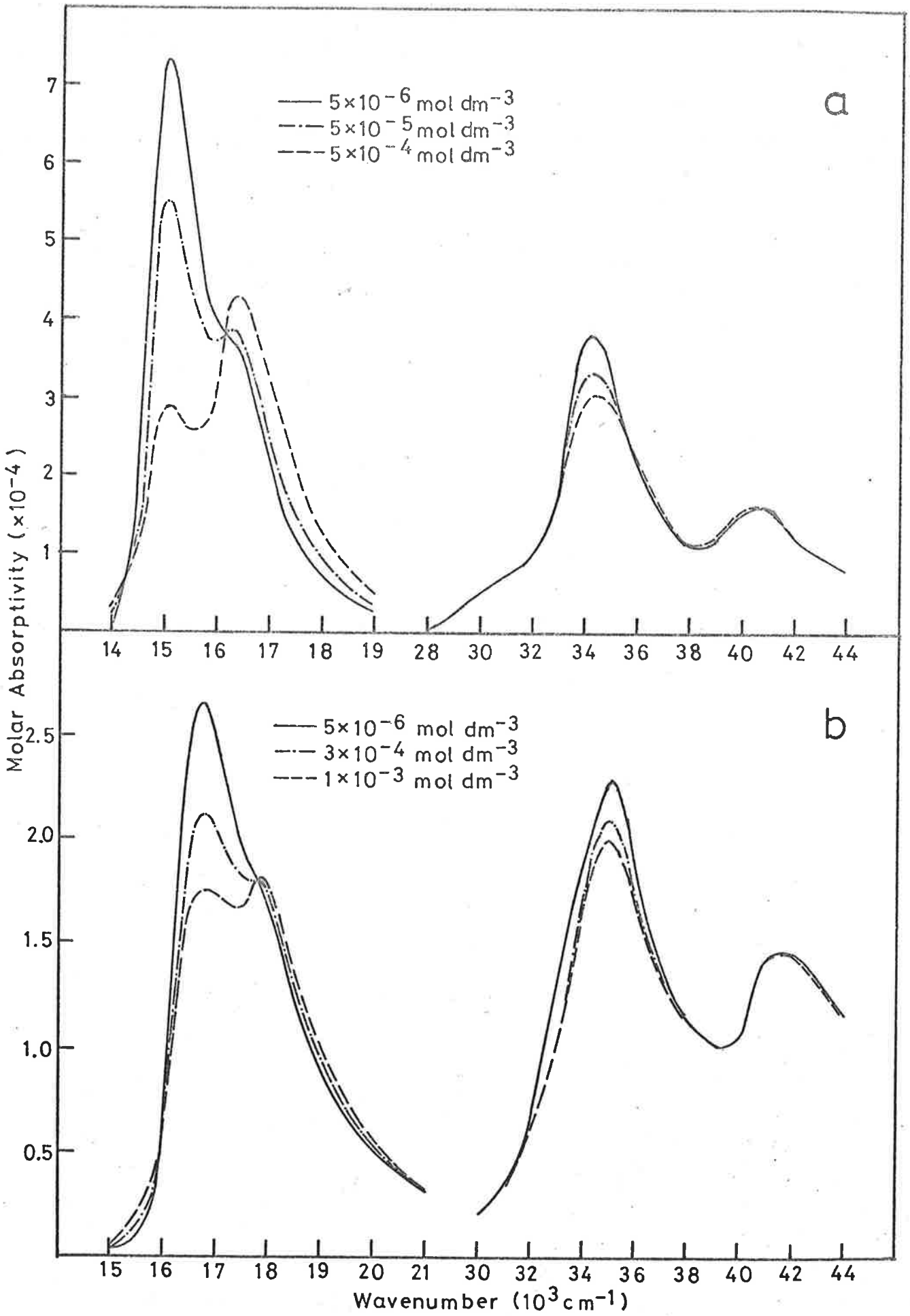

FIG. 15.3 SPECTRA OF PHENOTHIAZINE DYES AS FUNCTION OF CONCENTRATION. Approximate concentrations shown. (a) Methylene Blue; (b) Thionine.

concentrations could be calculated in terms of the dye to monomeric unit ratio (D/P). D/P ratios for the dyes in PVA were between 0.0002 and 0.0004, so that guest-guest interactions could be considered insignificant. Film spectra were measured at room temperature and at 77°K. The method developed for separating the dye and polymer spectra was as follows. It was assumed initially that the ratio of the maximum absorption intensity in the visible to the maximum absorption intensity in the ultraviolet was the same in both aqueous solution and PVA film for the dyes studied at very low concentrations. The polymer background was removed from the measured total dye-polymer spectrum by reproducing the polymer spectrum from an initial absorbance at 13000cm^{-1} as described in Section 15.1.1. This initial absorbance was treated as a parameter which could be varied so as to alter the polymer background and thus allow a computation of a dye spectrum which was as close as possible to the low concentration solution spectrum. This was carried out by means of the computed programme RESPECT in Appendix C in which the visible band intensity of the computed dye spectrum was normalized to the molar absorptivity of the solution spectrum at low concentration. The initial absorbance parameter for the polymer spectrum could then be varied in order to obtain a computed maximum ultraviolet molar absorptivity for the dye which was identical with the low concentration solution value. A comparison between solution and solid film band shapes then may be carried out.

An illustration of this method is given in figure 15.4 for Methylene Blue in PVA. Absorbances below 14000cm^{-1} cannot be considered accurate due to lack of photomultiplier response. It is apparent from this result that the lowering of temperature has only a marginal effect on dye spectrum resolution. There is, however, an increase in absorbance due

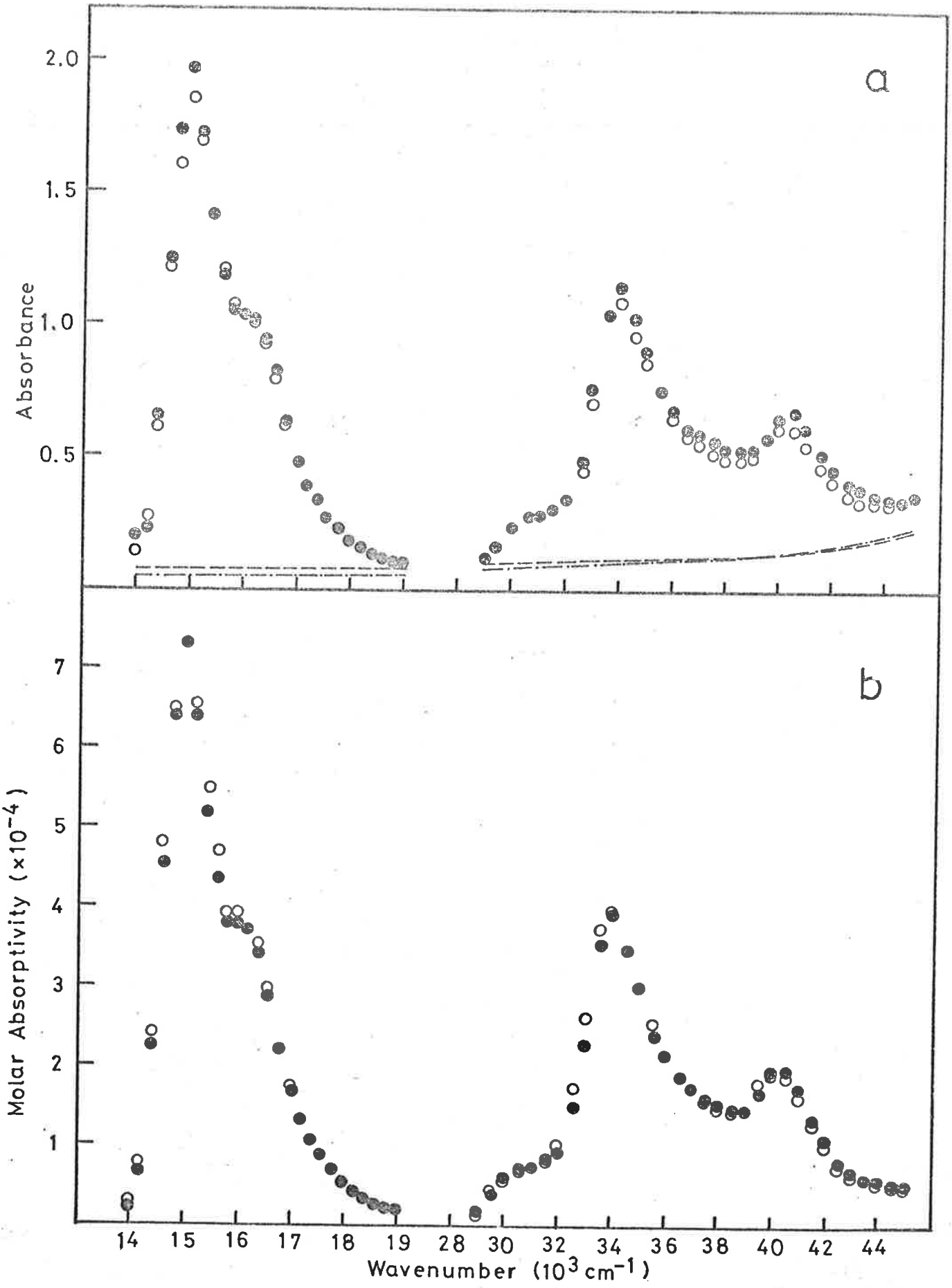

FIG. 15.4 SPECTRUM OF METHYLENE BLUE IN PVA. (a) Total spectrum of dye and PVA, at room temperature: o; at 77°K: ●. PVA background spectrum shown, at room temp: – – – –; at 77°K: —·—·—. (b) Corrected dye spectra at room temp: o; at 77°K: ●.

to contraction of the film. Figure 15.5 shows typical corrected dye spectra in PVA at room temperature for both dyes compared with the low concentration solution spectra. The solution spectra have been shifted in each of the visible and ultraviolet regions to achieve a coincidence between the positions of maximum absorptivity. Most transitions have been shifted by about $400cm^{-1}$ or less to the red in going from aqueous solution to PVA film, except for the far ultraviolet transition of Thionine which has been shifted $3400cm^{-1}$ to the red. Taking this into account, the correspondence between solution and film spectra are reasonable in the visible and near ultraviolet regions at least up to about $35000cm^{-1}$. Thus, at the concentrations prepared, these dyes are present predominantly as monomer in the PVA films and the correction technique is successful in deriving the dye spectra in PVA. There are differences, however, in the spectral shifts observed at room temperature and at $77^{o}K$ for Methylene Blue but not Thionine. These differences have been attributed to the contraction of the polymer structure in the films on *dehydration,* as shown in table 15.1. The transition peaks labelled A, B and C in each of the spectra in figure 15.5 have been tabulated. It is apparent from this data that solvent effects may be quite substantial and sensitive to environmental changes of the solvent. This will be a complicating factor in attempting to elucidate spectral shifts caused by resonance interactions in different polymers and at various temperatures.

The methods and procedures described above were applied to the spectra of Methylene Blue and Thionine in NaPSS. D/P ratios were between 0.0003 and 0.0004 for Methylene Blue and at about 0.0006 for Thionine. Again it was established from the visible spectra that the dyes were predominantly in the monomeric form in the NaPSS films and that, consequently, guest-guest

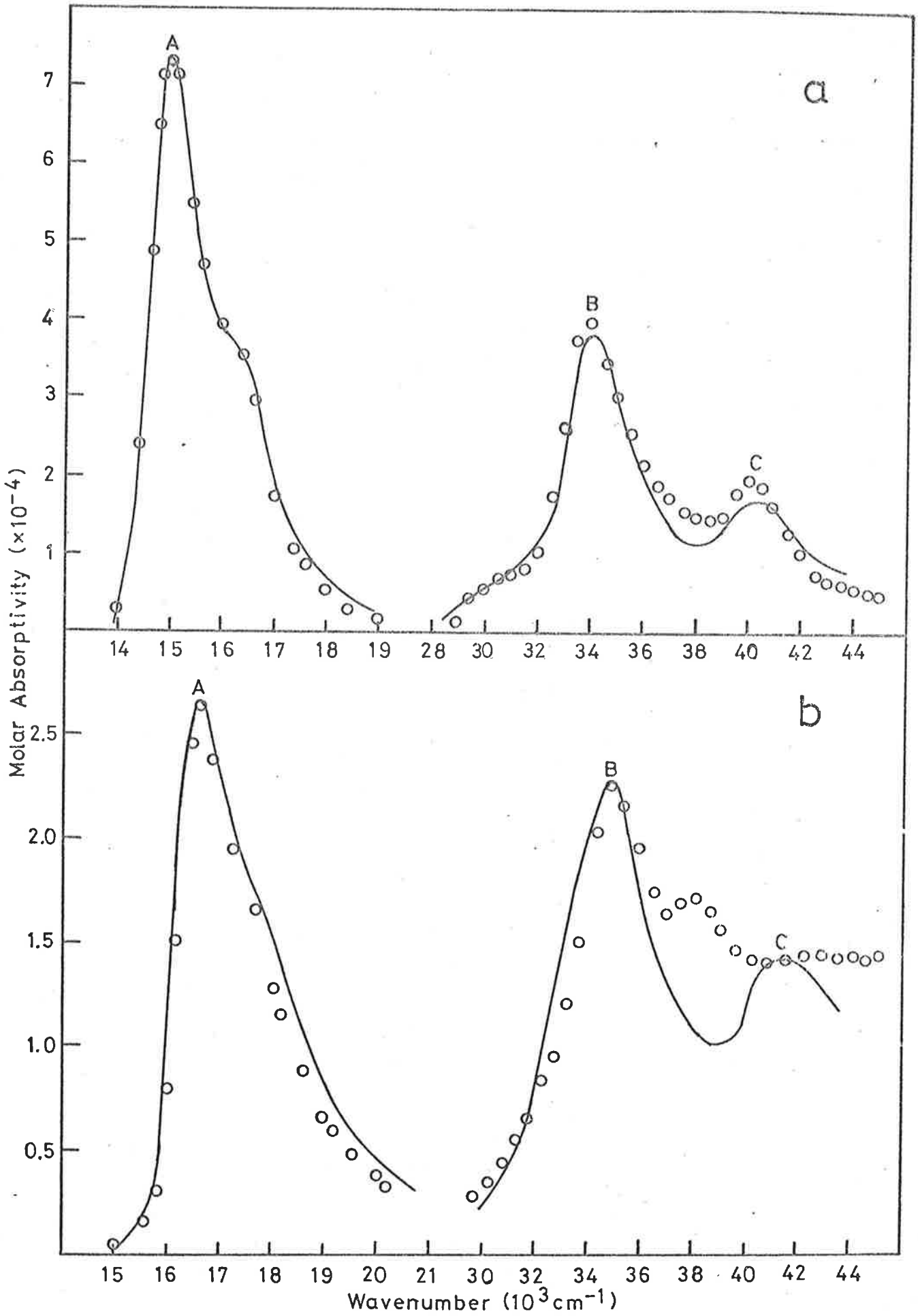

FIG. 15.5 SPECTRA OF PHENOTHIAZINE DYES IN PVA. (a) Methylene Blue; (b) Thionine. Spectrum in PVA at room temp: o; in solution, 5×10^{-6} mol dm^{-3}: ——.

Table 15.1 Spectral Shifts in PVA with respect to Solution Values

Transition Label	Conditions (Shifts in cm^{-1}) 293°K	293°K under vacuum	77°K under vacuum
Methylene Blue:			
A	-100	0	0
B	-200	-100	-100
C	-400	-200	-200
Thionine:			
A	-300	-300	-300
B	0	0	0
C	-3400	-3400	-3400

interactions were not significant. Figure 15.6 shows corrected dye spectra in NaPSS compared with solution spectra and, once more, the solution spectra have been shifted to affect a coincidence. However, due to the very substantial absorption by NaPSS in the region of $36000cm^{-1}$, the resolution of the corrected spectra could not be extended very far beyond $35000cm^{-1}$. The resolution improvement brought about by the lowering of temperature was marginal in the case of NaPSS films as well, resulting in the usual effect of increasing dye absorbances due to contraction. It is apparent from the spectra in figure 15.6 that the correlation between solution and film spectra is not favourable. By ensuring that the maximum molar absorptivity in the ultraviolet coincides with the solution value, a discrepancy occurs for both dyes in the region preceeding this maximum in the spectrum. However, the positions of peaks A and B in figure 15.6 may be resolved at both room temperature and 77°K

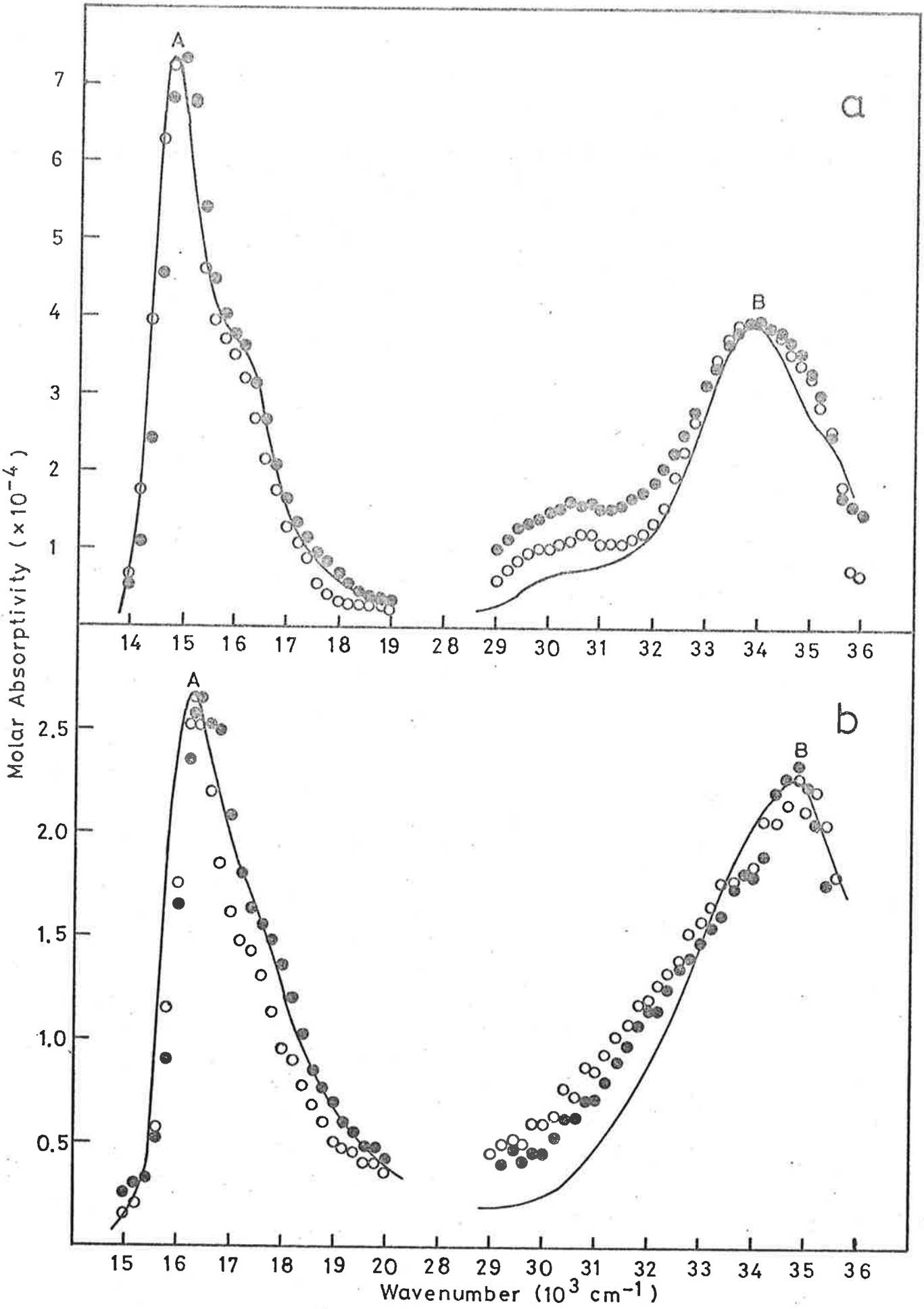

FIG. 15.6 SPECTRA OF PHENOTHIAZINE DYES IN NaPSS. (a) Methylene Blue; (b) Thionine. Spectrum in NaPSS at room temp: o; at 77°K: ●; in solution, 5×10^{-6} mol dm^{-3}: ——.

and compared with the solution values. The resultant spectral shifts are given in Table 15.2. It is seen that the shifts incurred in the dye spectra by the electrostatic forces in the case of NaPSS are somewhat larger than in the case of the polar PVA medium. These results are, however, very dependent on the validity of the correction procedure for resolving the dye spectra. The correlations between the Methylene Blue and Thionine results, unfortunately, leave the answer to this question ambiguous. Nevertheless it is of interest to explore them.

Table 15.2 Spectral Shifts in NaPSS with respect to Solution Values

Transition Label	Conditions (Shifts in cm^{-1})		
	$293^{o}K$	$293^{o}K$ under vacuum	$77^{o}K$ under vacuum
Methylene Blue:			
A	-300	-100	-100
B	-100	-200	-200
Thionine:			
A	-400	-300	-300
B	-500	-500	-500

The discrepancy between the corrected dye spectra in NaPSS and in solution are similar for both Methylene Blue and Thionine. In both cases, the intensity in the shoulder leading into the maximum ultraviolet absorption is larger than for the solution spectrum. Since, in the region of maximum absorptivity, the polymer absorbance is much larger than the dye absorbance, the error may well occur in this part of the spectrum. If each spectrum is then recorrected so that the low energy

"tail" of the ultraviolet absorption coincides with the solution spectrum, the peak absorptivity drops below the solution value in the case of both dye spectra. This was done for the dye spectra in NaPSS at room temperature. In addition, the shifts observed in PVA for the ultraviolet peaks labelled B are subtracted from those observed in NaPSS in an effort to correct for general solvent effects. It is seen that the Thionine transition is closer to the NaPSS absorption, suffers a larger spectral shift and undergoes a larger reduction in intensity. Whether this indicates that some form of guest-host interaction is occurring in the case of these dyes is clouded, however, by the uncertainty in the correction procedure employed which could have the very same effects. The correlation between the Methylene Blue and Thionine results tends to dismiss the premise that these effects are due to impurities.

16 DISCUSSION AND CONCLUSIONS

PVA is a reasonably simple, uncharged polymer which should act as a polar solvent. This is indeed what is found. The resolved dye spectra correspond quite closely to the solution spectra, except for red shifts in the various transitions. Various solvent effects are expected to cause spectral shifts and differences in structural resolution but marked changes in transition intensity do not appear to be caused by these perturbations as they are generally ascribed to additive intermolecular forces.[31] NaPSS is a polyelectrolyte which has been likened more to biopolymers than to other analogous synthetic polyelectrolytes.[32] Dye binding studies[32,33] with Pyronine Y and Acridine Orange suggest that there may be some form of intercalation of the dye into the polymer structure in the case of the acid form of NaPSS. If this were indeed true, interactions between dye and polymer chromophores could be substantial. However, exciton interactions would only be expected in a highly ordered structure such as the isotactic form, while the atactic form was used in this study. Absorption and fluorescence measurements[13,34,35] on the atactic and isotactic forms of polystyrene have indicated, in general, that the two structures are barely distinguishable. Similar results have been observed for the atactic and isotactic forms of poly (styrenesulphonic acid) although dye binding studies do indicate greater order in the isotactic form.[36] However, some form of order in the atactic structure has not been ruled out and may contribute to a certain degree of resonance interaction. Calculations for neutral-exciton interactions in isotactic polystyrene[13] have indicated Davydov splittings of the order of tens of wavenumbers so that guest-host interactions cannot be expected to be substantial.

The spectral changes observed for atactic sodium poly(styrenesulphonate) are quite marked. Assuming a polymer resonance interaction of $50cm^{-1}$ and a guest-host coupling constant of unity, the theory discussed in Section 14 predicts spectral shifts of only $-150cm^{-1}$ at trap depths corresponding to trap intensity changes of 40% to 50%. Such intensity changes are observed for Methylene Blue and Thionine but spectral shifts are as high as $-500cm^{-1}$. Thus, while it may be unreasonable to expect significant resonance interactions in the case of this atactic polymer, it has been shown that the various solvent effects involving polar and elecrostatic forces will have an overiding effect. In summary, the preliminary results presented indicate the limits faced and point to the analysis of the study of dye-polymer systems in solid films involving regions of significant spectral band overlap.

REFERENCES

1. M.R. Philpott, *J. Chem. Phys.*, 53, 968 (1970).

2. M.R. Philpott, *J. Chem. Phys.*, 54, 4223 (1971).

3. M.R. Philpott, *J. Chem. Phys.*, 55, 4005 (1971).

4. M.R. Philpott and J.W. Lee, *J. Chem. Phys.*, 57, 2026 (1972).

5. e.g. D.P. Craig and S.H. Walmsley, *Excitons in Molecular Crystals*, (W.A. Benjamin. 1968). pp. 46-48.

6. R.E. Merrifield, *J.Chem. Phys.*, 38, 920 (1963).

7. A.R. Peacocke and J.N.H. Skerrett, *Trans. Farad. Soc.*, 52, 261 (1956).

8. L.S. Lerman, *J. Mol. Biol.*, 3, 18 (1961).

9. L.S. Lerman, *Proc. Natl. Acad. Sci. (US)*, 49, 94 (1963).

10. J.N. Kikkert, G.R. Kelly and T. Kurucsev, *Biopolymers*, 12, 1459 (1973).

11. G.R. Kelly and T. Kurucsev, *Biopolymers*, 13, 769 (1974).

12. D.E. Joyce and T. Kurucsev, *Biophys. Chem.*, 2, 273 (1974).

13. M.T. Vala, J. Haebig and S.A. Rice, *J. Chem. Phys.*, 43, 886 (1965).

14. A. Bree, A.R. Lacey, I.G. Ross and R.Zwarich, *Chem. Phys. Lett.*, 26, 329 (1974).

15. A. Albert, *The Acridines*,(Edward Arnold, 1966).

16. E. Gurr, *Synthetic Dyes in Biology, Medicine and Chemistry*, (Academic Press. 1971).

17. W. Liptay, *Modern Quantum Chemistry* (Ed. O. Sinanoğlu; Academic Press. 1965). Part II, pp. 173-198.

18. G. Weill and M. Calvin, *Biopolymers*, 1, 401 (1963).

19. I.O. Walker, *Biochim. Biophys. Acta*, 109, 585 (1965).

20. (a) M. Nastasi, R.W. Yip, V.L. Seligy, A.G. Szabo and R.E. Williams, *Nature*, 249, 248 (1974).

    (b) A.G. Szabo, V.L. Seligy, M. Nastasi and R.W. Yip, *Biochem. Biophys. Res. Comm.*, 62, 830 (1975).

21. M. Nastasi, J.M. Morris, D.M. Rayner, V.L. Seligy, A.G.Szabo, D.F. Williams, R.E. Williams and R.W. Yip, *J. Amer, Chem. Soc.*, 98, 3979 (1976).

22. (a) A.F. Turback, *I & E.C. Product Research and Development*, 1, 275 (1962).

(b) A.F. Turback, *ibid*, 2, 229 (1963).

(c) A.F. Turback, *US Patents* 3,072,618; 3,072,619; 3,072,703.

23. T. Kurucsev and J.R. Zdysiewicz, *Biopolymers*, 10, 593 (1971).

24. S.W. Englander and H.T. Epstein, *Archs. Biochem. Biophys.*, 68, 144, (1957).

25. D.M. Gray and I. Rubenstein, *Biopolymers*, 6, 1605 (1968).

26. A. Rupprecht, R. Rigler, B. Forslind and G. Swanbeck, *Europ. J. Biochem.*, 10, 291 (1969).

27. G.R. Kelly, *Ph.D. Thesis*, (University of Adelaide.1974).

28. E. Braswell, *J. Phys. Chem.*, 72, 2477 (1968).

29. G.R. Haugen and E.R. Hardwick, *J. Phys. Chem.*, 67, 725 (1963).

30. H. Jacobi and H. Kuhn, *Z. Electrochem.*, 66, 47 (1962).

31. J.B. Birks, *Photophysics of Aromatic Molecules*, (Wiley-Interscience. 1970). pp. 109-119.

32. V. Vitagliano and L. Costantino, *J. Phys. Chem.*, 74, 197 (1970).

33. V. Vitagliano, L. Costantino and A. Zagari, *J. Phys. Chem.*, 77, 204 (1973).

34. M. Vala and S.A. Rice, *J. Chem. Phys.*, 39, 2348 (1963).

35. J.W. Longworth, *Biopolymers*, 4, 1131 (1966).

36. (a) D.O. Jordan, T. Kuruscev and M.L. Martin, *Trans. Farad. Soc.*, 64, 598 (1968).

(b) D.O. Jordan, T. Kuruscev and M.L. Martin, *ibid*, 64, 606 (1968).

(c) D.O. Jordan, T. Kuruscev and M.L. Martin, *ibid*, 65, 612, (1969).

Appendices

APPENDIX A PREDICTION ANALYSIS

The following is a description of the basic formulation of the statistical method of prediction analysis presented by J.R. Wolberg in "Prediction Analysis" (Van Nostrand, 1967). The application to a model monomer-dimer solution equilibrum was presented in part fulfilment of the degree of Bachelor of Science (Honours) at the University of Adelaide in November, 1972.

The purpose of prediction analysis is to make some estimate of the precision of the parameters determined in an experiment for which the physical law may be written in the general form

$$\eta_i = f(\xi_{1i}, \ldots \xi_{ji}, \ldots \xi_{mi} ; \alpha_1, \ldots \alpha_k, \ldots \alpha_p), \qquad (1)$$

where the dependent variable η_i, of the i th measurement, is a function of the m independent variables ξ_{ji} and of the p unknown parameters α_k. As a consequence, the precision of the results may be studied as a function of the experimental conditions including such entities as, for example, the number of data points taken, the distribution of these points and the accuracy of the instrumentation used. Prediction analysis is essentially a non-linear least squares procedure computing the standard deviations in the unknown parameters from the experimental variables and from the estimates of the parameters themselves. Four conditions must be fulfilled in order that prediction analysis may be applied to the problem on hand. Firstly, an explicit form of the physical law described in general form by eqn (1) is assumed to apply to the data. Secondly, estimates of the experimental variables and of their standard deviations

are required. Thirdly, it is assumed that data processing will be carried out by the method of least squares. Lastly, it is necessary that some estimate of the values of the unknown parameters be made.

The model monomer-dimer equilibrium was of interest in relation to the solution behaviour of the dye Pyronine Y. The physical law for such a system is written, as described in Chapter III, in the form

$$A_i^\lambda = \frac{b_i}{4K}(-1 + \sqrt{1 + 8KC_i})\{\varepsilon_1^\lambda + \frac{\varepsilon_2^\lambda}{4}(-1 + \sqrt{1 + 8KC_i})\} \qquad (2)$$

where A_i^λ, the solution absorbance at wavelength λ, is given as the function of the independent variables b_i, the path length of the cell, and C_i, the stoichiometric dye concentration, and of the unknown parameters to be determined, namely the dimerization constant K, and the molar absorptivities at wavelength λ of the monomeric species, ε_1^λ, and of the dimer species, ε_2^λ. Attention was confined to the wavelength λ^0 of the maximum absorption and the corresponding molar absorptivities $\varepsilon_1{}^0$ and $\varepsilon_2{}^0$ of the monomer and dimer species, respectively. The number of solutions to be included in this analysis was set arbitrarily at 20 and their concentrations were assumed to be evenly spaced between 1×10^{-5} mol dm^{-3} and 1×10^{-3} mol dm^{-3}. The initial set of parameters to be used in the calculation were selected as follows:

$$K = 1 \times 10^3 \text{ dm}^3 \text{ mol}^{-1}$$
$$\varepsilon_1{}^0 = 1 \times 10^5 \text{ dm}^3 \text{ mol}^{-1} \text{cm}^{-1}$$
$$\varepsilon_2{}^0 = 2 \times 10^4 \text{ dm}^3 \text{ mol}^{-1} \text{cm}^{-1}.$$

The standard deviations in the absorbances were calculated from a constant standard deviation of 0.3% in transmittance, and the relative standard deviations in the path lengths and concentrations both were estimated at

0.5%. Figure A.1 illustrates the results obtained from applying the procedure described by Wolberg to this model system varying each of the parameters K, ε_1^0 and ε_2^0 independently. It is seen, for example, that the value of ε_1^0 is determined quite precisely under all conditions considered since the monomer is present in relatively large amounts throughout the concentration range. However, the errors in both ε_2^0 and K are sensitive to the relative magnitudes of ε_1^0 and ε_2^0 and to the relative concentrations of the monomer and dimer species. The worst situation for determining K, in particular, corresponds to the case where ε_1^0 and ε_2^0 are close in value. Most of these results could have been anticipated qualitatively. However, the analysis has established the quantitative limits to the parameters within which the experiment could be considered worth performing and has illustrated the statistical correlation between the unknown parameters.

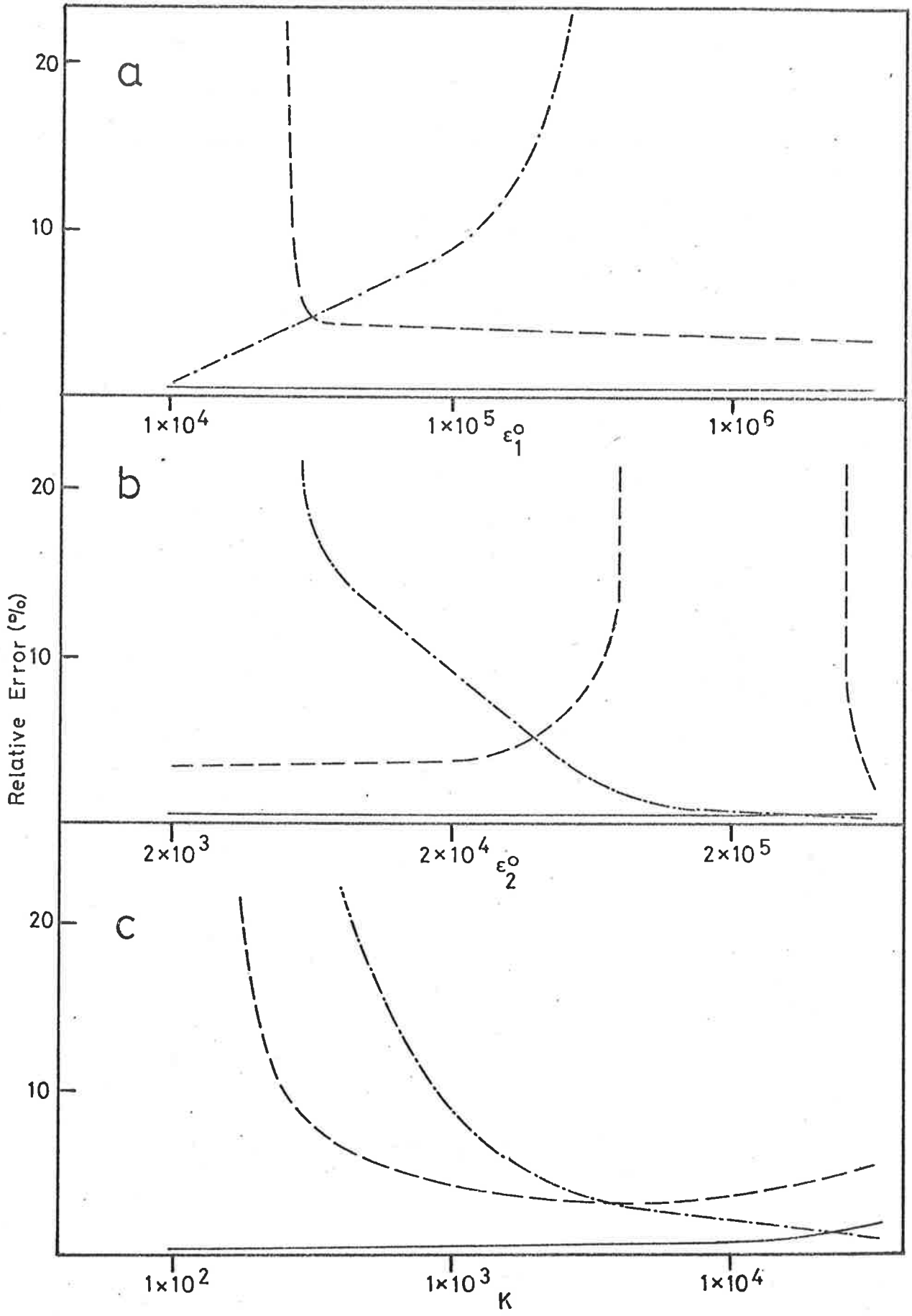

FIG. A.1 PREDICTED RELATIVE STANDARD DEVIATIONS IN DERIVED VALUES OF PARAMETERS K (– – –), ε_1^o (——) AND ε_2^o (—·—·—). (a) K and ε_2^o fixed at initial values and ε_1^o varied; (b) K and ε_1^o fixed, ε_2^o varied; (c) ε_1^o and ε_2^o fixed, K varied.

APPENDIX B EXPERIMENTAL DATA

B-1 Dimer Solution Data

Concentrations of dye solutions,

Cell path lengths.

Measured molar absorptivities.

B-2 Mixed Crystal Data

Crystal thicknesses at room temperature,

Guest concentrations,

Isotropic guest absorbances.

Polarized absorbance versus angle of incidence data,

B-3 Polymer Film Data

Film thicknesses at room temperature,

Poly (vinyl alcohol) and poly (styrenesulphonate) film absorbances at $77^{o}K$ and at room temperature,

B-1 Dimer Solution Data

Solution Label	Concentration (mol dm^{-3})	Path Length (cm)	Distribution*
1	4.805×10^{-6}	2.040	E, O
2	5.664×10^{-5}	0.105	E
3	1.043×10^{-4}	0.105	E
4	1.541×10^{-4}	0.0519	E
5	2.041×10^{-4}	0.0522	E, O
6	2.247×10^{-4}	0.0515	O
7	2.440×10^{-4}	0.0409	O
8	2.587×10^{-4}	0.0411	E, O
9	2.840×10^{-4}	0.0410	O
10	3.043×10^{-4}	0.0410	E, O
11	3.236×10^{-4}	0.0306	O
12	3.496×10^{-4}	0.0308	E, O
13	3.618×10^{-4}	0.0307	O
14	3.830×10^{-4}	0.0308	O
15	4.030×10^{-4}	0.0308	E, O
16	4.532×10^{-4}	0.0308	E
17	5.028×10^{-4}	0.0205	E
18	5.520×10^{-4}	0.0205	E
19	6.024×10^{-4}	0.0205	E, O
20	6.520×10^{-4}	0.0207	E
21	6.700×10^{-4}	0.0206	E
22	7.503×10^{-4}	0.0205	E
23	8.008×10^{-4}	0.0102	E, O
24	8.212×10^{-4}	0.0102	O
25	8.536×10^{-4}	0.0102	E, O
26	8.859×10^{-4}	0.0102	O
27	9.076×10^{-4}	0.0102	E, O
28	9.474×10^{-4}	0.0103	E, O
29	9.720×10^{-4}	0.0103	O
30	1.000×10^{-3}	0.0103	E, O

* E : 21 point even distribution) total of 30 quasi-evenly distributed points
O : 21 point optimum distribution)

On the next page, molar absorptivities are presented vertically with solution label and horizontally with wavenumber (cm^{-1}).

	16000.	16200.	16400.	16600.	16800.	17000.	17100.	17200.	17300.	17400.	17500.	17600.	17700.	17800.	17900.
(1)	400.	612.	612.	714.	714.	1122.	1428.	1938.	2959.	4591.	7549.	12344.	19281.	29687.	42235.
(2)	337.	337.	505.	506.	843.	1012.	1518.	2024.	3035.	4553.	7251.	11467.	17531.	26812.	37604.
(3)	275.	366.	458.	641.	1007.	1648.	2105.	2839.	3754.	5545.	8332.	12819.	19137.	27836.	38823.
(4)	250.	501.	501.	751.	1126.	1752.	2253.	2878.	4005.	5506.	8260.	12264.	18272.	27157.	36668.
(5)	375.	375.	469.	844.	1313.	1876.	2345.	3002.	4034.	5535.	8162.	12102.	17637.	25798.	35086.
(6)	346.	432.	432.	1037.	1383.	1902.	2334.	3112.	4149.	5792.	8126.	12103.	17462.	25502.	34406.
(7)	301.	401.	601.	1002.	1403.	2004.	2505.	3306.	4308.	5912.	8517.	12324.	17735.	25450.	34067.
(8)	376.	470.	658.	846.	1316.	2069.	2633.	3197.	4231.	5735.	8086.	11941.	16830.	24446.	32908.
(9)	258.	515.	687.	859.	1374.	2061.	2576.	3177.	4208.	5754.	8072.	11765.	16832.	24131.	32633.
(10)	321.	401.	641.	962.	1362.	2003.	2564.	3286.	4247.	5770.	8094.	11620.	16908.	24121.	32615.
(11)	303.	404.	606.	1010.	1515.	2222.	2828.	3534.	4342.	5857.	8281.	11916.	16461.	24034.	32012.
(12)	279.	558.	651.	1023.	1581.	2232.	2791.	3442.	4279.	5747.	8186.	11720.	16278.	23348.	31533.
(13)	360.	450.	631.	991.	1532.	2252.	2793.	3514.	4414.	5856.	8108.	11261.	16396.	23243.	30721.
(14)	340.	594.	679.	1019.	1528.	2293.	2717.	3481.	4415.	5774.	7997.	11293.	16218.	22841.	30567.
(15)	403.	565.	726.	1130.	1614.	2421.	2905.	3631.	4600.	5971.	8150.	11620.	16301.	22837.	30584.
(16)	287.	502.	718.	1220.	1650.	2440.	2942.	3660.	4592.	5956.	8252.	11338.	16002.	22101.	29564.
(17)	292.	584.	778.	1167.	1653.	2529.	3015.	3793.	4765.	6127.	8267.	11379.	15853.	22563.	29371.
(18)	353.	619.	795.	1326.	1856.	2563.	3005.	3800.	4772.	6009.	8307.	11311.	15465.	21474.	28632.
(19)	406.	568.	812.	1218.	1867.	2598.	3166.	3896.	4708.	6250.	8199.	11121.	15017.	21187.	27518.
(20)	446.	668.	891.	1263.	1931.	2600.	3119.	3936.	4902.	6239.	8096.	11290.	15152.	20722.	27333.
(21)	348.	626.	904.	1321.	1947.	2782.	3338.	4173.	4938.	6259.	8276.	11267.	15092.	20516.	26775.
(22)	456.	521.	847.	1303.	1955.	2737.	3324.	4041.	4953.	6257.	8277.	11210.	14990.	20530.	26526.
(23)	488.	732.	977.	1465.	1953.	2930.	3418.	4272.	5249.	6470.	8545.	11352.	15014.	20629.	26489.
(24)	476.	595.	952.	1428.	1905.	2738.	3452.	4166.	5119.	6428.	8332.	11189.	14998.	20355.	25116.
(25)	460.	575.	921.	1381.	1956.	2877.	3337.	4143.	5063.	6329.	8286.	10817.	14385.	19794.	25433.
(26)	441.	662.	993.	1324.	2096.	2979.	3641.	4303.	5296.	6621.	8496.	11255.	14896.	20082.	25820.
(27)	646.	646.	969.	1508.	2154.	3016.	3554.	4308.	5277.	6570.	8401.	11417.	14863.	19710.	25418.
(28)	411.	616.	924.	1335.	1951.	2875.	3491.	4107.	5031.	6151.	8009.	10473.	13964.	18482.	24026.
(29)	598.	797.	1096.	1494.	2191.	3087.	3685.	4382.	5278.	6474.	8465.	11155.	14342.	19222.	24899.
(30)	389.	681.	972.	1361.	1945.	2917.	3501.	4182.	5057.	6321.	8169.	10697.	14198.	19060.	24215.

	18000.	18100.	18200.	18300.	18400.	18500.	18600.	18700.	18800.	18900.	19000.	19100.	19200.	19300.	19400.
(1)	56824.	68862.	77228.	81104.	80186.	76105.	70290.	64373.	58456.	52641.	47846.	43868.	40807.	38665.	37033.
(2)	49914.	60200.	67957.	70824.	70149.	66777.	62224.	57155.	52443.	47890.	43575.	40977.	39290.	38110.	37604.
(3)	50635.	60158.	66934.	69314.	68032.	64828.	60158.	55671.	51001.	46973.	43768.	41662.	40563.	40288.	40380.
(4)	47681.	55191.	62323.	64451.	63325.	60321.	56066.	51936.	48182.	44552.	41924.	40548.	39797.	40297.	40923.
(5)	45218.	53661.	59665.	62010.	61259.	58257.	54505.	50659.	46906.	43904.	41653.	40527.	40433.	41090.	42216.
(6)	44434.	52474.	59043.	61032.	60254.	57487.	53770.	50053.	46422.	43397.	41235.	40284.	40284.	41062.	42186.
(7)	43986.	51801.	56511.	58214.	57112.	54206.	50699.	47192.	43986.	41281.	39778.	39077.	39678.	40880.	42082.
(8)	42781.	50585.	55755.	57637.	56885.	54252.	50579.	47294.	44003.	41371.	39584.	39020.	39302.	40336.	41653.
(9)	41993.	49808.	55218.	57107.	56420.	53930.	50495.	47317.	44054.	41134.	39760.	39073.	39503.	40791.	42165.
(10)	41109.	49203.	54171.	56095.	55453.	53049.	49684.	46398.	43353.	40869.	39426.	38946.	39667.	40789.	42391.
(11)	41202.	48776.	53522.	55542.	55139.	52411.	49180.	46049.	43222.	40697.	39182.	38879.	39687.	41101.	42818.
(12)	39905.	47068.	51998.	53765.	53300.	50695.	47626.	44556.	41858.	39719.	38417.	38138.	39068.	40556.	42324.
(13)	39820.	46576.	51802.	53794.	53063.	50901.	47658.	44695.	41982.	39820.	38649.	38378.	39189.	40901.	42793.
(14)	38549.	46191.	50861.	52729.	52219.	49842.	46700.	43898.	41266.	39313.	38039.	38039.	38973.	40587.	42540.
(15)	38815.	45512.	50273.	51958.	51403.	49063.	45996.	43172.	40590.	38815.	37846.	37846.	38695.	40832.	42769.
(16)	37457.	44131.	48436.	49871.	49369.	47288.	44418.	41691.	39466.	37816.	36955.	37314.	38605.	40615.	42911.
(17)	36860.	43570.	48044.	49795.	49308.	47363.	44640.	42014.	39680.	37979.	37249.	37735.	39096.	41042.	43376.
(18)	36055.	42064.	46306.	47985.	47367.	45511.	42948.	40562.	38618.	37116.	36585.	37116.	38706.	40916.	43478.
(19)	34662.	40669.	44890.	46513.	46270.	44321.	41724.	39695.	37828.	36285.	36042.	36610.	38233.	40587.	43104.
(20)	34017.	40182.	43970.	45455.	44787.	43227.	40925.	38771.	37062.	35800.	35651.	36468.	38102.	40627.	43227.
(21)	33800.	39085.	42910.	44301.	43914.	42145.	39989.	37903.	36303.	35260.	35191.	36095.	37972.	40685.	43258.
(22)	33304.	38583.	42363.	43797.	43340.	41711.	39560.	37540.	35976.	34998.	34998.	35976.	37865.	40539.	43340.
(23)	33080.	38573.	42113.	43822.	43334.	41747.	39794.	37841.	36254.	35278.	35278.	36498.	38329.	41015.	43822.
(24)	32854.	39091.	41662.	43210.	42353.	41424.	39282.	37377.	35930.	34996.	34996.	35949.	37972.	40591.	43567.
(25)	31762.	37056.	40853.	42464.	42119.	40623.	38782.	36941.	35444.	34639.	34754.	35905.	37861.	40508.	43385.
(26)	31999.	37185.	40385.	41709.	41268.	39944.	37847.	36082.	34758.	34096.	34427.	35530.	37737.	40606.	43475.
(27)	31773.	36835.	40173.	41574.	41143.	39635.	37804.	36188.	34788.	34142.	34142.	35434.	37589.	40497.	43405.
(28)	30084.	35218.	39223.	40968.	40968.	39531.	37785.	36142.	34705.	33996.	33986.	35116.	37169.	39941.	42919.
(29)	30874.	35655.	39240.	40435.	40435.	39140.	37248.	35655.	34760.	33653.	33962.	35157.	37348.	40236.	43124.
(30)	30147.	35106.	38704.	40260.	40066.	38802.	36954.	35301.	34036.	33453.	33745.	34912.	37246.	40066.	42983.

	19500.	19600.	19700.	19800.	19900.	20000.	20200.	20400.	20600.	20800.	21000.	21200.	21400.	21600.	21800.	22000.
(1)	35706.	34074.	32239.	29891.	27443.	24688.	19587.	15609.	12344.	10100.	8263.	6835.	5611.	4489.	3673.	2959.
(2)	36930.	35086.	34569.	32545.	29847.	27149.	21584.	17200.	13928.	11298.	9443.	7757.	6239.	4890.	3878.	3035.
(3)	40105.	39281.	37725.	35344.	32414.	29301.	23349.	18313.	14375.	11537.	9614.	7875.	6318.	5036.	4029.	3205.
(4)	41048.	40798.	39296.	37044.	34040.	30786.	24904.	20024.	15443.	12640.	10512.	8635.	6883.	5506.	4255.	3379.
(5)	42778.	42591.	41277.	39026.	36024.	32834.	26455.	21014.	16511.	13415.	10982.	9006.	7130.	5723.	4597.	3659.
(6)	42878.	42705.	41408.	39247.	36308.	33109.	26712.	21180.	16771.	13572.	11152.	9163.	7262.	5878.	4582.	3804.
(7)	43084.	42884.	41682.	39477.	36572.	33165.	27253.	21943.	17334.	14228.	11723.	9519.	7715.	6112.	4809.	3807.
(8)	42405.	42405.	41277.	39208.	36105.	33096.	26985.	21438.	17018.	13916.	11471.	9402.	7522.	5924.	4795.	3761.
(9)	43195.	43195.	42079.	40018.	37184.	33835.	27566.	21898.	17261.	13912.	11507.	9446.	7471.	6011.	4809.	3779.
(10)	43593.	43674.	42472.	40548.	37663.	34538.	28047.	22278.	17710.	14144.	11700.	9536.	7693.	6010.	4808.	3756.
(11)	43928.	44231.	42919.	40798.	38071.	34739.	28580.	22722.	18076.	14542.	11916.	9695.	7776.	6261.	5049.	3938.
(12)	43626.	43905.	42882.	40835.	38045.	34975.	28650.	22976.	18232.	14843.	12185.	9860.	8000.	6418.	5023.	4000.
(13)	44054.	44414.	43694.	41802.	38829.	35766.	29279.	23423.	18468.	14845.	12342.	10000.	8108.	6396.	5045.	4054.
(14)	43898.	44323.	43474.	41436.	38719.	35662.	29039.	23435.	18510.	14944.	12227.	10019.	8066.	6368.	5179.	4161.
(15)	44302.	44544.	43656.	41800.	38976.	35910.	29595.	23886.	18983.	15171.	12427.	10168.	8231.	6456.	5326.	4196.
(16)	44489.	44848.	43915.	42265.	39753.	35453.	30497.	24541.	19590.	15747.	12945.	10548.	8467.	6745.	5382.	4234.
(17)	44835.	45613.	44835.	42987.	40555.	37443.	31219.	25009.	20132.	16242.	13324.	10893.	8753.	6905.	5544.	4376.
(18)	45246.	45041.	45422.	43655.	41004.	37999.	31725.	25981.	20679.	16730.	13597.	11135.	8925.	7070.	5567.	4507.
(19)	45052.	45864.	45377.	43672.	41237.	39071.	32064.	26139.	20962.	16884.	13900.	11283.	9010.	7052.	5682.	4546.
(20)	45010.	45049.	45455.	43895.	41444.	39474.	32457.	26664.	21791.	17231.	14112.	11434.	9210.	7279.	5868.	4753.
(21)	45344.	45318.	45831.	44301.	41867.	39224.	33104.	27332.	21938.	17535.	14327.	11614.	9389.	7441.	5941.	4729.
(22)	45361.	46338.	45817.	44383.	41441.	39039.	33103.	27112.	21933.	17532.	14273.	11601.	9320.	7299.	5866.	4758.
(23)	46019.	45996.	46503.	45155.	42946.	40038.	34057.	28076.	22583.	18310.	14992.	12045.	9765.	7690.	6103.	5005.
(24)	45829.	45781.	46543.	45114.	42734.	39877.	33587.	27735.	22179.	17974.	14522.	11665.	9523.	7390.	5833.	4761.
(25)	45802.	45952.	46837.	45341.	43270.	40508.	34639.	28540.	23131.	18758.	15140.	12314.	9782.	7825.	6214.	5063.
(26)	45681.	45785.	46675.	45240.	42923.	40164.	34537.	28468.	22951.	18537.	15006.	12027.	9600.	7724.	6179.	4835.
(27)	45666.	45851.	46528.	45235.	43061.	40389.	34681.	28757.	23155.	18740.	15078.	12170.	9693.	7852.	6355.	5052.
(28)	45383.	45923.	47026.	45999.	43946.	41276.	35525.	29674.	24026.	19406.	14583.	12527.	10062.	8111.	6469.	5237.
(29)	45514.	45809.	46809.	45415.	43323.	40535.	34853.	28982.	23405.	19022.	15437.	12648.	10059.	7968.	6374.	5179.
(30)	45512.	45873.	46873.	45706.	43567.	41038.	35203.	29271.	23431.	19158.	15284.	12350.	9822.	7790.	6321.	5154.

B-2 Mixed Crystal Data

Crystal Label	Total Guest Concentration (mol/mol)	Isotropic Absorbance for trap shown	Thickness (cm)
Tetracene:		(TETA)	
1	0.0048	0.244	0.0014
2	0.0022	0.308	0.0039
3	-	-	0.0035
4	0.0018	0.166	0.0025
5	0.0020	0.170	0.0025
6	0.0037	0.214	0.0016
7	0.0030	0.518	0.0048
8	0.0043	0.344	0.0022
9	0.0014	0.223	0.0045
10	0.0022	0.262	0.0033
1-amino-anthracene:		(1A)	
1	0.0023	0.036	0.0007
2	0.0041	0.259	0.0029
3	0.0030	0.422	0.0064
4	0.0031	0.391	0.0058
5	0.0039	0.411	0.0049
6	0.0028	0.232	0.0038
7	0.0027	0.440	0.0075
8	0.0037	0.255	0.0032
9	0.0033	0.114	0.0016
2-amino-anthracene:		(2A)	
1	0.0119	0.335	0.0013
2	0.0030	0.408	0.0063
3	0.0061	0.199	0.0015
4	0.0018	0.181	0.0046
5	0.0044	0.240	0.0025
6	0.0037	0.304	0.0038
7	0.0051	0.233	0.0021
8	0.0019	0.160	0.0039
9	0.0038	0.351	0.0043
10	0.0032	0.317	0.0045

On the next page, ac- and b- polarized absorbances are presented vertically with crystal label and horizontally with angle of incidence (degrees). For each sample, ac- then b- polarized absorbances are presented one above the other.

	-15.0	-10.0	-5.0	0.0	5.0	10.0	15.0	20.0	25.0	30.0	35.0	40.0	43.5
TETA(1)	.116	.118	.112	.110	.119	.126	.123	.128	.133	.139	.137	.143	.139
	.635	.616	.606	.604	.625	.620	.625	.625	.627	.636	.646	.638	.633
TETB	.751	.747	.728	.739	.818	.913	.845	.943	.960	.879	.892	.899	.879
	-	-	-	-	-	-	-	-	-	-	-	-	-
TETC	.049	.062	.048	.041	.054	.068	.053	.070	.058	.066	.073	.062	.062
	.370	.357	.349	.348	.357	.361	.364	.359	.366	.363	.370	.374	.378
TETA(2)	.137	.137	.134	.127	.145	.157	.155	.165	.171	.168	.171	.173	.177
	.802	.793	.726	.728	.773	.807	.753	.817	.785	.837	.821	.834	.808
TETA(3)	-	.384	.376	.413	.400	.431	.430	.446	.451	.472	.478	.488	.491
	-	-	-	-	-	-	-	-	-	-	-	-	-
TETA(4)	.079	.081	.077	.084	.079	.085	.087	.088	.087	.094	-	.092	-
	.431	.420	.418	.416	.418	.413	.412	.411	.403	.416	-	.418	-
TETA(5)	.079	.079	.078	.082	.082	.081	.087	.093	.094	.093	.095	.096	.099
	.431	.424	.417	.424	.420	.428	.431	.424	.445	.439	.456	.445	.467
TETA(6)	-	-	-	.100	.103	.112	.114	.114	.117	-	.122	.122	-
	-	-	-	.535	.532	.538	.541	.540	.543	-	.561	.566	-
TETA(7)	.250	.246	.256	.263	.270	.280	.281	.285	.292	.300	.308	.310	.316
	1.33	1.32	1.26	1.28	1.27	1.29	1.29	1.33	1.34	1.33	1.33	1.36	1.36
TETA(8)	.140	.148	.149	.154	.166	.163	.172	.175	.183	.187	.190	.195	.190
	.832	.818	.857	.851	.854	.831	.884	.897	.892	.911	.905	.951	.979
TETA(9)	.119	.114	.118	.117	.125	.124	.123	.124	.131	.135	.139	.138	.146
	.544	.544	.539	.532	.575	.559	.559	.529	.574	.552	.598	.604	.599
TETA(10)	-	.122	.123	.127	.132	.140	.139	.140	.143	.145	.153	.152	.159
	-	.660	.652	.654	.664	.657	.664	.665	.665	.672	.687	.693	.707
1A(1)	-	-	-	.010	.013	.011	.010	.013	.013	.014	.014	.011	.012
	-	-	-	.102	.098	.102	.099	.099	.098	.103	.097	.098	.091
1A(2)	.065	.064	.070	.070	.078	.084	.085	.090	.095	.103	.104	.109	.112
	.562	.656	.673	.650	.676	.658	.673	.662	.670	.689	.686	.717	.693
1A(3)	.095	.110	.104	.110	.116	.125	.137	.140	.153	.154	.169	.171	.172
	1.11	1.08	1.11	1.08	1.06	1.08	1.11	1.13	1.11	1.12	1.09	1.15	1.11
1A(4)	.087	.092	.093	.099	.110	.111	.122	.125	.137	.142	.151	.155	.158
	1.02	1.01	.990	.996	.989	.990	.995	1.01	1.03	1.04	1.05	1.09	1.06
1A(5)	.065	.070	.077	.077	.082	.110	.094	.129	.160	.140	.178	.189	.187
	.785	.780	.784	.781	.789	.932	.781	.940	1.16	.964	1.19	1.21	1.18
1A(6)	.040	.049	.053	.056	.060	.067	.069	.075	.075	.081	.084	.090	.091
	.589	.598	.602	.591	.594	.600	.589	.599	.599	.608	.607	.627	.630
1A(7)	.090	.099	.101	.110	.124	.135	.135	.144	.150	.163	.169	.179	.189
	1.14	1.10	1.10	1.11	1.11	1.11	1.11	1.11	1.14	1.16	1.15	1.20	1.20
1A(8)	.053	.059	.059	.066	.072	.071	.083	.083	.083	.095	.091	.099	.100
	.552	.668	.636	.569	.692	.656	.673	.682	.655	.685	.671	.677	.676
1A(9)	.025	.028	.027	.029	.030	.032	.034	.036	.036	.039	.042	.044	.042
	.305	.312	.302	.308	.309	.297	.305	.301	.295	.299	.298	.301	.296
2A(1)	-	-	-	.009	.018	.017	.029	.027	.055	.060	.071	.081	.081
	-	-	-	.523	.535	.530	.545	.536	.559	.544	.556	.559	.569
2B	-	-	-	.102	.103	.095	.095	.078	.084	.075	.062	.052	.051
	-	-	-	.233	.246	.231	.244	.241	.244	.246	.250	.253	.248
2A(2)	.010	.012	.014	.020	.027	.030	.041	.060	.067	.092	-	.115	.116
	.599	.678	.679	.753	.664	.739	.699	.754	.724	.802	-	.799	.769
2B	.276	.254	.231	.236	.204	.211	.175	.185	.154	.149	-	.117	.127
	.578	.556	.552	.542	.542	.604	.531	.604	.553	.560	-	.562	.582
2A(3)	.005	-	.007	.010	.018	.016	.025	.028	.035	.041	.050	.053	.065
	.339	-	.348	.352	.346	.339	.362	.375	.342	.368	.352	.365	.392
2B	.111	-	.106	.099	.094	.084	.083	.079	.070	.068	.058	.053	.058
	.257	-	.267	.264	.261	.250	.275	.272	.254	.275	.262	.269	.285
2A(4)	.011	.010	.010	.009	.012	.021	.024	.026	.031	.039	.045	.052	.054
	.378	.377	.351	.357	.351	.377	.378	.359	.369	.364	.383	.369	.361
2B	-	-	-	.135	.124	.124	.115	.104	.096	.088	.083	.076	.072
	-	-	-	.341	.339	.358	.348	.337	.345	.343	.360	.363	.365
2A(5)	.005	.008	.006	.010	.013	.022	.024	.029	.037	.044	.051	.063	-
	.442	.434	.443	.454	.432	.432	.442	.424	.450	.447	.435	.457	-
2B	.153	.142	.136	.133	.117	.111	.103	.096	.092	.082	.077	.068	.059
	.331	.336	.333	.343	.330	.329	.323	.323	.341	.339	.331	.338	.338
2A(6)	.007	.011	.009	.016	.019	.024	.034	.039	.053	.064	.078	.079	.089
	.549	.522	.539	.515	.532	.515	.542	.522	.565	.547	.563	.576	.585
2B	.180	.171	.161	.153	.141	.132	.127	.118	.115	.106	.097	.092	.087
	.421	.398	.407	.392	.402	.403	.400	.409	.432	.423	.433	.447	.439
2A(7)	.008	.010	.010	.011	.017	.021	.029	.035	.045	.049	.063	.067	.066
	.442	.430	.407	.427	.414	.425	.442	.450	.436	.458	.448	.450	.441
2B	-	.156	.133	.135	.118	.117	.103	.102	.085	.080	.075	.067	.061
	-	.315	.305	.285	.296	.294	.317	.320	.309	.321	.308	.303	.323
2A(8)	.005	.011	.008	.011	.016	.015	.020	.021	.033	-	-	-	-
	.362	.355	.342	.322	.336	.351	.319	.325	.344	-	-	-	-
2B	.185	.168	.149	.146	.134	.134	.113	.112	.107	-	.092	-	.078
	.370	.367	.341	.338	.345	.362	.332	.346	.355	-	.345	-	.335
2A(9)	.007	.008	.009	.017	.023	.032	.043	.049	.058	.066	.090	.095	.108
	.599	.603	.517	.571	.580	.600	.599	.572	.597	.586	.618	.623	.642
2B	-	.265	.257	.231	.219	.210	.193	.178	.168	.158	.147	.136	.135
	-	.609	.618	.582	.593	.600	.622	.586	.610	.607	.623	.635	.642
2A(10)	.007	.011	.020	.019	.025	.035	.043	.051	.060	.079	.081	.096	-
	.551	.544	.547	.539	.536	.573	.551	.579	.582	.608	.585	.620	-
2B	.243	.249	.236	.231	.212	.208	.184	.181	.166	.161	.141	.138	.112
	.567	.552	.571	.580	.561	.589	.552	.602	.569	.594	.573	.599	.599

B-3 Polymer Film Data

Film Label		Thickness (cm)
Poly(vinyl alcohol):		
(PVA)	1	0.0052
	2	0.0046
	3	0.0037
	4	0.0046
	5	0.0065
	6	0.0057
	7	0.0067
	8	0.0076
Poly(styrenesulphonate):		
(PSS)	1	0.0021
	2	0.0034
	3	0.0027
	4	0.0061
	5	0.0045
	6	0.0040

On the next two pages, pure polymer film absorbances are presented vertically with film label and horizontally with wavenumber (cm^{-1}). For each sample, the absorbance at room temperature is presented above the $77^{o}K$ value.

	16000.	16500.	17000.	17500.	18000.	18500.	19000.	19500.	20000.	20500.	21000.	21500.	22000.	22500.	23000.
PVA 1	.036	.034	.032	.035	.035	.034	.032	.030	.030	.031	.032	.034	.033	.033	.033
	.036	.038	.039	.041	.041	.042	.042	.044	.044	.042	.043	.044	.044	.044	.045
PVA 2	.030	.032	.032	.034	.037	.037	.035	.035	.035	.036	.036	.038	.036	.036	.036
	.038	.036	.036	.035	.035	.036	.035	.036	.036	.035	.038	.038	.039	.039	.038
PVA 3	.029	.035	.035	.033	.035	.034	.034	.035	.036	.036	.035	.034	.036	.035	.034
	.037	.035	.036	.036	.036	.036	.036	.038	.038	.038	.039	.038	.038	.039	.038
PVA 4	.034	.031	.034	.034	.032	.035	.036	.036	.036	.036	.036	.037	.036	.036	.037
	.027	.029	.029	.032	.032	.033	.034	.035	.035	.035	.035	.036	.036	.037	.038
PVA 5	.034	.032	.032	.033	.032	.032	.030	.032	.036	.037	.037	.035	.037	.037	.038
	.035	.035	.036	.037	.037	.038	.039	.040	.040	.040	.040	.040	.040	.041	.041
PVA 6	.035	.032	.032	.035	.032	.032	.034	.035	.035	.035	.035	.032	.035	.037	.037
	.029	.028	.022	.022	.020	.020	.020	.020	.022	.023	.023	.023	.024	.027	.027
PVA 7	.034	.034	.035	.036	.036	.036	.036	.036	.035	.037	.037	.038	.037	.038	.038
	.029	.030	.030	.033	.033	.033	.033	.034	.034	.034	.034	.035	.035	.035	.035
PVA 8	.033	.033	.033	.036	.036	.037	.039	.040	.039	.039	.039	.039	.041	.042	.042
	.028	.030	.033	.035	.037	.038	.038	.039	.040	.041	.041	.042	.044	.046	.046

	23500.	24000.	24500.	25000.	25500.	26000.	26500.	27000.	27500.	28000.	28500.	29000.	29500.	30000.	30500.
PVA 1	.034	.034	.034	.034	.034	.034	.034	.034	.035	.035	.037	.037	.037	.037	.038
	.045	.046	.045	.046	.048	.050	.052	.050	.052	.053	.054	.054	.056	.058	.058
PVA 2	.036	.038	.037	.038	.038	.040	.040	.041	.043	.044	.045	.046	.047	.048	.049
	.039	.039	.040	.041	.042	.043	.043	.045	.046	.048	.049	.050	.052	.053	.053
PVA 3	.036	.036	.036	.036	.036	.037	.036	.038	.037	.039	.040	.040	.041	.042	.041
	.038	.039	.040	.040	.041	.041	.043	.043	.044	.045	.046	.047	.049	.050	.052
PVA 4	.037	.036	.037	.037	.038	.038	.038	.040	.041	.042	.042	.044	.044	.046	.047
	.038	.038	.038	.040	.040	.041	.043	.044	.044	.046	.047	.049	.052	.052	.053
PVA 5	.038	.039	.039	.039	.040	.041	.043	.044	.045	.046	.048	.049	.052	.052	.053
	.042	.043	.044	.044	.045	.046	.047	.047	.048	.049	.051	.053	.055	.056	.057
PVA 6	.037	.038	.038	.038	.039	.040	.041	.042	.043	.044	.046	.046	.047	.048	.047
	.027	.028	.030	.031	.033	.033	.034	.035	.035	.035	.035	.036	.039	.039	.041
PVA 7	.038	.039	.040	.040	.042	.042	.042	.044	.044	.045	.048	.049	.051	.053	.054
	.035	.035	.035	.035	.035	.036	.036	.040	.040	.040	.040	.042	.043	.044	.045
PVA 8	.041	.042	.042	.043	.044	.046	.046	.047	.049	.051	.052	.054	.056	.057	.059
	.046	.049	.049	.051	.053	.054	.056	.058	.060	.061	.065	.067	.070	.072	.075

	31000.	31500.	32000.	32500.	33000.	33500.	34000.	34500.	35000.	35500.	36000.	36500.	37000.	37500.	38000.
PVA 1	.034	.034	.034	.036	.037	.038	.038	.039	.040	.040	.040	.041	.041	.041	.041
	.060	.061	.064	.066	.071	.070	.074	.076	.080	.080	.083	.084	.085	.085	.086
PVA 2	.049	.049	.052	.053	.052	.054	.054	.055	.055	.056	.056	.057	.056	.057	.056
	.055	.057	.059	.061	.062	.066	.066	.069	.070	.072	.074	.076	.077	.077	.077
PVA 3	.042	.043	.042	.043	.043	.043	.044	.045	.046	.046	.046	.046	.047	.074	.074
	.053	.054	.057	.059	.061	.063	.064	.067	.069	.070	.072	.073	.073	.075	.077
PVA 4	.046	.048	.050	.051	.052	.054	.055	.056	.057	.059	.060	.061	.061	.062	.062
	.055	.058	.061	.063	.065	.068	.072	.075	.076	.078	.080	.082	.083	.084	.086
PVA 5	.052	.053	.056	.058	.061	.062	.063	.064	.065	.067	.068	.070	.071	.072	.073
	.060	.062	.066	.069	.072	.074	.076	.081	.082	.083	.084	.087	.089	.090	.093
PVA 6	.048	.050	.052	.054	.055	.056	.058	.059	.060	.061	.062	.063	.064	.065	.066
	.049	.050	.053	.057	.059	.060	.063	.065	.068	.070	.070	.072	.072	.074	.076
PVA 7	.056	.058	.058	.062	.064	.066	.070	.071	.073	.075	.077	.079	.080	.081	.082
	.045	.046	.048	.051	.052	.055	.057	.059	.061	.063	.063	.066	.066	.067	.068
PVA 8	.060	.062	.064	.068	.071	.073	.074	.076	.078	.079	.082	.082	.083	.084	.085
	.073	.075	.079	.082	.085	.088	.090	.093	.094	.096	.098	.101	.103	.105	.106

	38500.	39000.	39500.	40000.	40500.	41000.	41500.	42000.	42500.	43000.	43500.	44000.	44500.	45000.
PVA 1	.041	.042	.043	.045	.045	.049	.050	.055	.057	.062	.066	.072	.080	.085
	.086	.087	.089	.092	.094	.098	.103	.106	.113	.117	.124	.130	.136	.146
PVA 2	.056	.057	.058	.059	.061	.063	.064	.066	.071	.074	.076	.085	.090	.097
	.077	.080	.080	.082	.085	.088	.091	.095	.100	.106	.109	.114	.121	.128
PVA 3	.078	.074	.074	.078	.050	.052	.052	.055	.058	.061	.064	.068	.074	.081
	.077	.078	.079	.079	.082	.085	.089	.093	.096	.102	.106	.110	.116	.122
PVA 4	.062	.062	.063	.064	.066	.068	.070	.074	.078	.082	.088	.097	.105	.114
	.087	.087	.088	.090	.093	.098	.101	.105	.112	.117	.125	.129	.136	.144
PVA 5	.076	.078	.078	.079	.082	.085	.089	.095	.098	.105	.114	.120	.130	.145
	.095	.095	.095	.101	.103	.106	.112	.116	.125	.132	.139	.146	.155	.165
PVA 6	.066	.068	.068	.070	.072	.075	.079	.083	.089	.097	.104	.112	.120	.131
	.077	.079	.080	.084	.086	.090	.095	.103	.108	.114	.121	.129	.136	.146
PVA 7	.083	.083	.085	.087	.092	.096	.098	.099	.101	.115	.123	.134	.140	.153
	.070	.072	.072	.074	.077	.082	.086	.093	.100	.107	.115	.124	.134	.146
PVA 8	.086	.088	.090	.090	.093	.096	.101	.106	.110	.120	.123	.134	.144	.146
	.107	.108	.110	.114	.118	.122	.127	.134	.142	.146	.155	.162	.174	.185

	16000.	16500.	17000.	17500.	18000.	18500.	19000.	19500.	20000.	20500.	21000.	21500.	22000.	22500.	23000.
PSS 1	.043	.042	.042	.042	.042	.042	.043	.043	.043	.042	.043	.043	.043	.043	.044
	.040	.041	.042	.043	.043	.043	.043	.043	.043	.043	.043	.043	.043	.043	.045
PSS 2	.038	.038	.038	.040	.040	.039	.039	.040	.040	.040	.040	.040	.042	.042	.043
	.035	.035	.037	.037	.037	.038	.038	.039	.039	.040	.040	.040	.041	.042	.043
PSS 3	.044	.044	.046	.046	.046	.047	.047	.047	.047	.047	.047	.048	.048	.049	.051
	.045	.044	.044	.044	.044	.045	.045	.045	.045	.045	.045	.046	.047	.047	.048
PSS 4	.043	.043	.042	.042	.043	.043	.043	.044	.044	.044	.045	.045	.046	.046	.047
	.046	.047	.048	.049	.051	.051	.050	.050	.050	.050	.051	.051	.051	.052	.052
PSS 5	.037	.036	.036	.036	.038	.038	.038	.038	.040	.040	.039	.039	.041	.041	.042
	.040	.040	.038	.038	.038	.040	.041	.041	.041	.041	.041	.042	.043	.044	.044
PSS 6	.041	.040	.040	.041	.041	.041	.042	.042	.042	.042	.042	.042	.043	.043	.044
	.040	.040	.041	.042	.042	.043	.043	.044	.044	.044	.044	.045	.046	.046	.047

	23500.	24000.	24500.	25000.	25500.	26000.	26500.	27000.	27500.	28000.	28500.	29000.	29500.	30000.	30500.
PSS 1	.045	.045	.046	.047	.051	.054	.058	.061	.065	.070	.074	.079	.084	.089	.093
	.047	.048	.049	.051	.054	.059	.062	.066	.072	.077	.081	.087	.093	.099	.104
PSS 2	.044	.044	.046	.047	.050	.055	.060	.064	.068	.073	.077	.080	.086	.090	.097
	.044	.045	.048	.050	.054	.059	.065	.071	.078	.083	.088	.094	.100	.107	.116
PSS 3	.051	.052	.053	.055	.060	.064	.066	.072	.076	.081	.085	.090	.093	.099	.104
	.051	.052	.052	.054	.055	.058	.063	.071	.076	.077	.081	.087	.093	.098	.106
PSS 4	.048	.051	.052	.054	.057	.061	.063	.067	.069	.074	.078	.083	.087	.092	.098
	.055	.055	.057	.059	.063	.068	.072	.079	.083	.088	.093	.099	.103	.111	.116
PSS 5	.042	.044	.044	.045	.048	.052	.055	.061	.065	.068	.073	.077	.081	.087	.093
	.046	.047	.048	.050	.054	.057	.063	.066	.071	.074	.080	.086	.089	.096	.104
PSS 6	.045	.045	.045	.049	.051	.056	.060	.063	.069	.072	.077	.084	.089	.093	.099
	.047	.048	.049	.051	.055	.060	.065	.070	.076	.081	.086	.092	.098	.105	.113

	31000.	31200.	31400.	31600.	31800.	32000.	32200.	32400.	32600.	32800.	33000.	33200.	33400.	33600.	33800.
PSS 1	.101	.104	.106	.109	.113	.116	.119	.124	.129	.135	.145	.156	.160	.182	.200
	.114	.120	.124	.126	.131	.134	.139	.144	.150	.156	.166	.176	.188	.205	.224
PSS 2	.103	.105	.107	.110	.114	.116	.120	.124	.128	.136	.145	.156	.170	.186	.205
	.126	.128	.132	.136	.140	.144	.151	.155	.162	.168	.180	.192	.206	.224	.245
PSS 3	.111	.114	.116	.118	.120	.124	.127	.131	.136	.142	.150	.160	.172	.186	.204
	.115	.116	.119	.124	.126	.129	.134	.139	.143	.152	.160	.168	.183	.196	.214
PSS 4	.104	.108	.109	.113	.115	.119	.123	.126	.132	.138	.146	.156	.168	.184	.202
	.128	.131	.134	.138	.142	.145	.150	.155	.161	.168	.176	.186	.199	.214	.231
PSS 5	.099	.100	.104	.107	.110	.114	.116	.122	.126	.131	.140	.149	.162	.176	.194
	.112	.115	.116	.119	.124	.128	.132	.136	.142	.148	.156	.165	.176	.191	.209
PSS 6	.105	.108	.112	.114	.117	.121	.126	.130	.136	.143	.152	.164	.178	.194	.215
	.125	.128	.133	.137	.141	.146	.150	.156	.163	.170	.180	.193	.207	.226	.247

	34000.	34200.	34400.	34600.	34800.	35000.	35200.	35400.	35600.	35700.	35800.	35900.	36000.
PSS 1	.221	.243	.264	.284	.305	.330	.364	.417	.509	.600	.670	.800	.955
	.246	.271	.294	.316	.338	.366	.403	.457	.558	.630	.735	.870	1.040
PSS 2	.225	.249	.270	.291	.314	.340	.377	.434	.530	.608	.715	.855	1.040
	.269	.295	.323	.347	.372	.403	.446	.516	.637	.730	.865	1.040	1.250
PSS 3	.224	.245	.266	.286	.307	.335	.366	.417	.508	.591	.681	.805	.975
	.236	.257	.281	.301	.324	.353	.389	.450	.555	.637	.755	.895	1.080
PSS 4	.222	.245	.264	.284	.304	.326	.660	.408	.494	.558	.655	.775	.925
	.254	.276	.299	.319	.341	.366	.402	.455	.552	.628	.730	.855	1.000
PSS 5	.214	.235	.256	.277	.296	.322	.355	.408	.496	.568	.664	.790	.945
	.230	.254	.275	.294	.314	.337	.370	.420	.507	.575	.673	.805	.970
PSS 6	.238	.263	.285	.310	.332	.361	.400	.457	.558	.638	.750	.890	1.070
	.276	.305	.332	.357	.383	.413	.449	.506	.610	.691	.791	.940	1.140

APPENDIX C COMPUTER PROGRAMMES

All computer programmes have been written in the standard FORTRAN IV language.

C-1 PREDAN

C-2 ADFULGO

C-3 TROP

C-4 RESPECT

C-1 PREDAN

```
      PROGRAM PREDAN(INPUT,OUTPUT,TAPE5=INPUT,TAPE6=OUTPUT)
C*****THIS PROGRAM IS A PREDICTION ANALYSIS PROCEDURE (BASED ON BOOK,
C     PREDICTION ANALYSIS BY JOHN R. WOLBERG)
      COMMON XX(5,100),X(5),A(20),SX(5),SA(20),KX(5),CX(5),XCOMP(10),SY,
     1Y,CY,C(20,20),CINV(20,20),RE(20),BA(100),E(10,10),NMARK(10),YSIMP
      COMMON NP,N,M,KCY,KY,KF,KCT,KSET,KCOMP,NA,NB,NC,ND,NE,AA,AB,AC,KK,
     1NN,LL,I,NINT,PERC,IND,J,K,NM,NSIMP,NREJ,RULE,YLEV(2)
      DIMENSION DX(5),FA(20)
C*****MAIN CONTROL PART OF PROGRAM
C*****INITIALIZE INDICATORS, ETC
      LL=0
 1000 LL=LL+1
      PERC=1.
C*****READ IN INPUT AND PRINT THIS OUT
      CALL READ
C*****SET LIMITS
      IF(N.GT.200.OR.N.LT.NP+1) GO TO 1
      IF(M.GT.3) GO TO 2
      IF(NP.GT.20) GO TO 3
      IF(KCY.EQ.3.AND.NB.NE.3) GO TO 4
      GO TO 5
    1 PRINT 100 $ STOP
    2 PRINT 101 $ STOP
    3 PRINT 102 $ STOP
    4 PRINT 103 $ STOP
    5 KK=0 $ KCT=0 $ NSIMP=1

C*****IF SUBROUTINE OPL IS USED, X(2) IS INITIALIZED TO 0.5 AT THIS POIN
      X(2)=0.5

C*****IF EITHER OF THE ESTIMAT-PREDAN PROCEDURES USED, PUT THE FOLLOWING
C     AT THIS POINT          IF(NC.GE.2) CALL CYC                    CARD
      IF (NC.GE.2) CALL CYC

 2000 KK=KK+1 $ IND=1 $ NN=0
C*****CLEAR LOCATIONS FOR PREDICTED COEFFICIENT MATRIX
      DO 6 J=1,NP
      DO 6 K=1,NP
    6 C(J,K)=0.
C*****IF OPTIMIZING, TRANSFER CONTROL TO SIMPLEX
      IF(KCY.EQ.3.AND.KK.NE.1) 7,9
    7 CALL SIMPLEX $ IF(KK.EQ.0) 8,9
    8 GO TO (88,131,32),NE
   88 KCY=1 $ GO TO 2000
C*****INITIALIZE INDICATORS ETC
    9 I=1 $ NM=0 $ NINT=0
 3000 CONTINUE
C*****COMPUTE X(J,I) VALUES IF REQUIRED
      IF(KCOMP.NE.0) 10,12
   10 DO 11 J=1,KCOMP
   11 CALL XSPACE
      GO TO 14
   12 DO 13J=1,M
   13 X(J)=XX(J,I)
   14 CONTINUE
C*****IF OPL IS USED, Y NEED NOT BE RECOMPUTED
      IF(KCOMP.EQ.0.OR.KCOMP.EQ.M) 15,16
```

```
C*****COMPUTE Y AS REQUIRED
   15 Y=0.
      Y=EQN(MYDUMMY)
   16 CONTINUE
C*****COMPUTE SX AND SY VALUES AS REQUIRED
      SY=SIG(Y,KY,CY)
      DO 17 J=1,M
   17 SX(J)=SIG(X(J),KX(J),CX(J))
C*****COMPUTE DERIVATIVE OF RESIDUAL FUNCTION W.R.T X(J), NAMELY DX(J)
      ID=2
      DO 18 J=1,M
   18 DX(J)=DERIV(ID,X(J))
C*****COMPUTE THE RESIDUAL MATRIX DL
      DL=SY**2
      DO 19 J=1,M
   19 DL=DL+(SX(J)*DX(J))**2
C*****COMPUTE DERIVATIVE OF RESIDUAL FUNCTION W.R.T A(K), NAMELY FA(K)
      ID=1
      DO 20 K=1,NP
   20 FA(K)=DERIV(ID,A(K))
C*****COMPUTE EACH ELEMENT OF THE MATRIX C
      DO 21 J=1,NP
      DO 21 K=J,NP
   21 C(J,K)=C(J,K)+FA(J)*FA(K)/DL
C*****PRINT OUT PRESENT INFORMATION IF APPLICABLE
      IF(KCY.EQ.3) GO TO 22
      CALL PRINT $ IND=2
C*****MOVE ONTO A NEW DATA POINT OR CARRY ON
   22 CONTINUE $ IF(I.EQ.N) 24,23
   23 I=I+1
      GO TO 3000
   24 CONTINUE
C*****C IS SYMMETRIC-FILL IN ALL ELEMENTS
      DO 25 J=1,NP
      DO 25 K=J,NP
   25 C(K,J)=C(J,K)
C*****INVERT C TO GIVE CINV(K,J)
      CALL MTXINV
      IF(NM.EQ.110) 26,28
   26 IND=3 $ CALL PRINT $ IF(KCY.EQ.3) 27,30
   27 RE(1)=1.0E+30 $ GO TO 2000
C*****COMPUTE PREDICTED UNCERTAINTIES SA(K) AND REL. ERRORS RE(K)
   28 DO 29 K=1,NP
      SA(K)=SQRT(CINV(K,K))
   29 RE(K)=SA(K)/A(K)
C*****PRINT OUT SA(K) VALUES TOGETHER WITH THE A(K) AND RE(K) VALUES
C     AND/OR CYCLE REQUIRED PARAMETERS OR GO BACK TO SIMPLEX
      IF(KCY.EQ.3) GO TO 30 $ IND=3 $ CALL PRINT
   30 CONTINUE $ GO TO (32,31,2000),KCY
   31 CALL CYC $ IF(NV.EQ.1) 32,2000
  131 CALL CYC $ IF(NV.EQ.1) 32,5
   32 CONTINUE $ IF(LL.EQ.KSET) 4000,1000
  100 FORMAT (1H1,*NO MORE THAN 200 OR LESS THAN NP+1 POINTS ALLOWED*)
  101 FORMAT(1H1,*ONLY 3 INDEPENDENT VARIABLES ALLOWED*)
  102 FORMAT(1H1,*ONLY 20 UNKNOWN PARAMETERS ALLOWED*)
  103 FORMAT(1H1,*INCORRECT FORMULATION IN XSPACE USED WITH SIMPLEX*)
 4000 STOP $ END
```

```
      SUBROUTINE READ
C*****THIS SUBROUTINE READS IN THE RELEVANT INDICATORS,PARAMETERS AND
C     AND PRINTS THESE OUT                                    VARIABLES
      COMMON XX(5,100),X(5),A(20),SX(5),SA(20),KX(5),CX(5),XCOMP(10),SY,
     1Y,CY,C(20,20),CINV(20,20),RE(20),BA(100),E(10,10),NMARK(10),YSIMP
      COMMON NP,N,M,KCY,KY,KF,KCT,KSET,KCOMP,NA,NB,NC,ND,NE,AA,AB,AC,KK,
     1NN,LL,I,NINT,PERC,IND,J,K,NM,NSIMP,NREJ,RULE,YLEV(2)
      READ 50,NP,N,M,KCY,KY,KF,KSET,KCOMP,NA,NB,NC,ND,NE,CY,AA,AB,AC
      READ 51,(KX(J),J=1,M)
      READ 52,(A(K),K=1,NP)
      READ 52,(CX(J),J=1,M)
      IF(KCOMP.EQ.0) 1,2
    1 READ 52,((XX(J,I),J=1,M),I=1,N) $ GO TO 3
    2 L=2*KCOMP
      READ 52,(XCOMP(J),J=1,L)
    3 CONTINUE $ IF(NE .NE.3) GO TO 4 $ READ 53,(NMARK(K),K=1,ND)
C*****PRINT INPUT
    4 PRINT 100
      PRINT 101,NP,N,M,KCY,KY,KF,KSET,KCOMP,NA,NB,NC,ND,NE,CY,AA,AB,AC
      PRINT 102
      PRINT 103,(KX(J),J=1,M)
      PRINT 104
      PRINT 105,(CX(J),J=1,M)
      PRINT 106
      PRINT 107,(XCOMP(J),J=1,L)
      PRINT 110 $ PRINT 111,(A(K),K=1,NP)
      IF(NE .NE.3) GO TO 5
      PRINT 108 $ PRINT 109,(NMARK(K),K=1,ND)
   50 FORMAT(13I4,4E7.0)
   51 FORMAT(20I4)
   52 FORMAT(8E10.0)
   53 FORMAT(5I4)
  100 FORMAT(1H1,55X,*INPUT INFORMATION*/////)
  101 FORMAT(1H , 9X,*NP=*I4,26X,*N=*I4,28X,*M=*I4,27X,*KCY=*I4//10X,*KY
     1=*I4,25X,*KF=*I4,25X,*KSET=*I4,25X,*KCOMP=*I4,//10X,*NA=*I4,25X,*N
     1B=*I4,27X,*NC=*I4,28X,*ND=*I4//10X,*NE=*I4//10X,*CY=*E9.2,20X,*AA=
     1*E9.2,22X,*AB=*E9.2,23X,*AC=*E9.2////)
  102 FORMAT(1H ,10X,*KX(J) VALUES ARE* 5X)
  103 FORMAT(1H ,2X,3(I3,7X))
  104 FORMAT(1H ,//10X,*CX(J) VALUES ARE*,5X)
  105 FORMAT(1H ,1X,3(E10.3,5X))
  106 FORMAT(1H ,//10X,*XCOMP(J) VALUES ARE*,5X)
  107 FORMAT (1H ,1X,6(E10.3,5X))
  108 FORMAT(1H ,//10X,*NMARK(K) VALUES ARE*5X)
  109 FORMAT(1H ,1X,5(I5,5X))
  110 FORMAT(1H ,//10X,*A(K) VALUES ARE*5X)
  111 FORMAT(1H ,1X,3(E10.3,5X))
    5 RETURN $ END
```

```
      SUBROUTINE SIMPLEX
C*****THIS SUBROUTINE MINIMIZES THE FUNCTION YSIM(K) WHICH DEPENDS ON
C     ND VARIABLES. THE METHOD USED IS THE SEQUENTIAL SIMPLEX METHOD WITH
C     A STEP SIZE AB (BASED ON BOOK, OPTIMIZATION: THEORY AND PRACTICE
C     BY BEVERIDGE AND SCHECHTER)
C*****NOTE: RESTRICTED TO (1) POSITIVE INTEGRAL VALUES OF THE OUTPUT
C                              GREATER THAN OR EQUAL TO 2        VARIABLES
C                          (2) FIXED ITERATION NUMBER (YLEV(1))
C                          (3) A FIXED YSIM(MIN) VALUE IS TAKEN AS THE
C                              (YLEV(2))                          OPTIMUM
C                          (4) STEP SIZE SHOULD NOT BE LESS THAN 2
C                          (5) ND CANNOT BE GREATER THAN 5 WITH PRESENT
C                              SUBROUTINE XSPACE
C                          (6) NMARK(K) VALUES SHOULD NOT BE LESS THAN 3 IN
C                              STARTING SIMPLEX (ONLY) OR WILL OBTAIN
      COMMON XX(5,100),X(5),A(20),SX(5),SA(20),KX(5),CX(5),XCOMP(10),SY,
     1Y,CY,C(20,20),CINV(20,20),RE(20),BA(100),E(10,10),NMARK(10),YSIMP
      COMMON NP,N,M,KCY,KY,KF,KCT,KSET,KCOMP,NA,NB,NC,ND,NE,AA,AB,AC,KK,
     1NN,LL,I,NINT,PERC,IND,J,K,NM,NSIMP,NREJ,RULE,YLEV(2)
      DIMENSION YSIM(10),R(10),NS(10),NT(50)
      YLEV(1)=30. $ YLEV(2)=0.001
      GO TO (1,2,9),NSIMP
C*****CONTROL FACTORS COMPUTED
    1 MIT=1.65*ND+0.05*ND*ND
      DO 66 K=1,ND
   66 E(K,1)=NMARK(K)
      AZ=AB/(ND*SQRT(2.)) $ BZ=ND+1 $ BZ=SQRT(BZ)
      P=AZ*(BZ+ND-1) $ Q=AZ*(BZ-1)
      NSUM=0 $ NSIND=1 $ NDAB=1 $ MM=0 $ NSIMP=2 $ NAUX=1
C*****YSIM CALCULATED FOR FIRST ND+1 POINTS
    2 J=KK-1 $ YSIM(J)=0. $ MM=MM+1 $ KCT=KCT+1 $ NT(J)=KCT
      DO 3 K=1,NP
    3 YSIM(J)=RE(K)+YSIM(J)
      YSIMP=YSIM(J) $ IND=1 $ CALL PRINT
      IF(MM.EQ.ND+1) 4,5
    4 NSIMP=3 $ GO TO 11
    5 DO 8 L=1,ND
      IF(L.EQ.MM) 6,7
    6 R(L)=P $ GO TO 77
    7 R(L)=Q
   77 E(L,KK)=E(L,1)+R(L)
    8 NMARK(L)=E(L,KK)
      RETURN
C*****YSIM CALCULATED FOR REST OF POINTS
    9 J=KK-1 $ L=NREJ $ YSIM(L)=0. $ KCT=KCT+1 $ NT(L)=KCT
      DO 10 K=1,NP
   10 YSIM(L)=RE(K)+YSIM(L)
      YSIMP=YSIM(L) $ NREJ=NS(NREJ) $ IND=2 $ CALL PRINT
C*****MAXIMUM YSIM VALUE CALCULATED AND POINT REJECTED BY RULE 1 OR 2
C     RULE 1: POINT IN SIMPLEX FIGURE WITH MAXIMUM YSIMP VALUE IS REJECT-
C     RULE 2: NO POINT SHALL BE RETURNED TO ONCE IT HAS BEEN REJECTED  ED
   11 L=1 $ J=0 $ IF(KK.GT.YLEV(1)) GO TO 20
   12 J=J+1
      K=L+J $ IF(YSIM(L).LT.YSIM(K)) 13,14
   13 L=K $ J=0
   14 CONTINUE $ IF(K.EQ.ND+1.OR.L.EQ.ND+1) 15,12
   15 NREJ=L $ NS(L)=NT(L) $ GO TO (19,18,16),NSIND
```

```
   16 CONTINUE $ IF(NREJ.EQ.NREJA) 17,19
   17 ALOK=YSIM(NREJ) $ LREJ=NREJ $ YSIM(NREJ)=0.
      NSIND =2 $ GO TO 11
   18 RULE=2 $ YSIM(LREJ)=ALOK $ NREJA=NREJ $ GO TO 20
   19 RULE=1 $ NREJA=NREJ
C*****MINIMUM YSIM VALUE CALCULATED
   20 L=1 $ J=0 $ NSIND=3
   21 J=J+1
      K=L+J $ IF(YSIM(L).GT.YSIM(K)) 22,23
   22 L=K $ J=0
   23 CONTINUE $ IF(K.EQ.ND+1.OR.L.EQ.ND+1) 24,21
C*****STEP SIZE REDUCED OR SIMPLEX STOPPED BY CONVERGENCE, EXCESS ITER-
C  OR MAXIMUM ITERATIONS ATTAINED                                  ATIONS
   24 CONTINUE $ IF(YSIM(L).LE.YLEV(2).OR.KK.GT.YLEV(1)) GO TO 35
      GO TO (30,25),NAUX
   25 CONTINUE $ IF(L.EQ.NBEST) 26,29
   26 NSUM=NSUM+1 $ IF(NSUM.GT.MIT) 27,30
   27 CONTINUE $ GO TO (28,33),INDAB
   28 AB=AB/ 2. $ PRINT100,AB $ INDAB=2 $ KK=2 $ GO TO 1
   29 NSUM=0
C*****NEW POINT COMPUTED IN SIMPLEX POLYHEDRON
   30 DO 32 J=1,ND
      SUM=0.
      NV=ND+1 $ DO 31 K=1,NV
   31 SUM=SUM+E(J,K)
      SUM=(SUM-E(J,NREJ))*2./ND
      E(J,NREJ)=SUM-E(J,NREJ)
      IF(E(J,NREJ).LE.1.) E(J,NREJ)=2.
   32 NMARK(J)=E(J,NREJ)
      NAUX=2 $ NBEST=L $ RETURN
   33 DO 34 K=1,ND
   34 NMARK(K)=E(K,L)
      IND=4 $ CALL PRINT $ KK=0 $ RETURN
   35 DO 36 K=1,ND
   36 NMARK(K)=E(K,L)
      IND=5 $ CALL PRINT $ KK=0 $ RETURN
  100 FORMAT(1H ,//,43X,*NEW STEP SIZE INTRODUCED*/50X,*=*,E10.3//)
      END
```

```
      SUBROUTINE XSPACE                                        [VARIABLES]
C*****THIS SUBROUTINE EVALUATES VALUES AND SPACINGS OF THE INDEPENDENT
      COMMON XX(5,100),X(5),A(20),SX(5),SA(20),KX(5),CX(5),XCOMP(10),SY,
     1Y,CY,C(20,20),CINV(20,20),RE(20),BA(100),E(10,10),NMARK(10),YSIMP
      COMMON NP,N,M,KCY,KY,KF,KCT,KSET,KCOMP,NA,NB,NC,ND,NE,AA,AB,AC,KK,
     1NN,LL,I,NINT,PERC,IND,J,K,NM,NSIMP,NREJ,RULE,YLEV(2)
      DIMENSION XA(10),XB(10),XBA(10),XK(20),X1(10),X2(10),X3(10),X4(10)
      GO TO (1,6,13),NB
C*****CASE 1- EQUAL SPACING FOR EACH OF THE X(J) VALUES TREATED
C             XCOMP(ODD)=INITIAL VALUES OF X(J) FOR SET I
C             XCOMP(EVEN)=FINAL VALUE OF X(J) FOR SET I
    1 CONTINUE
      IF(I.GT.1) GO TO 3
      JN=2*J $ J1=JN-1
      XI=(XCOMP(JN)-XCOMP(J1))/(N-1)
    2 XA(J)=XCOMP(J1)-(XI/2.)
      XB(J)=XCOMP(JN)+(XI/2.)
      XBA(J)=(XB(J)-XA(J))/N
    3 X(J)=XA(J)+(I-0.5)*XBA(J)
      IF(J.EQ.KCOMP) 4,5
    4 CONTINUE
```

```
C*****IF SUBROUTINE OPL USED, CALL IT AT THIS POINT, AS FOLLOWS
      IF(KCOMP.NE.M) CALL OPL
    5 RETURN
C*****CASE 2-SPACING FROM HIGHEST POINT XCOMP(EVEN) TO LOWEST POINT
C             XCOMP(ODD) WITH AN INTERVAL INCREASING BY A MULTIPLICATION
C             FACTOR AA
    6 CONTINUE $ IF(I.GT.1) GO TO 9
      IF(J.GT.1) GO TO 8
      ZZ=1 $ Z=1 $ NX=1
    7 NX=NX+1
      IF(NX.EQ.N) GO TO 8
      Z=Z*AA
      ZZ=ZZ+Z $ GO TO 7
    8 JN=2*J $ J1=JN-1
      XK(J)=XCOMP(JN)-XCOMP(J1) $ XK(J)=XK(J)/ZZ
      X(J)=XCOMP(JN) $ GO TO 10
    9 X(J)=X(J)-XK(J) $ XK(J)=XK(J)*AA
   10 CONTINUE $ IF(J.EQ.KCOMP) 11,12
C*****IF SUBROUTINE OPL USED, CALL IT AT THIS POINT, AS FOLLOWS
   11 CONTINUE $ IF(KCOMP.NE.M) CALL OPL
   12 RETURN
C*****CASE 3 - MULTI SECTION EQUAL INTERVAL SPACING FOR SIMPLEX WITH 5
   13 CONTINUE $ IF(I.GT.1) GO TO 15                                VARIABLES
      N=0 $ DO 14 K=1,ND
   14 N=NMARK(K)+N $ N=N-4 $ NAUX=1 $ NAU=5 $ IK=1
      JN=2*J $ J1=JN-1
      ABT=(XCOMP(JN)-XCOMP(J1))/5.
      X1(J)=XCOMP(J1)+ABT $ X2(J)=X1(J)+ABT $ X3(J)=X2(J)+ABT
      X4(J)=X3(J)+ABT
      IF(KK .EQ.1) PRINT 100,X1(J),X2(J),X3(J),X4(J)
   15 GO TO (16,17,18,20,21,23),NAUX
   16 F=X1(J) $ G=XCOMP(J1) $ MM=NMARK(1) $ GO TO 19
   17 F=X2(J) $ G=X1(J) $ MM=NMARK(2) $ GO TO 19
   18 F=X3(J) $ G=X2(J) $ MM=NMARK(3) $ GO TO 19
   20 F=X4(J) $ G=X3(J) $ MM=NMARK(4) $ GO TO 19
   21 F=XCOMP(JN) $ G=X4(J) $ MM=NMARK(5)
   19 XI=(F-G)/(MM-1)
      XA(J)=G-(XI/2.)
      XB(J)=F+(XI/2.)
      XBA(J)=(XB(J)-XA(J))/MM
   23 X(J)=XA(J)+(IK-0.5)*XBA(J) $ NAUX=6
      ZA=ABS(X(J)-F) $ ZB=XI*1.0E-01 $ IF(ZA.LE.ZB) 24,25
   24 NAU=NAU-1 $ NAUX=NAUX-NAU $ IK=1
   25 IK=IK+1  $ IF(J.EQ.KCOMP) 26,27
C*****IF SUBROUTINE OPL USED, CALL IT AT THIS POINT, AS FOLLOWS
   26 CONTINUE $ IF(KCOMP.NE.M) CALL OPL
   27 RETURN
  100 FORMAT(1H ,//10X,*SPACED INTERVALS IN XSPACE ARE*/2X,4(E10.3,5X))
      END

      FUNCTION EQN(MYDUMMY)                                        [FORMS
C*****THIS SUBROUTINE PROVIDES THE REQUIRED MODELS IN NORMAL AND RESIDUAL
      COMMON XX(5,100),X(5),A(20),SX(5),SA(20),KX(5),CX(5),XCOMP(10),SY,
     1Y,CY,C(20,20),CINV(20,20),RE(20),BA(100),E(10,10),NMARK(10),YSIMP
      COMMON NP,N,M,KCY,KY,KF,KCT,KSET,KCOMP,NA,NB,NC,ND,NE,AA,AB,AC,KK,
     1NN,LL,I,NINT,PERC,IND,J,K,NM,NSIMP,NREJ,RULE,YLEV(2)
      DIMENSION B(5)
      GO TO (1,2,2,3,3), KF
C*****MONOMER-DIMER MODEL, 3 PARAMETERS
    1 EPS1=A(1) $ EPS2=2.*A(2) $ EK=A(3)
      C1=1.+8.*EK* X(1) $ C1=SQRT(C1) $ C1=C1-1. $ C1=C1/(4.*EK)
```

```
      C2=EK*C1*C1 $ F=(EPS1*C1+EPS2*C2)* X(2)-Y
      EQN=F
      RETURN
    2 EPS1=ABS(A(1)) $ EPS2=ABS(A(2)) $ EPS3=ABS(A(3))
      B(1)=- X(1) $ B(2)=1. $ B(3)=ABS(A(4)*2.) $ IF(KF .EQ.2)21,22
C*****MONOMER-DIMER-TRIMER MODEL, 4 PARAMETERS (K3=K2**2)
   21 B(4)=ABS(A(4)*A(4)*3.) $ GOTO23
C*****MONOMER-DIMER-TRIMER MODEL, 5 PARAMETERS
   22 B(4)=ABS(A(5)*3.)
   23 C1= X(1)*PERC $ CALL NEWRAP(B,4,C1) $ PERC=C1/ X(1)
      F=EPS1*C1+B(3)*EPS2*C1*C1+B(4)*EPS3*C1*C1*C1
      F=F* X(2)- Y
      EQN=F
      RETURN
    3 EPS1=ABS(A(1)) $ EPS2=ABS(A(2)) $ EPS4=ABS(A(3))
      B(1)=- X(1) $ B(2)=1. $ B(3)=ABS(A(4)*2.) $ B(4)=0.
      IF(KF .EQ.4)31,32
C*****MONOMER-DIMER-TETRAMER MODEL, 4 PARAMETERS (K4=K2**3)
   31 B(5)=ABS(A(4)*A(4)*A(4)*4.) $ GOTO33
C*****MONOMER-DIMER-TETRAMER MODEL, 5 PARAMETERS
   32 B(5)=ABS(A(5)*4.)
   33 C1= X(1)*PERC $ CALL NEWRAP(B,5,C1) $ PERC=C1/ X(1)
      F=EPS1*C1+B(3)*EPS2*C1*C1+B(5)*EPS4*C1*C1*C1*C1
      F=F* X(2)-Y
      EQN=F
      RETURN $ END
```

```
      SUBROUTINE OPL
C*****THIS SUBROUTINE IS RELEVANT TO THIS EXAMPLE ONLY. IT EVALUATES AN
C     OPTIMUM VALUE OF THE OPTICAL PATH LENGTH VARIABLE SO THAT THE OPTI-
C     DENSITY IS WITHIN THE RANGE 0.3-0.7 IF POSSIBLE                  CAL
      COMMON XX(5,100),X(5),A(20),SX(5),SA(20),KX(5),CX(5),XCOMP(10),SY,
     1Y,CY,C(20,20),CINV(20,20),RE(20),BA(100),E(10,10),NMARK(10),YSIMP
      COMMON NP,N,M,KCY,KY,KF,KCT,KSET,KCOMP,NA,NB,NC,ND,NE,AA,AB,AC,KK,
     1NN,LL,I,NINT,PERC,IND,J,K,NM,NSIMP,NREJ,RULE,YLEV(2)
      DIMENSION CL(20)
      DATA(CL(L),L=1,15)/4.000,2.000,1.000,0.5,0.2,0.1,0.09,0.08,0.07,0.
     C06,0.05,0.04,0.03,0.02,0.01/
      KND=1
    1 Y=0. $  Y=EQN(MYDUMMY)
      IF(Y.LE.0.7.AND.Y.GE.0.5) RETURN
      GO TO (2,11),KND
    2 CONST=Y/X(2) $ Y=0.6  $ X(2)=Y/CONST
      DO 3 L=1,14
      IF(X(2).GE.CL(L)) GO TO 4
    3 CONTINUE
      IF(X(2).LT.CL(L)) X(2)=CL(L) $ KND=2 $ GO TO 1
    4 CONTINUE $ IF(L.EQ.1) 5,6
    5 X(2)=CL(L) $ KND=2 $ GO TO 1
    6 TEST1=X(2)-CL(L) $ TEST2=CL(L-1)-X(2)
      IF(TEST1.EQ.TEST2) 7,8
    7 X(2)=CL(L) $ KND=2 $ GO TO 1
    8 CONTINUE $ IF(TEST1.LT.TEST2) 9,10
    9 X(2)=CL(L) $ KND=2 $ GO TO 1
   10 X(2)=CL(L-1) $ KND=2 $ GO TO 1
   11 NM=NM+1 $ BA(NM)=X(2) $ RETURN
      END
```

```
      SUBROUTINE NEWRAP(B,N,X)
C*****REQUIRED FOR THIS PARTICULAR FORM OF FUNCTION EQN ONLY
      DIMENSION B(5)
      XLIM=X*1E-10 $ DO1 I=1,10 $ XL=X $ X1=1. $ F=B(1) $ FD=0.
      DO2 J=2,N $ FD=FD+B(J)*(J-1)*X1 $ X1=X1*X
    2 F=F+B(J)*X1 $ X=X-F/FD $ IF(ABS(X-XL).LE.XLIM)3,1
    1 CONTINUE
    3 RETURN $ END
```

```
      FUNCTION DERIV (ID,Z)
C*****THIS FUNCTION EVALUATES THE DERIVATIVE OF THE RESIDUAL FUNCTION W.R.T.
C     PARAMETERS OR VARIABLES AS SPECIFIED BY THE INPUT VALUE Z
      COMMON XX(5,100),X(5),A(20),SX(5),SA(20),KX(5),CX(5),XCOMP(10),SY,
     1Y,CY,C(20,20),CINV(20,20),RE(20),BA(100),E(10,10),NMARK(10),YSIMP
      COMMON NP,N,M,KCY,KY,KF,KCT,KSET,KCOMP,NA,NB,NC,ND,NE,AA,AB,AC,KK,
     1NN,LL,I,NINT,PERC,IND,J,K,NM,NSIMP,NREJ,RULE,YLEV(2)
      F0= EQN(MYDUMMY)
      ZZ=Z
      Z=ZZ*1.005
      DZ=Z-ZZ
      IF(ID.EQ.1) 1,2
    1 A(K)=Z $ GO TO 3
    2 X(J)=Z
    3 F1= EQN(MYDUMMY)
      DERIV=(F1-F0)/DZ
      IF(ID.EQ.1) 4,5
    4 A(K)=ZZ $ GO TO 6
    5 X(J)=ZZ
    6 RETURN $ END
```

```
      SUBROUTINE CYC
C*****THIS SUBROUTINE CYCLES THE REQUIRED PARAMETER(S)-WRITTEN AS REQUIRED
      COMMON XX(5,100),X(5),A(20),SX(5),SA(20),KX(5),CX(5),XCOMP(10),SY,
     1Y,CY,C(20,20),CINV(20,20),RE(20),BA(100),E(10,10),NMARK(10),YSIMP
      COMMON NP,N,M,KCY,KY,KF,KCT,KSET,KCOMP,NA,NB,NC,ND,NE,AA,AB,AC,KK,
     1NN,LL,I,NINT,PERC,IND,J,K,NM,NSIMP,NREJ,RULE,YLEV(2)
      DIMENSION SORBM(6),SORBD(6)
      DATA(SORBM(L),L=1,6)/.383,.551,.474,.298,.253,.186/,
     C(SORBD(L),L=1,6)/.278,.385,.350,.284,.298,.222/,CTM,CTD/1.07026E-0
     C5,1.00017E-03/,PLM,PLD/1.00686,0.0102248/
      GO TO (1,2,3) NC
C*****CASE (1) - N VARIED
    1 N=N+1 $ IF(N.GT.NA) 4,5
C*****CASE (2) - ESTIMAT-PREDAN PROCEDURE, K VARIED AT ONE POINT
    2 A(1)=SORBM(2)/(CTM*PLM) $ A(3)=A(3)+20.  $ IF(A(3).GT.NA) GO TO 4
      C1=1.+8.*A(3)*CTD $ C1=SQRT(C1) $ C1=(C1-1.)/(4.*A(3))
      SL=SORBD(2)/PLD $ A(2)=(SL-A(1)*C1)/((CTD-C1)*2.)
      GO TO 5
C*****CASE (3) - ESTIMAT-PREDAN PROCEDURE, CALCULATION OVER SPECTRUM
    3 L=KK+1
      IF(L.GT.6) GO TO 4
      A(1)=SORBM(L)/(CTM*PLM)
      C1=1.+8.*A(3)*CTD $ C1=SQRT(C1) $ C1=(C1-1.)/(4.*A(3))
      SL=SORBD(L)/PLD $ A(2)=(SL-A(1)*C1)/((CTD-C1)*2.)
      GO TO 5
    4 NN=1
    5 RETURN $ END
```

```
      SUBROUTINE MTXINV
C*****MATRIX INVERSION SUBROUTINE
      COMMON XX(5,100),X(5),A(20),SX(5),SA(20),KX(5),CX(5),XCOMP(10),SY,
     1Y,CY,C(20,20),CINV(20,20),RE(20),BA(100),E(10,10),NMARK(10),YSIMP
      COMMON NP,N,M,KCY,KY,KF,KCT,KSET,KCOMP,NA,NB,NC,ND,NE,AA,AB,AC,KK,
     1NN,LL,I,NINT,PERC,IND,J,K,NM,NSIMP,NREJ,RULE,YLEV(2)
      DIMENSION JC(20),IR(20),IORD(20),YY(20)
      EPS=1.E-60
    1 DET=1. $ DO2 K=1,NP$ IR(K)=0 $ JC(K)=0
    2 CONTINUE $ DO19 K=1,NP$ T=0. $ DO9 J=1,NP$ DO3 I=1,NP
      KLES=K-1 $ IF(KLES)6,6,3
    3 CONTINUE $ DO5 L=1,KLES $ DO5 MM=1,KLES $ IF(J-JC(L))4,9,4
    4 IF(I-IR(MM))5,8,5
    5 CONTINUE
    6 CONTINUE $ IF(T-ABS(C(I,J)))7,8,8
    7 T=ABS(C(I,J)) $ IR(K)=I $ JC(K)=J
    8 CONTINUE
    9 CONTINUE $ IK=IR(K) $ JK=JC(K) $ D=C(IK,JK)
      IF(ABS(D)-ABS(EPS))36,36,10
   10 DET=DET*D $ DO13 J=1,NP $ IF(J-JK)11,12,11
   11  C(IK,J)=C(IK,J)/D $ GOTO13
   12 C(IK,JK)=1./D
   13 CONTINUE $ DO18 I=1,NP$ IF(I-IK)14,18,14
   14 F=C(I,JK) $ DO17 J=1,NP $ IF(J-JK)15,16,15
   15 C(I,J)=C(I,J)-F*C(IK,J) $ GOTO17
   16 C(I,J)=-F*C(IK,JK)
   17 CONTINUE
   18 CONTINUE
   19 CONTINUE $ DO20 K=1,NP$ I=IR(K) $ J=JC(K) $ IORD(I)=J
   20 CONTINUE $ ICT=0 $ LIM=NP
   21 LND=1 $ IF(LIM-2)25,22,22
   22 CONTINUE $ DO24K=2,LIM $ IF(IORD(K-1)-IORD(K))24,24,23
   23 T=IORD(K-1) $ IORD(K-1)=IORD(K) $ IORD(K)=T $ LND=K-1 $ ICT=ICT+1
   24 CONTINUE
   25 CONTINUE $ IF(LND-1)27,27,26
   26 LIM=LND $ GOTO21
   27 IF((ICT/2)*2-ICT)28,29,28
   28 DET=-DET
   29 DO32 J=1,NP $ DO30 I=1,NP$ J1=JC(I) $ I1=IR(I) $ YY(J1)=C(I1,J)
   30 CONTINUE $ DO31 I=1,NP$ C(I,J)=YY(I)
   31 CONTINUE
   32 CONTINUE$DO35I=1,NP$DO33J=1,NP$J1=JC(J)$I1=IR(J)$YY(I1)=C(I,J1)
   33 CONTINUE $ DO34 J=1,NP$ C(I,J)=YY(J)
      CINV(I,J)=C(I,J)
   34 CONTINUE
   35 CONTINUE $ RETURN
   36 NM=110 $ IF(KCY.NE.3) PRINT 100 $ RETURN
  100 FORMAT(1H ,//,5X,*MATRIX NON-SINGULAR, NO SOLUTIONS POSSIBLE*/)
      END
```

```
      FUNCTION SIG(XX,KK,CC)
C*****THIS FUNCTION EVALUATES UNCERTAINTIES IN EITHER X(J) OR Y AS REQU-
                                                                  IRED
      GO TO (1,2,3,4) KK
C*****CASE 1-CONSTANT UNCERTAINTY
    1 SIG=CC $ RETURN
C*****CASE 2-CONSTANT FRACTIONAL UNCERTAINTY
    2 SIG=CC*XX $ RETURN
C*****CASE 3-COUNTING STATISTICS
    3 SIG=CC*SQRT(XX) $ RETURN
C*****CASE 4 - LOGARITHMIC RELATIONSHIP TO DETERMINE UNCERTAINTY IN
C              ABSORBANCE FROM CONSTANT UNCERTAINTY IN TRANSMITTANCE
    4 TRANS=2.-XX $ TRANS=10.**(TRANS)
      TRANS=TRANS + CC
      SIG = XX- (2. - ALOG10(TRANS)) $ RETURN $ END
```

```
      SUBROUTINE PRINT
C*****THIS SUBROUTINE PRINTS OUT RESULTS AND HEADINGS
      COMMON XX(5,100),X(5),A(20),SX(5),SA(20),KX(5),CX(5),XCOMP(10),SY,
     1Y,CY,C(20,20),CINV(20,20),RE(20),BA(100),E(10,10),NMARK(10),YSIMP
      COMMON NP,N,M,KCY,KY,KF,KCT,KSET,KCOMP,NA,NB,NC,ND,NE,AA,AB,AC,KK,
     1NN,LL,I,NINT,PERC,IND,J,K,NM,NSIMP,NREJ,RULE,YLEV(2)
      IF(KCY.EQ.3) GO TO 23
      GO TO (1,19,20),IND
    1 CONTINUE $ IF(KK.EQ.1) 2,17
    2 CONTINUE $ IF(LL.EQ.1) 32,33
   32 PRINT 100 $ GO TO 34
   33 PRINT 113
   34 CONTINUE $ IF(KCY.EQ.1) GO TO 6
C*****SELECT CYC VARIATION STATEMENT
      GO TO (3,4,5),NC
    3 PRINT 101 $ GO TO 6
    4 PRINT 102 $ GO TO 6
    5 PRINT 103 $ GO TO 6
C*****SELECT XSPACE VARIATION STATEMENT
    6 CONTINUE $ IF(KCOMP.EQ.0) 35,36
   35 PRINT 203 $ GO TO 10
   36 GO TO (7,8,9),NB
    7 PRINT 104 $ GO TO 10
    8 PRINT 105,AA $ GO TO 10
    9 PRINT 106 $ GO TO 10
C*****SELECT OUTPUT FOR RELEVANT MODELS AS STATED
   10 GO TO (11,12,13,14,15),KF
   11 PRINT 107 $ GO TO 16
   12 PRINT 108 $ GO TO 16
   13 PRINT 109 $ GO TO 16
   14 PRINT 110 $ GO TO 16
   15 PRINT 111 $ GO TO 16
   16 PRINT 112,LL,KK
      GO TO 18
   17 PRINT 113 $ PRINT 112,LL,KK
   18 PRINT 114,N
   19 PRINT 115,(X(J),J=1,M),(SX(J),J=1,M),Y,SY
      GO TO 1000
   20 CONTINUE $ IF(NM.EQ.110) 21,22
   21 PRINT 116,(A(K),K=1,NP) $ GO TO 1000
   22 PRINT 117,(A(K),SA(K),RE(K),K=1,NP)
      IF(NM.EQ.0) GO TO 31
      PRINT 118 $ PRINT 119,(BA(K),K=1,NM) $ GO TO 31
   23 CONTINUE $ GO TO(24,27,28,30,29),IND
   24 CONTINUE $ IF(KK.EQ.2) 25,26
   25 PRINT 120,AB
   26 PRINT 121,J,(NMARK(K),K=1,ND),YSIMP,N  $ RETURN
   27 PRINT 122,J,(NMARK(K),K=1,ND),YSIMP,NREJ,RULE,N $ RETURN
   28 J=KK-1 $ PRINT 123,J $ RETURN
   29 PRINT 124, (YLEV(L),L=1,2)
   30 PRINT 125,(NMARK(K),K=1,ND)
   31 NDF=N-M $ IF(NDF.LE.15) PRINT 126,NDF
  100 FORMAT(1H1,52X,*PREDICTION ANALYSIS OUTPUT*///,5X,*QUANTITIES ARE
     1SET OUT IN GROUPS IN THE FOLLOWING MANNER-*/5X,*N, BELOW WHICH ARE
     1 X(J),SX(J), Y AND SY, BELOW THESE ARE A(K) AND CORRESPONDING SA(K
     1) AND RE(K) VALUES, IF APPLICABLE*///)
  101 FORMAT(1H ,10X,*N VARIED*)
```

```
 102 FORMAT(1H ,10X,*ESTIMAT-PREDAN PROCEDURE*/11X,*K VARIED AT ONE POI
    1NT*)
 103 FORMAT(1H ,10X,*ESTIMAT-PREDAN PROCEDURE*/11X,*CALCULATIONS OVER S
    1PECTRUM*)
 203 FORMAT(1H ,10X,*X(J) VALUES READ IN*///)
 104 FORMAT(1H ,10X,*EQUAL SPACING*///)
 105 FORMAT(1H ,10X,*SPACING*,F7.4 ,*-TUPLED CONSECUTIVELY*///)
 106 FORMAT(1H ,10X,*SIMPLEX VARIATION*///)
 107 FORMAT(1H ,47X,*MONOMER-DIMER MODEL, 3 PARAMETERS*/////)
 108 FORMAT(1H ,44X,*MONOMER-DIMER-TRIMER MODEL, 4 PARAMETERS*/////)
 109 FORMAT(1H ,44X,*MONOMER-DIMER-TRIMER MODEL, 5 PARAMETERS*/////)
 110 FORMAT(1H ,43X,*MONOMER-DIMER-TETRAMER MODEL, 4 PARAMETERS*/////)
 111 FORMAT(1H ,43X,*MONOMER-DIMER-TETRAMER MODEL, 5 PARAMETERS*/////)
 112 FORMAT(1H ,43X,    *RESULTS OF COMPUTATIONS FOR SET*I3,1X,*CASE*I3/
    1//)
 113 FORMAT(1H1)
 114 FORMAT(1H ,//,66X,I3//)
 115 FORMAT(1H ,22X,E10.3,2X,F7.4,10X,2(E10.3,4X),4X,F7.4,4X,E10.3)
 116 FORMAT(1H ,//60X,E10.3)
 117 FORMAT(1H ,//50X,2(  E10.3,2X ),F6.3)
 118 FORMAT(1H ,//10X,*THE FOLLOWING ARE VALUES OF THE PATH LENGTH WHIC
    1H DO NOT FIT BETWEEN ABSORBANCES 0.5 AND 0.7 AND MUST BE TAKEN*)
 119 FORMAT(1H ,21X,10(F7.4,2X))
 120 FORMAT(1H1,56X,*SIMPLEX OUTPUT*///,5X,*QUANTITIES SPAN THE PAGE IN
    1 THE FOLLOWING MANNER-*/5X,       *POINT,NMARK(K) VALUES,YSIMP,POIN
    1T REJECTED,RULE FOR REJECTION AND N*///53X,*STEP SIZE=*,E10.3//)
 121 FORMAT(1H ,10X,I3,10X,5(I5,5 X),F8.3,10X,*STARTING SIMPLEX*,10X,I3
    1)
 122 FORMAT(1H ,10X,I3,10X,   5(I5, 5X),       F8.3,10X,I3,10X,F3.0,10X
    1,I3)
 123 FORMAT(1H ,10X,I3,10X,*THIS POINT REJECTED DUE TO IMPOSSIBILITY OF
    1 SOLUTION-MATRIX NON-SINGULAR*)
 124 FORMAT(1H ,//20X,F2.0,1X,*ITERATIONS EXCEEDED OR YLEV(2) HAS BEEN
    1SURPASSED AT A VALUE OF*1X,F6.3,1X,*IN SIMPLEX*/)
 125 FORMAT(1H ,35X,*THE OPTIMUM SET OF VALUES NMARK(K) ARE RESPECTIVEL
    1Y*/37X,5(I5,5X)//)
 126 FORMAT(1H ,//51X,*NO. OF DEGREES OF FREEDOM IS*1X,I3/37X,*CONFIDEN
    1CE INTERVAL MUST BE USED AS DEFINED BY THE FOLLOWING:*//49X,*A(K)-
    1SA(K).F(Z)<B(K)<A(K)+SA(K).F(Z)*//40X,*WHERE B(K) ARE THE TRUE VAL
    1UES OF THE PARAMETERS*/40X,*F(Z) ARE VALUES OF THE T-DISTRIBUTION
    1AT THE Z-LEVEL*/40X,*AND THE REST OF THE ENTITIES HAVE BEEN DEFINE
    1D*)
1000 RETURN $ END
```

C-2 ADFULGO

```
      PROGRAM ADFULGO(INPUT,OUTPUT,TAPE5=INPUT,TAPE6=OUTPUT)
C*****DIMER SPECTRUM CALCULATION BASED ON ADIABATIC MODEL OF FULTON, JCP
C     VOL. 56, P.1210,(1972) AND THE THEORETICAL DEVELOPEMENT OF FULTON
C AND GOUTERMAN JCP VOL. 41, P.2280 (1964)
      COMMON ZR(50,50),ZI(50,50),X(101),SUM(101,2),TOTAL(101),
     1EV(2,10,10),EI(2,10,10),CV(2,10,10),CI(2,10,10),BN(50,10)
      COMMON EPS,BML,BMK,THETA,W,V,BG,AMAX,WMIN,WINCR,N,NM,NINCR,NMAX,
     1IPLOT,NEV,XS
      DIMENSION AR(50,50),AI(50,50),Z(50,50),D1(50),D2(50),E(50),E2(50),
     1TAU(2,50),SC(2),INEV(2)
      EQUIVALENCE (ZR,Z)
C     READ IN NUMBER OF DATA SETS
      READ(5,100) NDATA
      LADD=0
 1000 LADD=LADD+1
C     READ INPUT INFORMATION
      CALL READ (LADD,NDATA)
C     ESTABLISH CONSTANTS, ETC.
C     IF READ IN BML USE NEXT CARD, OTHERWISE TAKE OUT
      XL=BML*BML
C     IF READ IN XL USE NEXT TWO CARDS, OTHERWISE REMOVE THEM
      XL=BML
      BML=SQRT(XL)
C     XS MAY BE USED AS AN ALTERATION FACTOR FOR ANY VARIABLE PARAMETER
      BMK=W/V
      BMK=2.*BML/BMK
      BGC=2.7726/(BG*BG)
      NEV=10
      INEV(1)=NEV
      INEV(2)=NEV
      ILIM1=1
      ILIM2=2
      IF(LADD.EQ.1) GO TO 1
      IF(EPS.NE.X1) GO TO 1
      IF(BML.NE.X2) GO TO 1
      IF(BMK.NE.X5) GO TO 1
      IF(X3.EQ.0..AND.THETA.NE.X3) GO TO 2
      IF(X3.EQ.180. .AND.THETA.NE.X3) GO TO 1
      IF(THETA.NE.X3) GO TO 19
      IF(BG.NE.X4) GO TO 21
    1 IF(THETA.EQ.0.) GO TO 3
    2 IF(THETA.EQ.180.) GO TO 4
      GO TO 5
    3 DO 33 I=1,NEV
      DO 33 J=1,NEV
      CV(2,I,J)=0.
      CV(2,J,I)=CV(2,I,J)
      CI(2,I,J)=0.
   33 CI(2,J,I)=CI(2,I,J)
      ILIM2=1
      GO TO 5
    4 WRITE(6,499)
      DO 44 I=1,NEV
      DO 44 J=1,NEV
      CV(1,I,J)=0.
      CV(1,J,I)=CV(1,I,J)
      CI(1,I,J)=0.
```

```
   44 CI(1,J,I)=CI(1,I,J)
      ILIM1=2
    5 DO 18 NQ=ILIM1,ILIM2
C     COMPUTE BN COEFFICIENTS AND D1 EIGENVALUES
      NEV=10
      DO 52 K=1,N
      DO 52 J=K,N
      Z(J,K)=0.
   52 Z(K,J)=Z(J,K)
      SIGN=-1.
      CHANGE=-1.
      PQ=3-2*NQ
      DO 53 K=1,N
      I=K-1
      SIGN=SIGN*CHANGE
      D1(K)=I+0.5+BMK*BMK*0.5
      E(K)=SQRT(0.5*I)*BML
   53 Z(K,K)=1.
      CALL IMTQL2(NM,N,D1,E,Z,IERR)
      IF(IERR.NE.0)  56,51
   56 WRITE(6,503) IERR
      GO TO 30
   51 IF(PQ.GT.0.) 54,55
   54 WRITE(6,505)
      GO TO 57
   55 WRITE(6,5051)
   57 WRITE(6,502) (D1(I),I=1,NEV)
      DO 58 I=1,N
   58 WRITE(6,5052) I,(Z(I,J),J=1,NEV)
      DO 59 I=1,N
      DO 59 J=1,NEV
   59 BN(I,J)=Z(I,J)
C     COMPUTE CM COEFFICIENTS AND D2 EIGENVALUES
      DO 6 K=1,N
      DO 6 J=K,N
      AR(J,K)=0.
      AI(J,K)=0.
      Z(J,K)=0.
    6 Z(K,J)=Z(J,K)
      SIGN=-1
      CHANGE=-1
      PQ=3-2*NQ
      DO 7 K=1,N
      I=K-1
      SIGN = SIGN*CHANGE
      AR(K,K)=(I+0.5)+SIGN*PQ*EPS
    7 Z(K,K)=1.
      N1=N-1
      SIGN=1
      CHANGE=-1
      DO 8 K=1,N1
      J=K+1
      SIGN=SIGN*CHANGE
    8 AI(J,K)=SQRT(0.5*K)*(BMK+PQ*SIGN*(-BML))
C     IMTQL2, HTRIDI AND HTRIBK ARE LIBRARY PROGRAMS FOR COMPUTATION OF
C     EIGENVALUES AND EIGENFUNCTIONS OR COMPLEX HERMITIAN MATRIX
      CALL HTRIDI(NM,N,AR,AI,D2,E,E2,TAU)
```

```
      CALL IMTQL2(NM,N,D2,E,Z,IERR)
      DO 9 K=1,N
      DO 9 J=1,N
    9 ZR(J,K)=Z(J,K)
      CALL HTRIBK(NM,N,AR,AI,TAU,N,ZR,ZI)
      IF(IERR.NE.0) 91,92
   91 WRITE(6,503) IERR
      GO TO 30
   92 IF(PQ.GT.0) 10,11
   10 WRITE(6,500)
      GO TO 12
   11 WRITE(6,501)
   12 WRITE(6,502) (D2(I),I=1,NEV)
      DO 15 I=1,N
   15 WRITE(6,504) I,(ZR(I,J),ZI(I,J),J=1,NEV)
      NN=NEV
C     COMPUTE NON-ANGULAR FACTORS IN INTENSITIES
      CALL SUMINT(NQ,NN)
      INEV(NQ)=NEV
C     ESTABLISH TRANSITION ENERGIES IN DIMENSIONLESS UNITS
      DO 18 I=1,NN
      DO 18 J=1,NN
      EV(NQ,I,J)=D1(I)+D2(J)-1.
   18 CONTINUE
      NEV=MIN0(INEV(1),INEV(2))
C     COMPUTE ANGLE FACTOR IN INTENSITIES
   19 T=THETA*0.017453
      COST=COS(T)
      SC(1)=1.+COST
      SC(2)=1.-COST
C     COMPUTE ENERGIES IN CM-1 AND INTENSITIES
      DO 20 NQ=ILIM1,ILIM2
      DO 20 I=1,NEV
      DO 20 J=1,NEV
      CV(NQ,I,J)=EV(NQ,I,J)*V+W+XL*V
   20 CI(NQ,I,J)=EI(NQ,I,J)*SC(NQ)
      NI=NINCR+1
C     FIT GAUSSIAN BANDSHAPE TO LINE SPECTRUM
   21 DO 22 I=1,NI
      SUM(I,1)=0.
      SUM(I,2)=0.
      TOTAL(I)=0.
   22 X(I)=WMIN+WINCR*(I-1)
      DO 23 NQ=ILIM1,ILIM2
      DO 23 I=1,NEV
      DO 23 J=1,NEV
      DO 23 K=1,NI
      XEN=ABS(X(K)-CV(NQ,I,J))
      XEN=XEN*XEN
      XEN=-BGC*XEN
      IF(XEN.LT.-675.83) 221,222
  221 XEN=0.
      GO TO 23
  222 XEN=EXP(XEN)
   23 SUM(K,NQ)=SUM(K,NQ)+XEN*CI(NQ,I,J)
      DO 24 K=1,NI
   24 TOTAL(K)=SUM(K,1)+SUM(K,2)
```

```
C       NORMALIZE SPECTRUM TO MEASURED INTENSITY MAXIMUM
        PEAK=TOTAL(1)
        DO 26 I=1,NI
        IF(TOTAL(I).GE.PEAK) 25,26
   25   PEAK=TOTAL(I)
   26   CONTINUE
        IF(PEAK.EQ.0.) 27,28
   27   WRITE(6,507) CV(NQ,1,1)
        GO TO 30
   28   FACTOR=AMAX/PEAK
        DO 29 I=1,NI
        TOTAL(I)=TOTAL(I)*FACTOR
        SUM(I,1)=SUM(I,1)*FACTOR
   29   SUM(I,2)=SUM(I,2)*FACTOR
        CALL PRINT
   30   X1=EPS
        X2=BML
        X3=THETA
        X4=BG
        X5=BMK
        X6=XS
        IF(LADD.EQ.NDATA) RETURN
        GO TO 1000
  100   FORMAT(I2)
  499   FORMAT(1H1)
  500   FORMAT(1H ,/////,40X,*EIGENVALUES AND CM COEFFICIENTS FOR THE PLUS
       1 SERIES*/)
  501   FORMAT(1H ,/////,40X,*EIGENVALUES AND CM COEFFICIENTS FOR THE MINU
       1S SERIES*/)
  502   FORMAT(1H , 4X,10(5X,F7.3)///)
  503   FORMAT(1H ,///,20X,*MORE THAN 30 ITERATIONS REQIURED FOR EIGENVALU
       1E *,I3,1X,*LOWER EIGENVALUES UNORDERED - MUST TERMINATE*)
  504   FORMAT(4X,I3,1X,20(1X,F5.3))
  505   FORMAT(1H1,/////,40X,*EIGENVALUES AND BN COEFFICIENTS FOR PLUS SER
       1IES*/)
 5051   FORMAT(1H1,/////,40X,*EIGENVALUES AND BN COEFFICIENTS FOR MINUS SE
       1RIES*/)
 5052   FORMAT(4X,I3,2X,10(F7.3,5X))
  507   FORMAT(1H ,///20X,*ALL POINTS IN SPECTRUM ARE ZERO - TERMINATE*/,
       120X,*ONE OF THE FIRST ENERGIES IS *,E10.3,1X,*CM-1*)
        END
```

```
      SUBROUTINE SUMINT(NQ,NN)
C     SUBROUTINE FOR COMPUTATION OF INTENSITY SUMS
      COMMON ZR(50,50),ZI(50,50),X(101),SUM(101,2),TOTAL(101),
     1EV(2,10,10),EI(2,10,10),CV(2,10,10),CI(2,10,10),BN(50,10)
      COMMON EPS,BML,BMK,THETA,W,V,BG,AMAX,WMIN,WINCR,N,NM,NINCR,NMAX,
     1IPLOT,NEV,XS
      COMPLEX CTERM1,CTERM2,CTERM3,CTERM4,CTERM5,CSUM(2,100)
      DIMENSION CONV(2),SSUM(2),XSUM(2,10)
      X1=0.
      X2=1.
      BMA=BMK/2.
      CTERM1=CMPLX(X1,BMA)
      DO 50 J=1,NN
      CTERM2=CMPLX(ZR(1,J),ZI(1,J))
      CTERM2=CONJG(CTERM2)
      CTERM3=CMPLX(X2,X1)
      CTERM4=CMPLX(BN(1,J),X1)
      CTERM5=CTERM3
      CSUM(1,1)=CTERM2*CTERM3
      CSUM(2,1)=CTERM4*CTERM5
      DO 1 L=2,N
      K=L
      KK=L-1
      CTERM2=CMPLX(ZR(K,J),ZI(K,J))
      CTERM2=CONJG(CTERM2)
      CTERM4=CMPLX(BN(K,J),X1)
      XFAC=FLOAT(KK)
      XFAC=1./SQRT(XFAC)
      CTERM3=CTERM1*CTERM3*XFAC
      CTERM5=CTERM1*CTERM5*XFAC
      CSUM(1,K)=CSUM(1,KK)+CTERM2*CTERM3*(-1)**KK
    1 CSUM(2,K) =CSUM(2,KK)+CTERM4*CTERM5*(-1)**KK
      DO 2 L=1,2
      SUM2=CABS(CSUM(L,K))
      SSUM(L)=SUM2
      SUM1=CABS(CSUM(L,KK))
      XSUM(L,J)=SUM2*SUM2
      CONV(L)=ABS(SUM2-SUM1)
      IF(SUM2.EQ.0.) 11,12
   11 CONV(L)=0.
      GO TO 2
   12 CONV(L)=CONV(L)/SUM2
    2 CONTINUE
C     ERROR TAKEN AT 5 P.C. OF ACTUAL SUM
      IF(CONV(1).LE.0.05.AND.CONV(2).LE.0.05) GO TO 50
      IF(J.GT.6) 3,4
    3 NEV=J-1
      NN=J
   50 CONTINUE
      DO 51 I=1,NN
      DO 51 J=1,NN
   51 EI(NQ,I,J)=XSUM(2,I)*XSUM(1,J)
      RETURN
    4 WRITE(6,500) CONV(2),CONV(1)
      STOP
  500 FORMAT (1H ,//20X,*TERMINATED AS NO MORE THAN 6 SUMS IN SUMINT HA
     1E CONVERGED TO BETTER THAN 5 P.C.*/20X,*FRACTIONAL CHANGE IN LAST
     1BN SUM AT END WAS *,F5.2,/20X,*FRACTIONAL CHANGE IN LAST CM SUM
     2 END WAS *,F5.2)
      END
```

```
      SUBROUTINE READ (LADD,NDATA)
C*****INPUT SUBROUTINE
      COMMON ZR(50,50),ZI(50,50),X(101),SUM(101,2),TOTAL(101),
     1EV(2,10,10),EI(2,10,10),CV(2,10,10),CI(2,10,10),BN(50,10)
      COMMON EPS,BML,BMK,THETA,W,V,BG,AMAX,WMIN,WINCR,N,NM,NINCR,NMAX,
     1IPLOT,NEV,XS
C     READ AND WRITE 1 HEADER CARD
      READ(5,100) (X(I),I=1,10)
C     READ ALL OTHER DATA AND PRINT IT OUT
      READ(5,101) EPS,BML,THETA,W,V,BG,AMAX,WMIN,WINCR,N,NM,NINCR,NMAX,
     1IPLOT,XS
      WRITE(6,500) EPS,BML,THETA,W,V,BG,AMAX,WMIN,WINCR,N,NM,NINCR,NMAX,
     1IPLOT,XS
      WRITE(6,501) LADD,NDATA,(X(I),I=1,10)
      RETURN
  100 FORMAT(10A8)
  101 FORMAT(9F6.0,2I3,3I2,F6.0)
  500 FORMAT(1H1,///20X,   *ABSORPTION SPECTRA OF DIMERS CALCULATED BY T
     1HE ADIABATIC MODEL OF FULTON (JCP, VOL. 56, 1210 (1972))*,/,35X,*A
     2ND THE TECHNIQUE OF FULTON AND GOUTERMAN (JCP, VOL. 41, 2280 (1964
     3))*,/////,60X,*INPUT INFORMATION*///,40X,*EPS= *,F6.2,8X,*BML= *,
     4F6.2,7X,*THETA= *,F5.1//40X,*W= *,F6.0,8X,*V= *,F6.0,8X,*BG= *,
     5F5.0,//40X,*AMAX= *,F6.0,5X,*WMIN= *,F6.0,5X,*WINCR= *,F5.0//40X,*
     6N= *,I3,13X,*NM= *,I3,11X,*NINCR= *,I2//40X,*NMAX= *,I2,9X,*IPLOT=
     7 *,I2,8X,*XS= *,F6.3)
  501 FORMAT(1H ,////,10X,*SET *,I2,1X,*IN *,I2,1X,*SETS OF DATA*,//,10X
     1,10A8)
      END
      SUBROUTINE PRINT
C*****OUTPUT SUBROUTINE
      COMMON ZR(50,50),ZI(50,50),X(101),SUM(101,2),TOTAL(101),
     1EV(2,10,10),EI(2,10,10),CV(2,10,10),CI(2,10,10),BN(50,10)
      COMMON EPS,BML,BMK,THETA,W,V,BG,AMAX,WMIN,WINCR,N,NM,NINCR,NMAX,
     1IPLOT,NEV,XS
      EVS=EPS*V
      WRITE(6,500) EPS,EVS,BML,BMK,BG,THETA
      NN=NEV
      IF(NEV.EQ.10) NN=9
      DO 1 I=1,NN
      DO 1 J=1,I
      K=I-1
      L=I-J+1
    1 WRITE(6,501) K,CV(1,L,J),CI(1,L,J),CV(2,L,J),CI(2,L,J)
      WRITE(6,502)
      NI=NINCR+1
      DO 2 K=1,NI
    2 WRITE(6,503)  X(K),SUM(K,1),SUM(K,2),TOTAL(K)
C     PLOT RESULTS IF REQUIRED
      IF(IPLOT.EQ.1) CALL OVERSA(1H ,1H.,NI,TOTAL,X)
      RETURN
  500 FORMAT(1H1,///,32X,*ADIABATIC MODEL OF THE DIMER*//32X,*CALCULATED
     1 SPECTRUM FOR THE FOLLOWING SET OF PARAMETERS*/32X,*EXCITON COUPLI
     2NG PARAMETER IS *,F6.3,3X,*OR *,F5.0,1X,*CM-1.*/32X, *POSITION COU
     3PLING PARAMETER IS *,F6.3/32X,*MOMENTUM COUPLING PARAMETER IS *,
     4F6.3/32X,*GAUSSIAN BANDWIDTH IS *,F5.0,/32X,*ANGLE BETWEEN TRANSIT
     5ION MOMENTS IS *,F6.2,1X,*DEGREES*///,17X,*POSITIONS IN CM-1, WN(+
     6/-), AND RELATIVE INTENSITIES, XI(+/-), OF DIMER BANDS*//21X,*QUAN
     7TA*,10X,*WN(+)*,15X,*XI(+)*,16X,*WN(-)*,18X,*XI(-)*/)
  501 FORMAT(20X,I5,12X,F6.0,9X,E13.4,12X,F6.0,16X,E13.4)
  502 FORMAT(1H ,////,50X,*CALCULATED SPECTRUM*//27X,*WAVENUMBER*,11X,
     2*PLUS SERIES*,5X,*MINUS SERIES*,3X,*TOTAL INTENSITY*)
  503 FORMAT(30X,F6.0,8X,3(5X,E12.5))
      END
```

SUBROUTINE OVERSA as in programme RESPECT

C-3 TROP

```
      PROGRAM TROP(INPUT,OUTPUT,TAPE5=INPUT,TAPE6=OUTPUT)
C*****THIS PROGRAM CALCULATES TRANSITION MOMENT ORIENTATIONS
      COMMON Y(50),X(5,50),XX(5),SY(50),SX(5,50),A(5),B(10),R(50),F(50)
     1,SA(5),C(5,5),CINV(5,5),DL(50),S
      COMMON N,M,NP,NC,KE,KSET,ISTAT,ITER,CONMIN
      DIMENSION AB(20),AY(20)
      KK=0
 1000 CALL DATAFIT
      KK=KK+1
      IF(ISTAT.EQ.4) GO TO 9
C     READ B-POL ABSORBANCES
    1 READ(5,50) (AB(I),I=1,N)
      B1=B(1)*B(1)
      B2=B(2)*B(2)
      B3=B(3)*B(3)
      B4=B(4)*0.01745
      A1=A(1)*0.01745
      A2=A(2)
      SUMX2=0.
      SUMY2=0.
      SUMXY=0.
      MIND=1
      DO 2 I=1,N
      XX(1)=X(1,I)
      IF(XX(1).GT.B4) GO TO 5
      Z1=COS(B4-XX(1))/B1
      Z2=SIN(B4-XX(1))/B3
      RINDEX=1./SQRT(Z1*Z1+Z2*Z2)
      AY1=SIN(XX(1))*RINDEX
      AY1=B2-AY1*AY1
      AY2=1./AY1
      AY1=SQRT(AY2)
      AY(I)=AY1
      SUMX2=SUMX2+AY2
      SUMY2=SUMY2+AB(I)
    2 SUMXY=SUMXY+(AY1*AB(I))
C     A3  IS THE SCALE FACTOR FOR B-POL ABSORPTION SAME AS FOR AC-POL
      A3  = SUMXY/SUMX2
      SD3=SUMX2*SUMY2-SUMXY*SUMXY
      SD3=SD3/((N-2)*SUMX2*SUMX2)
      SD3=ABS(SD3)
      SD3=SQRT(SD3)
      DO 3 I=1,N
    3 AY(I)=AY(I)*A3
C     DO CALCULATION FOR TRANSMISSION OF RAY ALONG C(DASHED) AXIS
      WN=B3/B1*TAN(B4)
      WN=B4-ATAN(WN)
      Z1=COS(B4-WN)/B1
      Z2=SIN(B4-WN)/B3
      RINDEX=1./SQRT(Z1*Z1+Z2*Z2)
      AY0=SIN(WN)*RINDEX
      AY0=B2-AY0*AY0
      AY0=A3 *SQRT(1./AY0)
      T=10.**(-AY0)
      T=T+0.01
      YY=-ALOG10(T)
      SDAY=ABS(AY0-YY)
```

```
   31 THETA=A2/A3
      AX0=THETA
      THETA=SQRT(THETA)
      THETA=ATAN(THETA)/0.01745
      AX0=AY0*COS(A1)*COS(A1)*AX0
      AX0=ABS(AX0)
      AZ0=TAN(A1)
      AZ0=AX0*AZ0*AZ0
      AZ0=ABS(AZ0)
C     COMPUTE STD. DEV. IN AX,AZ0 AND THETA
      IF(MIND.EQ.2) GO TO 33
      Z1=A1
      Z2=A2
      Z3=AX0
      Z4=AY0
      Z5=AZ0
      Z6=THETA
      Z7=A3
      A1=A1+SA(1)*0.01745
      A2=A2+SA(2)
      A3=A3+SD3
      AY0=AY0+SDAY
      MIND=2
      GO TO 31
   33 SDAX=ABS(AX0-Z3)
      SDAZ=ABS(AZ0-Z5)
      SDTH=ABS(THETA-Z6)
      A1=Z1
      A2=Z2
      AX0=Z3
      AY0=Z4
      AZ0=Z5
      THETA=Z6
      A3=Z7
C     COMPUTE TOTAL ASORBANCE AND A MEAN STD. DEV. IN THIS VALUE
      AT=(AX0+AY0+AZ0)/3.
      SDAT=(SDAX+SDAY+SDAZ)/3.
      WN=WN/0.01745
      WRITE(6,100) A3,SD3
      WRITE(6,101)
      DO 4 I=1,N
      T=10.**(-AB(I))
      T=T+0.01
      YY=-ALOG10(T)
      ERR=ABS(AB(I)-YY)
    4 WRITE(6,102) AY(I),AB(I),ERR
      WRITE(6,103) WN,AX0,AY0,AZ0,SDAX,SDAY,SDAZ
      WRITE(6,104) AT,SDAT
      A1=A1/0.01745
      Z1=A1
      IF(Z1.LE.180..AND.Z1.GE.0.) GO TO 44
      IF(Z1.LT.0..AND.Z1.GE.-180.) 40,41
   40 Z1=Z1+180.
      GO TO 44
   41 SIGN=Z1/ABS(Z1)
      DO 42 J=1,5
      Z2=Z1-SIGN*360.*J
```

```
      IF(Z2.GE.-180..AND.Z2.LT.0.) 411,412
  411 Z1=Z2+180.
      GO TO 44
  412 IF(Z2.LE.180..AND.Z2.GE.0.) GO TO 43
   42 CONTINUE
   43 A1=Z2
      GO TO 45
   44 A1=Z1
   45 WRITE(6,105) A1,SA(I),THETA,SOTH
      GO TO 8
    5 WRITE(6,106)
    8 IF(KK.NE.KSET) 1000,2000
    9 WRITE(6,500)
      A(1)=-10.
      WRITE(6,501) A(2)
      A(2)=A(2)*0.01745
      A(2)=SIN(A(2))
      A(2)=A(2)*A(2)
   10 A(1)=A(1)+10.
      DO 11 I=1,13
      XX(1)=X(1,I)
   11 AB(I)=-EQN(I)
      WRITE(6,502) A(1),(AB(I),I=1,13)
      IF(A(1).LT.180.) 10,8
 2000 STOP
   50 FORMAT(20F4.0)
  100 FORMAT(1H ,///50X,*ORIENTATION EXPERIMENT RESULTS*////10X,*LINEAR
     1LEAST SQUARES ON B-POL. ABSORPTION DATA*//20X,*SCALE FACTOR AND ST
     2D. DEV. IS*,10X,2(E10.3,5X))
  101 FORMAT(1H ,///20X,*CALCULATED AND EXPT. B-POL ABSORBANCES AND ERRO
     1RS IN EXPT. VALUES ARE, RESPECTIVELY*//)
  102 FORMAT(25X,3(F5.3,10X))
  103 FORMAT(1H ,/////10X,*ABSORBANCE CALCULATIONS*//20X,*WAVENORMAL ANG
     1LE FOR RAY COLLINEAR WITH C(PRIMED)-AXIS IS *,F6.2///20X,*A-, B- A
     2ND C(PRIMED)-POL. ABSORBANCES ARE*,3(5X,F6.3)//20X,*ERRORS IN THES
     3E ABSORBANCES ARE *,9X,3(5X,F6.3))
  104 FORMAT(1H ,////20X,*TOTAL ABSORBANCE AND ITS ERROR IS *,
     1  2(5X,F6.3))
  105 FORMAT(1H ,/////10X,*SUMMARY OF EFFECTIVE TRANSITION MOMENT ANGLES
     1 WITH RESPECTIVE ERRORS*,//20X,*ANGLE TO A-AXIS IN AC(PRIMED)-PLAN
     2E IS*,2(F7.2,5X)//  20X,*ANGLE TO B-AXIS IS *,2(F7.2,5X))
  106 FORMAT(1H ,///10X,*XX(1) CANNOT EXCEED B(4) IN MAIN*)
  500 FORMAT(1H1,///5X,*THEORETICAL ABSORBANCES FROM -15 TO 45 DEGREES A
     1CROSS PAGE*/5X,*AND AT 10 DEGREE INTERVALS FOR THE ANGLE IN AC-PLA
     2NE DOWN PAGE*///)
  501 FORMAT(1H ,10X,*VALUE OF ANGLE TO B-AXIS IS *,F7.2///)
  502 FORMAT(5X,F6.1,5X,13(2X,F6.3))
      END
```

```
      SUBROUTINE DATAFIT
C*****WEIGHTED NON-LINEAR LEAST SQUARES PROCEDURE (AFTER J.R. WOLBERG,
C     PREDICTION ANALYSIS, D. VAN NOSTRAND. 1967)
      COMMON Y(50),X(5,50),XX(5),SY(50),SX(5,50),A(5),B(10),R(50),F(50)
     1,SA(5),C(5,5),CINV(5,5),DL(50),S
      COMMON N,M,NP,NC,KE,KSET,ISTAT,ITER,CONMIN
      DIMENSION V(5),AA(5),FA(5)
      KK=0
 1000 KK=KK+1
      II=-1
      KP=1
C     READ INPUT
      CALL READ
C*****NEXT STATEMENT FOR THIS PARTICULAR PROGRAMME ONLY
      IF(ISTAT.EQ.4) GO TO 20
C     CHECK DIMENSIONS
      IF(N.GT.50) GO TO 1
      IF(M.GT.5) GO TO 2
      IF(NP.GT.5) GO TO 3
      IF(NC.GT.10) GO TO 4
      GO TO 2000
    1 WRITE(6,100)
      GO TO 4000
    2 WRITE(6,101)
      GO TO 4000
    3 WRITE(6,102)
      GO TO 4000
    4 WRITE(6,103)
      GO TO 4000
C     CLEAR RELEVANT MATRICES
 2000 DO 6 J=1,NP
      DO 5 K=1,NP
    5 C(J,K)=0.
    6 V(J)=0.
C     START COMPUTATION OF C AND V MATRICES
      S=0.
      II=II+1
      DO 3000 I=1,N
      DO 7 J=1,M
    7 XX(J)=X(J,I)
      R(I)=EQN(I)
C     COMPUTE WEIGHT FACTOR DL AND REQUIRED DERIVATIVES
      DL(I)=SY(I)*SY(I)
      DO 8 J=1,M
      DUM=SX(J,I)*DERIV(J,I,1)
    8 DL(I)=DL(I)+DUM*DUM
      DO 9 K=1,NP
    9 FA(K)=DERIV(K,I,2)
C     COMPUTE C AND V MATRICES
      DO 11 J=1,NP
      DO 10 K=J,NP
   10 C(J,K)=C(J,K)+FA(J)*FA(K)/DL(I)
   11 V(J)=V(J)+FA(J)*R(I)/DL(I)
C     COMPUTE WEIGHTED SUM S AND THE CALCULATED DEPENDENT VARIABLE
      S=S+R(I)*R(I)/DL(I)
      F(I)=Y(I)-R(I)
 3000 CONTINUE
```

```
C       PRINT INITIAL AND INTERIM RESULTS
        CALL PRINT(KP)
        KP=2
C       COMPLETE C MATRIX AND INVERT
        DO 12 J=1,NP
        DO 12 K=J,NP
   12 C(K,J)=C(J,K)
        CALL MATINV
C       COMPUTE AA MATRIX
        DO 13 K=1,NP
        AA(K)=0.
        DO 13 J=1,NP
   13 AA(K)=AA(K)+CINV(J,K)*V(J)
        DO 14 K=1,NP
        IF(A(K).EQ.0.) GO TO 131
        TEST=ABS(AA(K)/A(K))
        GO TO 132
  131 TEST=ABS(AA(K))
  132 IF(TEST.GT.CONMIN) GO TO 15
   14 CONTINUE
        GO TO 18
   15 IF(II.EQ.ITER) GO TO 17
        DO 16 K=1,NP
   16 A(K)=A(K)-AA(K)
        GO TO 2000
   17 WRITE(6,104)
C       COMPUTE ESTIMATES OF STANDARD DEVIATIONS
   18 SNP=S/(N-NP)
        DO 19 K=1,NP
        DUM=SNP*CINV(K,K)
   19 SA(K)=SQRT(DUM)
C       PRINT FINAL RESULTS
        KP=3
        CALL PRINT(KP)
C       IF ISTAT=1 CONTINUE GENERAL LEAST SQUARES PROCEDURE
C       IF ISTAT=2 RETURN TO MAIN FOR ADDITIONAL SPECIAL COMPUTATIONS
        IF(ISTAT.NE.1) GO TO 20
C       IF NO MORE DATA STOP
        IF(KK.NE.KSET) GO TO 1000
 4000 STOP
   20 RETURN
  100 FORMAT(1H ,///10X,*N HAS EXCEEDED 50*)
  101 FORMAT(1H ,///10X,*M HAS EXCEEDED 5*)
  102 FORMAT(1H ,///10X,*NP HAS EXCEEDED 5*)
  103 FORMAT(1H ,///10X,*NC HAS EXCEEDED 10*)
  104 FORMAT(1H ,///10X,      * MAX NUMBER OF ITERATIONS EXCEEDED*/16X,
     1*PROCEDURE HAS NOT CONVERGED BUT THE FOLLOWING ARE GIVEN FOR THE L
     2AST ITERATION *)
        END
```

```
      SUBROUTINE READ
C*****INPUT SUBROUTINE
      COMMON Y(50),X(5,50),XX(5),SY(50),SX(5,50),A(5),B(10),R(50),F(50)
     1,SA(5),C(5,5),CINV(5,5),DL(50),S
      COMMON N,M,NP,NC,KE,KSET,ISTAT,ITER,CONMIN
      WRITE(6,99)
C     READ 3 HEADER CARDS
      DO 1 J=1,3
      READ(5,50) (X(J,I),I=1,20)
    1 WRITE(6,50) (X(J,I),I=1,20)
C     READ INDICATORS
      READ(5,51) N,M,NP,NC,KE,KSET,ISTAT,ITER,CONMIN
C     READ INITIAL GUESSES AT PARAMETERS A(K)
      READ(5,511) (A(K),K=1,NP)
C     READ DEP. AND INDEP. VARIABLES OR CALC. ERRORS IN THESE
C     READ REQUIRED CONSTANTS IN THIS ORDER
C        (1) 3 REFRACTIVE INDICES
C        (2) ANGLE BETWEEN Z- AND C(PRIMED)-AXES
      READ(5,53) (B(I),I=1,NC)
C     READ ABSORBANCES AND ANGLES OF INCIDENCE - TRANSMISSION ANGLES
C     CALCULATED IN ETA.  ANGLES OF INCIDENCE READ IN AS X(1,I) AND
C        (1) MUST BE POSITIVE IF TRANSMITTED ANGLE WILL BE ON Z-AXIS SIDE
C        (2) MUST BE NEGATIVE IF TRANSMITTED ANGLE WILL BE ON OPTIC AXIS
C     ALL ANGULAR QUANTITIES READ IN AND PRINTED OUT IN DEGREES    SIDE
      READ(5,54) (Y(I),I=1,N)
      READ(5,54) (X(1,I),I=1,N)
      DO 4 I=1,N
      DL(I)=X(1,I)
      X(1,I)=ETA(I)
      SX(1,I)=0.5
      T=10.**(-Y(I))
      T=T+0.01
      YY=-ALOG10(T)
    4 SY(I)=ABS(Y(I)-YY)
C     WRITE HEADINGS ETC
      WRITE(6,100)
      WRITE(6,101) N,M,NP,NC,KE,KSET,ISTAT,ITER,CONMIN
      WRITE(6,102) (B(I),I=1,NC)
      WRITE(6,104)
      DO 5 I=1,N
      WRITE(6,105) I,Y(I),SY(I),X(1,I),SX(1,I),DL(I)
      SX(1,I)=SX(1,I)*0.01745
    5 X(1,I)=X(1,I)*0.01745
      RETURN
   50 FORMAT(20A4)
   51 FORMAT(8I2,F6.0)
  511 FORMAT(5E10.3)
   52 FORMAT(3F10.0)
   53 FORMAT(4F10.0)
   54 FORMAT(20F4.0)
   99 FORMAT(1H1)
  100 FORMAT(1H ,///50X,*INPUT INFORMATION*)
  101 FORMAT(1H ,///40X,*N=*,I3,11X,*M=*,I3,11X,*NP=*,I3///40X,*NC=*,
     1I3,10X,*KE=*,I3,10X,*KSET=*,I3,10X//40X,*ISTAT=*,I3,7X,*ITER=*,I3,
     28X,*CONMIN=*,F6.4)
  102 FORMAT(1H ,///10X,*B(I) VALUES ARE*/20X,4(F10.3,5X))
  104 FORMAT(1H ,///20X,*POINT*,10X,*Y(I)*,10X,*SY(I)*,10X,*X(1,I)*,10X,
     1*SX(1,I)*,10X,*ANGLE OF INCIDENCE*//)
  105 FORMAT(21X,I2,10X,2(F6.3,9X),F6.2,11X,F6.2,15X,F6.2)
      END
```

```
      FUNCTION ETA(L)
C*****DERIVES INTERNAL ANGLE OF TRANSMISSION FROM ANGLE OF INCIDENCE BY
C     NEWTONS METHOD
      COMMON Y(50),X(5,50),XX(5),SY(50),SX(5,50),A(5),B(10),R(50),F(50)
     1,SA(5),C(5,5),CINV(5,5),DL(50),S
      COMMON N,M,NP,NC,KE,KSET,ISTAT,ITER,CONMIN
      V1=1./B(1)
      V3=1./B(3)
      IEX1=0
      AIF=X(1,L)*0.01745
      ETA=AIF
      IF(ETA.EQ.0.) GO TO 7
      AC=B(4)*0.01745
    1 IEX1=IEX1+1
      IF(IEX1.GT.10) GO TO 6
      IEX2=1
    2 IF(ETA.LT.0) GO TO 3
      IF(ETA.LT.AC) GO TO 3
      AD=ETA-AC
      GO TO 4
    3 AD=AC-ETA
    4 A1=V1*COS(AD)
      A3=V3*SIN(AD)
      VPE=SQRT(A1*A1+A3*A3)
      CF=1./VPE
      Z=SIN(AIF)-SIN(ETA)*CF
      IF(IEX2.EQ.2) GO TO 5
      IEX2=2
      ZZ=Z
      XZ=ETA
      ETA=ETA*1.005
      GO TO 2
    5 DX=ETA-XZ
      DZ=(Z-ZZ)/DX
      ADD=ZZ/DZ
      ETA=XZ-ADD
      TEST=ABS(ADD)
      ELIM=0.05*0.01745
      IF(TEST.LE.ELIM) GO TO 7
      GO TO 1
    6 AIF=AIF/0.01745
      XZ=XZ/0.01745
      ETA=ETA/0.01745
      WRITE(6,100) AIF,XZ,ETA
      STOP
    7 ETA=ETA/0.01745
      RETURN
  100 FORMAT(1H ,///10X,*10 ITERATIONS EXCEEDED IN ETA BY AIF= *,F6.2/
     110X,*LAST TWO VALUES OF ETA WERE *,2(F7.2,5X))
      END
```

```
      FUNCTION EQN(L)
C*****EQUATION SUBROUTINE
      COMMON Y(50),X(5,50),XX(5),SY(50),SX(5,50),A(5),B(10),R(50),F(50)
     1,SA(5),C(5,5),CINV(5,5),DL(50),S
      COMMON N,M,NP,NC,KE,KSET,ISTAT,ITER,CONMIN
      B1=B(1)
      B3=B(3)
      B4=B(4)*0.01745
      A1=A(1)*0.01745
      A2=A(2)
      IF(XX(1).LE.0.) GO TO 3
      BB=ABS(XX(1))
      IF(BB.LT.B4) GO TO 3
      Z=XX(1)-B4
      GO TO 4
    3 Z=B4-XX(1)
    4 Z1=COS(Z)/B1
      Z2=SIN(Z)/B3
      RINDEX=1./SQRT(Z1*Z1+Z2*Z2)
      RAY=(Z2*B1)/(Z1*B3)
      RAY=B4-ATAN(RAY)
      CRAY=COS(RAY)
      AB=COS(A1)*CRAY
      AB=AB+SIN(A1)*SIN(RAY)
      AB=AB*AB
      AB=AB/(COS(XX(1))*RINDEX*COS(RAY-XX(1)))
      EQN=Y(L)-A2*AB
      RETURN
      END
```

```
      FUNCTION DERIV(L,LL,IND)
C*****A GENERAL DIFFERENTIATION PROCEDURE
      COMMON Y(50),X(5,50),XX(5),SY(50),SX(5,50),A(5),B(10),R(50),F(50)
     1,SA(5),C(5,5),CINV(5,5),DL(50),S
      COMMON N,M,NP,NC,KE,KSET,ISTAT,ITER,CONMIN
      IF(IND.EQ.2) GO TO 2
C     DIFFERENTIATE W.R.T INDEP. VARIABLE
      Z=XX(L)
      IF(Z.EQ.0.) GO TO 11
      XX(L)=XX(L)*1.005
      GO TO 12
   11 XX(L)=XX(L)+0.005
   12 ZZ=XX(L)
      E=EQN(LL)
      XX(L)=Z
      GO TO 3
C     DIFFERENTIATE W.R.T UNKNOWN PARAMETERS
    2 Z=A(L)
      IF(Z.EQ.0.) GO TO 21
      A(L)=A(L)*1.005
      GO TO 22
   21 A(L)=A(L)+0.005
   22 ZZ=A(L)
      E=EQN(LL)
      A(L)=Z
    3 DERIV=(E-R(LL))/(ZZ-Z)
      RETURN
      END
```

```
      SUBROUTINE PRINT(KP)
C*****OUTPUT SUBROUTINE
      COMMON Y(50),X(5,50),XX(5),SY(50),SX(5,50),A(5),B(10),R(50),F(50)
     1,SA(5),C(5,5),CINV(5,5),DL(50),S
      COMMON N,M,NP,NC,KE,KSET,ISTAT,ITER,CONMIN
      GO TO (1,2,3),KP
    1 WRITE(6,100)
      WRITE(6,101) S,(A(K),K=1,NP)
      WRITE(6,102)
      L=0
      GO TO 1000
    2 L=L+1
      WRITE(6,103) L,S,(A(K),K=1,NP)
      GO TO 1000
    3 WRITE(6,104)
      WRITE(6,105) (A(K),SA(K),K=1,NP)
      WRITE(6,106)
      DO 4 I=1,N
    4 WRITE(6,107) I,R(I),DL(I),F(I)
 1000 RETURN
  100 FORMAT(1H1,///50X,*LEAST SQUARES RESULTS*,/////20X,*STARTING S*,
     130X,*INITIAL GUESSES*//)
  101 FORMAT(20X,1PE10.3,25X,2(E10.3,5X))
  102 FORMAT(1H ,/////20X,*ITERATION*,15X,*S*,30X,*VALUES OF PARAMETERS*
     1///)
  103 FORMAT(24X,I2,13X,1PE10.3,22X,2(E10.3,5X))
  104 FORMAT(1H ,/////20X,*INITIAL RESULTS*,//25X,*EACH PARAMETER AND IT
     1S STANDARD DEVIATION LISTED ACROSS PAGE*///)
  105 FORMAT(30X,2(1PE10.3,5X),10X,2(E10.3,5X))
  106 FORMAT(1H ,/////20X,*RESIDUALS IN DEPENDENT VARIABLE AND WEIGHTS U
     1SED*,//25X,*POINT*,15X,*RESIDUAL*,20X,*WEIGHT*,15X,*Y(CALC)*///)
  107 FORMAT(27X,I2,17X,F6.3,18X,E10.3,14X,F6.3)
      END
```

```
      SUBROUTINE MATINV
C*****INVERSION SUBROUTINE FOR A 2X2 MATRIX ONLY
      COMMON Y(50),X(5,50),XX(5),SY(50),SX(5,50),A(5),B(10),R(50),F(50)
     1,SA(5),C(5,5),CINV(5,5),DL(50),S
      COMMON N,M,NP,NC,KE,KSET,ISTAT,ITER,CONMIN
      IF(NP.GT.2) GO TO 1000
C     CALC. DETERMINANT AND SEE IF MATRIX IS NON-SINGULAR
      C1=C(1,1)*C(2,2)
      C2=C(1,2)*C(1,2)
      DET=C1-C2
      IF(ABS(DET).GE.0.001) GO TO 2
    1 WRITE(6,100) DET
      GO TO 2000
    2 CINV(1,1)=C(2,2)/DET
      CINV(2,2)=C(1,1)/DET
      CINV(2,1)=-C(2,1)/DET
      CINV(1,2)=CINV(2,1)
      GO TO 3000
 1000 WRITE(6,101)
 2000 STOP
 3000 RETURN
  100 FORMAT(1H ,///10X,*DET= *,1PE10.3,1X,*MATRIX NON-SINGULAR - NO SOL
     1UTION POSSIBLE*)
  101 FORMAT(1H ,///10X,*ONLY 2X2 MATRIX CAN BE INVERTED*)
      END
```

C-4 RESPECT

```
      PROGRAM RESPECT(INPUT,OUTPUT,TAPE5=INPUT,TAPE6=OUTPUT)
C*****COMPUTES CORRECTED GUEST SPECTRA FROM TOTAL GUEST-POLYMER SPECTRA
C     FOR PVA AND NAPSS AT 293 AND 77 K
      COMMON AA,WLIM(4),VMAX,UVMAX,IPOLY,ITEMP,NI,IPLOTV,IPLOTUV,IGYD,
     1TS(200),BS(200),CS(200),W(200)
C     READ IN NO. OF DATA SETS
      READ(5,100) NDATA
      ICOUNT=0
C     READ INPUT INFORMATION
 1000 CALL READ
      ICOUNT=ICOUNT+1
C     COMPUTE BACKGROUND SPECTRUM BS AND CORRECTED SPECTRUM CS FROM
      CALL BKSPEC                                              TOTAL TS
      DO 1 I=1,NI
    1 CS(I)=TS(I) - BS(I)
      IF(IGYD.NE.1) GO TO 3
      IF(IPLOTV.EQ.1) GO TO 2
      CALL PEAK(VMAX,WLIM(1),WLIM(2))
      CALL PRINT(2)
    2 IF(IPLOTUV.EQ.1) GO TO 3
      CALL PEAK(UVMAX,WLIM(3),WLIM(4))
      CALL PRINT(3)
      GO TO 4
    3 CALL PEAK(VMAX,WLIM(1),WLIM(2))
      CALL PRINT(1)
    4 IF(ICOUNT.LT.NDATA) GO TO 1000
      STOP
  100 FORMAT(I2)
      END
```

```
      SUBROUTINE READ
C*****INPUT SUBROUTINE
      COMMON AA,WLIM(4),VMAX,UVMAX,IPOLY,ITEMP,NI,IPLOTV,IPLOTUV,IGYD,
     1TS(200),BS(200),CS(200),W(200)
C     1 HEADER CARD
      READ(5,100) (BS(I),I=1,10)
C     READ CONSTANTS, ETC.
      READ(5,101) AA,(WLIM(I),I=1,4),VMAX,UVMAX,IPOLY,ITEMP,NI,IPLOTV,
     1IPLOTUV,IGYD
C     READ MEASURED TOTAL SPECTRUM TS AS A FUNCTION OF WAVENUMBER W
      READ (5,102) (W(I),I=1,NI)
      READ(5,103) (TS(I),I=1,NI)
C     WRITE INPUT DATA OUT
      WRITE(6,500)AA,(WLIM(I),I=1,4),VMAX,UVMAX,IPOLY,ITEMP,NI,IPLOTV,
     1IPLOTUV,IGYD
      WRITE(6,100) (BS(I),I=1,10)
      DO 1 I=1,NI
    1 WRITE(6,501) I,W(I),TS(I)
      RETURN
  100 FORMAT(10A8)
  101 FORMAT(F10.3,6F5.0,6I3)
  102 FORMAT(13F6.0)
  103 FORMAT(20F4.0)
  500 FORMAT(1H1,///35X,*DYE ABSORPTION SPECTRA IN POLYMER MATRICES*,///
     1//,50X,*INPUT DATA*///,10X,*AA,WLIM(4),VMAX,UVMAX,IPOLY,ITEMP,NI,I
     1PLOTV,IPLOTUV,IGYD, RESPECTIVELY*//5X,7(1PE10.3,2X),/,5X,6(I4,8X))
  501 FORMAT(10X,I4,10X,F6.0,10X,F6.3)
      END
```

```
      SUBROUTINE BKSPEC                                                ABSOR-
C*****THIS SUBROUTINE COMPUTES BACKGROUND SPECTRUM FROM AN INITIAL BANCE
      COMMON AA,WLIM(4),VMAX,UVMAX,IPOLY,ITEMP,NI,IPLOTV,IPLOTUV,IGYD,
     1TS(200),BS(200),CS(200),W(200)
      IF(IPOLY.NE.1) GO TO 3
      IF(ITEMP.NE.1) GO TO 2
      CALL PVA293
      ND=64
      ALIM=45000.
      GO TO 5
    2 CALL PVA77
      ND=64
      ALIM=45000.
      GO TO 5
    3 IF(ITEMP.NE.1) GO TO 4
      CALL PSS293
      ND=61
      ALIM=31000.
      GO TO 5
    4 CALL PSS77
      ND=61
      ALIM=31000.
    5 CS(1)=AA
      DO 6 I=1,ND
      II=I+1
    6 CS(II)=CS(I)*BS(I)
      WN=12500.
      DO 7 I=1,10
      WN=WN+500.
      IF(W(1).LT.WN) GO TO 8
    7 CONTINUE
    8 NW=I-1
      NL=1
      DIV=500.
    9 J=NW
      JJ=J+1
      A1=CS(J)
      A2=CS(JJ)
      S=ABS(A2-A1)/DIV
      DO 10 I=NL,NI
      IF(W(I).GE.WN) GO TO 11
      X=W(I)/1000.
      XX=AINT(X)
      XX=(X-XX)*1000.
      IF(X.GT.DIV) X=X-DIV
   10 BS(I)=S*X+A1
      GO TO 12
   11 NL=I
      NW=NW+1
      WN=WN+DIV
      IF(WN.NE.ALIM) GO TO 9
      IF(ALIM.NE.31000.) GO TO 110
      DIV=200.
      ALIM=36000.
      GO TO 9
  110 WN=WN+0.1
      GO TO 9
   12 RETURN
      END
```

```
      SUBROUTINE PEAK (AMAX,XLIM1,XLIM2)
C*****THIS SUBROUTINE COMPUTES NORMALIZED CORRECTED SPECTRA
      COMMON AA,WLIM(4),VMAX,UVMAX,IPOLY,ITEMP,NI,IPLOTV,IPLOTUV,IGYD,
     1TS(200),BS(200),CS(200),W(200)
      DO 11 J=1,200
      IF(XLIM1.NE.W(J)) GO TO 1
      N=J
    1 IF(XLIM2.NE.W(J)) GO TO 11
      M=J
      GO TO 2
   11 CONTINUE
    2 IF(IGYD.NE.1) N=1
      PK=CS(N)
      DO 4 I=N,M
      IF(CS(I).GT.PK) 3,4
    3 PK=CS(I)
    4 CONTINUE
      IF(PK.LE.0) 6,7
    6 WRITE(6,500)
      STOP
    7 FACTOR=AMAX/PK
      J=N
      IF(IGYD.NE.1) M=NI
      MM=M + 1
      DO 8 I=1,200
      CS(I)=CS(J)*FACTOR
      W(I)=W(J)
      J=J + 1
      IF(J.EQ.MM) GO TO 9
    8 CONTINUE
    9 NI=I
      RETURN
  500 FORMAT(1H ,///,10X,*SPECTRUM INTENSITIES LESS THAN OR EQUAL TO ZER
     10 - TERMINATE*)
      END

      SUBROUTINE PRINT (IP)
C*****OUTPUT SUBROUTINE
      COMMON AA,WLIM(4),VMAX,UVMAX,IPOLY,ITEMP,NI,IPLOTV,IPLOTUV,IGYD,
     1TS(200),BS(200),CS(200),W(200)
      IF(IP.EQ.1) GO TO 1
      IF(IP.EQ.2) GO TO 3
      IF(IP.EQ.3) GO TO 5
    1 WRITE(6,500) AA
      DO 2 I=1,NI
      TS(I)=TS(I)-BS(I)
    2 WRITE(6,501) W(I),CS(I),TS(I),BS(I)
      GO TO 7
    3 WRITE(6,502)
      DO 4 I=1,NI
    4 WRITE(6,503) W(I),CS(I)
      CALL OVERSA (1H ,1H.,NI,CS,W)
      GO TO 7
    5 WRITE(6,504)
      DO 6 I=1,NI
    6 WRITE(6,503) W(I),CS(I)
      CALL OVERSA (1H ,1H.,NI,CS,W)
    7 RETURN
  500 FORMAT(1H ,///,10X,*FOLLOWING ARE WAVENUMBERS AND CORRECTED MOLAR
     1ABSORPTIVITIES OF DYE SPECTRUM*/,10X,*NORMALIZED TO VISIBLE MAX IN
     2 SOLUTION FOLLOWED BY ABSORBANCES OF DYE AND POLYMER SPECTRA*///,
     320X,*INITIAL ABSORBANCE IS *,F6.3//)
  501 FORMAT(20X,F6.0,10X,E10.3,2(10X,F6.3))
  502 FORMAT(1H1,/////,10X,*NORMALIZED VISIBLE SPECTRUM*//)
  503 FORMAT(10X,F6.0,10X,E10.3)
  504 FORMAT(1H1,/////,10X,*NORMALIZED UV SPECTRUM*//)
      END
```

```
      SUBROUTINE OVERSA(IZERO,IPOINT,N,O,A)
C*****PLOTTING SUBROUTINE
      DIMENSION O(101),A(101),IO(101),IA(101),IP(101)
      OMAX=AMAX=-1.E25
      OMIN=AMIN=1.E25
      DO 8 I=1,N
      IF(O(I)-OMAX) 2,2,1
    1 OMAX=O(I)
    2 IF(O(I)-OMIN) 3,4,4
    3 OMIN=O(I)
    4 IF(A(I)-AMAX) 6,6,5
    5 AMAX=A(I)
    6 IF(A(I)-AMIN) 7,8,8
    7 AMIN=A(I)
    8 CONTINUE
      AINC=(AMAX-AMIN)/99.
      OINC=(OMAX-OMIN)/49.
      WRITE(6,101) AMIN,AMAX,AINC,OMAX,OMIN,OINC
      WRITE(6,102)
      DO 9 I=1,100
      IO(I)=0
    9 IA(I)=0
      DO 10 I=1,N
      IK=(O(I)-OMIN)/OINC
      II=50-IK
      IO(I)=II
      IK=(A(I)-AMIN)/AINC
      II=IK+1
      IA(I)=II
   10 CONTINUE
      L=0
      I=0
   11 I=I+1
      L=6+1
      IF(I-51) 12,20,20
   12 DO 121 K=1,100
  121 IP(K)=0
      DO 14 J=1,N
      IF(IO(J)-I) 14,13,14
   13 JJ=IA(J)
      IP(JJ)=1
   14 CONTINUE
      DO 17 J=1,100
      IF(IP(J)) 16,15,16
   15 IP(J)=IZERO
      GO TO 17
   16 IP(J)=IPOINT
   17 CONTINUE
      IF(L-5) 18,19,18
   18 WRITE(6,103) (IP(J),J=1,100)
      GO TO 11
   19 WRITE(6,104) (IP(J),J=1,100)
      L=0
      GO TO 11
   20 WRITE(6,102)
      RETURN
  101 FORMAT(1H1,*ABCISSA SCALE --- VALUE AT THE LEFT =*E10.3,*, VALUE A
     1T THE RIGHT =*E10.3,*, INCREMENT =*E10.3,/,* ORDINATE SCALE --- VA
     2LUE AT THE TOP =*E10.3,*, VALUE AT THE BOTTOM =*E10.3,*, INCREMENT
     3 =*E10.3,//)
  102 FORMAT(10X,102HI----5----5----5----5----5----5----5----5----5----5
     1----5----5----5----5----5----5----5----5----5----5I)
  103 FORMAT(10X,1HI,100A1,1H1)
  104 FORMAT(10X,1H5,100A1,1H5)
      END
```

```
      SUBROUTINE PVA293
C*****THIS CONTAINS PVA DATA AT 293K
      COMMON AA,WLIM(4),VMAX,UVMAX,IPOLY,ITEMP,NI,IPLOTV,IPLOTUV,IGYD,
     1TS(200),BS(200),CS(200),W(200)
      DIMENSION AS(65)
      DATA(AS(L),L=1,64)/1.00,1.00,1.00,1.00,1.00,1.00,1.00,1.01,1.02,
     11.00,1.01,1.00,1.01,1.02,1.02,1.00,1.00,1.02,1.01,1.00,1.01,1.01,
     21.01,1.01,1.02,1.02,1.01,1.03,1.02,1.03,1.04,1.02,1.03,1.02,1.01,
     31.00,1.02,1.03,1.02,1.02,1.03,1.02,1.02,1.02,1.02,1.02,1.02,1.01,
     41.01,1.00,1.01,1.01,1.01,1.02,1.03,1.04,1.03,1.05,1.05,1.08,1.06,
     51.09,1.08,1.08/
      DO 1 L=1,64
    1 BS(L)=AS(L)
      RETURN
      END

      SUBROUTINE PVA77
C*****THIS CONTAINS PVA DATA AT 77K
      COMMON AA,WLIM(4),VMAX,UVMAX,IPOLY,ITEMP,NI,IPLOTV,IPLOTUV,IGYD,
     1TS(200),BS(200),CS(200),W(200)
      DIMENSION AS(65)
      DATA(AS(L),L=1,64)/1.00,1.00,1.00,1.00,1.00,1.00,1.01,1.02,1.04,
     11.00,1.02,1.00,1.03,1.02,1.00,1.02,1.01,1.02,1.03,1.00,1.01,1.02,
     21.02,1.02,1.03,1.02,1.03,1.03,1.02,1.02,1.02,1.03,1.05,1.02,1.02,
     31.02,1.03,1.05,1.05,1.04,1.04,1.04,1.04,1.03,1.02,1.02,1.03,1.01,
     51.02,1.02,1.01,1.02,1.01,1.04,1.03,1.04,1.05,1.05,1.06,1.05,1.06,
     61.05,1.06,1.07/
      DO 1 L=1,64
    1 BS(L)=AS(L)
      RETURN
      END

      SUBROUTINE PSS293
C*****THIS CONTAINS NAPSS DATA AT 293K
      COMMON AA,WLIM(4),VMAX,UVMAX,IPOLY,ITEMP,NI,IPLOTV,IPLOTUV,IGYD,
     1TS(200),BS(200),CS(200),W(200)
      DIMENSION AS(65)
      DATA(AS(L),L=1,61)/1.00,1.00,1.00,1.00,1.00,1.00,1.00,1.01,1.01,
     11.01,1.00,1.01,1.01,1.01,1.00,1.00,1.00,1.03,1.00,1.02,1.01,1.03,
     21.02,1.04,1.07,1.08,1.06,1.07,1.07,1.06,1.06,1.06,1.06,1.06,1.06,
     31.07,1.03,1.03,1.03,1.03,1.03,1.03,1.04,1.05,1.07,1.07,1.09,
     41.10,1.10,1.10,1.10,1.09,1.08,1.07,1.08,1.10,1.14,1.22,1.34,1.43/
      DO 1 L=1,61
    1 BS(L)=AS(L)
      RETURN
      END

      SUBROUTINE PSS77
C*****THIS CONTAINS NAPSS DATA AT 77K
      COMMON AA,WLIM(4),VMAX,UVMAX,IPOLY,ITEMP,NI,IPLOTV,IPLOTUV,IGYD,
     1TS(200),BS(200),CS(200),W(200)
      DIMENSION AS(65)
      DATA(AS(L),L=1,61)/1.00,1.00,1.00,1.00,1.00,1.00,1.01,1.01,1.01,
     11.01,1.02,1.00,1.01,1.00,1.01,1.00,1.01,1.02,1.01,1.02,1.04,1.02,
     21.03,1.04,1.07,1.08,1.08,1.09,1.08,1.05,1.06,1.07,1.06,1.07,1.07,
     31.09,1.02,1.03,1.03,1.03,1.03,1.04,1.04,1.04,1.04,1.06,1.06,1.07,
     41.09,1.09,1.10,1.10,1.09,1.07,1.07,1.08,1.10,1.14,1.22,1.33,1.42/
      DO 1 L=1,61
    1 BS(L)=AS(L)
      RETURN
      END
```

Offprinted from the *Journal of The Chemical Society, Faraday Transactions II*, 1974, vol. 70.

DERIVATION AND INTERPRETATION OF THE SPECTRA OF AGGREGATES

PART 3.—PREDICTION ANALYTICAL STUDY OF THE SPECTRUM OF PYRONINE Y IN AQUEOUS SOLUTION

Gianneschi, L. P. & Kurucsev, T. (1974). Derivation and interpretation of the spectra of aggregates. Part 3.-Prediction analytical study of the spectrum of pyronine Y in aqueous solution. *Journal of the Chemical Society, Faraday Transactions 2: Molecular and Chemical Physics, 70,* 1334-1342.

Gianneschi, L. P. & Kurucsev, T. (1976). Derivation and interpretation of the spectra of aggregates. Part 4. - Adiabatic theory of exciton interactions in dimers. *Journal of the Chemical Society, Faraday Transactions 2: Molecular and Chemical Physics*, *72*, 2095-2104.